Alma Mater Studiorum – Università di Bologna

DOTTORATO DI RICERCA IN

Meccanica e scienze avanzate dell'Ingegneria

Ciclo XXVIII

Settore Concorsuale di afferenza: 09/C2

Settore Scientifico disciplinare: ING-IND/18

DESIGN AND DIAGNOSTICS OF NON-EQUILIBRIUM ATMOSPHERIC PLASMA SOURCES FOR CELL TREATMENT AND BACTERIAL DECONTAMINATION

Presentata da: Augusto Stancampiano

Coordinatore Dottorato

Prof. Vincenzo Parenti Castelli

Relatore

Prof. Vittorio Colombo

Esame finale anno 2016

Progress is made by trial and failure; the failures are generally a hundred times more numerous than the successes; yet they are usually left unchronicled.

William Ramsay

Every great advance in science has issued from a new audacity of imagination.

John Dewey

INDEX

INTRODUCTION

In the last two decades non-equilibrium atmospheric plasma, also known as cold atmospheric plasma (CAP), has undeniably risen an increasingly amount of interest both in the scientific and industrial worlds. While its potential is still to be fully discovered, its role as one of the leading scientific innovations of the 21st century is less and less questioned.
Through their wide variety of operating conditions, CAP sources offer a tremendous number of degrees of freedom for the tailoring of plasma characteristics to specific applications requirements. As a result, the field of applications of CAP is expanding steadily and, being true to its pervasive nature, nowadays include many processes like the decontamination of surfaces and liquids, thin film deposition, wound healing and dental applications.
Driven by encouraging results and the desire to exploit the full potential of this emerging technology, the past years have witnessed strong interdisciplinary research efforts in the study of the still not completely understood plasma phenomena. The increasing number of scientific publications and new applications presented every year lead to believe that the future of plasma technology is still mostly unseen and up to now we have only barely scratched the surface.

During my Ph.D. studies at Alma Mater Studiorum - Università di Bologna, I have been thoroughly involved in the activities of the Research Group for Industrial Application of Plasmas (IAP group) and I focused my studies mainly on the design, the diagnostic and the optimization of CAP sources for biomedical applications, such as cell treatment and bacterial decontamination. To achieve this purpose, during my research activities, I studied and adopted several diagnostic techniques and had the opportunity to cooperate with other researchers, especially for the analysis of plasma biological effects. I also took part in various research activities dealing with other applications and CAP sources outside the core activity of my study. I devoted a fair share of time also in the investigation of possible use of an inductively coupled plasma for biomedical purposes, that, as a matter of facts, falls under thermal plasma applications. During these three years I had the opportunity to contribute to the widening of the IAP group multidisciplinary network of collaborations within and without the Università di Bologna, also in the framework of international projects such as the European COST action MP1101 "Biomedical applications of atmospheric pressure plasma technology" and COST action TD1208: "Electrical discharges with liquids for future applications".

In this dissertation, I will discuss results from my activities on the design and diagnostic of CAP sources for biomedical applications. First, I will briefly introduce the CAP technology, providing an overview of the state of the art and a selection of chosen references. Second, I will focus on the

characterization of a single electrode jet plasma source with the aim to highlight the fundamental processes involved in the plasma propagation both in the case of the effluent freely extending into open air environment and impinging on a water substrate; in this section, the expertise and methodology developed for the proper use of ICCD cameras in plasma diagnostic will be also presented. In the second half of the dissertation, the investigation of potential applications of plasmas in the biomedical field will be presented. More in detail, the reported results will focus on: the plasma treatment effect on early bacterial adhesion and decontamination of soft reline palatal obturators; the plasma treatment of a lymphoma cell line for the promotion of cell death and cell-cycle arrest; the plasma treatment of tooth dentin to improve later adhesion of composite and implants mechanical properties in order to reduce failures.
These results have been reported in the following papers on international journals:

1. Stancampiano A. *et al.*, *Practical and theoretical considerations on the use of ICCD imaging for the characterization of non-equilibrium plasmas*, Plasma Sources Science and Technology 2015, 24:064004. doi: 10.1088/0963-0252/24/6/064004
2. Stancampiano A. *et al.*, *Atmospheric Non-Equilibrium Plasma Promotes Cell Death and Cell-Cycle Arrest in a Lymphoma Cell Line*, Plasma Processes and Polymers 2015, 12:1354-63. doi: 10.1002/ppap.201500033
3. Stancampiano A. *et al.*, *Characterization of a cold atmospheric pressure plasma jet device driven by nanosecond voltage pulses*, IEEE Transactions on Plasma Science 2015, 43:713-25. doi: 10.1109/TPS.2014.2381854
4. Stancampiano A. *et al.*, *Schlieren high-speed imaging of a nanosecond pulsed atmospheric pressure non-equilibrium plasma jet*, Plasma Chemistry and Plasma Processes 2014, 34:853-69. doi: 10.1007/s11090-014-9537-1
5. Stancampiano A. *et al.*, *ICCD Imaging of the Transition From Uncoupled to Coupled Mode in a Plasma Source for Biomedical and Materials Treatment Applications*, IEEE Transactions on Plasma Science 2014, 42:2746-7. doi: 10.1109/TPS.2014.2321012
6. Stancampiano A. *et al.*, *High-speed multi-imaging of repetitive unipolar nanosecond-pulsed DBDs.* IEEE Transactions on Plasma Science 2014, 42:2744-5. doi: 10.1109/TPS.2014.2330954
7. Stancampiano A. *et al.*, *Cold atmospheric plasma treatment affects early bacterial adhesion and decontamination of soft reline palatal obturators,* submitted to Journal of Biomedical Materials Research: Part B - Applied Biomaterials 2016

In addition, some results were presented at international conferences:

1. Stancampiano A. *et al.*, *Advanced investigation of the interaction between a plasma jet and a liquid surface: influence of electrical and fluid dynamic parameters,* oral presentation at the 11th biennial Frontiers in Low Temperature Plasma Diagnostic (FLTPD), Porquerolles Island (France), May 2015
2. Stancampiano A. *et al.*, *Effective decontamination of soft reline-based oral cancer shutters by means of non-thermal atmospheric plasma*, poster presentation at Joint meeting of COST Actions CMST TD1208 and MPNS MP1101, Bertinoro, Italy, 13-16 September 2015
3. Stancampiano A. *et al.*, *Characterization of a cold nanopulsed plasma jet in free-flow configuration and imping on different substrates,* poster presentation at Joint meeting of COST Actions CMST TD1208 and MPNS MP1101, Bertinoro, Italy, 13-16 September 2015.
4. Stancampiano A. *et al.*, *Advanced investigation of electrical and fluid-dynamic parameters on a nanopulsed plasma jet impinging on a liquid substrate,* poster presentation at Joint meeting of COST Actions CMST TD1208 and MPNS MP1101, Bertinoro, Italy, 13-16 September 2015.

5. Stancampiano A. *et al.*, *Multi-diagnostic investigation of a non-equilibrium atmospheric pressure plasma jet driven by nanosecond voltage pulses in free-flow configuration and while imping on different substrate,* oral presentation at Sixth Central European Symposium on Plasma Chemistry (CESPC-6),Bressanone (Italy), September 2015.
6. Stancampiano A. *et al.*, *Characterization of a cold nanopulsed plasma jet in free-flow configuration and imping on different substrates* poster presentation at 22th ISPC, Antwerp, Belgium, July 2015.
7. Stancampiano A. *et al.*, *Advanced investigation of electrical and fluid-dynamic parameters on a nanopulsed plasma jet impinging on a liquid substrate,* poster presentation at 22th ISPC, Antwerp, Belgium, July 2015.
8. Stancampiano A. *et al.*, *Effective decontamination of soft reline-based oral cancer shutters by means of non-thermal atmospheric plasma*, poster presentation at 22th ISPC, Antwerp, Belgium, July 2015
9. Stancampiano A. *et al.*, *Effective decontamination of soft reline-based oral cancer shutters by means of non-thermal atmospheric plasma "* poster presentation at Congresso Nazionale Biomateriali SIB, Portonovo, Ancona(Italy), June 2015, [Best Poster Award]
10. Stancampiano A. *et al.*, *Characterization of a cold atmospheric pressure plasma jet driven by nanosecond high-voltage pulses,* oral presentation at the 42nd IEEE International Conference on Plasma Science (ICOPS) Belek, Antalya (Turkey), May 2015.
11. Stancampiano A. *et al.*, *Advanced investigation of the interaction between a plasma jet and a liquid surface: influence of atmosphere and substrate composition,* poster presentation at the 11th biennial Frontiers in Low Temperature Plasma Diagnostic (FLTPD), Porquerolles Island (France), May 2015.
12. Stancampiano A. *et al.*, *Characterization of a non-equilibrium atmospheric pressure plasma jet driven by nanosecond voltage pulses*, oral presentation at 20th Symposium on Application of Plasma Processes - SAPP XX, Tatranská Lomnica, Vysoké Tatry, Slovakia, 17-22 September 2014
13. Stancampiano A. *et al.*, *Non-thermal plasma promotes apoptosis and cell-cycle arrest in a lymphoma cell line*, oral presentation at 5th International Conference on Plasma Medicine (ICPM5), Nara, Japan, 18 - 23 May 2014
14. Stancampiano A. *et al.*, *Characterization of a plasma jet for biomedical applications: composition, temperature, fluid dynamics and plasma structure*, poster presentation at ISPC21, Cairns, Australia, 4-9 August 2013
15. Stancampiano A. *et al.*, *Study of the role of dielectric material in a dielectric barrier discharge (DBD) plasma source for dermatological application*, poster presentation at ISPC21, Cairns, Australia, 4-9 August 2013
16. Stancampiano A. *et al.*, *Characterization of a plasma jet for biomedical applications: composition, temperature, fluid dynamics and plasma structure*, poster presentation at FLTPD-X, Kerkrade, the Netherlands, 28 April - 2 May 2013

In this research field, I have been co-supervisor for the following MA and BA thesis:

1. L. Fontanili, "Studio dell'interazione tra un plasma jet nanopulsato con substrati metallici, dielettrici e liquidi", laurea triennale in Ingegneria Clinica, Alma Mater Studiorum - Università di Cesena 2015
2. S. Antoci, "*Diagnostica in spettroscopia ottica di emissione (OES) di una sorgente plasma jet in condizioni di free flow e incidente su substrato liquido*", Alma Mater Studiorum - Università di Bologna 2015
3. E. Simoncelli, *"Progettazione, realizzazione e caratterizzazione di una sorgente Plasma Gun"*, Alma Mater Studiorum - Università di Bologna 2014

As a member of the IAP group, during my Ph.D., I also took part into other researches related to plasma biomedical and industrial processes. Through design and optimization oriented diagnostics I contributed to the investigation and development of a large variety of plasma sources for many different applications such as water treatment, thin film polymeric deposition, decontamination for endodontic procedure, *multijet* plasma sources, dermatological treatment, tooth bleaching, microplasma sources, mesenchymal cells treatment.
Since these researches are outside the core activity of my Ph.D., as they have been unexpected pleasant digressions, their results are not presented in this thesis. Nonetheless, these studies have been reported in the following papers on international journals were a complete description of the motivations, experimental set-ups and results can be found:

1. Stancampiano A. *et al.*, *Atmospheric plasma assisted PLA/microfibrillated cellulose (MFC) multilayer biocomposite for sustainable barrier application,* Industrial Crops and Products 2016, doi: 10.1016/j.indcrop.2016.03.020
2. Stancampiano A. *et al.*, *Deposition of plasma-polymerized polyacrylic acid coatings by a nonequilibrium atmospheric pressure nanopulsed plasma jet*, Plasma Processes and Polymers 2015, 13:375-86 doi: 10.1002/ppap.201500080
3. Stancampiano A. *et al.*, *Investigation of the antimicrobial activity at safe levels for eukaryotic cells of a low power atmospheric pressure inductively coupled plasma source*, Biointerphases 2015, 10, 029519. doi:10.1116/1.4919018
4. Stancampiano A. *et al.*, *Solid-State Crosslinking of Polysaccharide Electrospun Fibers by Atmospheric Pressure Non-Equilibrium Plasma: A Novel Straightforward Approach*, Plasma Processes and Polymers 2015, 12:1195-9. doi: 10.1002/ppap.201500054
5. Stancampiano A. *et al.*, *Preliminary investigation of the antibacterial efficacy of a handheld plasma gun source for endodontic procedures,* Clinical Plasma Medicine 2015; 3:77–86. doi:10.1016/j.cpme.2015.11.001
6. Stancampiano A. *et al.*, *High-speed and Schlieren imaging of a low power inductively coupled plasma source for potential biomedical applications*, IEEE Transactions on Plasma Science, Images in Plasma Science 2014, 42, 10. doi:10.1109/TPS.2014.2319856.

Also, many results were presented at international conferences:

1. Stancampiano A. *et al.*, *Atmospheric non-equilibrium plasma sources and processes with a focus on plasma medicine and antibacterial applications*, oral presentation at GEC-68/ICRP-9/SPP-33, Honolulu, USA, 12-16 October 2015.
2. Stancampiano A. *et al*, *PlasmMi-Plasma Mobile Inactivator: cold plasma smartphone sanitizer to reduce hospital and community-acquired bacterial diseases*, poster presentation at Joint meeting of COST Actions CMST TD1208 and MPNS MP1101, Bertinoro, Italy, 13-16 September 2015.
3. Stancampiano A. *et al*, *In vivo investigation on the effects of plasma activated water against plant pathogenic bacteria,* poster presentation at Joint meeting of COST Actions CMST TD1208 and MPNS MP1101, Bertinoro, Italy, 13-16 September 2015.
4. Stancampiano A. *et al.*, *Investigation of the antimicrobial activity at safe levels for eukaryotic cells of a low power atmospheric pressure inductively coupled plasma source*, poster presentation at Joint meeting of COST Actions CMST TD1208 and MPNS MP1101, Bertinoro, Italy, 13-16 September 2015
5. Stancampiano A. *et al.*, *Solid-state crosslinking of polysaccharide electrospun fibers by atmospheric pressure non-equilibrium plasma: a novel straightforward approach*, poster presentation at Joint meeting of COST Actions CMST TD1208 and MPNS MP1101, Bertinoro, Italy, 13-16 September 2015

6. Stancampiano A. *et al*, *Investigation of antibacterial efficacy of a plasma gun source for endodontic applications*, oral presentation at Joint meeting of COST Actions CMST TD1208 and MPNS MP1101, Bertinoro, Italy, 13-16 September 2015.
7. Stancampiano A. *et al*, *Non-equilibrium atmospheric pressure plasma jet driven by a nanosecond pulse generator for acrylic acidi plasma-polymerization*, poster presentation at Joint meeting of COST Actions CMST TD1208 and MPNS MP1101, Bertinoro, Italy, 13-16 September 2015.
8. Stancampiano A. *et al*, *Atmospheric pressure DC microplasma for the surfactant-free synthesis of CuO nanoparticles in a liquid environment*, oral presentation at Joint meeting of COST Actions CMST TD1208 and MPNS MP1101, Bertinoro, Italy, 13-16 September 2015.
9. Stancampiano A. *et al.*, *Investigation of the antimicrobial activity at safe levels for eukaryotic cells of a low power atmospheric pressure inductively coupled plasma source,* poster presentation at Sixth Central European Symposium on Plasma Chemistry (CESPC-6),Bressanone (Italy), September 2015
10. Stancampiano A. *et al.*, *Surface characterization of plasma-polymerized polyacrylic acid thin film deposited by means of a nanosecond pulsed plasma jet,* oral presentation at Sixth Central European Symposium on Plasma Chemistry (CESPC-6),Bressanone (Italy), September 2015.
11. Stancampiano A. *et al.*, *Investigation of the efficacy of plasma gun decontamination of realistic root canal models for endodontic applications*, oral presentation at Sixth Central European Symposium on Plasma Chemistry (CESPC-6),Bressanone (Italy), September 2015.
12. Stancampiano A. *et al, In vivo investigation on the effects of plasma activated water against plant pathogenic bacteria* poster presentation at 22th ISPC, Antwerp, Belgium, July 2015.
13. Stancampiano A. *et al*, *Investigation of the antimicrobial activity at safe levels for eukaryotic cells of a low power atmospheric pressure inductively coupled plasma source,* poster presentation at 22th ISPC, Antwerp, Belgium, July 2015.
14. Stancampiano A. *et al*, *Investigation of antibacterial efficacy of a plasma gun source for endodontic applications* poster presentation at 22th ISPC, Antwerp, Belgium, July 2015.
15. Stancampiano A. *et al.*, *Solid-state crosslinking of polysaccharide electrospun fibers by atmospheric pressure non-equilibrium plasma: a novel straightforward approach*, poster presentation at 22th ISPC, Antwerp, Belgium, July 2015.
16. Stancampiano A. *et al*, *Effective deposition of plasma-polymerized polyacrilic acid thin film by means of a plasma jet driven by nanosecond high voltage pulses*, oral presentation at 22th ISPC, Antwerp, Belgium, July 2015.
17. Stancampiano A. *et al.*, *Characterization and evaluation of bactericidal effect and cytocompatibility of a low power ICP source for biomedical applications,* oral presentation at the 42nd IEEE International Conference on Plasma Science (ICOPS) Belek, Antalya (Turkey), May 2015.
18. Stancampiano A. *et al.*, *Investigation of antibacterial efficacy of a plasma gun source for endodontic applications,* oral presentation at the 42nd IEEE International Conference on Plasma Science (ICOPS) Belek, Antalya (Turkey), May 2015.
19. Stancampiano A. *et al.*, *Atmospheric pressure non-thermal plasma for the production of composite materials*, oral presentation at the 42nd IEEE International Conference on Plasma Science (ICOPS) Belek, Antalya (Turkey), May 2015.
20. Stancampiano A. *et al.*, *Solid-state crosslinking of polysaccharide electrospun fibers by atmospheric pressure non-equilibrium plasma: a novel straightforward approach*, oral presentation at the 42nd IEEE International Conference on Plasma Science (ICOPS) Belek, Antalya (Turkey), May 2015.
21. Stancampiano A. *et al.*, *Direct and indirect treatment of prokaryotic and eukaryotic cells in liquid medium by means of a low power inductively coupled plasma (icp) torch: evaluation of antibacterial effects and cytocompatibility,* oral presentation at the 2nd Annual meeting of COST Action TD1208, Barcelona, Spain, 2015.
22. Stancampiano A. *et al.*, *Plasma gun decontamination of bacteria in liquid suspensions,* poster presentation at the 2nd Annual meeting of COST Action TD1208, Barcelona, Spain, 2015.

23. Stancampiano A. *et al.*, *Mass spectrometry analysis of coupled and uncoupled mode in a Gatling-gun like plasma source*, oral presentation at COST MP1101 Topical Workshop, Paris, France, 2014
24. Stancampiano A. *et al.*, *Plasma gun decontamination of bacteria in liquid suspensions*, poster presentation at 20th Symposium on Application of Plasma Processes - SAPP XX, Tatranská Lomnica, Vysoké Tatry, Slovakia, 17-22 September 2014
25. Stancampiano A. *et al.*, *Investigation of the effectiveness of a gatling machine gun-like plasma source for biomedical applications and materials treatment*, poster presentation at 14th International Conference on Plasma Surface Engineering, Garmisch-Partenkirchen, Germany, 15-19 September 2014
26. Stancampiano A. *et al.*, *Non-equilibrium plasma sources and processes with a focus on antibacterial applications and sterilization*, keynote lecture at 14th International Conference on Plasma Surface Engineering, Garmisch-Partenkirchen, Germany, 15-19 September 2014
27. Stancampiano A. *et al.*, *Processes and sources for biomedical and material applications in UNIBO*, poster presentation at Gordon Research Conference on Plasma Processing Science - Many Scales, Many Applications, One Discipline, Bryant University, Smithfield, USA, 22-27 July 2014
28. Stancampiano A. *et al.*, *Processes and sources for biomedical and material applications in UNIBO*, oral presentation at Gordon Research Seminar on Plasma Processing Science: Non-Equilibrium Plasma Diagnostics, Modeling, and Applications, Bryant University, Smithfield, USA, 26-27 July 2014
29. Stancampiano A. *et al.*, *Investigation of the effectiveness of a low power inductively coupled plasma source for biomedical applications*, oral presentation at 5th International Conference on Plasma Medicine (ICPM5), Nara, Japan, 18 - 23 May 2014
30. Stancampiano A. *et al.*, *Plasma source for fast and continuous purification of water flows*, poster presentation at 5th International Conference on Plasma Medicine (ICPM5), Nara, Japan, 18 - 23 May 2014
31. Stancampiano A. *et al.*, *A novel plasma based teeth whitening technology*, poster presentation at 5th International Conference on Plasma Medicine (ICPM5), Nara, Japan, 18 - 23 May 2014
32. Stancampiano A. *et al.*, *Diagnostics of a low power inductively coupled plasma source for potential biomedical applications*, poster presentation at 5th International Conference on Plasma Medicine (ICPM5), Nara, Japan, 18 - 23 May 2014
33. Stancampiano A. *et al.*, *Antimicrobial activity of a low power inductively coupled plasma source at safe levels for eukaryotic cells*, poster presentation at 5th International Conference on Plasma Medicine (ICPM5), Nara, Japan, 18 - 23 May 2014
34. Stancampiano A. *et al.*, *Atmospheric pressure non-equilibrium plasma for the production of composite materials*, poster presentation at 5th International Conference on Plasma Medicine (ICPM5), Nara, Japan, 18 - 23 May 2014
35. Stancampiano A. *et al.*, *Investigation of the effectiveness of a Gatling machine gun-like plasma source for biomedical applications and materials treatment*, poster presentation at 5th International Conference on Plasma Medicine (ICPM5), Nara, Japan, 18 - 23 May 2014
36. Stancampiano A. *et al.*, *Comparison of the growth inhibition potential of different dielectric barrier discharge operating regimes*, poster presentation at 5th International Conference on Plasma Medicine (ICPM5), Nara, Japan, 18 - 23 May 2014
37. Stancampiano A. *et al.*, *Plasma as a new odontoiatric tool to improve implants adhesion*, poster presentation at 5th International Conference on Plasma Medicine (ICPM5), Nara, Japan, 18 - 23 May 2014
38. Stancampiano A.. *et al.*, *Investigation of the effectiveness of a low power inductively coupled plasma source for biomedical applications*, invited presentation at COST TD1208 Annual meeting, Lisboa, Portugal, 10 – 13 March 2014

39. Stancampiano A.. *et al.*, *Investigation of the effectiveness of a gatling machine gun-like plasma source for biomedical applications and materials treatment*, poster presentation at COST TD1208 Annual meeting, Lisboa, Portugal, 10 – 13 March 2014
40. Stancampiano A.. *et al.*, *Plasma-assisted electrospinning: the many facets of a process*, oral presentation at Workshop on Atmospheric Plasma Processes and Sources, EU COST MP1101, Bohinjska Bistrica, Slovenia, 22 – 23 January 2014
41. Stancampiano A.. *et al.*, *Processes and sources for biomedical and surface treatment applications in UNIBO*, invited presentation at Workshop on Atmospheric Plasma Processes and Sources, EU COST MP1101, Bohinjska Bistrica, Slovenia, 22 – 23 January 2014
42. Stancampiano A. *et al.*, *Atmospheric plasma surface modification of electrospun poly(L-lactic acid): effect on mat properties and cell culturing*, oral presentation at MiMe-Materials in Medicine 2013, Faenza, Italy, 8-11 October 2013
43. Stancampiano A. *et al.*, *Surface modification of poly(L-lactic acid) electrospun scaffold by atmospheric plasma: scaffold properties and fibroblast morphological response*, oral presentation at ISSIB-IV, Roma, Italy, 24-28 September 2013
44. Stancampiano A. *et al.*, *Increasing cell viability of 3D scaffolds for tissue engineering by means of an atmospheric pressure plasma jet*, poster presentation at ISPC21, Cairns, Australia, 4-9 August 2013
45. Stancampiano A. *et al.*, *Effect of atmospheric pressure non-equilibrium plasma treatment on poly-L-lactic acid electrospinnability*, poster presentation at ISPC21, Cairns, Australia, 4-9 August 2013
46. Stancampiano A. *et al.*, *Study of the effect of atmospheric pressure plasma treatment on electrospinnability of poly-L-lactic acid solutions: voltage waveform effect*, poster presentation at ISPC21, Cairns, Australia, 4-9 August 2013
47. Stancampiano A. *et al.*, *High speed imaging characterization of a Dielectric Barrier Discharge Roller plasma source*, poster presentation at ISPC21, Cairns, Australia, 4-9 August 2013
48. Stancampiano A. *et al.*, *Atmospheric plasma surface modification of electrospun poly(L-lactic acid): effect on mat properties and cell culturing*, oral presentation at ISPC21, Cairns, Australia, 4-9 August 2013
49. Stancampiano A. *et al.*, *Study of the effect on human mesenchymal and epithelial cells of an atmospheric pressure plasma source driven by different voltage waveforms*, poster presentation at ISPC21, Cairns, Australia, 4-9 August 2013
50. Stancampiano A. *et al.*, *Parametric study on the effectiveness of treatment of polyethylene (PE) foils for pharmaceutical packaging with a large area atmospheric pressure plasma source*, poster presentation at ISPC21, Cairns, Australia, 4-9 August 2013
51. Stancampiano A. *et al.*, *Plasma-assisted electrospinning: the many facets of a process*, oral presentation at ISPC21, Cairns, Australia, 4-9 August 2013
52. Stancampiano A. *et al.*, *Comparison of localized treatment effectiveness on biocompatible glass with different atmospheric pressure plasma sources*, poster presentation at ISPC21, Cairns, Australia, 4-9 August 2013
53. Stancampiano A. *et al.*, *Study of the role of dielectric material in a dielectric barrier discharge (DBD) plasma source for dermatological applications*, poster presentation at 11th ICSD, Bologna, Italy, 30 June - 4 July 2013
54. Stancampiano A. *et al.*, *Parametric study on the effectiveness of treatment of polyethylene (PE) foils for pharmaceutical packaging with a large area atmospheric pressure plasma source*, poster presentation at PPPS 2013, San Francisco, USA, 16-21 June 2013
55. Stancampiano A. *et al.*, *Atmospheric plasma surface modification of electrospun poly(L-lactic acid): effect on mat properties and cell culturing*, oral presentation at PPPS 2013, San Francisco, USA, 16-21 June 2013
56. Stancampiano A. *et al.*, *Comparison of localized treatment effectiveness on biocompatible glass with different atmospheric pressure plasma sources*, poster presentation at PPPS 2013, San Francisco, USA, 16-21 June 2013

57. Stancampiano A. *et al.*, *Plasma meets electrospinning: the many facets of a process*, oral presentation at Congresso AIV, Catania, Italy, 15-17 May 2013
58. Stancampiano A. *et al.*, *Bioplasma: on the industrial and social potential of cold atmospheric plasma applications*, keynote presentation at Congresso AIV, Catania, Italy, 15-17 May 2013
59. Stancampiano A. *et al.*, *Characterization of the plasma structure of a Dielectric Barrier Discharge roller plasma source for material treatment at atmospheric pressure*, poster presentation at FLTPD-X, Kerkrade, the Netherlands, 28 April - 2 May 2013
60. Stancampiano A. *et al.*, *Multi-imaging techniques for the characterization of a nanopulsed DBD system for biomedical applications*, oral presentation at Plasma to Plasma!, Leiden, The Netherlands, 7-11 January 2013

In these research fields, I have been co-supervisor for the following MA and BA thesis:

1. F. Manghi, *"Realizzazione e caratterizzazione funzionale di una sorgente di plasma atmosferico di non equilibrio per l'abbattimento di inquinanti organici in soluzione acquosa"*, Alma Mater Studiorum - Università di Bologna 2015
2. Patria, *"Analisi dell'efficacia antibatterica di sorgenti di plasma di non equilibrio per applicazioni medicali"*, Alma Mater Studiorum - Università di Bologna 2015
3. S. Polverini, *"Analisi dell'efficacia antibatterica e di degradazione di inquinanti chimici di una sorgente plasma a pressione atmosferica per la purificazione di flussi d'acqua"*, Alma Mater Studiorum - Università di Bologna
4. G. Anceschi, *"Sviluppo di processi di inattivazione batterica assistiti da sorgenti di plasma freddo a pressione atmosferica"*, Alma Mater Studiorum - Università di Bologna
5. F. Marani, *"Realizzazione e caratterizzazione chimico-fisica di una sorgente di plasma di non equilibrio operante a pressione atmosferica per la modifica superficiale di materiali polimerici in ambiente controllato"*, Alma Mater Studiorum - Università di Bologna
6. S. Bianconi, *"Progettazione, realizzazione e caratterizzazione di fasci di sorgenti microplasma (gatling plasma) per applicazioni biomedicali e di modificazione superficiale"*, Alma Mater Studiorum - Università di Bologna

ABBREVIATIONS

APPJ	Atmospheric Pressure Plasma Jet
AC	Alternating Current
CAP	Cold Atmospheric Plasma
DBD	Dielectric Barrier Discharge
DC	Direct Current
HS	High Speed
HIS	High Speed Imaging
ICCD	Intensified Charge Coupled Device
LTE	Local Thermal Equilibrium
PAPS	Pulsed Atmospheric-pressure Plasma Streamer
PV	Peak Voltage
PRF	Pulse Repetition Frequency
RF	Radio Frequency
RNS	Reactive Nitrogen Species
RONS	Reactive Oxygen and Nitrogen Species
ROS	Reactive Oxygen Species
SLPM	Standard Liters Per Minute

CHAPTER 1
NON-EQUILIBRIUM ATMOSPHERIC PRESSURE PLASMA

1.1 Literature overview

Nowadays, it is still quite uncommon for an ordinary person to come directly and knowingly into contact with plasma, the fourth state of matter. Our daily lives are dominated by the presence of the other three states (solid, liquid and gas), which we therefore perceive as more familiar. Despite the general belief, plasma is not rare, quite the opposite. More than 99% of the visible matter in the universe is in the plasma state [1]. It can be seen in its natural form on earth as lightning or as polar light in proximity of the North and South Poles. During a solar eclipse, plasma can be observed as a bright corona around the Sun. Plasma, in various forms and aspects, already plays an important role in many technologies of everyday life. A common example are neon lamps, widely diffuse all over the world as light sources.

The plasma is an ionized gas and consists of neutral, reactive and charged species. As can be easily found in nearly all textbooks and thesis on plasma technology, the term *plasma* was first introduced in 1928 by the Noble prize winner Irving Langmuir during his research on the extension of the lifetime of tungsten filament light bulbs [2]. In analogy with the blood plasma, the way ions and electrons are carried in gases with high applied voltages reminded Langmuir the way blood carries red and white corpuscles. Nearly 90 years have passed since that moment and plasma physics has become a large object of research worldwide aiming at exploring the intrinsic properties of matter [3,4], but also, especially in recent years, directed towards a multitude of applications [5–7].

Not all ionized gas can be called plasma. In fact, there is always a small degree of ionization in any gas. An ionized gas is defined as plasma when it is electrically neutral and contains a significant number of electrically charged particles, sufficient to affect its electrical properties and behaviour [5]. Plasmas can be divided either in thermal or non-thermal plasmas according to the neutrals, ions and electron temperatures. Thermal plasmas are also called *hot* plasmas or *equilibrium* plasmas and are nearly completely ionized. In those plasmas, the temperatures of neutral species, ions and electrons are nearly the same, so in thermodynamic equilibrium. Thermal plasmas applications are typically conducted at atmospheric pressure and include, for example, cutting of metal pieces and nanoparticle synthesis.
In non-thermal plasma, or *cold* plasmas, the temperatures of the neutrals and ions are much lower than the temperature of electrons and the plasma results far from thermodynamic equilibrium [3,8]. For these reason this kind of plasma is usually referred to as *non-equilibrium plasma.* Historically, these plasmas are produced in low pressure and used for applications such as lighting, microelectronics manufacturing and surface functionalization. It's worth reminding that most computer and smart phones hardware have undergone production processes relying on plasma technology [8].

To generate plasma, energy is needed in order to strip electrons from atoms. This energy can be of various origins including thermal and electrical. In the case on non-equilibrium plasma usually a high voltage is applied across two electrodes. If the applied voltage exceeds the breakdown voltage of the gas occupying the volume between the two electrodes, some molecules and atoms in the gas will be ionized and an electron avalanche is formed, possibly leading to the formation of a plasma discharge. The breakdown voltage may depend on different factors as described by the Paschen law [9] that basically expresses this threshold value depends as a function of the product of pressure and distance. In order to allow electrons to reach a high enough energy and be able to collide and ionize enough atoms, a minimum distance between the electrodes as to be granted. Similarly, if the distance between the electrode or the pressure is increased the applied voltage required to ignite the plasma has to increase as well. As the voltage to sustain a plasma is typically smaller than the breakdown voltage, if a large applied voltage, necessary to initially ignite the plasma, is sustained after breakdown, it will lead to rapid ionization and heating. In practice, while at low pressure relatively low voltages may be sufficient to achieve a stable plasma generation over gaps of several centimeters, at atmospheric pressure the voltage required to generate plasma over a few millimetres gap is usually in the order of some kilovolts [8,10].

Recent developments in physical electronics and pulsed power engineering have promoted significant developments in non-equilibrium atmospheric pressure plasma science and engineering [8,10]. Cold, uniform and well-controlled atmospheric pressure plasma sources have become a reality, creating the opportunity to apply plasma to heat sensitive materials and even living tissue, including the human body. The extensive work conducted by several research groups and companies around the world in the last decade demonstrated that CAP can provide breakthrough solutions to challenging problems and potentially revolutionize many technological fields, including the medical one.

Plasmas are able to produce a high concentration of energetic and chemically active species such as: electrons, positive and negative ions, atoms and radicals, excited atoms and molecules, photons with a wide spectral range. A high concentration of active species is crucial for plasma applications like plasma assisted combustion, surface sterilization and tissue engineering [6] . Moreover, as mentioned earlier, CAPs can be very far from thermodynamic equilibrium, thus providing an extremely high concentration of chemically active species and energetic electrons while maintaining macroscopic temperatures as low as room temperature. Thus, they can sustain complex chemistries, usually characteristic of high temperature systems, while remaining cold.
This feature determines the main advantage of CAPs and their wide application in many fields. Nowadays, CAPs are taking part in a variety of applications, including decontamination of heat-sensitive materials [11], food [12–14] and packaging [15–17], surface functionalization in implantology [18,19] and the treatment and deposition of polymers [5,20,21] [PAPER IV]. Recently, the use of non-thermal plasmas in the large field of biomedicine [22–31][PAPER VII], including promise of novel cancer therapies [26,32–36][PAPER VI], has gained significant interest. Another promising area of application is the treatment of wounds to improve an accelerate the healing process [37–39].

Without detailed understanding of the physical and chemical mechanisms, new plasma devices have little chance of successful application in any field and especially in medicine where the safety and controllability of devices is a major issue. Diagnostic investigation is crucial to achieve a complete control over plasma generation and plasma assisted processes. In the last years many works have helped in increasing knowledge on the principles of plasma generation and propagation through the use of several diagnostic techniques [40–45][PAPER I, II, III, IV, V] and modelling [46–48]. This aspect of non-thermal plasma diagnostic will be discussed in detail in Chapter 2 and 3.

Concluding, non-thermal plasma is a very exciting and new multidisciplinary branch of modern science and technology. In this dissertation, some of the results achieved during my Ph.D. research will be presented. More specifically, I will focus on the diagnostic investigation of a promising group of plasma devices usually named APPJs (Atmospheric Pressure Plasma Jets) and on three different promising

medical applications such as decontamination of soft reline implants, promotion of lymphoma cell death and adhesion enhancement for dental applications.

1.2 References

[1] C. Tendero, C. Tixier, P. Tristant, J. Desmaison, and P. Leprince, "Atmospheric pressure plasmas: A review," Spectrochim. Acta Part B At. Spectrosc., vol. 61, no. 1, pp. 2–30, 2006.

[2] L. Tonks, "The Birth of 'Plasma,'" Am. J. Phys., vol. 35, no. 9, p. 857, 1967.

[3] Y. P. Raizer, Gas discharge physics. Berlin: Springer-Verlag, 1991.

[4] J.-L. Delcroix and A. Bers, Physique des plasmas. Les Ulis (Essonne) : EDP sciences, 1994.

[5] A. Fridman and G. Friedman, Plasma medicine. John Wiley & Sons, 2012.

[6] R. Hippler, S. Pfau, and M. Schmidt, Low temperature plasma physics: fundamental aspects and applications. Wiley-VCH, 2001.

[7] J. E. Harry, Introduction to Plasma Technology: Science, Engineering, and Applications. John Wiley & Sons, 2011.

[8] A. Fridman, Plasma chemistry. Cambridge university press, 2008.

[9] F. Paschen, "Ueber die zum Funkenübergang in Luft, Wasserstoff und Kohlensäure bei verschiedenen Drucken erforderliche Potentialdifferenz," Ann. Phys., vol. 273, no. 5, pp. 69–96, 1889.

[10] U. Kogelschatz, "Dielectric-barrier Discharges: Their History, Discharge Physics, and Industrial Applications," Plasma Chem. Plasma Process., vol. 23, no. 1, 2003.

[11] S. Bekeschus, A. Schmidt, K.-D. Weltmann, and T. von Woedtke, "The plasma jet kINPen – A powerful tool for wound healing," Clin. Plasma Med., pp. 1–10, 2016.

[12] N. N. Misra, B. K. Tiwari, K. S. M. S. Raghavarao, and P. J. Cullen, "Nonthermal Plasma Inactivation of Food-Borne Pathogens," Food Eng. Rev., vol. 3, no. 3–4, pp. 159–170, Dec. 2011.

[13] P. Basaran, N. Basaran-Akgul, and L. Oksuz, "Elimination of Aspergillus parasiticus from nut surface with low pressure cold plasma (LPCP) treatment," Food Microbiol., vol. 25, no. 4, pp. 626–632, 2008.

[14] S. Perni, D. W. Liu, G. Shama, and M. G. Kong, "Cold Atmospheric Plasma Decontamination of the Pericarps of Fruit."

[15] A. S. Chiper, W. Chen, O. Mejlholm, P. Dalgaard, and E. Stamate, "Atmospheric pressure plasma produced inside a closed package by a dielectric barrier discharge in Ar/CO 2 for bacterial inactivation of biological samples," Plasma Sources Sci. Technol., vol. 20, no. 2, p. 025008, Apr. 2011.

[16] D. Ziuzina, S. Patil, P. J. Cullen, K. M. Keener, and P. Bourke, "Atmospheric cold plasma inactivation of Escherichia coli in liquid media inside a sealed package," J. Appl. Microbiol., vol. 114, no. 3, pp. 778–787, Mar. 2013.

[17] P. Muranyi, J. Wunderlich, and H.-C. Langowski, "Modification of bacterial structures by a low-temperature gas plasma and influence on packaging material," J. Appl. Microbiol., vol. 109, no. 6, pp. 1875–1885, Dec. 2010.

[18] K. Duske, L. Jablonowski, I. Koban, R. Matthes, B. Holtfreter, A. Sckell, J. B. Nebe, T. von Woedtke, K. D. Weltmann, and T. Kocher, "Cold atmospheric plasma in combination with mechanical treatment improves osteoblast growth on biofilm covered titanium discs," Biomaterials, vol. 52, pp. 327–334, 2015.

[19] C. Gabler, C. Zietz, R. Göhler, A. Fritsche, T. Lindner, M. Haenle, B. Finke, J. Meichsner, S. Lenz, B. Frerich, F. Lüthen, J. Nebe, and R. Bader, "Evaluation of Osseointegration of Titanium Alloyed Implants Modified by Plasma Polymerization," Int. J. Mol. Sci., vol. 15, no. 2, pp. 2454–2464, Feb. 2014.

[20] A. Liguori, A. Pollicino, A. Stancampiano, F. Tarterini, M. L. Focarete, V. Colombo, and M. Gherardi, "Deposition of Plasma-Polymerized Polyacrylic Acid Coatings by a Non-Equilibrium Atmospheric Pressure Nanopulsed Plasma Jet," Plasma Process. Polym., vol. 13, no. 3, pp. 375–386, 2016.

[21] F. Intranuovo, P. Favia, E. Sardella, C. Ingrosso, M. Nardulli, R. d'Agostino, and R. Gristina, "Osteoblast-Like Cell Behavior on Plasma Deposited Micro/Nanopatterned Coatings," Biomacromolecules, vol. 12, no. 2, pp. 380–387, Feb. 2011.

[22] G. Fridman, G. Friedman, A. Gutsol, A. B. Shekhter, V. N. Vasilets, and A. Fridman, "Applied plasma medicine," Plasma Process. Polym., vol. 5, no. 6, pp. 503–533, 2008.

[23] D. B. Graves, "Low temperature plasma biomedicine: A tutorial reviewa)," Phys. Plasmas, vol. 21, no. 8, p. 080901, Aug. 2014.

[24] T. von Woedtke, S. Reuter, K. Masur, and K.-D. Weltmann, "Plasmas for medicine," Phys. Rep., vol. 530, no. 4, pp. 291–320, Sep. 2013.

[25] D. B. Graves, "The emerging role of reactive oxygen and nitrogen species in redox biology and some implications for plasma applications to medicine and biology," J. Phys. D. Appl. Phys., vol. 45, no. 26, p. 263001, 2012.

[26] M. Vandamme, E. Robert, S. Lerondel, V. Sarron, D. Ries, S. Dozias, J. Sobilo, D. Gosset, C. Kieda, B. Legrain, J.-M. Pouvesle, and A. Le Pape, "ROS implication in a new antitumor strategy based on non thermal plasma.," Int. J. Cancer, 2011.

[27] J. Schlegel, J. Köritzer, and V. Boxhammer, "Plasma in cancer treatment," Clin. Plasma Med., vol. 1, no. 2, pp. 2–7, 2013.

[28] K.-D. Weltmann, M. Polak, K. Masur, T. von Woedtke, J. Winter, and S. Reuter, "Plasma Processes and Plasma Sources in Medicine," Contrib. to Plasma Phys., vol. 52, no. 7, pp. 644–654, Aug. 2012.

[29] M. G. Kong, G. Kroesen, G. Morfill, T. Nosenko, T. Shimizu, J. van Dijk, and J. L. Zimmermann, "Plasma medicine: an introductory review," New J. Phys., vol. 11, no. 11, p. 115012, 2009.

[30] F. Iza, G. J. Kim, S. M. Lee, J. K. Lee, J. L. Walsh, Y. T. Zhang, and M. G. Kong, "Microplasmas: Sources, particle kinetics, and biomedical applications," Plasma Process. Polym., vol. 5, no. 4, pp. 322–344, 2008.

[31] N. O'Connor, O. Cahill, S. Daniels, S. Galvin, and H. Humphreys, "Cold atmospheric pressure plasma and decontamination. Can it contribute to preventing hospital-acquired infections?," J. Hosp. Infect., vol. 88, no. 2, pp. 59–65, 2014.

[32] G. Collet, E. Robert, A. Lenoir, M. Vandamme, T. Darny, S. Dozias, C. Kieda, and J. M. Pouvesle, "Plasma jet-induced tissue oxygenation: potentialities for new therapeutic strategies," Plasma Sources Sci. Technol., vol. 23, no. 1, p. 012005, Feb. 2014.

[33] A. R. Gibson, H. O. McCarthy, A. A. Ali, D. O'Connell, and W. G. Graham, "Interactions of a Non-Thermal Atmospheric Pressure Plasma Effluent with PC-3 Prostate Cancer Cells," Plasma Process. Polym., vol. 11, no. 12, pp. 1142–1149, Dec. 2014.

[34] M. Keidar, "Plasma for cancer treatment," Plasma Sources Sci. Technol., vol. 24, no. 3, p. 033001, Jun. 2015.

[35] A. M. Hirst, M. S. Simms, V. M. Mann, N. J. Maitland, D. O'Connell, and F. M. Frame, "Low-temperature plasma treatment induces DNA damage leading to necrotic cell death in primary prostate epithelial cells," Br. J. Cancer, vol. 112, no. 9, pp. 1536–1545, Apr. 2015.

[36] N. Barekzi and M. Laroussi, "Dose-dependent killing of leukemia cells by low-temperature plasma," J. Phys. D. Appl. Phys., vol. 45, no. 42, p. 422002, Oct. 2012.

[37] S. Salehi, A. Shokri, M. R. Khani, M. Bigdeli, and B. Shokri, "Investigating effects of atmospheric-pressure plasma on the process of wound healing," Biointerphases, vol. 10, no. 2, p. 029504, Jun. 2015.

[38] V. N. Vasilets, A. Gutsol, A. B. Shekhter, and A. Fridman, "Plasma medicine," High Energy Chem., vol. 43, no. 3, pp. 229–233, May 2009.

[39] A. S. Wu, S. Kalghatgi, D. Dobrynin, R. Sensenig, E. Cerchar, E. Podolsky, E. Dulaimi, M. Paff, K. Wasko, K. P. Arjunan, K. Garcia, G. Fridman, M. Balasubramanian, R. Ownbey, K. A. Barbee, A. Fridman, G. Friedman, S. G. Joshi, and A. D. Brooks, "Porcine intact and wounded skin responses to atmospheric nonthermal plasma," J. Surg. Res., vol. 179, no. 1, pp. e1–e12, 2013.

[40] M. Boselli, V. Colombo, E. Ghedini, M. Gherardi, R. Laurita, a. Liguori, P. Sanibondi, and a. Stancampiano, "Schlieren high-speed imaging of a nanosecond pulsed atmospheric pressure non-equilibrium plasma jet," Plasma Chem. Plasma Process., vol. 34, no. 4, pp. 853–869, 2014.

[41] M. Boselli, V. Colombo, M. Gherardi, R. Laurita, A. Liguori, P. Sanibondi, E. Simoncelli, and A. Stancampiano, "Characterization of a Cold Atmospheric Pressure Plasma Jet Device Driven by Nanosecond Voltage Pulses," IEEE Trans. Plasma Sci., vol. 43, no. 3, pp. 713–725, 2015.

[42] J. W. Bradley, J. Oh, O. T. Olabanji, C. Hale, R. Mariani, and K. Kontis, "Schlieren Photography of the Outflow From a Plasma Jet," Trans. Plasma Sci., vol. 39, no. 11, pp. 2312–2313, 2011.

[43] E. Robert, V. Sarron, T. Darny, D. Riès, S. Dozias, J. Fontane, L. Joly, and J.-M. Pouvesle, "Rare gas flow structuration in plasma jet experiments," Plasma Sources Sci. Technol., vol. 23, no. 1, p. 012003, 2014.

[44] A. V Nastuta, I. Topala, and G. Popa, "ICCD Imaging of Atmospheric Pressure Plasma Jet Behavior in Different Electrode Configurations," vol. 39, no. 11, 2011.

[45] D. Maletić, N. Puač, N. Selaković, S. Lazović, G. Malović, A. Đorđević, and Z. L. Petrović, "Time-resolved optical emission imaging of an atmospheric plasma jet for different electrode

positions with a constant electrode gap," Plasma Sources Sci. Technol., vol. 24, no. 2, p. 025006, 2015.

[46] S. a Norberg, E. Johnsen, and M. J. Kushner, "Formation of reactive oxygen and nitrogen species by repetitive negatively pulsed helium atmospheric pressure plasma jets propagating into humid air," Plasma Sources Sci. Technol., vol. 24, no. 3, p. 035026, 2015.

[47] N. Y. Babaeva and M. J. Kushner, "Interaction of multiple atmospheric-pressure micro-plasma jets in small arrays: He/O 2 into humid air," Plasma Sources Sci. Technol., vol. 23, no. 1, p. 015007, 2014.

[48] S. Reuter, J. Winter, A. Schmidt-Bleker, H. Tresp, M. U. Hammer, and K. D. Weltmann, "Controlling the ambient air affected reactive species composition in the effluent of an argon plasma jet," IEEE Trans. Plasma Sci., vol. 40, no. 11 PART1, pp. 2788–2794, 2012.

CHAPTER 2
DIAGNOSTIC OF A PLASMA JET SOURCE EXPANDING IN OPEN AIR

2.1 Literature overview

The term "APPJ" (Atmospheric Pressure Plasma Jets) usually refers to a group of plasma sources comprehensive of a large number of different configurations (number of electrodes, gas channel geometry/length, etc…), driving voltage profiles (sinusoidal, square wave, DC, micro/nano pulsed) and working gas (He, Ar, air etc…) united by their characteristic ability to generate a plasma plume in the surrounding atmosphere [1]. The common characteristic that unite these sources is the distinguish ability to use a gas flow to generate a plasma plume in the surrounding atmosphere. The plasma plume can be generated over distance up to several tens of centimetres from the powered electrodes (contrarily to dielectric barrier discharges for example) allowing both radical and charged species to be delivered far away from the region where the discharge is originally ignited. This feature of APPJs results particular appealing for applications, like biological one, where an irregular or bulky substrates have to be treated. The great variety and versatility of APPJs has strongly boosted their study and adoption in biomedical applications and material processing in the last decade [2–17]. Many of these aspects of the APPJs will be analyzed through this dissertation. The aim of this part of the thesis is to present a general introduction on APPJs with an eye on the parameters and terminology that will be later used and analyzed more in detail in the following sections.

Nowadays the term APPJ is usually used to referee to cold plasmas, nevertheless in its more ample meaning it also includes thermal plasmas. From this point of view, the development of APPJ devices can be track down to more than 50 years ago. Already in the late '50s, arc based atmospheric pressure plasma jets were studied and proposed for propulsion purposes [18,19] and cutting applications [20]. In the following decades, fundamental studies were performed on these thermal jets and their possible applications. By the end of the '80s, huge efforts were made to transfer low-pressure plasma processes to atmospheric pressure conditions and thus get rid of expensive vacuum facilities. In the 1991, Lu *et al.* reported on successful diamond synthesis at atmospheric pressure by coalescing three DC jets with respective power input of 12 kW and a feed gas mixture of argon and hydrogen [21]. Up to that moment, apart from sporadic applications, thermal arc based plasmas were mostly used as heat sources instead of fully exploiting their plasma characteristic [22].

By the end of the '90s, new concepts emerged on how to generate plasma jets at atmospheric pressure without using transferred arcs. This was achieved by the use of pointed electrodes similar to those employed in corona discharges, the use of a dielectric material to cover at least one electrode, the miniaturization of the discharge region, discharge pulsing and the applications of alternating voltage signals [23,24]. Along with these alternative generation concepts, plasma properties changed as well. Thermal plasma jets operate in local thermal equilibrium (LTE), meaning that the electron temperature is equal to the temperature of heavy particles. Thus, high electron densities in the order of 10^{21} - 10^{26} m^{-3} are produced [25]. On the contrary, non-LTE plasma jets also named in literature as *cold* or *non-equilibrium*

plasma jets have a heavy particle temperature in the range of 300–500 K, which is at least one order of magnitude lower than the electron temperature. Electron densities are typically below 10^{19} m^{-3} in non-LTE plasma jets [25]. The presence of atmospheric pressure plasma jets operated in open air at moderate gas temperatures, but nevertheless with high plasma-chemical activity, triggered a multiplicity of interesting applications. Nowadays, non-equilibrium APPJs are regarded as promising tools for a wide and constantly expanding range of applications. In the following an overview on APPJs applications that can be found in the literature is given. Although knowing that completeness in this list is by far not achievable, the selection aims to give the reader an overview of the APPJs possibilities and versatility. For every APPJs application, one or more references will be provided where more details and further information on the specific application could be found.

- Wound healing [26,27]
- Bacteria inactivation [6,11] [PAPER IV and VII]
- Thin film deposition [15,28]
- Dentistry [14,29]
- Anticancer therapy [30] [PAPER VI]
- Removal of environmental pollutants [31]
- Combustion assistances [32–34]
- Surface modification [35,36]
- Inactivation of biofilm [37] [PAPER VII]
- Yeast inactivation [38]

Driven by encouraging results and the desire to understand and optimize the aforementioned processes, the past decade has witnessed strong research efforts on various atmospheric pressure plasma jets. As reported in a review from Weltmann *et al.* [39] between the years 2003 and 2014 the annual publication number increased more than tenfold, from 15 to 211 publications per year. During this period, many studies have also been devoted to the understanding of the physical mechanisms involved in plasma jet sources. A particular attention in APPJs characterization has been dedicated to the ignition mechanism of the discharge. As it will be later discussed more in details, plasma jet does not generate continuous plasma, but the discharge is actually driven by the propagation of an ionization wave which then forms a partially ionized gas channel called streamer [40,41]. The phenomenological description of the ionization wave propagation in APPJs, firstly named *plasma bullet* [42,43] and more recently PAPS (Pulsed Atmospheric-pressure Plasma Streamer) [44,45], has been the subject of extensive research in the last decade. A brief overview of the formation of PAPS will be presented prior to discuss APPJs possible architectures.

Ionization waves can have various spatial structures. The most common type of ionization wave in atmospheric pressure plasma is the streamer, a growing plasma channel with a head typically of spherical form. The concept of streamers was formulated in the '60-'70s by Loeb, Raether and Meek [46–48] and a detailed description of streamers in atmospheric air can be found in the work by Raizer [49]. The streamer channel radius is usually of several hundreds of micrometers in atmospheric pressure gases and may assume an annular front in the case of cold plasma jets [50]. In propagating ionization waves, charged species (electrons and ions) are produced in localized regions of enhanced electric field, like the wave front, due to ionization of atoms and molecules of the medium by electron impact [50]. The value of the enhanced electric field in the front region is governed by the density of volumetric electric charge formed by the wave itself and can greatly exceed the local applied electric field. The property of ionization waves to produce strong electric fields in their fronts, capable to ionize medium, allows their penetration into low-electric field region. Being formed in the region of strong applied electric field, streamers propagate to the opposite electrode, forming conductive channels.

Depending on the direction of propagation, streamers are called *positive* (or *cathode directed*) and *negative* (or *anode directed*) streamers. These two streamer mechanisms, extracted from the original work of Raizer [49]

are illustrated in Figure 2.1 and 2.2. In his work, Raizer affirms that the formation of a streamer requires an electron avalanche at the head of the streamer itself as shown in Figure 2.2. The electron avalanche is produced by the repulsion of electrons from the negative voltage applied to the cathode (true for both type of streamers). In the case of positive streamer, seed electrons ahead of the streamer front are produced due to ionization of medium species by energetic photons emitted from the excited atoms in the primary avalanche, a region of strong electric field. These electrons moving to the head of the streamer generate secondary avalanches that are pulled into the trail due to the direction of the local electric field. Secondary avalanches ions enhance the positive space charge at the cathode end of the evolving plasma channel enhancing the electric field ahead of its front. In this way the streamers grow toward the cathode. Figure 2.1. For negative streamers if the field and gap between the electrodes is large enough the avalanche will transition to anode directed streamer (Figure 2.2). The mechanisms of propagation towards the anode are different than those in the positive streamers because in this case the drift of electrons has the same direction as the streamer front. The electrons at the streamer front join the ionic trails of secondary avalanches initiated by photoionization and together form the plasma.

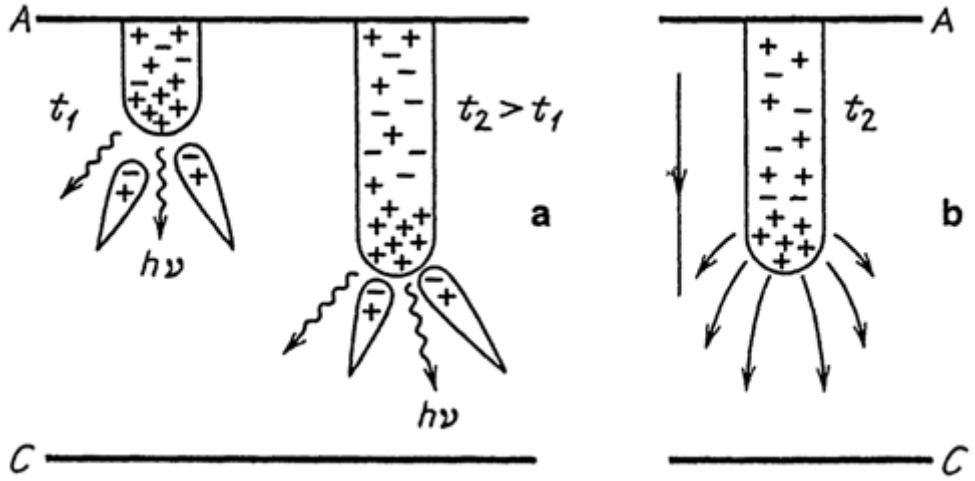

Figure 2.1 Cathode-directed streamer. (a) Streamer at two consecutive moments of time, with secondary avalanches moving towards the positive head of the streamer; wavy arrows are photons that generate seed electrons for avalanches. (b) Lines of force of the field near the streamer head [49].

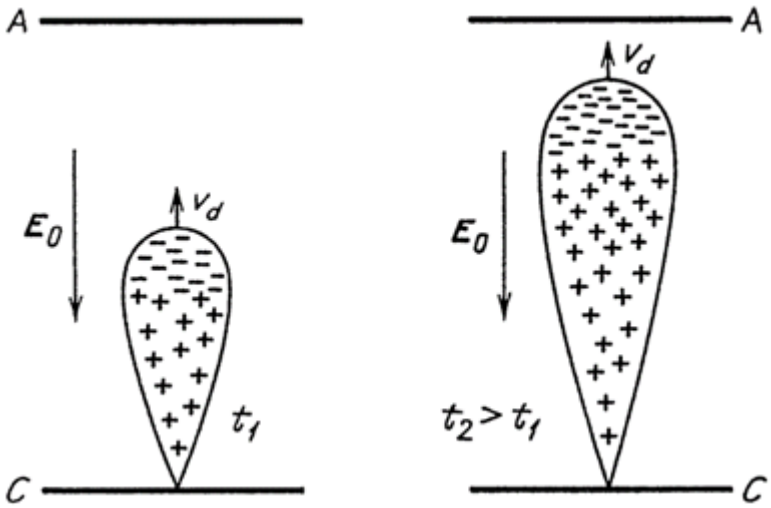

Figure 2.2 Shape and charge distribution of an electron avalanche at two consecutive moments of time. Arrows indicate direction of external electric field E_0 and avalanche head velocity v_d [49].

In nature, and in most laboratory experiments, the propagation of ionization waves has no preferential direction. However, it is possible to arrange conditions such as that ionization waves move along a predetermined path. A specific form of ionization waves, named *guided ionization wave* or *guided streamer*, has been discovered recently in experiments with atmospheric-pressure plasma jets (APPJs) formed by DBD discharges in noble gas flows (usually He or Ar) in thin dielectric tubes and injected into ambient air [42,43,50].
In plasma technology the term *plasma jet* is used to refer to many different configurations and types of plasmas, having in common that the gas discharge is operated in an open volume electrodes arrangement and plasma is projected outside the electrode arrangement into the environment. The expansion of the plasma is often due to a high flow of a working gas, usually a noble gas, flown through a capillary before expansion into ambient air, where it forms a channel, also named plume, surrounded by air. In APPJs, the *guided* aspect results from local differences in the required E/N (electric field/gas number density) for avalanche being lower in the noble gas dominated plume than in the surrounding air. The ionization front is then prevented from spreading laterally into air and remains in the rare-gas channel. From this *guiding* of the ionization wave along the noble gas channel, the term *guided ionization wave* or *guided streamer* was coined. The speed of the front has been measured in several studies at about $10^5 – 10^8$ cm/s [1,51,52] [PAPER II and III]. In contrast to streamers in a free space that propagate in a stochastic manner and often branch, guided ionization waves are repetitive and highly reproducible and propagate along the same path (usually the jet axis). This property of guided streamers, in comparison with streamers in a free space, enables many advanced time resolved experimental studies of ionization waves with nanosecond precision. This has prompt the study of this typology of sources in last years as testified by the large number of publication on the subject found in literature [1,50] [PAPER II and III].
The dynamics of the plasma bullets involves two stages. At the first stage, ionization waves formed in strong field regions inside dielectric tubes move along the tube walls similarly to streamers observed in surface barrier discharges [50]. After leaving the tube, plasma bullets propagate inside the plume in a mixture of a noble gas with ambient air. At both stages, the plasma volume moves along a predetermined path, the jet axis, as a guided ionization wave [50]. As the plasma produced ions, electrons and excited species interact with ambient air, other RONS are generated. The RONS produced in this manner are believed to be the main agents in biomedical applications including atomic oxygen (O), hydroxyl radicals (OH), ozone (O_3), hydrogen peroxide (H_2O_2) and nitric oxide (NO) [53].

Many different APPJ architectures have been designed and presented, ranging from single electrode sources [PAPER I, II, III] to DBD jet [44,45] through more exotic configurations like *multijet* arrays [PAPER IV] and multielectrode DBD jets [54]. The control of plasma parameters and properties is still a key challenge for the emerging applications of these plasma sources. While the general mechanisms of plasma jet generation are understood, there still is a lack of knowledge on the basic plasma parameters for most of the APPJs. This is due to the discharge having a small size and a transient behaviour, which makes them very challenging objects for plasma diagnostics.
Diagnostic investigation is crucial to achieve a complete control over plasma generation of reactive species and their delivery. Because of the complexity of plasma interaction with biological and thermo-sensitive materials, diagnostic analysis is strongly required to evaluate process feasibility and to develop plasma sources optimized for specific applications. Integrated approaches relying not only on the effectiveness of the plasma treatment, but also the characterization of plasma sources, are required in order to promote a multi-step optimization of the process.
Particular attention in APPJs characterization has been dedicated to discharge structure since the first works reporting on the observation of "plasma bullets" [42,43], whose fundamental aspects have been strongly debated within the international scientific community and now mostly discarded in favour of a new theory recently introduced along with a new nomenclature, "pulsed atmospheric-pressure plasma streams" (PAPS) [44,45]. Another important aspect that is being more and more addressed is the study of the fluid-dynamic behaviour of the jet effluent, as it strongly affects the structure and propagation of the plasma discharge. For this purpose, among the principal tools that have been adopted are numerical

simulations [45] and Schlieren photography [55,56] [PAPER I and II], occasionally in combination with each other [45].
In the next paragraphs of this chapter the results concerning the characterization of a single electrode plasma jet will be presented. The presented results were achieved with both standard diagnostic techniques (such as low speed imaging) and more complex diagnostic setups like high speed Schlieren imaging and ICCD camera with sub-nanosecond synchronisation. These results, presented at international conferences and published in two papers on international journals, have received good response from the plasma scientific community and contributed in their way to expand our knowledge on APPJ.

2.2 Atmospheric pressure plasma jet source architectures

Many different plasma jet arrangements exist and many different classifications can be done according to various parameters like discharge geometry, electrode arrangement, field configuration, excitation frequency, type of gas and other. A comprehensive collection of nearly all possible APPJ arrangements was given by Lu, Laroussi and Puech in 2012 [1] and recently recalled and updated by Weltmann *et al.* in another review in 2015 [39]. The original classification is still up to date and many of the recently developed APPJ devices can be tracked down to the main group there defined. In light of the work that will be presented in this dissertation these classification will be shortly presented with an eye on the architecture that include the plasma jet sources investigated during my Ph.D.
A very wide and common category of plasma jets is falls under the name of *DBD jets*. As shown in Figure 2.3 various different configurations are possible. The common feature of this category is the DBD architecture [57,58] which requires the presence of a dielectric barrier interposed between the high voltage electrode and the grounded electrode or the target. The geometry of the electrodes can greatly vary but usually ring or pin electrode geometries are adopted.
All these configuration can be operated either by kHz AC excitation or by pulsed DC excitation and the length of the plasma jet can easily reach several centimeters [52]. This characteristic makes the operation of these plasma jets easy and practical. Moreover, due to the low power delivered to the plasma, the gas temperature of the plasma remains close to room temperature. Another important advantage is the use of a dielectric that prevents the risk of arcing whether the object to be treated is placed far away or close to the nozzle. Both these two characteristic are very important for medical application, where safety is a strict requirement.

A second group of APPJs, presented in Figure 2.4, is those of the *DBD-like* plasma jets. When the plasma is not in contact with any object, the discharge works more or less like in a DBD jet. However, when the plasma plume is impinging on a target, the discharge may run directly between the high voltage electrode and the target to treat. For this reason, the risk of arcing should be carefully avoided. On the other hand, this architecture demonstrated the ability to produce plasma plumes of several tens of centimeters (up to meters) in length inside dielectric capillaries. Therefore, as long as arcing is carefully avoided, the DBD-like jets have some advantages. In fact, the number of papers on medical application of DBD-like plasma sources is steadily increasing [27,59]. The *Plasma Gun* jet source that will be described in detail in the following paragraph (Paragraph 2.2.1) and that has been designed for endodontic medical treatments (Chapter 4) falls into this group.

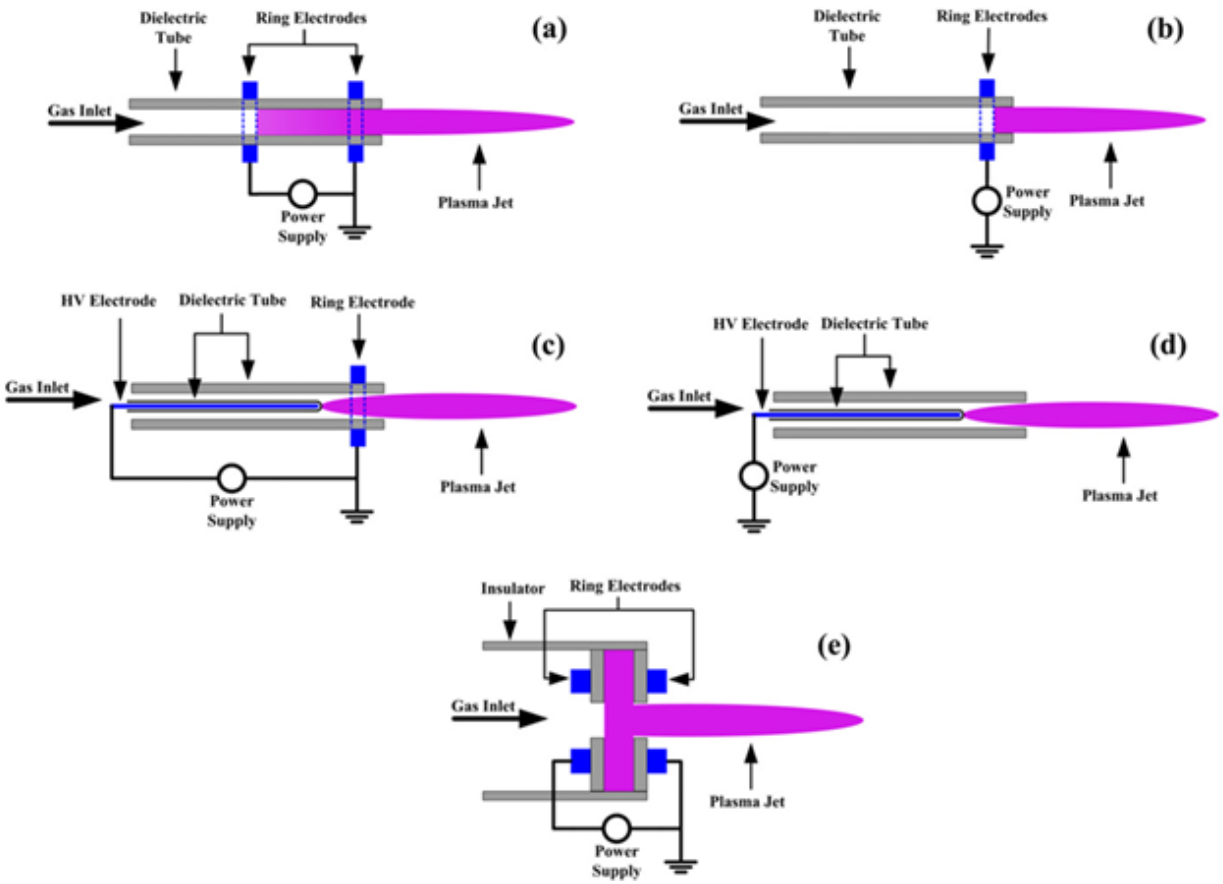

Figure 2.3 Schematic of DBD plasma jets [1]

The last group of APPJs that will be here reported is the single electrode jets, represented schematically in Figure 2.5. In this configuration, the dielectric tube only plays the role of guiding the gas flow. These sources usually can be driven by DC, kHz AC, RF or pulsed DC power. To avoid the risk of arcing and make it suitable also for the treatment of thermosensitive materials and medical applications, several solutions may be implemented in this configuration. One example is represented in Figure 2.5c, where a capacitance and a resistance have been used to control and limit the discharge current and voltage on the high voltage electrode. Another solution is the adoption of extremely short excitation pulses (few tens of nanosecond) as in the case of the *Plasma Jet* that will be presented in detail in Paragraph 2.2.1 and that has been extensively characterized by means of several diagnostics during my Ph.D. [PAPER I, II, III].

A new group of APPJs that is raising interest in the scientific community and that was not originally included in the classification are the so called *multijets* or *jets-array* [60–63] [PAPER IV]. These sources are based on an array of multiple plasma jets sources. Ideally developed for the treatment of large planar surfaces [64–66] and 3-D objects even with complex geometry [67–71], they have shown characteristics far more complex and interesting than being simply the sum of the single jets. While partially overcoming the limitation of classical single plasma jets, the scaling of plasma jet arrays has presented a unique challenge due to the tendency of individual plasma jets to interact with each other, which can lead to the merging of some jets when posed in close proximity and in the right conditions. This phenomenon, usually referred to as *jet-to-jet coupling,* has also been shown to be able to generate plasma plumes with unique characteristics [72–74] that may open new field of applications.

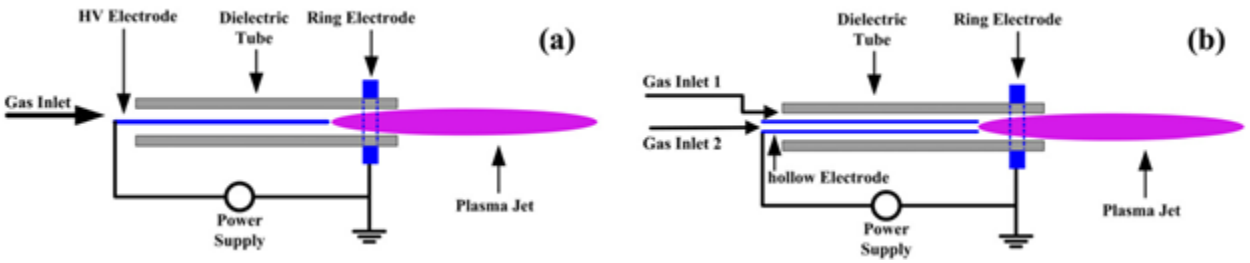

Figure 2.4 Schematic of DBD-like plasma jets [1]

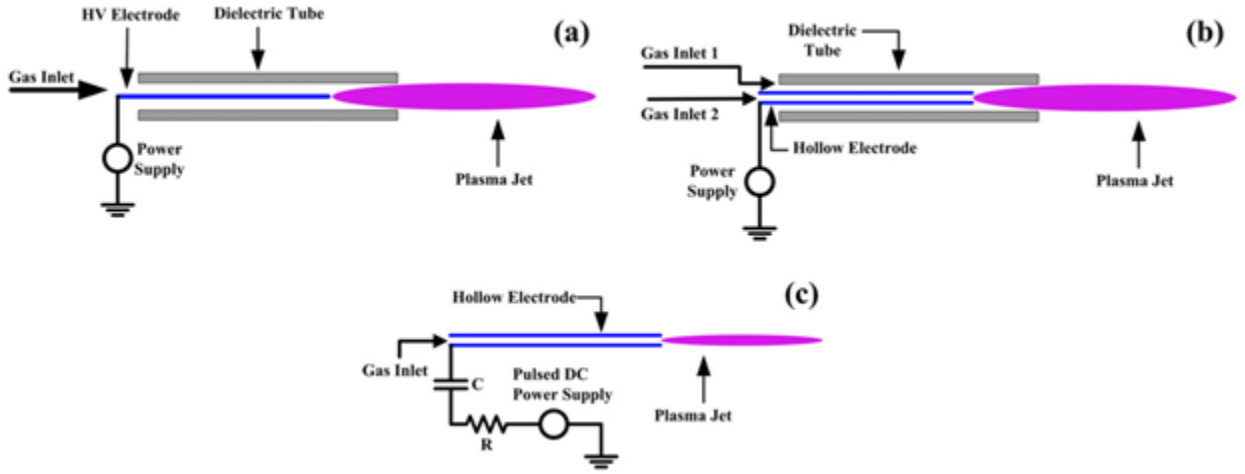

Figure 2.5 Schematic of single electrode plasma jets [1]

Nevertheless, to take full advantage of this jet-to-jet coupling behavior in the development of new plasma sources, increasing our understanding of the phenomenon is of the most importance. While extensive studies and considerable advances have been made with individual plasma jets [52,75–80] [PAPER I, II and III], *multijet* arrays are far less studied although the number of work on the subject is rapidly increasing [63,65,67,73,74,81–84][PAPER IV]. During my Ph.D., I have spent a fair amount of time investigating a *multijet* plasma source named *Gatling Gun* for its reminding in shape of a Gatling machine gun. An initial characterization of the plasma source and the occurrence of the jet-to-jet coupling phenomenon and its potential application can be found in PAPER IV.

This brief description of the most common APPJ architectures is inevitably not exhaustive and many configurations have been left outside (multi electrodes jets [54], dielectric free electrode DFE jets [85,86], etc…). The APPJ field is in rapid expansion and many new architectures are created even in this moment in different labs around the world. As reported APPJs have a broad range of possible configurations and this lead to a difficulty in comparing different devices and their performances. A proper characterization of the plasma should be done whenever a new plasma device is developed. This was exactly one of the aims my Ph.D. as I focused on the characterization of a new design single electrode APPJ called *Plasma Jet*. In the following sections of this chapter this plasma source will be described in detail along with some results of its intensive characterization by means of several diagnostic techniques.

2.2.1 Plasma Jet

The plasma source here described is a single electrode plasma jet developed in the laboratory of the IAP group at Alma Mater Studiorum - Università di Bologna by Colombo *et al.* and described in several published works [87] [PAPER I, II, III]. The characterization of this particular source was one of the main topics of my research and it was investigated in depth with several diagnostic techniques in many different operating conditions. A general schematic of the source is presented in Figure 2.6. The plasma source consists of a high-voltage electrode (a stainless steel sharpened metallic needle with a diameter of 0.3 mm) centered inside a dielectric channel. In this source, a primary working gas (usually He or Ar) is injected through a 12-hole (0.3 mm diameter) diffuser aimed at ensuring a uniform and laminar flow along the electrode and at sustaining the plasma discharge, while the secondary gas is introduced in the discharge region downstream the electrode tip through twelve 0.3 mm holes, tilted with respect to the plasma source axis. The plasma is ejected from the source into the surrounding atmosphere through a 1 mm orifice. The plasma source has been mostly investigated when driven by a commercial pulse generator (FPG 20–1NMK, FID GmbH) producing high-voltage pulses with nanosecond rise time but other driving power supply like sinusoidal or DC may be adopted. Is worth mentioning that ionization waves generated by nanosecond pulses have recently attracted interest due to their emerging applications in plasma-assisted combustion, high-speed flow control and plasma assisted film deposition [16,88–90]. As mentioned in the previous paragraph, this source falls in the group of the single electrode APPJs. A peculiarity of this source is the possibility to use two distinct gas flows in the primary and secondary channel according with specific applications. In fact, the versatility of this source is confirmed by the variety of applications it has been used for, including thin film deposition [16], treatment of polymeric solutions [87], co-deposition of acrylic acid and nanoparticles [15].

.

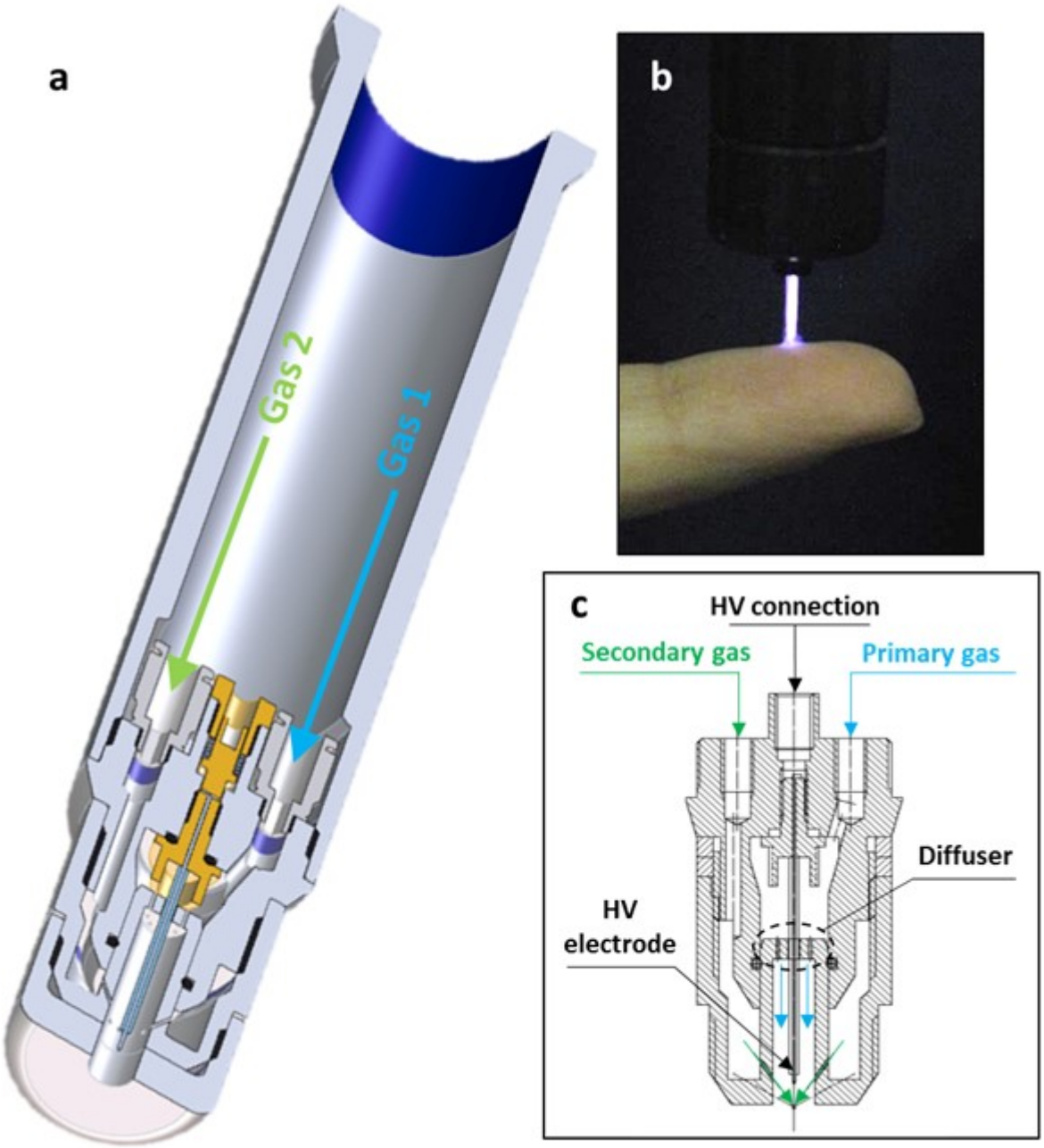

Figure 2.6 Schematics (a,c) and picture (b) of the *Plasma Jet* device developed at the Alma Mater Studiorum - Università di Bologna

2.2.2 Plasma Gun

This plasma source, here referred to as *Plasma Gun,* is a DBD-like plasma jet developed in the laboratory of the IAP group at Università di Bologna and specifically designed for dental applications [14]. During my Ph.D. research, I was involved in the development of this particular plasma source and, as it will be later reported in Chapter 4, I had the opportunity to test this APPJ source to investigate the feasibility of its use in dental applications.
A schematic of the source is shown in Figure 2.7. As high-voltage (HV) electrode, a 50mm long tungsten wire having a 1 mm diameter is used; the wire is positioned on the axis of a borosilicate glass capillary (4 and 6 mm of inner and outer diameter, respectively) having a relative dielectric constant $\varepsilon_r = 7$. A PTFE support is used to guarantee the coaxial geometry of the HV wire and the borosilicate glass capillary, while it is also machined to provide the inlet for the gas injection. As grounded electrode, a 40mm width aluminum foil was wrapped outside the dielectric capillary. In order to make the PG suitable for endodontic applications, the borosilicate glass capillary terminates with a 25mm long section characterized by an inclination of 75° and a tapered orifice (inner diameter of 2 mm), resembling in shape typical endodontic instruments. As working gas, 99.999% pure He is introduced for sustaining and propagating the plasma; a plasma plume is produced downstream the source orifice, where the mixing of He plasma with the surrounding ambient air occurs. The plasma source is usually driven by a micropulsed generator producing high-voltage sinusoidal pulses having a peak voltage (PV) of 7–18 kV, frequency (f)of 20–50 kHz, variable pulse duration (around 700 ms at the lowest duty cycle (DC) of 7%) and fixed pulsed repetition frequency (PRF) of 100 Hz.

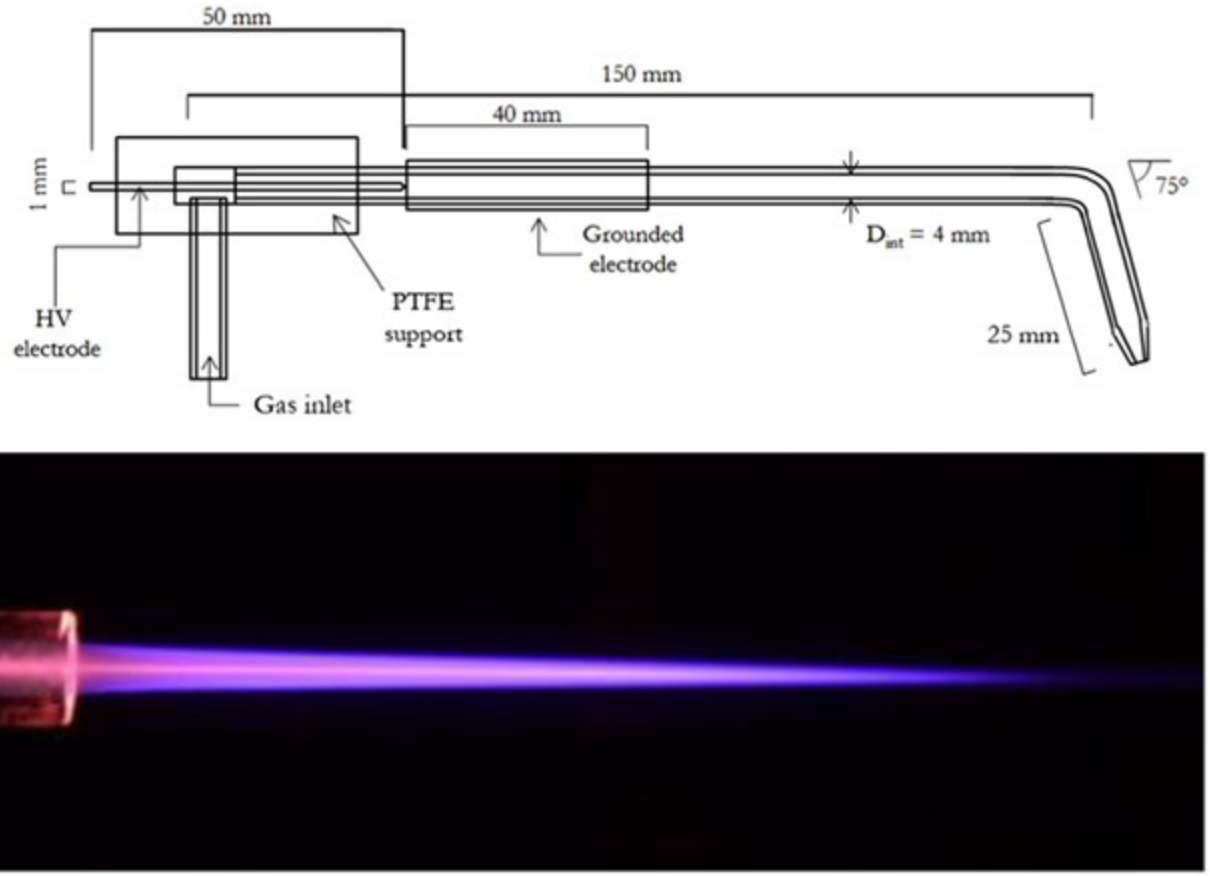

Figure 2.7 Schematic and picture of the *Plasma Gun* plasma source developed at the Alma Mater Studiorum - Università di Bologna [14]

2.3 Conventional diagnostic techniques

The characteristics of APPJs expanding freely in the surrounding atmosphere have been extensively investigated and many relevant parameters such as electron density, electric field, gas temperature, fluid dynamics as well as the reactive species produced by APPJs plasmas, whether metastables, radicals or molecules, have been measured for several different APPJ configurations [1,50].
During my Ph.D. research I had the opportunity to learn and adopt several diagnostic techniques including ICCD imaging, Schlieren, High Speed Imaging, Optical Emission Spectroscopy, FTIR, mass spectroscopy analysis and many other. Due to time and space limitation, only the results concerning the characterization of the single electrode source *Plasma Jet* (described in Paragraph 2.2.1) will be here presented.

To the human eye plasma plumes of most common APPJs are perceived as a continuous stationary glow discharge. In reality, the plasma plumes are made of small and fast moving PAPS that cannot be discerned as individual object by the eye. Because the PAPSs propagate with a speed of $\sim 10^5$–10^8 cm s^{-1} [1,50], to characterize such rapid propagation behavior, diagnostics methods with high temporal and spatial resolution are needed. Nevertheless, these diagnostics usually are quite sophisticated and the configuration of the proper set-up may result particularly time-demanding. Consequently, especially in the earlier stages of the characterization of new plasma devices, more common and ready to use diagnostics are usually adopted, which, while being limited in time and space resolution and sensitivity, they may become a powerful tool if properly implemented. The first example here presented is the adoption of standard photographic cameras for the visualization of APPJs plumes. This imaging technique, usually referred to as *low speed imaging*, has been adopted in several papers for the characterization of different plasma devices [91–95]. The optical emission intensity of the plasma is usually very low. This makes it necessary to adopt considerably long exposure times when using conventional cameras and collect the emission of multiple plasma discharges. The limit of this technique is that the acquisition of long exposure time images of the plasma plume does not allow discerning the propagation of a single ionization front.
Nevertheless, standard cameras allow visualizing the average behavior of the plasma plume and are commonly adopted to compare different operating conditions. As an example, in Figure 2.8 is reported a picture from a work of Yamamoto and coworkers [95]. In the paper a standard imaging technique is efficiently used to compare the lengths of plasma plumes generated using the same APPJ driven by different power supplies. Another good example may be found in the work of Kushner *et al.* [93] where very interesting pictures of a plasma plume impinging and transferring into a dielectric channel are directly compared to simulation results.
In line with the literature, a first characterization of the *Plasma Jet* was performed by means of a standard photographic camera. Different working gases where investigated, as shown in Figure 2.9 where Ar and He plumes produced in the same operating conditions are directly compared. It is easy to observe the substantial differences both in terms of length and radial diffusion between the two gases. As it will be discussed more in detail in the following paragraph, these differences may be, at least in part, attributed to the different fluid dynamic behavior characterizing the two gas flows. As reported in PAPER I and II the Reynolds number at the outlet of the jet for the He case may be estimated to be about 500, while for the Ar case it results to be approximately 5000. According to Ungate *et al.* [96] the Reynolds number for the He case falls inside a transition range (between 500 and 1000) in which the jet becomes unstable at a certain distance from the nozzle while in the Ar case a nearly completely turbulent flow should be established already at the nozzle outlet, in agreement with what observed in the picture.

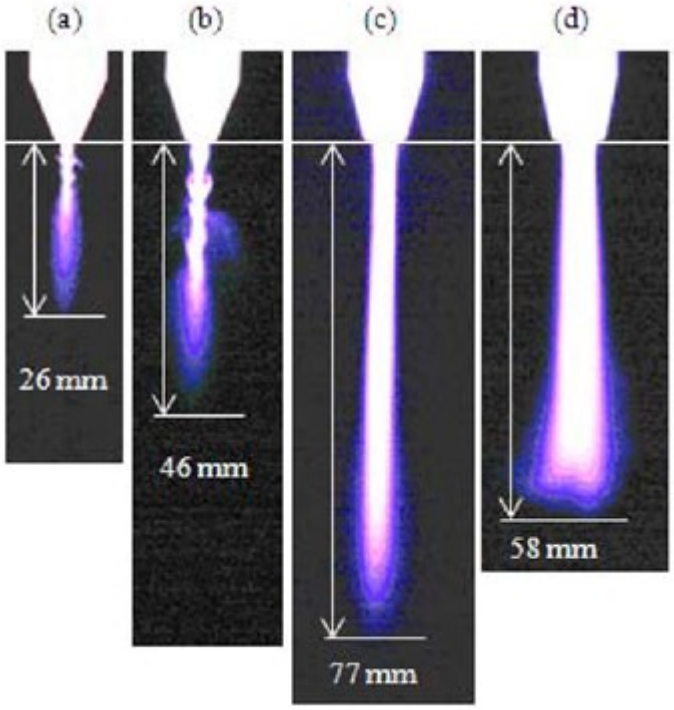

Figure 2.8 Evaluation of plasma emission length for different nozzle configurations [95]

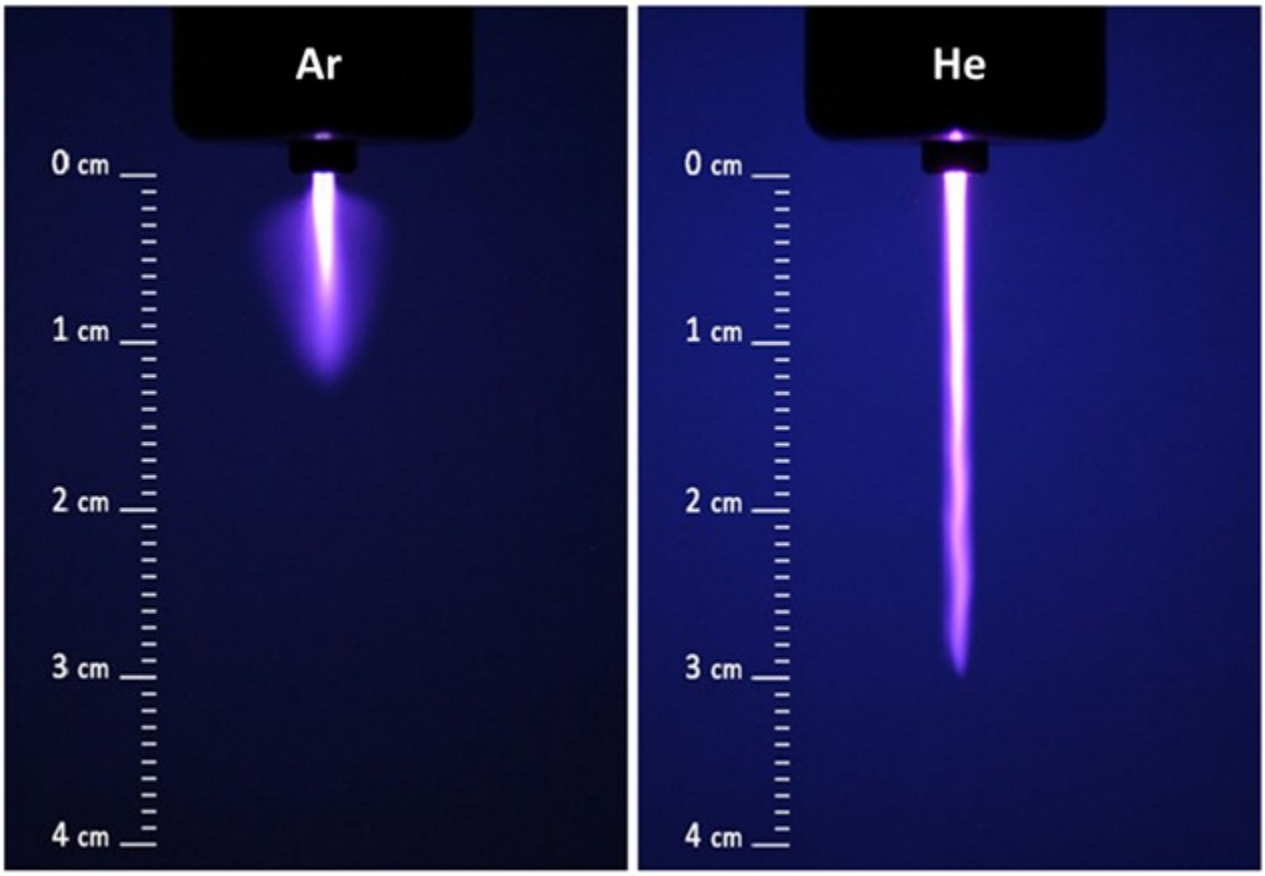

Figure 2.9 Low speed imaging of the *Plasma Jet* operating in Ar and He. PV =17 kV, PRF=1 kHz and mass flow rate = 3 slpm [PAPER I]

A parametrical investigation on the flow rate influence on the plasma plume length and morphology was effectuated for the case with He and is briefly resumed in PAPER I. It was reported how an increase from 1 to 3 He slpm (Re 170 and 500 respectively) causes a length increase in the plasma plume, whereas a further increase up to 5 slpm (Re 1000) results in a turbulent behavior of the plume, due to the increased shear force between the high velocity jet and the surrounding stagnant air, that leads to a shortening of the visible plasma plume. This evident strong correlation between the fluid dynamic regime at the outlet of the jet source and the discharge propagation length triggered the investigation of the phenomenon by means of a combination of ICCD and Schlieren imaging [PAPER I and II]. These results will be later presented in this same chapter. Another relatively common technique adopted for the characterization of APPJs is the use of temperature probes to measure the effluent gas global temperature. Nevertheless, due to the conductive nature of the plasma and the fact that most common thermocouples are made of metallic material, also for this relatively easy measurement special precautions have to be taken. The adoption of a metallic thermocouple would in fact introduce another conductive electrode in the plasma source electrical system, therefore interfering with the plasma discharge. To avoid this possibility, during my research I have adopted a fiber optic temperature sensor completely made of dielectric material. Fiber optic sensors were chosen for measurements also because they are immune from electromagnetic interferences possibly generated by the discharge [97] and they only slightly affect the discharge because of the small diameter and the dielectric properties of the sensor head. An example of the axial temperature profiles acquired with this method is presented in Figure 10, while a complete description of the experimental setup can be found in PAPER II. The study demonstrated the relevant influence of flow rate and peak repetition frequency on the gas macroscopic maximum temperature and profile. Higher flow rate in fact induced a flattening of the axial temperature profile that instead resulted much higher in proximity of the nozzle for smaller gas flow rates. The main purpose of this part of the study [ARTICE II] was a preliminary investigation of the feasibility to operate the source for biomedical applications. For these applications a temperature lower of 40 °C is preferable in order to avoid any possible thermal damage to the cells. As demonstrated in PAPER II the choice of the right operating conditions plays an important role in the fulfillment of this requirement as an increase of the PRF or a reduction of the flow rate may induce a critical increase in the effluent temperature.

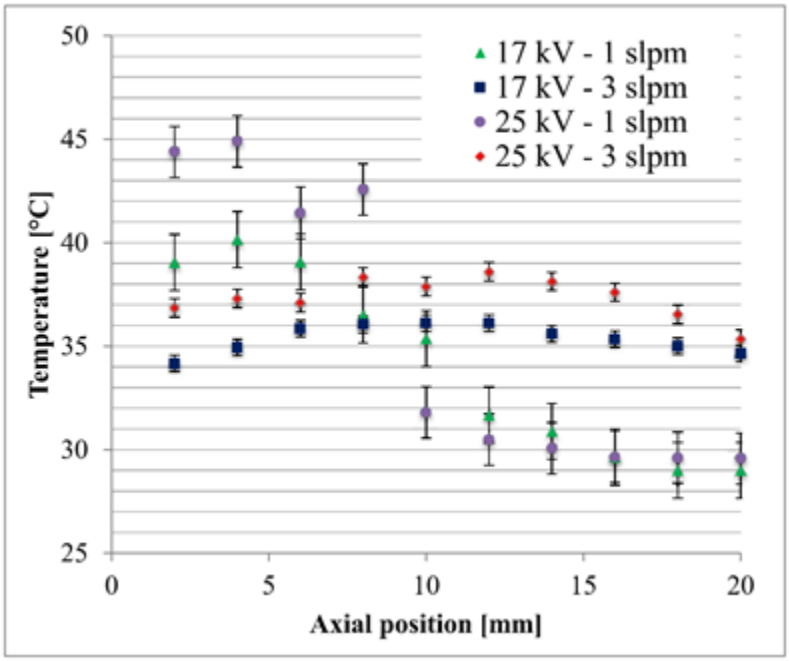

Figure 2.10 Axial temperature profile of the *Plasma Jet* at constant PRF (1 kHz) for different values of PV (17 and 25 kV) and He flow rate (1 and 3 SLPM). Room temperature during measurements: around 29 °C. Axial position = 0 mm corresponds to the source outlet. [PAPER II]

2.4 ICCD imaging for time resolved analysis of plasma structure

Over the past decade, the use of ICCD cameras as a means for characterizing CAP has been steadily increasing. Due to their high sensitivity and high speed gateability, ICCD cameras enable time-resolved studies of the anatomy and time-resolved investigation of physical and chemical properties of non-equilibrium plasma discharges. During my Ph.D, I had the opportunity to use an ICCD camera (Princeton Instruments PIMAX3, spectral response 180–900 nm, Filmless Gen III intensifiers). I adopted this powerful tool to investigate several plasma sources, ranging from large area DBDs to APPJs, including micro plasma sources and in water discharges. Anyway, in this dissertation I will present mainly the results concerning the ICCD characterization of the Plasma Jet source, as this was one of the first sources I worked on and that I continued investigating during all my Ph.D. The results presented in PAPER II and III and those still unpublished reported in Chapter 3 very well show the temporal evolution of my research and experience for what concern the use of ICCD imaging for plasma diagnostic. In this paragraph, the content of PAPER I, II and III will be summarised in order to better introduce the inedited results presented in Chapter 3.

As mentioned above, plasma bullets propagate at very high speed. The total propagating distance is typically about several centimeters. Thus the propagating time could be as short as of the order of hundreds ns. In the meantime, the optical emission intensity of the plasma is low. Thus, in order to capture the temporal dynamics of the plasma bullets, high speed intensified charge coupled device (ICCD) cameras are normally used.
A charge coupled device (CCD) is a semiconductor architecture whose operation is based on the movement of electrical charge through storage areas until the area where manipulation with the collected charge can be performed. The three basic functions of the device are: charge collection, charge transfer and conversion of collected charge into a measurable parameter (usually voltage). The initial concept of operation of CCD devices was given by Boyle and Smith [98]. When an image intensifier is mounted in front of the CCD this makes an intensified charge coupled device (ICCD). An ICCD consists of photocathode, microchannel plate (MCP) and phosphor screen. The image intensifier can be connected to the CCD either by a fiberoptic bundle or a relay lens. The sensitivity of the ICCD camera is mainly determined by the photocathode responsivity. Nowadays, photocathodes of GenII (multialkali photocathode) and GenIII (GaAs photocathode) are used in most of the ICCD cameras. The main advantage of ICCD cameras, beside high sensitivity, is high speed gateability. Due to their construction, ICCD cameras can enable shutter times of the order of picoseconds.

ICCD cameras have been relied on extensively for the investigation of plasma jets and several characteristics of plasma jets have been discovered using this technology; as an example, plasma jets seen as a continuous plasma flow by the human eye were recently revealed, by means of fast imaging systems, to be often composed of the sequences of fast moving discrete luminous clusters also known either as pulsed atmospheric pressure streamers (PAPS) or plasma 'bullets'. Photographs captured by high speed cameras can give us two-dimensional (2D) distributions of the optical emission intensity at any given time. As a consequence of these features and their versatility, over the past decade ICCD cameras have become a standard tool in diagnostics of non-equilibrium discharges, especially at atmospheric pressure where small dimensions and fast developing phenomena can impede other diagnostic techniques. Our ability to do so critically depends on the characteristics of the adopted ICCD cameras, among which the time resolution, that is required to match the speed of the observed phenomenon (e.g. propagation speed of PAPS), and the dynamic range, that has to be large enough to record the entire plasma discharge at once; this is especially relevant for the case of plasma jets, typically characterized by a brighter region (PAPS head) as well as a weaker continuous region behind the ionization front [44,45].

ICCD cameras with down to nanosecond expositions were adopted to record PAPS speeds by using freeze frame detection and careful triggering at numerous points during the phase between subsequent plasma formations (repeating voltage pulses or high frequency sinusoidal field). An example of this kind

of analysis is presented in Figure 2.11 from PAPER II were a sequence of representative ICCD frame showing the PAPS evolution is presented. This sequence allowed to estimate the average ionization front velocity in the order of 10^8 cm/s. This velocity may be considered quite high for PAPS generated by APPJs and is usually a characteristic of plasma jets sources driven by voltage pulses with nanosecond rise time [44,92,99].

The appearance of the ionization front 5 ns after the start of the voltage rise, which corresponds to a voltage in the range 5–10 kV, is visible in Figure 2.11. After this instant, the PAPS can be observed in all the subsequent frames. Nevertheless, its intensity and extension seem to fluctuate during the high-voltage pulse. For example, from the frame starting at 5 ns to the one at 9.75 ns, both the intensity and the length of the plasma plume increase up to a maximum reached at 6.75 ns and then they start to decrease. A similar behavior can be observed every 5 ns: from 10 to 15 ns, from 15 to 20 ns, and from 20 to 25 ns. To the best of my knowledge, this fluctuating behavior had never been reported in other study in the literature. Considering only the brightest frame in each fluctuation (6.75, 11.75, 16.75, and 21.75 ns), a progressive elongation of the plasma plume is clearly visible. As it can be observed in the frames reported in Fig. 11 with a chromatic scale modified to enhance the light emissions with lower intensity, the propagating plasma front remains connected to the plasma source by a visible channel even in the frames in which the plasma plume is characterized by weaker intensity. This structure characterized by a moving front connected to the source, similar to that reported in literature for other plasma jet sources and is usually referred to as PAPS [44,100,101].

In PAPER II two different operating conditions were investigated through ICCD imaging. The second set of operating condition presented a higher peak voltage and flow rate. The second case presented a fluctuation of both the intensity and the length of the plasma plume with a period (5 ns) similar to that observed in the first case. Nevertheless, the structure of the plasma evolves in a sensibly different way. While in the first case (Figure 2.11), only one front can be observed in the plasma jet, in the second case, the final part of the plasma jet resulted at first distorted and then branched in several fronts connected to the plasma source by converging tails characterized by weaker emission. A similar behavior of the plasma front has been observed in [102] and described as snake-like mode. This aspect, as well as the subsequent branching of the plasma jet front, is probably related to hydrodynamic instabilities of the He gas flow, which result in turbulent mixing of He species with the surrounding ambient air; as the plasma discharge is propagating preferentially in regions with high He concentration [103], the turbulent mixing of He and surrounding air can induce several pathways for the plasma discharge, resulting in branching of the plasma jet front. To investigate the correlation between the gas flow instabilities and discharge structure, further investigations exploiting Schlieren imaging have been conducted and the results are presented in the following Paragraph 2.5.

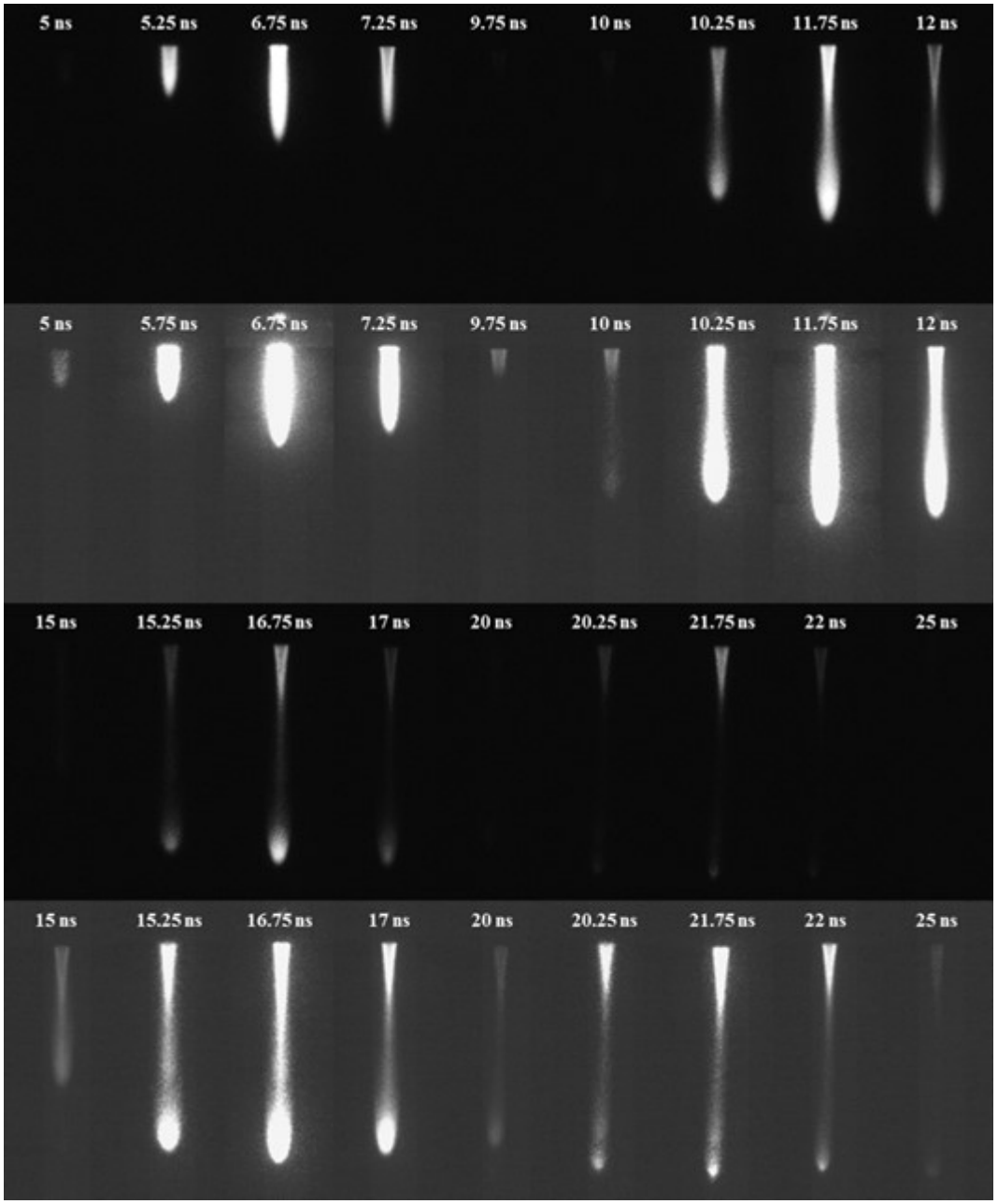

Figure 2.11 ICCD frames (3ns exposure time, 50 accumulations, 0.25 ns of delay increase from one frame to the following) of a plasma jet driven by nanosecond pulses (17 kV, 1000 Hz, 2 slpm of He). Two different chromatic scales were adopted to make all the frames clearly visible (top: higher intensity scale, bottom: low intensity scale). Time values reported on top of each frame are indicative of the time lapse between the start of the voltage pulse and the corresponding opening of the ICCD gate. [PAPER II].

2.4.1 Signal delay compensation method for sub-microsecond synchronization

The ICCD acquisition presented in Figure 2.11 can only be achieved by means of a precisely designed and controlled setup that include far more components than just the ICCD camera. Indeed, to achieve a properly time-resolved visualization of the discharge phenomenon it is extremely important that the gating of the camera sensor is correctly synchronized with the discharge event and, as a consequence, with the voltage pulse driving the plasma discharge.
The development and realization of a diagnostic setup (Figure 2.12) able to guarantee a synchronization level that would allow to achieve ICCD acquisitions with nanosecond resolution and sub-nanosecond synchronization was one of the main topic of my Ph.D. research. While the acquisitions achieved with this setup have been published in PAPER II and in Chapter 3, the methodology and consideration to achieve this kind of synchronization have been presented separately in PAPER III.

An important part for the correct gate setting of the ICCD acquisition is the evaluation of signal transmission delays, which include the delay related to cable transmission and the internal response time of instrumentations; these delays may greatly affect the accuracy of ICCD acquisitions, especially in the case of plasma jet sources excited by sub-microsecond pulses. As presented in PAPER III, it is possible to estimate these delays and compensate for them following a series of best practices to realize a correct synchronization between the ICCD camera and the plasma discharge.
While ICCD cameras are widely adopted for the study of atmospheric pressure plasma discharges, in literature any reference or guideline for the correct synchronization of these instruments could hardly be found before the publication of PAPER III. This is probably due to the magnitude of the signal delays that is usually in the order of nanoseconds; as it will be discussed in the following, this error results relevant in the case of sub-microsecond excitation but less in the case of microsecond pulses, which are generally more diffuse.

In brief, for a general ICCD setup like the one represented in Figure 2.12, to achieve an accurate acquisition is important to synchronize the recorded waveform of the excitation voltage pulse and the gate signal generated by the ICCD camera. This can be achieved only if the delays between the aforementioned signals and their measurement and visualization on the oscilloscope are properly taken into account. In particular, for the excitation signal we should consider the cable delay from the high voltage electrode to the high voltage probe, the high voltage probe characteristic delay and the cable delay from the high voltage probe to the oscilloscope; on the other hand, for the case of the ICCD gate signal we should take into account the delay related to light transmission from the plasma discharge to the ICCD sensor, the ICCD camera internal delay for gate signal generation and the cable delay from the ICCD camera output to the oscilloscope. To estimate these delays is useful, as a first step, to define a starting point (zero value, t_0) from which to calculate the delay of the two signals. Any instant can be chosen in principle but, as suggested in PAPER III, a good option is to taken as t_0 the instant when the high voltage excitation signal reaches the high voltage electrode where the ionization phenomenon takes place. Once all the delays have been estimated or measured they should be introduced as an adjustment in the corresponding channel of the oscilloscope dedicated to the measurement.

Following the procedure described in PAPER III and summarized above, for setting the proper adjustments on the oscilloscope in order to compensate for the delays, the voltage waveform and camera gate signal should be properly synchronized allowing the correct acquisition of time-resolved pictured and the proper interpretation of results; on the other hand, either failing to properly estimate the delays or neglecting the issue can lead to the misinterpretation of results due to incorrect synchronization. The higher the difference between the total delay on the side of the excitation pulse reading and the total delay on the side of the ICCD gate signal (14.6 ns in our setup), the greater can be the negative effect of neglecting or miscalculating the delays.

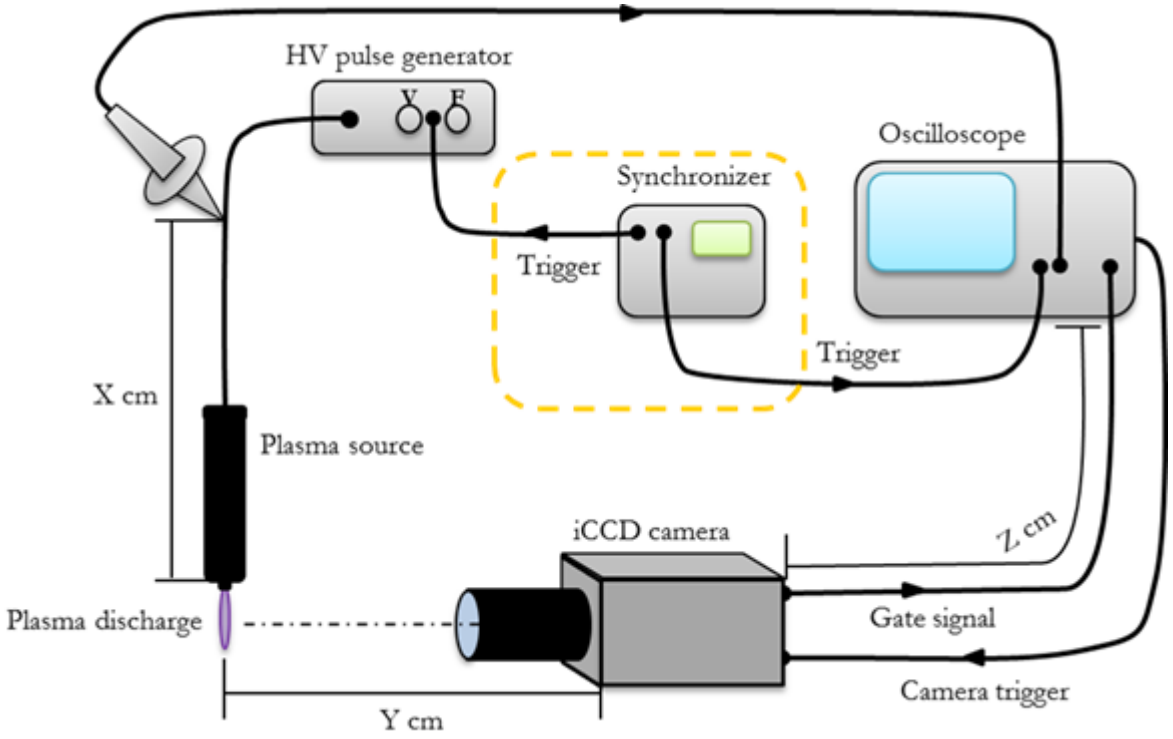

Figure 2.12 Experimental setup adopted for the ICCD imaging experiments reported in Chapter 2. The delay generator (or synchronizer, circled in orange), which is used to synchronize the generator and the oscilloscope, was required only by the experiments with the nanopulse generator; for the tests with the micropulse generator this element was removed. [PAPER III]

In order to clarify the issue, ICCD images obtained with the setup presented in Figure 2.12 and adopting the "best practice", thus taking delays into account and applying the appropriate adjustments to achieve good synchronization, or the "bad practice", thus failing to take into account the aforementioned delays, are reported and compared in Figure 2.13.
As it is possible to observe and as already mentioned before, for the micropulsed generator no significant difference can be observed between "best practice" and "bad practice" acquisitions, since the signal delay difference (in this case 14.6 ns) is at least three orders of magnitude smaller than the gate width necessary to record the PAPS propagation. On the contrary, when the plasma source is powered by a nanopulsed generator, the shorter pulses require the use of shorter camera gates, of the same order of magnitude of signal delay difference, and therefore a proper synchronization is required. In the third row of Fig. 13, "best practice" and "bad practice" acquisitions are reported for the camera gate set to extend over an entire voltage pulse (35 ns). Even if the two plasma discharges are very similar, in the case of the "bad practice" the plasma discharge is shorter and its emission intensity is slightly lower. The reported images are the result of 30 accumulations and the experiment was repeated several times, therefore the reduction in the discharge length is unlikely to be due to random fluctuation in the electrical or fluid dynamic parameters, but has to be appointed to the incorrect synchronization between the gate timing and the excitation pulse. Indeed, in the "bad practice" case, the real camera gate (blue rectangle in Figure 2.13) is shifted 14.6 ns earlier than the supposed camera gate (red rectangle in Figure 2.13) and as a consequence the light emission related to the second half of the HV pulse was not recorded in this acquisition and is the reason of the observed differences.

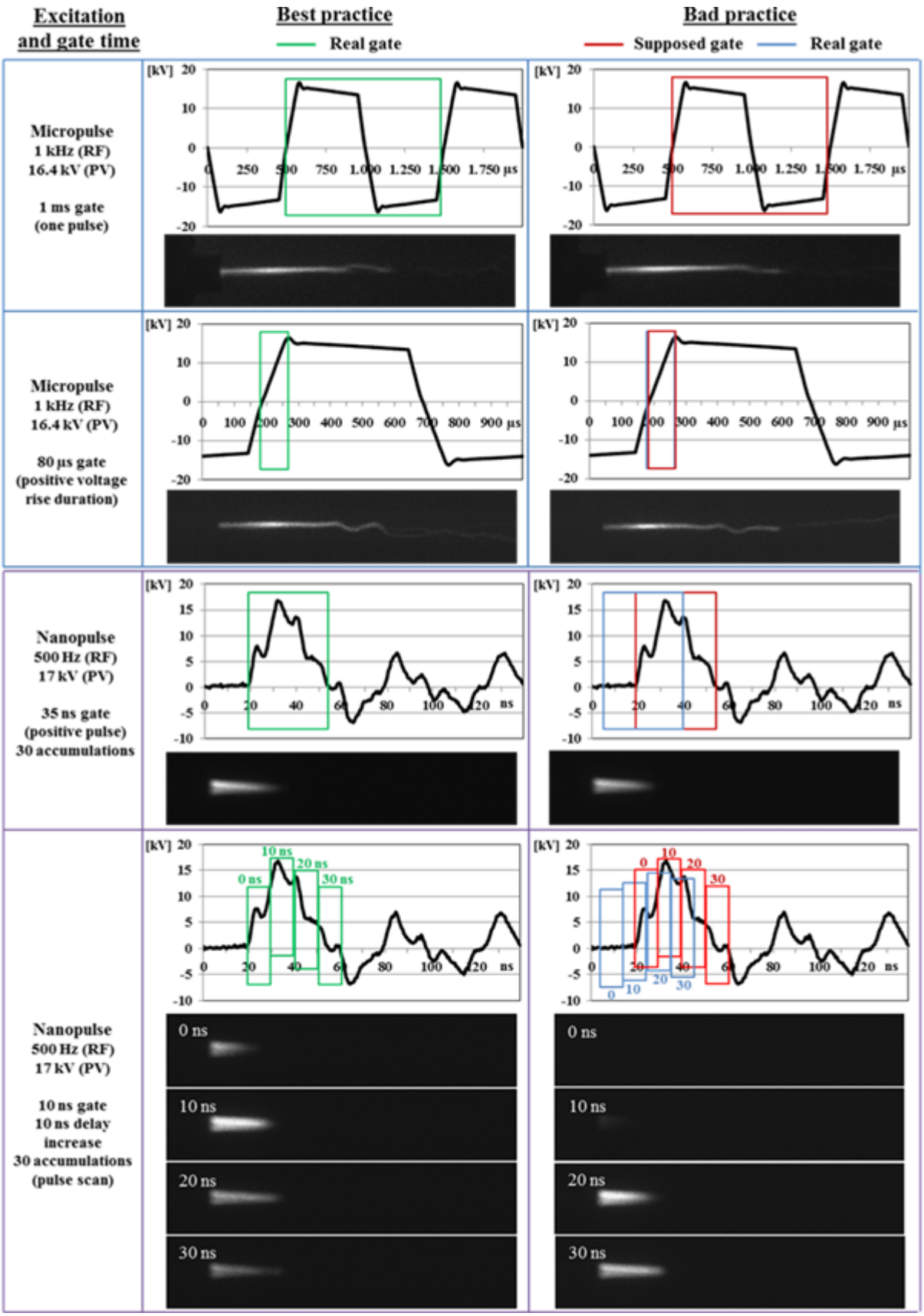

Figure 2.13 ICCD acquisitions and voltage waveforms for the *Plasma Jet* operated with micropulsed and nanopulsed generators. Results obtained compensating ("Best practice") and not compensating ("Bad practice") signal delays are compared. Recorded ICCD gate are superimposed on the voltage waveform with green ("Best practice") and red ("Bad practice") rectangles. For the bad practice case, the real position (artificially compensating the delays) of the gates is shown in blue rectangles.[PAPER III]

This issue is even more pronounced when the gate width is further reduced to investigate the temporal evolution of the plasma jet during the HV pulse. In the last row of Figure 2.13 a sequence of ICCD acquisitions (camera gate 10 ns and 30 accumulations) is shown, together with the recorded voltage waveforms with the camera gates super imposed; the ICCD gate opening for the first frame of each scan was set at t_0 and subsequent frames were recorded at fixed time steps (delays) of 10 ns. In the best practice case, the ICCD acquisitions show the formation of the plasma plume in the first 10 ns of the HV pulse, its increase in length along the entire voltage pulse duration and a maximum emission intensity in correspondence of the voltage peak; these results are in good agreement with other previously obtained for the same plasma source in similar operating conditions, but analyzed with a different setup [PAPER II]. Instead, in the "bad practice" case no light emission is observed in the first frame (first 10 ns of the HV pulse) and only a faint plasma discharge is discernable in the second one; considering the supposed camera gates (red rectangles in Figure 2.13), these misleading results would suggest that the plasma is not generated during the entire HV rising front and that the highest emission intensity is not reached in correspondence of the HV peak. Indeed, if the real camera gates (blue rectangles in Figure 2.13) are considered, it can be observed that the gate corresponding to the first frame is entirely located before the HV pulse and that the gate corresponding to the second frame overlaps only partially with the HV pulse, and this is in agreement with the corresponding ICCD images of the plasma discharge. In conclusion, failing to account for signal delays may lead to an unrealistic interpretation of the investigated phenomenon for the case of nanosecond pulsed excitation; this because the time scale of the signal delays and the camera gates usually adopted for these experiments are of the same order of magnitude (tens of nanoseconds).

2.5. Schlieren imaging for flow regime visualization

Schlieren photography is used for the imaging of the flow of fluids of varying density [104]. The basic optical Schlieren system uses light from a single collimated source to investigate a target object or medium. Variations in refractive index caused by density gradients in the fluid bend the collimated light beam. This distortion creates a spatial variation in the intensity of the light, which can be visualized directly with a shadowgraph system. In Schlieren photography, the collimated light is focused with a lens, and a knife-edge is placed at the focal point. By moving the knife edge more closely to the axis of the light beam, the overall photograph brightness can be progressively reduced. However, in a flow with density variations the distorted beam focuses imperfectly, and parts which have been focused in an area covered by the knife-edge are blocked. The result is a set of lighter and darker patches corresponding to positive and negative fluid density gradients in the direction normal to the knife-edge. When a knife-edge is used, the system is generally referred to as a Schlieren system, which measures the first derivative of the density in the direction of the knife-edge. If a knife-edge is not used, the system is generally referred to as a shadowgraph system, which measures the second derivative of density.
Schlieren imaging is a very powerful tool for APPJs diagnostic. By using Schlieren photography, the distribution of the working gas (mainly He or Ar) flow in the surrounding air can be achieved and the flow mode (turbulent or laminar flow) of the working gas can be determined, which is very important for understanding the propagation behaviour of the plasma bullet.

The gas flow rate is one of the important parameters used to control not only the discharge characteristics but also the effluent temperature and the transportation of reactive species. In the context of biomedical applications, gas mixing is an important factor influencing the delivery of reactive species via the plasma jet effluent to a treatment surface. Since the first work of Bradley *et al.* [55] in 2011 the number of published studies investigating of the influence of the gas flow rate on APPJs by means of Schlieren photography has steadily increased. As part of my Ph.D. research I contributed to deepen the understanding of the gas dynamics in APPJs through the PAPER I and II, which was, together with the work of Robert *et al.* [105] published in the same year, one of the first to visualize the evolution of the

turbulent phenomena induced in APPJ effluent. The result was achieved coupling the Schlieren setup with a high speed camera recording at 4000 fps. An example of the acquisition achieved is presented in Figure 2.14 from PAPER I. From these selected frames, at 1.5 ms from the voltage pulse it is possible to observe a turbulent front propagating in the downstream region of the plasma jet. The observed turbulent front propagation is similar for each voltage pulse; comparing the frame at 2.5 ms and 14.5 ms the fluid dynamic structure of the APPJ source effluent results very similar, with the formation of a turbulent front 1.5 cm downstream the nozzle. The propagation velocity of the turbulent front along the laminar region was estimated, by analysing the high-speed Schlieren acquisitions, to be about 60 m/s, which is close to the mean gas velocity and far below the estimated PAPS velocity (10^8 cm/s). In PAPER I different possible mechanisms to explain the phenomenon are advanced, such as gas heating, local pressure increase, the change of transport properties of the fluid and the momentum transfer between ions and neutrals. As it will be discussed in Chapter 3 most of this hypothesis have been later abandoned in favour of a new one featuring the indirect heating of the gas as a consequence of the sharp increase of the high voltage electrode as a consequence of the current flow generated by the plasma discharge.
Another very powerful use of the Schlieren technique for the diagnostic of APPJs is in combination with ICCD imaging. An example of this multidiagnostic approach is presented in Figure 2.15 from PAPER II. In the picture ICCD acquisitions paired with the corresponding Schlieren frames of the Plasma Jet operating at different operating conditions are presented. From Schlieren images, it can be noted that the flow at the source outlet is almost laminar (Reynolds number is approximately 500 for the plasma source operated with 3 slpm of He) while fluid-dynamic instabilities can be observed in a more downstream position. With increasing PRF (from 125 to 1000 Hz), the length of the laminar region becomes shorter and fluid-dynamic instabilities of higher intensity can be observed. With PV increasing from 17 to 30 kV, the same trend is observed, but the effect is weaker in comparison with the change in PRF. From ICCD images, it can be noted that the length of the plasma plume is increased as the PV is increased, whereas with increasing PRF, the plasma plume length is generally reduced.

From the comparison of Schlieren frames and ICCD images, a clear correspondence between fluid-dynamic instabilities and branching of the plasma plume can be observed. The ending part of the plasma plume becomes branched in the cases in which the operating conditions induce the plasma plume to propagate into the spatial region where the flow is turbulent. This phenomenon is mostly evident for the cases with highest PV (30 kV), which are characterized by a longer plasma plume that can penetrate the regions with higher intensity of fluid-dynamics instabilities. It can be observed that the branching of the plasma plume appears in correspondence of the region where the transition from laminar to turbulent flow is observed. On the contrary, in the cases with lowest PV (17 kV), the plasma plume is propagating in the laminar region only and no branching of the front is observed. These results support the idea that fluid-dynamic instabilities of the jet induce a turbulent mixing of He and the surrounding air and, consequently, the formation of more than one preferential pathways through which the plasma plume can propagate, resulting in branching of the plasma front.

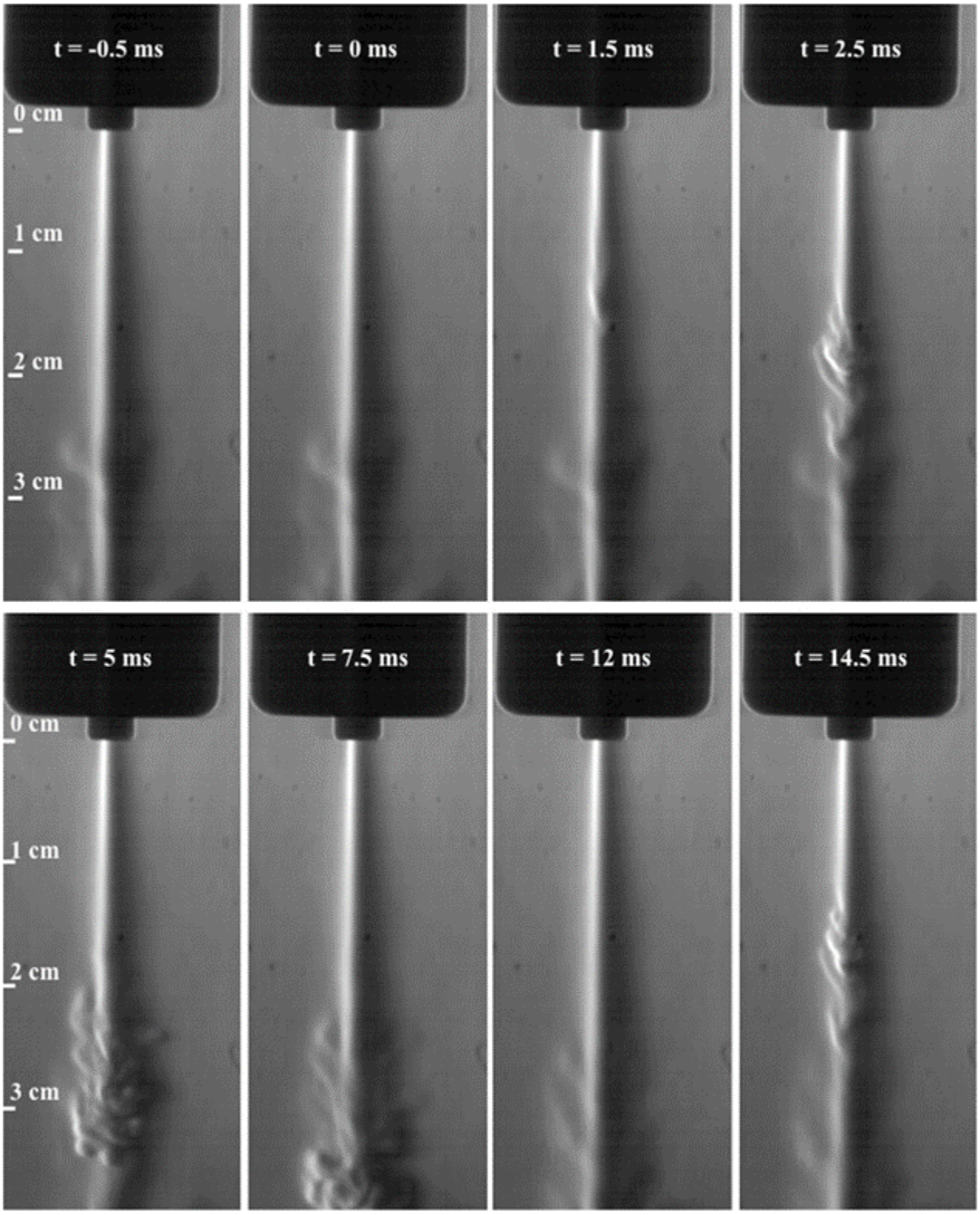

Figure 2.14 Schlieren imaging of the plasma jet evolution between two voltage pulses, at t=0 ms and t=12 ms. (PV=20kV, PRF=83 Hz and He mass flow rate = 3slm) [PAPER I]

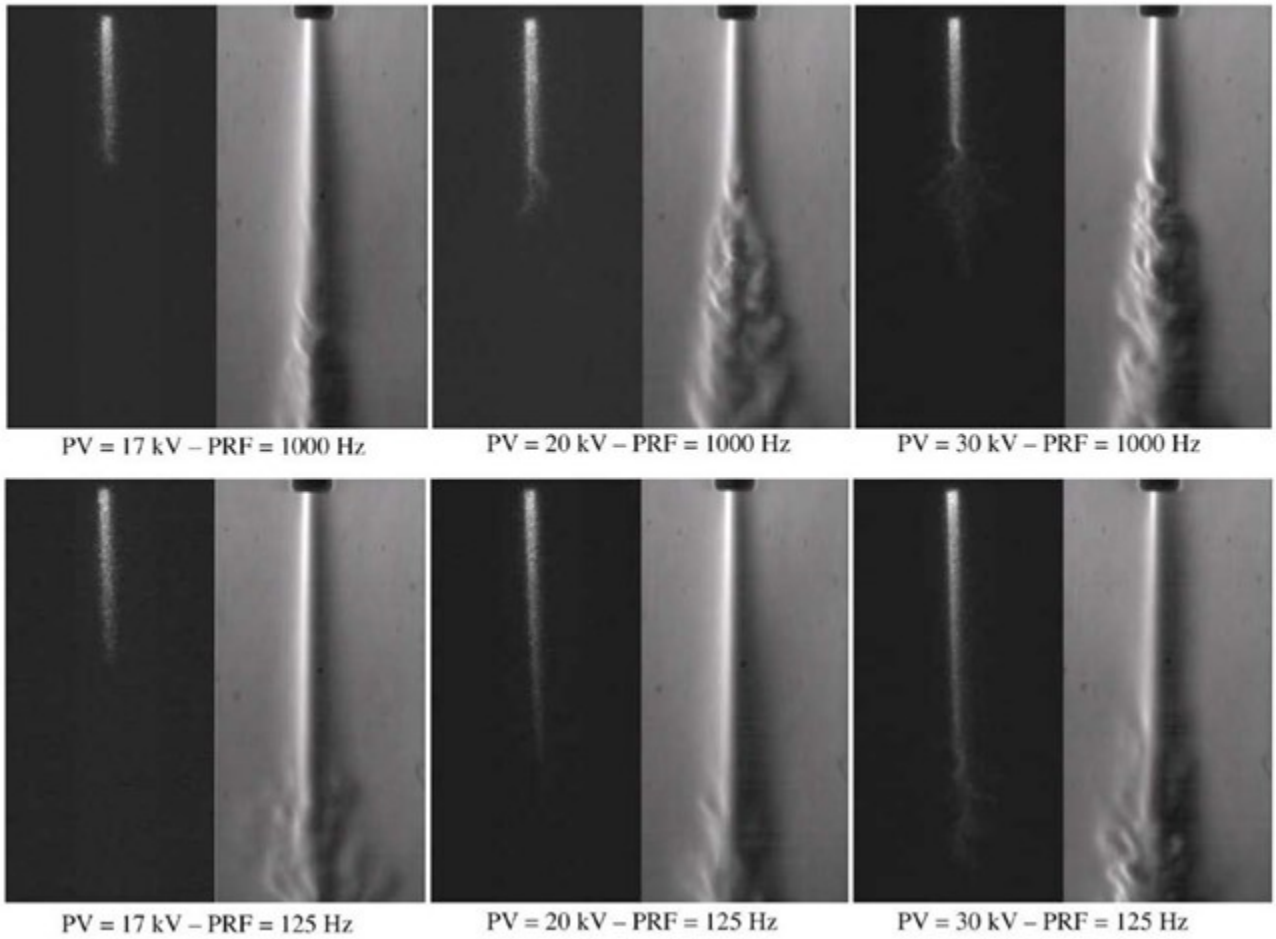

Figure 2.15 Comparison of synchronized (left) ICCD and (right) Schlieren acquisitions of the plasma jet for different values of PV (17, 20, and 30 kV) and PRF (125 and 1000 Hz). Flow rate set at 3 slpm of He for all cases. [PAPER II]

2.6 References

[1] X. Lu, M. Laroussi, and V. Puech, "On atmospheric-pressure non-equilibrium plasma jets and plasma bullets," Plasma Sources Sci. Technol., vol. 21, no. 3, p. 034005, 2012.

[2] L. Taghizadeh, G. Brackman, A. Nikiforov, J. van der Mullen, C. Leys, and T. Coenye, "Inactivation of Biofilms Using a Low Power Atmospheric Pressure Argon Plasma Jet; the Role of Entrained Nitrogen," Plasma Process. Polym., vol. 12, no. 1, pp. 75–81, Jan. 2015.

[3] X. Deng, A. Yu Nikiforov, P. Vanraes, and C. Leys, "DEPOSITION OF NANOSILVER-ORGANOSILICON COMPOSITE FILMS USING AN ATMOSPHERIC PRESSURE DC PLASMA JET," Rom. Reports Phys., vol. 66, no. 4, pp. 1088–1098, 2014.

[4] a. Van Deynse, P. Cools, C. Leys, R. Morent, and N. De Geyter, "Surface modification of polyethylene in an argon atmospheric pressure plasma jet," Surf. Coatings Technol., vol. 276, pp. 384–390, 2015.

[5] a. Sarani, N. De Geyter, A. Y. Nikiforov, R. Morent, C. Leys, J. Hubert, and F. Reniers, "Surface modification of PTFE using an atmospheric pressure plasma jet in argon and argon+CO2," Surf. Coatings Technol., vol. 206, no. 8–9, pp. 2226–2232, 2012.

[6] T. von Woedtke, S. Reuter, K. Masur, and K.-D. Weltmann, "Plasmas for medicine," Phys. Rep., vol. 530, no. 4, pp. 291–320, Sep. 2013.

[7] J. L. Walsh and M. G. Kong, "Contrasting characteristics of linear-field and cross-field atmospheric plasma jets," Appl. Phys. Lett., vol. 93, no. 11, pp. 13–16, 2008.

[8] M. Noeske, J. Degenhardt, S. Strudthoff, and U. Lommatzsch, "Plasma jet treatment of five polymers at atmospheric pressure: surface modifications and the relevance for adhesion," Int. J. Adhes. Adhes., vol. 24, no. 2, pp. 171–177, 2004.

[9] E. Stoffels, a J. Flikweert, W. W. Stoffels, and G. M. W. Kroesen, "Plasma needle: a non-destructive atmospheric plasma source for fine surface treatment of (bio)materials," Plasma Sources Sci. Technol., vol. 11, no. 4, pp. 383–388, 2002.

[10] F. Iza, G. J. Kim, S. M. Lee, J. K. Lee, J. L. Walsh, Y. T. Zhang, and M. G. Kong, "Microplasmas: Sources, particle kinetics, and biomedical applications," Plasma Process. Polym., vol. 5, no. 4, pp. 322–344, 2008.

[11] G. Fridman, G. Friedman, A. Gutsol, A. B. Shekhter, V. N. Vasilets, and A. Fridman, "Applied plasma medicine," Plasma Process. Polym., vol. 5, no. 6, pp. 503–533, 2008.

[12] M. Laroussi, "Low-temperature plasmas for medicine?," IEEE Trans. Plasma Sci., vol. 37, no. 6 PART 1, pp. 714–725, 2009.

[13] R. Laurita, M. Zaccaria, M. Gherardi, D. Fabiani, A. Merlettini, A. Pollicino, M. L. Focarete, and V. Colombo, "Plasma Processing of Electrospun Li-Ion Battery Separators to Improve Electrolyte Uptake," Plasma Process. Polym., vol. 13, no. 1, pp. 124–133, Jan. 2016.

[14] E. Simoncelli, D. Barbieri, R. Laurita, A. Liguori, A. Stancampiano, L. Viola, R. Tonini, M. Gherardi, and V. Colombo, "Preliminary investigation of the antibacterial efficacy of a handheld

Plasma Gun source for endodontic procedures," Clin. Plasma Med., vol. 3, no. 2, pp. 77–86, 2015.

[15] A. Liguori, E. Traldi, E. Toccaceli, R. Laurita, A. Pollicino, M. L. Focarete, V. Colombo, and M. Gherardi, "Co-Deposition of Plasma-Polymerized Polyacrylic Acid and Silver Nanoparticles for the Production of Nanocomposite Coatings Using a Non-Equilibrium Atmospheric Pressure Plasma Jet," Plasma Process. Polym., p. n/a–n/a, Oct. 2015.

[16] A. Liguori, A. Pollicino, A. Stancampiano, F. Tarterini, M. L. Focarete, V. Colombo, and M. Gherardi, "Deposition of Plasma-Polymerized Polyacrylic Acid Coatings by a Non-Equilibrium Atmospheric Pressure Nanopulsed Plasma Jet," Plasma Process. Polym., vol. 13, no. 3, pp. 375–386, 2016.

[17] S. Bianconi, F. Cavrini, V. Colombo, M. Gherardi, R. Laurita, A. Liguori, P. Sanibondi, and A. Stancampiano, "iCCD Imaging of the Transition From Uncoupled to Coupled Mode in a Plasma Source for Biomedical and Materials Treatment Applications," vol. 42, no. 10, pp. 2746–2747, 2014.

[18] G. M. Giannini, "The Plasma Jet," Sci. Am., vol. 197, no. 2, pp. 80–90, Aug. 1957.

[19] M. Andrenucci, "Giannini, Ducati and the dawn of MPD propulsion," in Space Propulsion Conf., 2010.

[20] G. R. Gage, "Arc torch and process," US 2,806,124 A, 1957.

[21] Z. P. Lu, L. Stachowicz, P. Kong, J. Heberlein, and E. Pfender, "Diamond synthesis by DC thermal plasma CVD at 1 atm," Plasma Chem. Plasma Process., vol. 11, no. 3, pp. 387–394, Sep. 1991.

[22] H. Akatsuka and M. Suzuki, "Arc-heated magnetically trapped expanding plasma jet generator," Rev. Sci. Instrum., vol. 64, no. 7, p. 1734, 1993.

[23] A. Schutze, J. Y. Jeong, S. E. Babayan, Jaeyoung Park, G. S. Selwyn, and R. F. Hicks, "The atmospheric-pressure plasma jet: a review and comparison to other plasma sources," IEEE Trans. Plasma Sci., vol. 26, no. 6, pp. 1685–1694, 1998.

[24] K. H. Schoenbach, M. Moselhy, W. Shi, and R. Bentley, "Microhollow cathode discharges," J. Vac. Sci. Technol. A Vacuum, Surfaces, Film., vol. 21, no. 4, p. 1260, 2003.

[25] C. Tendero, C. Tixier, P. Tristant, J. Desmaison, and P. Leprince, "Atmospheric pressure plasmas: A review," Spectrochim. Acta Part B At. Spectrosc., vol. 61, no. 1, pp. 2–30, 2006.

[26] Nasruddin, Y. Nakajima, K. Mukai, H. S. E. Rahayu, M. Nur, T. Ishijima, H. Enomoto, Y. Uesugi, J. Sugama, and T. Nakatani, "Cold plasma on full-thickness cutaneous wound accelerates healing through promoting inflammation, re-epithelialization and wound contraction," Clin. Plasma Med., pp. 1–8, 2014.

[27] S. Bekeschus, A. Schmidt, K.-D. Weltmann, and T. von Woedtke, "The plasma jet kINPen – A powerful tool for wound healing," Clin. Plasma Med., pp. 1–10, 2016.

[28] A. Liguori, A. Pollicino, A. Stancampiano, F. Tarterini, M. L. Focarete, V. Colombo, and M. Gherardi, "Deposition of Plasma-Polymerized Polyacrylic Acid Coatings by a Non-Equilibrium Atmospheric Pressure Nanopulsed Plasma Jet," Plasma Process. Polym., p. n/a–n/a, 2015.

[29] H. W. Lee, S. H. Nam, A. A. H. Mohamed, G. C. Kim, and J. K. Lee, "Atmospheric pressure plasma jet composed of three electrodes: Application to tooth bleaching," Plasma Process. Polym., vol. 7, no. 3–4, pp. 274–280, 2010.

[30] D. Yan, A. Talbot, N. Nourmohammadi, J. H. Sherman, X. Cheng, and M. Keidar, "Toward understanding the selective anticancer capacity of cold atmospheric plasma — A model based on aquaporins (Review) Toward understanding the selective anticancer capacity of cold atmospheric plasma — A model based on aquaporins (Review)," vol. 040801, 2015.

[31] R. Brandenburg, V. V. Kova??evi??, M. Schmidt, R. Basner, M. Kettlitz, G. B. Sretenovi??, B. M. Obradovi??, M. M. Kuraica, and K. D. Weltmann, "Plasma-Based Pollutant Degradation in Gas Streams: Status, Examples and Outlook," Contrib. to Plasma Phys., vol. 54, no. 2, pp. 202–214, 2014.

[32] S. M. Starikovskaia, "Plasma assisted ignition and combustion," J. Phys. D. Appl. Phys., vol. 39, no. 16, pp. R265–R299, 2006.

[33] J. K. Lefkowitz, "Plasma Assisted Combustion : Fundamental Studies and Engine Applications," no. January, 2016.

[34] A. Starikovskiy and N. Aleksandrov, "Plasma-assisted ignition and combustion," Progress in Energy and Combustion Science, vol. 39, no. 1. pp. 61–110, 2013.

[35] H. T. Kim and O. C. Jeong, "PDMS surface modification using atmospheric pressure plasma," in Microelectronic Engineering, 2011, vol. 88, no. 8, pp. 2281–2285.

[36] A. Sarani, A. Y. Nikiforov, N. De Geyter, R. Morent, and C. Leys, "Surface modification of polypropylene with an atmospheric pressure plasma jet sustained in argon and an argon/water vapour mixture," Appl. Surf. Sci., vol. 257, no. 20, pp. 8737–8741, 2011.

[37] F. Marchal, H. Robert, N. Merbahi, C. Fontagné-Faucher, M. Yousfi, C. E. Romain, O. Eichwald, C. Rondel, and B. Gabriel, "Inactivation of Gram-positive biofilms by low-temperature plasma jet at atmospheric pressure," J. Phys. D. Appl. Phys., vol. 45, no. 34, p. 345202, Aug. 2012.

[38] J. F. Kolb, A. M. Mattson, C. M. Edelblute, X. Hao, M. A. Malik, and L. C. Heller, "Cold DC-Operated Air Plasma Jet for the Inactivation of Infectious Microorganisms," IEEE Trans. Plasma Sci., vol. 40, no. 11, pp. 3007–3026, Nov. 2012.

[39] J. Winter, R. Brandenburg, and K.-D. Weltmann, "Atmospheric pressure plasma jets: an overview of devices and new directions," Plasma Sources Sci. Technol., vol. 24, no. 6, p. 064001, 2015.

[40] L. B. Loeb and J. M. Meek, "The Mechanism of Spark Discharge in Air at Atmospheric Pressure. I," J. Appl. Phys., vol. 11, no. 6, p. 438, 1940.

[41] L. B. Loeb and J. M. Meek, "The Mechanism of Spark Discharge in Air at Atmospheric Pressure. II," J. Appl. Phys., vol. 11, no. 7, p. 459, 1940.

[42] X. Lu and M. Laroussi, "Dynamics of an atmospheric pressure plasma plume generated by submicrosecond voltage pulses," J. Appl. Phys., vol. 100, no. 6, p. 063302, 2006.

[43] M. Teschke, J. Kedzierski, E. G. Finantu-Dinu, D. Korzec, and J. Engemann, "High-speed photographs of a dielectric barrier atmospheric pressure plasma jet," IEEE Trans. Plasma Sci., vol. 33, no. 2, pp. 310–311, Apr. 2005.

[44] E. Robert, V. Sarron, D. Riès, S. Dozias, M. Vandamme, and J.-M. Pouvesle, "Characterization of pulsed atmospheric-pressure plasma streams (PAPS) generated by a plasma gun," Plasma Sources Sci. Technol., vol. 21, no. 3, p. 034017, 2012.

[45] Z. Xiong, E. Robert, V. Sarron, J.-M. Pouvesle, and M. J. Kushner, "Dynamics of ionization wave splitting and merging of atmospheric-pressure plasmas in branched dielectric tubes and channels," J. Phys. D. Appl. Phys., vol. 45, no. 27, p. 275201, Jul. 2012.

[46] L. B. Loeb, "Basic Processes of Gaseous Electronics." Univ. California Press, 1955.

[47] H. Raether, Electron avalanches and breakdown in gases. Butterworths, 1964.

[48] R. S. Sigmond, J. M. Meek, and J. D. Craggs, "Electrical breakdown of gases," New York Wiley, 1978.

[49] Y. P. Raizer, Gas discharge physics. Berlin: Springer-Verlag, 1991.

[50] X. Lu, G. V. Naidis, M. Laroussi, and K. Ostrikov, "Guided ionization waves: Theory and experiments," Phys. Rep., vol. 540, no. 3, pp. 123–166, 2014.

[51] M. Keidar, A. Shashurin, O. Volotskova, M. Ann Stepp, P. Srinivasan, A. Sandler, and B. Trink, "Cold atmospheric plasma in cancer therapy," Phys. Plasmas, vol. 20, no. 5, p. 057101, 2013.

[52] X. Lu, Z. Jiang, Q. Xiong, Z. Tang, X. Hu, and Y. Pan, "An 11 cm long atmospheric pressure cold plasma plume for applications of plasma medicine," Appl. Phys. Lett., vol. 92, no. 8, p. 081502, 2008.

[53] D. B. Graves, "The emerging role of reactive oxygen and nitrogen species in redox biology and some implications for plasma applications to medicine and biology," J. Phys. D. Appl. Phys., vol. 45, no. 26, p. 263001, Jul. 2012.

[54] Y. Yue, X. Pei, and X. Lu, "electrodes OH density optimization in atmospheric-pressure plasma jet by using multiple ring electrodes," vol. 033301, 2016.

[55] J. W. Bradley, J. Oh, O. T. Olabanji, C. Hale, R. Mariani, and K. Kontis, "Schlieren Photography of the Outflow From a Plasma Jet," Trans. Plasma Sci., vol. 39, no. 11, pp. 2312–2313, 2011.

[56] a Schmidt-Bleker, S. Reuter, and K.-D. Weltmann, "Quantitative schlieren diagnostics for the determination of ambient species density, gas temperature and calorimetric power of cold atmospheric plasma jets," J. Phys. D. Appl. Phys., vol. 48, no. 17, p. 175202, 2015.

[57] U. Kogelschatz, "Collective phenomena in volume and surface barrier discharges," J. Phys. Conf. Ser., vol. 257, p. 012015, 2010.

[58] U. Kogelschatz, "Dielectric-Barrier Discharges: Their History, Discharge Physics, and Industrial Applications," Plasma Chem. Plasma Process., vol. 23, no. 1, pp. 1–46, 2003.

[59] E. Robert, M. Vandamme, L. Brullé, S. Lerondel, a. Le Pape, V. Sarron, D. Riès, T. Darny, S. Dozias, G. Collet, C. Kieda, and J. M. Pouvesle, "Perspectives of endoscopic plasma applications," Clin. Plasma Med., vol. 1, no. 2, pp. 8–16, 2013.

[60] X. P. Lu, Q. Xiong, Z. Y. Tang, Z. H. Jiang, and Y. Pan, "A cold plasma jet device with multiple plasma plumes merged," IEEE Trans. Plasma Sci., vol. 36, no. 4 PART 1, pp. 990–991, 2008.

[61] X. Pei, Z. Wang, Q. Huang, S. Wu, and X. Lu, "Dynamics of a plasma jet array," IEEE Trans. Plasma Sci., vol. 39, no. 11 PART 1, pp. 2276–2277, 2011.

[62] R. a. Ganeev, M. Suzuki, and H. Kuroda, "Quasi-phase-matching of high-order harmonics in multiple plasma jets," Phys. Rev. A - At. Mol. Opt. Phys., vol. 89, no. 3, pp. 2–7, 2014.

[63] C. Qian, Z. Fang, J. Yang, and M. Kang, "Investigation on Atmospheric Pressure Plasma Jet Array in Ar," IEEE Trans. Plasma Sci., vol. 1, no. l, pp. 1–1, 2014.

[64] C. Zhang, T. Shao, Y. Zhou, Z. Fang, P. Yan, and W. Yang, "Effect of O2 additive on spatial uniformity of atmospheric-pressure helium plasma jet array driven by microsecond-duration pulses," Appl. Phys. Lett., vol. 105, no. 4, p. 044102, 2014.

[65] S. J. Kim, T. H. Chung, H. M. Joh, J. Cha, I. S. Eom, and H. Lee, "Characteristics of Multiple Plasma Plumes and Formation of Bullets in an Atmospheric- Pressure Plasma Jet Array," vol. 43, no. 3, pp. 753–759, 2015.

[66] J. G. Eden and S. J. Park, "New opportunities for plasma science in nonequilibrium low-temperature plasmas confined to microcavities: There's plenty of room at the bottom," Phys. Plasmas, vol. 13, no. 5, pp. 3–8, 2006.

[67] Q. Q. Fan, M. Y. Qian, C. S. Ren, D. Wang, and X. Wen, "Discharge characteristics of a cold-atmospheric-plasma jet array generated with single-electrode configuration," IEEE Trans. Plasma Sci., vol. 40, no. 6 PART 2, pp. 1724–1729, 2012.

[68] N. O'Connor, H. Humphreys, and S. Daniels, "Cooperative Merging of Atmospheric Pressure Plasma Jet Arrays," IEEE Trans. Plasma Sci., vol. 42, no. 3, pp. 756–758, Mar. 2014.

[69] Z. Cao, J. L. Walsh, and M. G. Kong, "Atmospheric plasma jet array in parallel electric and gas flow fields for three-dimensional surface treatment," Appl. Phys. Lett., vol. 94, no. 2, p. 021501, 2009.

[70] Q. Y. Nie, Z. Cao, C. S. Ren, D. Z. Wang, and M. G. Kong, "A two-dimensional cold atmospheric plasma jet array for uniform treatment of large-area surfaces for plasma medicine," New J. Phys., vol. 11, 2009.

[71] V. Zablotskii, O. Churpita, Z. Hubicka, L. Jastrabik, and a. Dejneka, "Multijet atmospheric plasma device for biomedical applications," Plasma Med., vol. 1, no. 2, pp. 135–141, 2011.

[72] J. Y. Kim and S. O. Kim, "Intense plasma emission from atmospheric-pressure plasma jet array by jet-to-jet coupling," IEEE Trans. Plasma Sci., vol. 39, no. 11 PART 1, pp. 2278–2279, 2011.

[73] J. Furmanski, J. Y. Kim, and S. O. Kim, "Triple-coupled intense atmospheric pressure plasma jet from honeycomb structural plasma device," IEEE Trans. Plasma Sci., vol. 39, no. 11 PART 1, pp. 2338–2339, 2011.

[74] J. Y. Kim, J. Ballato, and S. O. Kim, "Intense and energetic atmospheric pressure plasma jet arrays," Plasma Process. Polym., vol. 9, no. 3, pp. 253–260, 2012.

[75] M. Boselli, F. Cavrini, V. Colombo, E. Ghedini, M. Gherardi, R. Laurita, A. Liguori, P. Sanibondi, and A. Stancampiano, "High-Speed and Schlieren Imaging of a Low Power Inductively Coupled Plasma Source for Potential Biomedical Applications," pp. 1–2, 2014.

[76] S. a. Norberg, E. Johnsen, and M. J. Kushner, "Helium atmospheric pressure plasma jets touching dielectric and metal surfaces," J. Appl. Phys., vol. 118, no. 1, p. 013301, 2015.

[77] S. a Norberg, E. Johnsen, and M. J. Kushner, "Formation of reactive oxygen and nitrogen species by repetitive negatively pulsed helium atmospheric pressure plasma jets propagating into humid air," Plasma Sources Sci. Technol., vol. 24, no. 3, p. 035026, 2015.

[78] S. Zhang, a Sobota, E. M. van Veldhuizen, and P. J. Bruggeman, "Gas flow characteristics of a time modulated APPJ: the effect of gas heating on flow dynamics," J. Phys. D. Appl. Phys., vol. 48, no. 1, p. 015203, 2015.

[79] Q. Muyang, R. Chunsheng, W. Dezhen, F. Yan, and Z. Jialiang, "Atmospheric Pressure Cold Argon/Oxygen Plasma Jet Assisted by Preionization of Syringe Needle Electrode," Plasma Sci. Technol., vol. 12, no. 5, pp. 561–565, Oct. 2010.

[80] Q. Xiong, X. P. Lu, K. Ostrikov, Y. Xian, C. Zou, Z. Xiong, and Y. Pan, "Pulsed dc- and sine-wave-excited cold atmospheric plasma plumes: A comparative analysis," Phys. Plasmas, vol. 17, no. 4, p. 043506, 2010.

[81] N. Y. Babaeva and M. J. Kushner, "Interaction of multiple atmospheric-pressure micro-plasma jets in small arrays: He/O 2 into humid air," Plasma Sources Sci. Technol., vol. 23, no. 1, p. 015007, 2014.

[82] Z. Chang, G. Zhang, C. Yao, W. Liao, and X. Shi, "Atmospheric Pressure Plasma Jet Array With Multivariate Cells," vol. 42, no. 10, pp. 2440–2441, 2014.

[83] Y. Zhou, T. Shao, Z. Fang, C. Zhang, Z. Niu, P. Yan, W. Huang, and H. Ma, "Discharge characteristics of one-dimensional plasma jet array at atmospheric pressure," in 2013 Annual Report Conference on Electrical Insulation and Dielectric Phenomena, 2013, pp. 1034–1037.

[84] M. Ghasemi, P. Olszewski, J. W. Bradley, and J. L. Walsh, "Interaction of multiple plasma plumes in an atmospheric pressure plasma jet array," J. Phys. D. Appl. Phys., vol. 46, no. 5, p. 052001, 2013.

[85] J. Y. Jeong, S. E. Babayan, V. J. Tu, J. Park, I. Henins, R. F. Hicks, and G. S. Selwyn, "Etching materials with an atmospheric-pressure plasma jet," Plasma Sources Sci. Technol., vol. 7, no. 3, pp. 282–285, Aug. 1998.

[86] "Etching polyimide with a nonequilibrium atmospheric-pressure plasma jet," . Vac. Sci. Technol. …, 1999.

[87] V. Colombo, D. Fabiani, M. L. Focarete, M. Gherardi, C. Gualandi, R. Laurita, and M. Zaccaria, "Atmospheric Pressure Non-Equilibrium Plasma Treatment to Improve the Electrospinnability of Poly(L -Lactic Acid) Polymeric Solution," Plasma Process. Polym., vol. 11, no. 3, pp. 247–255, Mar. 2014.

[88] S. M. Starikovskaia, N. B. Anikin, S. V Pancheshnyi, D. V Zatsepin, and A. Y. Starikovskii, "Pulsed breakdown at high overvoltage: development, propagation and energy branching," Plasma Sources Sci. Technol., vol. 10, no. 2, pp. 344–355, May 2001.

[89] I. V Adamovich, I. Choi, N. Jiang, J.-H. Kim, S. Keshav, W. R. Lempert, E. Mintusov, M. Nishihara, M. Samimy, and M. Uddi, "Plasma assisted ignition and high-speed flow control: non-thermal and thermal effects," Plasma Sources Sci. Technol., vol. 18, no. 3, p. 034018, Aug. 2009.

[90] R. Pothiraja, N. Bibinov, and P. Awakowicz, "Amorphous carbon film deposition on the inner surface of tubes using atmospheric pressure pulsed filamentary plasma source," J. Phys. D. Appl. Phys., vol. 44, no. 35, p. 355206, Sep. 2011.

[91] D. Zou, X. Cao, X. Lu, and K. K. Ostrikov, "Chiral streamers," Phys. Plasmas, vol. 22, no. 10, 2015.

[92] S. Wu, H. Xu, X. Lu, and Y. Pan, "Effect of Pulse Rising Time of Pulse dc Voltage on Atmospheric Pressure Non-Equilibrium Plasma," Plasma Process. Polym., vol. 10, no. 2, pp. 136–140, Feb. 2013.

[93] Z. Xiong, E. Robert, V. Sarron, J.-M. Pouvesle, and M. J. Kushner, "Atmospheric-pressure plasma transfer across dielectric channels and tubes," J. Phys. D. Appl. Phys., vol. 46, no. 15, p. 12pp, 2013.

[94] G. Uchida, A. Nakajima, K. Takenaka, K. Koga, M. Shiratani, and Y. Setsuhara, "Gas Flow Rate Dependence of the Discharge Characteristics of a Plasma Jet Impinging Onto the Liquid Surface," pp. 1–7, 2015.

[95] A. Yamamoto, Y. Kawano, M. Nakai, T. Nakagawa, T. Sakugawa, H. Hosseini, and H. Akiyama, "Investigation of Gas Flow Dependence of Plasma Jet Produced by Pulsed Power," IEEE Trans. Plasma Sci., vol. 43, no. 10, pp. 3451–3455, 2015.

[96] C. Ungate, D. Harleman, and G. Jirka, "Stability and mixing of submerged turbulent jets at low Reynolds numbers," Energy Lab. Rep., 1975.

[97] M. R. Wertheimer, M. Ahlawat, B. Saoudi, and R. Kashyap, "Accurate in-situ gas temperature measurements in dielectric barrier discharges at atmospheric pressure," Appl. Phys. Lett., vol. 100, no. 20, p. 201112, 2012.

[98] W. S. Boyle and G. E. Smith, "Charge Coupled Semiconductor Devices," Bell Syst. Tech. J., vol. 49, no. 4, pp. 587–593, Apr. 1970.

[99] J.-P. Boeuf, L. L. Yang, and L. C. Pitchford, "Dynamics of a guided streamer ('plasma bullet') in a helium jet in air at atmospheric pressure," J. Phys. D. Appl. Phys., vol. 46, no. 1, p. 015201, Jan. 2013.

[100] A. Shashurin, M. N. Shneider, and M. Keidar, "Measurements of streamer head potential and conductivity of streamer column in cold nonequilibrium atmospheric plasmas," Plasma Sources Sci. Technol., vol. 21, no. 3, p. 034006, Jun. 2012.

[101] Y. Xian, P. Zhang, X. Lu, X. Pei, S. Wu, Q. Xiong, and K. (Ken) Ostrikov, "From short pulses to short breaks: exotic plasma bullets via residual electron control," Sci. Rep., vol. 3, Apr. 2013.

[102] S. Wu, Z. Wang, Q. Huang, X. Tan, X. Lu, and K. Ostrikov, "Atmospheric-pressure plasma jets: Effect of gas flow, active species, and snake-like bullet propagation," Phys. Plasmas, vol. 20, no. 2, p. 023503, 2013.

[103] R. Xiong, Q. Xiong, A. Y. Nikiforov, P. Vanraes, and C. Leys, "Influence of helium mole fraction distribution on the properties of cold atmospheric pressure helium plasma jets," J. Appl. Phys., vol. 112, no. 3, p. 033305, 2012.

[104] I. H. Hutchinson, "Principles of plasma diagnostics.," Princ. plasma diagnostics., by Hutchinson, I. H.. Cambridge Univ. Press. Cambridge (UK), 1990, 379 p., ISBN 0-521-32622-2, Price £ 55.00 (cloth). ISBN 0-521-38583-0, Price £ 14.95 (paper)., 1990.

[105] E. Robert, V. Sarron, T. Darny, D. Riès, S. Dozias, J. Fontane, L. Joly, and J.-M. Pouvesle, "Rare gas flow structuration in plasma jet experiments," Plasma Sources Sci. Technol., vol. 23, no. 1, p. 012003, 2014.

CHAPTER 3

DIAGNOSTIC OF A PLASMA JET SOURCE IMPINGING ON A LIQUID SUBSTRATE

3.1 Literature overview

Diagnostic investigation is crucial to achieve a complete control over plasma generation of reactive species and their delivery to the target substrate for applications purposes. In the last years, the characteristics of APPJs plumes expanding freely in the surrounding atmosphere have been extensively investigated and many relevant parameters such as electron density, electric field, gas temperature, fluid dynamics as well as the reactive species (metastables, radicals and molecules) produced in the plasma plume, have been measured for several different APPJ configurations.
Although the great majority of APPJs applications involve the interaction between the plasma and a surface, nevertheless, up to now the number of published papers focusing on the characteristics of this interaction is extremely limited. Unfortunately, the link between the characteristics of a plasma expanding freely in surrounding gas and the effect on a treated surface of the plasma produced by the same APPJ in identical operating conditions is not trivial, as the presence of a target will in many cases change the properties of the plasma. The reason of this sensitivity of APPJs to the electrical characteristics of the treated surface results from the fact that the surface itself is an element in the electrical circuit of the APPJ. This, together with the alteration of the gas fluid dynamic and composition, results in the properties of the surface not being negligible variables as they effect the dynamics of the incident plasma.

The need for fundamental understanding of the physics of plasma jets interaction with various materials, required for the optimisation of processes of practical use, has prompted the scientific community to address this phenomenon. In a recent paper Robert *et al.* [1] studied the influence of the presence of a metallic target on the gas fluid dynamic in a He plasma jet. Their hypothesis is that the plasma action on the He flow is mainly driven by the drift of ionic species generated in the helium PAPS; in the same paper they underline how the non-negligible modification of the He flow induced by the presence of the target may have large impacts in applications. In another very interesting paper, Guaitella and Sobota [2] reported on the propagation of a plasma jet over different dielectric surfaces and the relative influence, on the propagation dynamics, of gas flow characteristics, voltage amplitude, source dimensions and the capacitance of the target. They attribute the influence of the target on the plasma characteristics to two main mechanism: the local enhancement of the electric field and the supply of pre-deposited charge. They conclude asserting that the development of the jet on a glass surface depends mainly on the gas

flow dynamics over the surface and the capacitance of the target, while voltage amplitude and source geometry play a minor role.

Recently, also computational investigations have been conducted to examine the behaviour of APPJ plasmas interacting with surfaces. In an interesting paper Kushner *et al.* [3] studied the influence of the relative permittivity of a solid target on the characteristics of a He plasma jet impinging on it. Five different values of the relative permittivity were selected to simulate different possible materials ranging from fluorocarbon polymers to metal. The authors found that increasing the permittivity increases the speed of the ionization wave and the electron and ion density in the plasma column increased as well. A lower permittivity instead favoured a larger spread of the plasma across the surface due to the establishment of a surface ionization wave (SIW). Also very recently, Breden and Raja [4] presented their study on the role of the target proximity and the target thickness and dielectric properties on APPJ-surface interaction. They observed that the distance between the APPJ and the surface strongly influence the composition of the species reaching the target surface. For example, short-lived species, such as O and N and charged particles, are relevant only in the case of short gap distance as they are produced on site by the ionization wave while propagating across the target surface.

In APPJs applications, the composition of the surface being treated can greatly differ from case to case, ranging from plastics to biological tissues, from metals to liquids. Especially the treatment of liquids by means of atmospheric plasma is raising increasing interest for its potential use in many application fields. Many recent papers have been focused on the subject of plasma activated water (PAW), produced by means of plasma discharges generated in water or above its surface, for a wide variety of applications [5–8]. Furthermore, common to plasma system interacting with living matter is the presence of a gas-liquid environment (due to blood serum-like liquids), in which the plasma not only is generated in a humid atmosphere but also impinges on a thin layer of liquid covering the tissue [9]. In fact the plasma-produced reactive species and photons mainly react with the liquid film that covers the tissue instead of interacting directly with the tissue itself. Varying the plasma jet characteristics and mediating the plasma-tissue interaction even a thin layer of liquid can greatly influence the treatment response.

If the amount of literature on plasma interaction with substrate is not abundant even less is the amount of papers tackling the subject of plasma in contact with liquid substrate. The subject is computationally addressed in a recent work of Kushner *et al.* [10]. In the paper the interaction of a single electrode APPJ with a 200 μm water layer covering a tissue-like dielectric is investigated. The work is focused on the comparison of cases where the plasma plume is in contact with the liquid surface and other where it is not. Two major modes for delivery of active species to the water layer are identified according to the authors of the paper: one, based on the spreading of the plasma over the liquid surface and enabling photolysis, direct charge exchange reactions and solvation of electrons, dominates in the cases where the plasma touches the water; the other, based on convection and diffusion into the liquid of neutral species formed remotely from the surface, is relevant both in touching and non-touching conditions and is mostly influenced by the residence time of the species at the surface of the water that increase the likelihood of their solvation.

The present study aims to provide further understanding of APPJ-liquid interaction presenting experimental evidences acquired investigating a nanopulsed He APPJ interacting with a water surface. The choice of a water substrate was driven, as already mentioned, by the increasing interest concerning plasma and water applications and the fact that most of the biological tissues usually present a high level of water content. Also motivated by application interests we investigated the APPJ-liquid distance, the applied peak voltage and the pulse repetition frequency as variable parameters because often used to tune plasma surface processes. As mentioned above, the characteristics of the substrate significantly affect plasma characteristics and, in case of liquids, plasma can in turn significantly alter the liquid

characteristics; to minimize the variation of liquid characteristics during plasma treatment we used a buffered saline solution of known conductivity as a substrate; the conductivity of the solutions was monitored during the test and resulted very stable.

Similarly to our previous study on the same plasma source freely expanding in ambient air [PAPER I, II, III], in this chapter we use a combination of two different optical diagnostic techniques (ICCD and Schlieren) to provide insights on APPJ-liquid surface interaction. The achieved results, both confirm the computational work of Kushner and co-workers [10] and present many interesting novel observations. ICCD and Schlieren acquisitions suggest a key effect of gap distance and peak voltage on discharge morphology, propagation velocity and effluent fluid dynamic behaviour. As already observed in previous works [PAPER I and II], a transient turbulent structure propagating along the gas flow after the plasma ignition was also observed in this conditions. The nature of the turbulence, and consequently the induced turbulent structures at the liquid surface, is also strongly affected by the gap distance.

The presented results further confirm that the gas dynamics and the discharge behaviour are strongly influenced by the presence of the liquid substrate and its relative position with respect to the plasma source. It is important to take into account these features, since they in turn play an important role in determining the distribution of gas phase reactive species over the liquid surface and therefore on the effect of the eventual liquid treatment. This study, providing inedited experimental results, may be regarded as a further step in increasing our knowledge of the APPJ-liquid interaction and in the gathering of useful information for the optimisation of plasma jet assisted processes involving liquid substrates.

3.2 Experimental setup

3.2.1 Plasma source and liquid substrate

The schematic of the experimental setup is shown in Figure 1. The plasma source adopted in this work is the *Plasma Jet* developed by Colombo *et al.* and already described in Chapter 2 and in published works [PAPER I and II] along with several results on the characterisation of the source in free flow conditions and its use for different applications [11–13]. For this study the plasma source is driven by a commercial pulse generator (FPG 20–1NMK, FID GmbH) producing high-voltage pulses with nanosecond rise time. The setup adopted for this study is schematically represented in Figure 3.2. The plasma source is in vertical position above the surface of a liquid substrate. The electrical conductivity of the target affects plasma characteristics [1,14] and in turn plasma treatment may alter alters the electrical conductivity of liquid solution [6,15]. For these reasons, the liquid target was realised with a phosphate buffer solution made dissolving sodium phosphate dibasic (Na2HPO4) and monobasic potassium phosphate (KH2PO4) in distilled water, whose conductivity (119 μS/cm) and pH (7.2) are unaffected by plasma treatment. For the tests, a vessel with quartz sidewalls, to allow visualization, and a grounded bottom realized in aluminium plate, was filled with 120 ml of the solution. During experiments, the plasma plume was investigated while impinging on the liquid surface located 5, 10, 15 and 20 mm away from the nozzle and in free flow condition. Furthermore, the influence of the electrical operating conditions was analysed varying the PV from 10 kV to 15 kV and the PRF from 50 Hz to 125 Hz.

3.2.2 Diagnostic techniques

The morphology and the temporal evolution of the plasma discharge interacting with the liquid substrate were investigated by means of an ICCD camera (Princeton Instruments PIMAX3, spectral response 180–900 nm). As shown in Figure 3.1, voltage waveforms were collected on the high voltage cable connecting the plasma source to the pulse generator by means of a high voltage probe (Tektronix P6015A) and a current probe (Pearson 6585) connected to an oscilloscope (Tektronix DPO 40034). To achieve a properly time-resolved visualization of the discharge phenomenon the synchronisation of the camera sensor with the voltage pulse was performed taking into account all possible signal transmission delays with a delay generator (BNC 575 digital pulse/delay generator) in accordance with the guidelines reported in ARTICLE III and already summarized in Chapter 2. The ICCD acquisitions were performed to study the spatial and temporal evolution of the plasma discharge luminous emission during the whole voltage pulse (sequential 10 ns camera gate exposures, 30 accumulations, subsequent frames recorded at fixed time steps of 5 ns).

The Schlieren setup adopted is presented in Figure 3.2 and similar to that described in detail in PAPER I and II. In order to visualize refractive-index gradients generated in the region above and inside the vessel filled with buffer solution, the plasma source was positioned in the middle of the optical path between two parabolic mirrors, as shown in Figure 3.2. Also in this case the camera and the voltage pulse were synchronised by means of the setup already described in Figure 3.1.

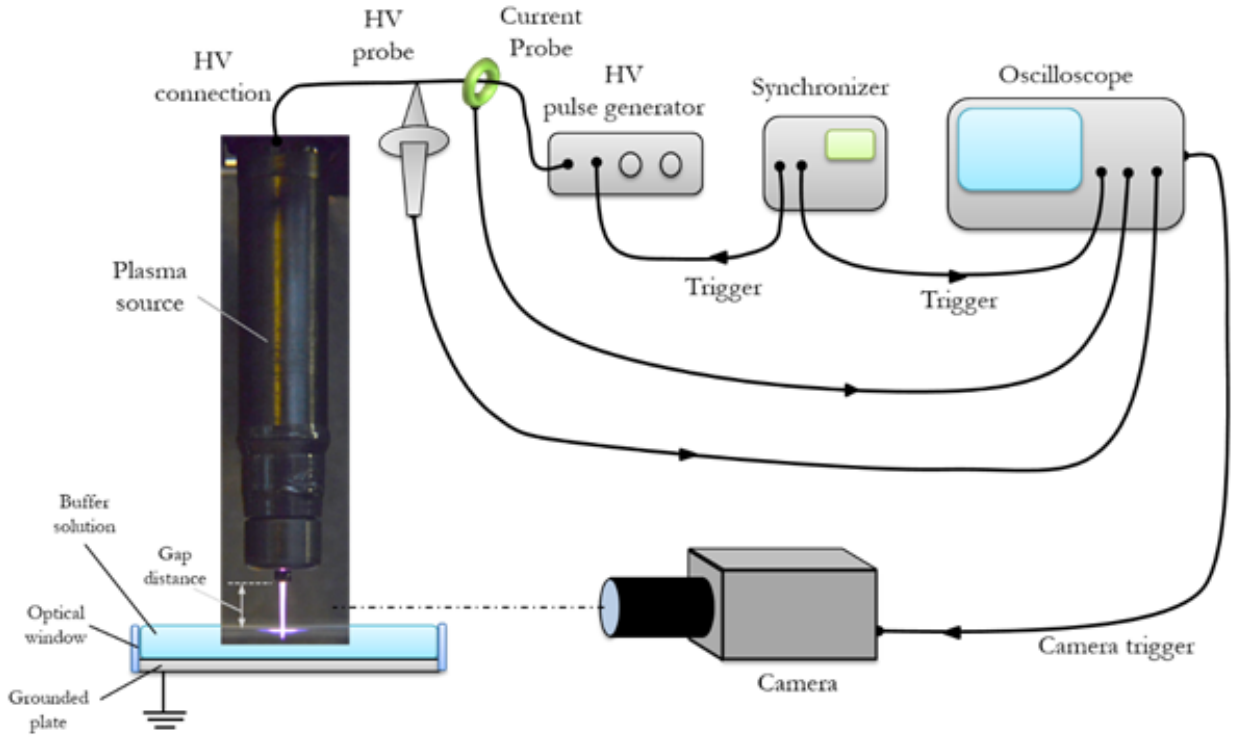

Figure 3.1 Experimental setup

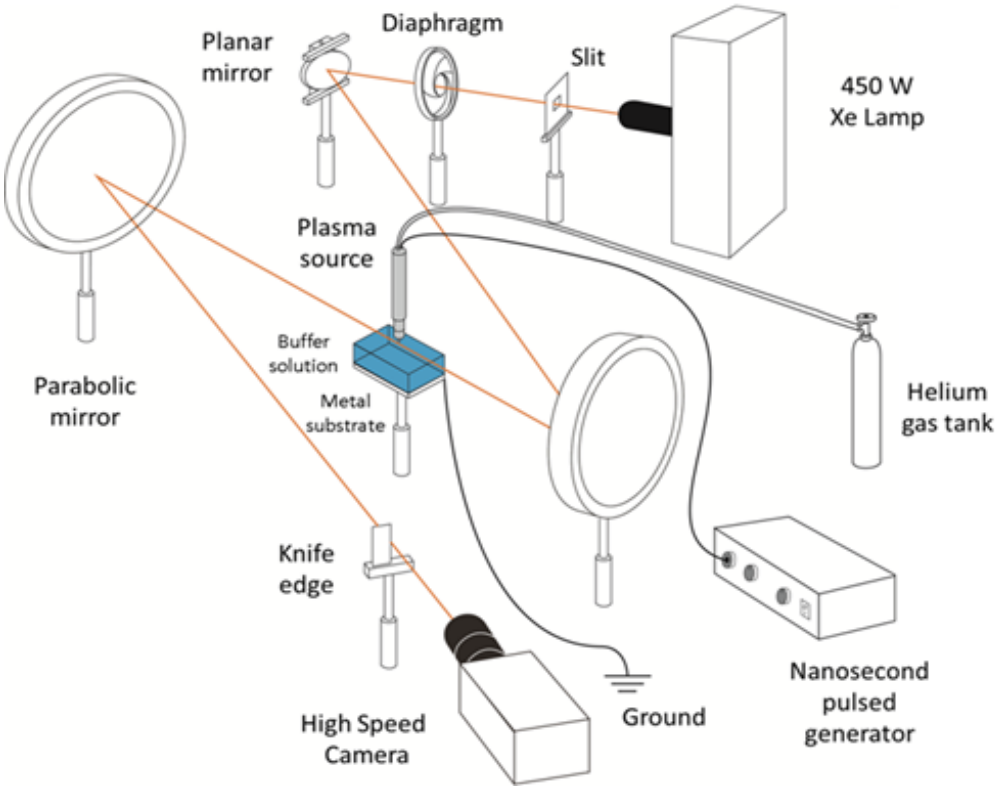

Figure 3.2 High-speed Schlieren imaging setup

3.3 Time resolved plasma emission analysis with ICCD camera

Figure 3.3 presents results for the ICCD imaging of the plasma jet plume, generated at 125 HZ (PRF) and 15 kV (PV), impinging on the liquid substrate for different gap distances. For each condition, a sequence of ICCD images (10 ns exposure) is shown. For the sake of clarity the ICCD camera gates of the presented frames are super imposed on the excitation voltage waveforms in Figure 3.4; the ICCD gate opening for the first frame of each scan was set at t_0 and subsequent frames were recorded at fixed time steps (delays) of 5 ns. The time values reported on each frame are indicative of the time lapse between t_0 and the corresponding camera gate opening. The acquisitions in Figure 3.3 clearly show how the visible plasma emission is strongly influenced by the gap width. The ionization wave generated in the plasma source propagates through the helium channel flowing out of the APPJ and, after a certain time lapse and length, impinges onto the liquid substrate (except for the free flow case). Due to different gap distances and ionization wave velocities, the time required for the plasma to reach the substrate varies depending on the gap width: the closer the distance, the faster the plasma front reaches the substrates. Furthermore, the intensity of the plasma emission for the 5 mm case is higher than in the other cases at the beginning of the voltage rising front. Also only for this case is possible to observe a spreading of the plasma across the liquid surface, sideways respect to the point of impingement. Comparing the 20 mm gap and the free flow cases, the visible plasma emission reaches a greater maximum extension in the case were the substrate is present. Figure 3.5 shows time resolved plasma emission structures for different PV and PRF values with a fixed 10 mm gap. The plasma emission structure and evolution results nearly unaffected by a variation of the peak repetition frequency between from 125 Hz to 50 Hz. On the other hand, a significant modification of the intensity and the structure of the plasma emission is noted when the applied peak voltage is varied. Reducing the peak voltage from 15 kV to 10 kV the appearance of the plasma emission outside the jet nozzle is delayed and its propagation toward the liquid substrate is considerably slower (see second row of frame Figure 3.5). Moreover, in every acquisition the intensity of the plasma emission related to the cases at 10 kV is lower than that of the cases at 15 kV.

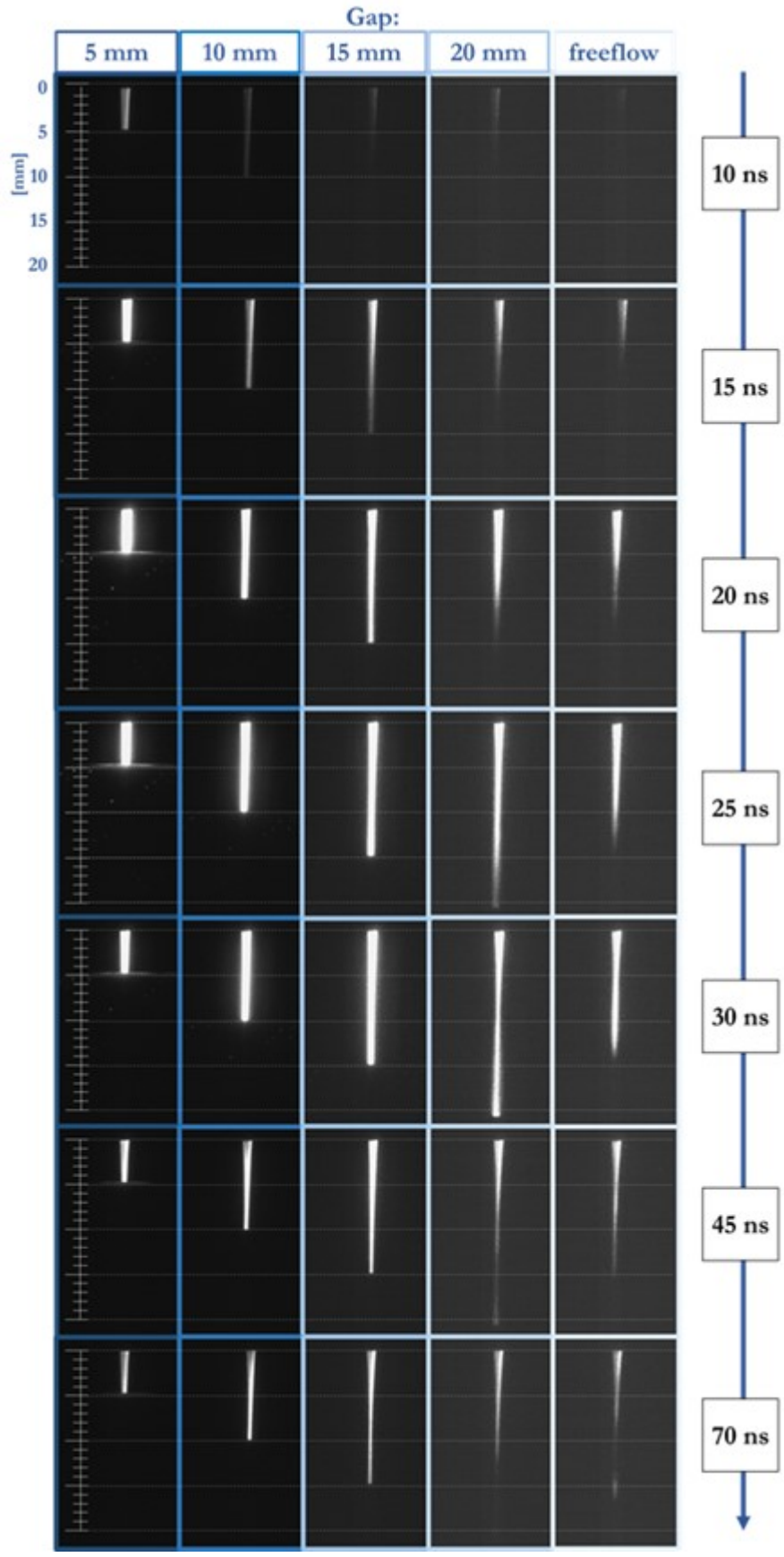

Figure 3.3 Time resolved ICCD imaging of the P*lasma Jet* plume, generated at 125 HZ (PRF) and 15 kV (PV), impinging on the liquid substrate for different gap distances. The time values reported aside are indicative of the time lapse between the trigger at t_0 and the corresponding opening of the ICCD gate.

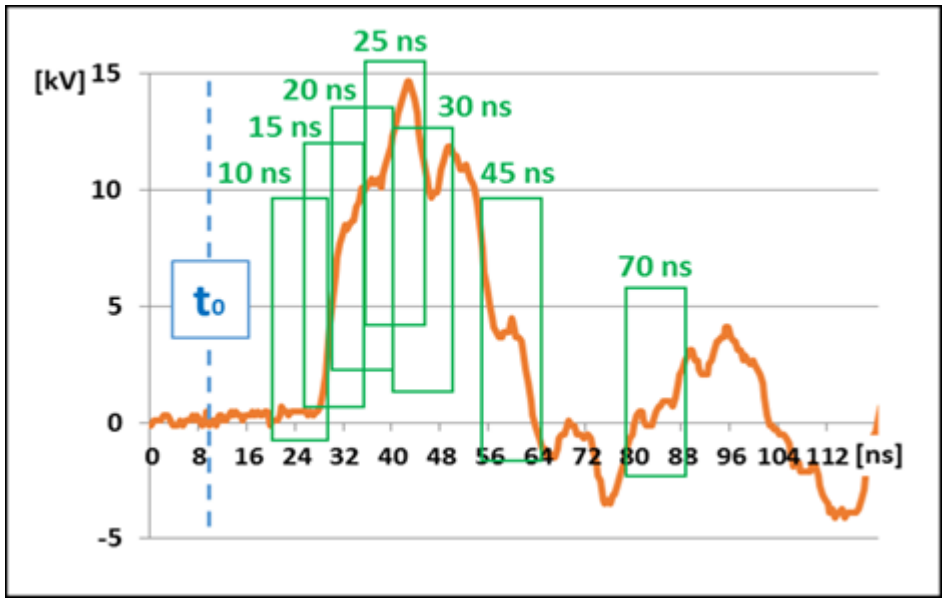

Figure 3.4 Voltage waveform for the case at 15 kV (PV) 125 Hz (PRF) and 10 mm distance. Recorded ICCD gates are superimposed on the voltage waveform with green rectangles. The time values reported on top of each exposure are indicative of the time lapse between the trigger at t_0 and the opening of the ICCD gate.

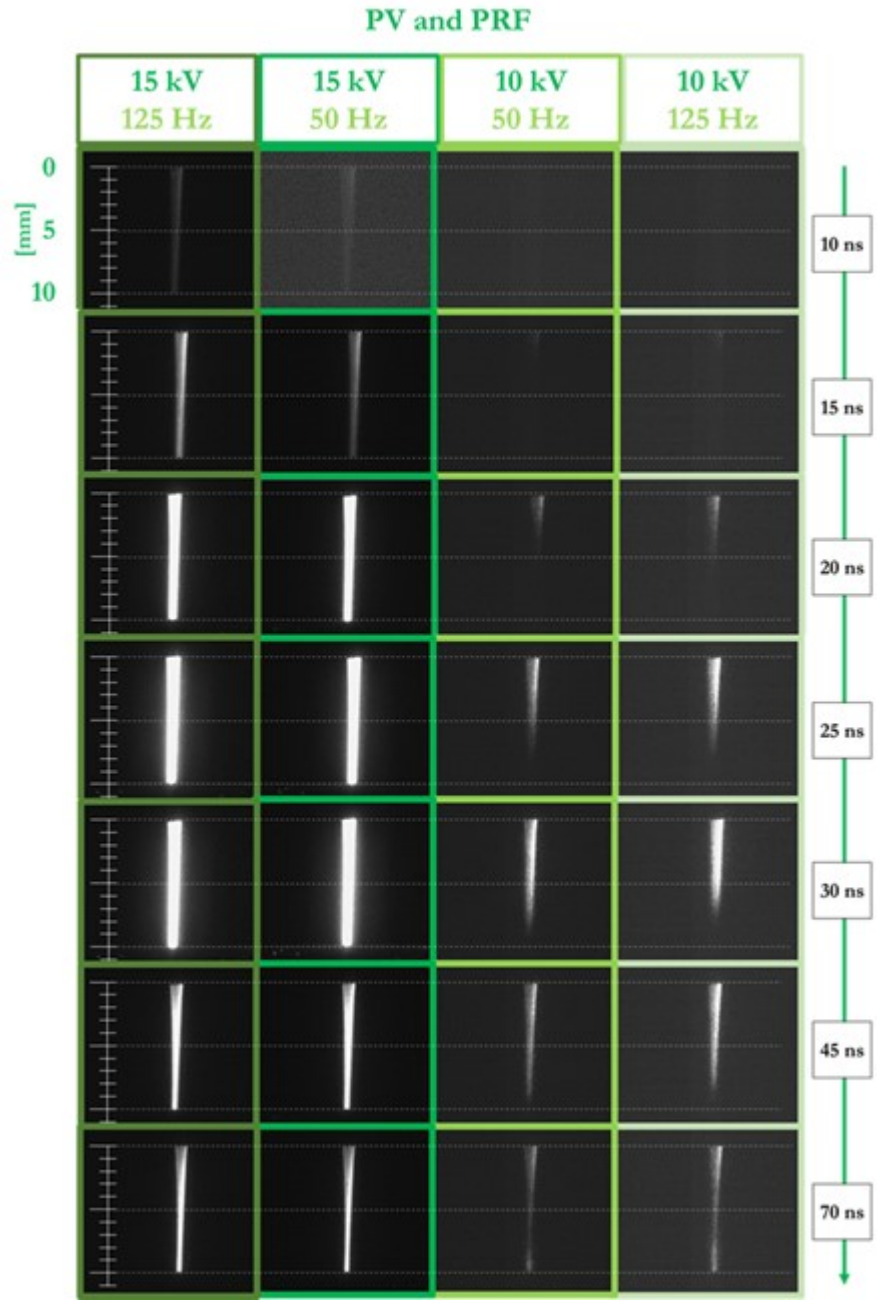

Figure 3.5 Time resolved ICCD imaging of the *Plasma Jet* plume, generated at different PRF and PV, impinging on the liquid substrate at 10 mm gap distances. The reported time values are indicative of the time lapse between the trigger at t_0 and the corresponding opening of the ICCD gate.

3.4 Ionization front velocity and dissipated power

The time resolved ICCD images allowed to estimate the mean velocity of the ionization front during its propagation from the nozzle to the substrate (for the free flow case the mean has been evaluated averaging over the same time lapse as for the 20 mm case); results are reported in Figure 3.6. Both the presence of a liquid substrate and its distance from the plasma source affect the ionization front propagation velocity: the smaller the distance from the liquid substrate, the higher the ionization front velocity. It should be noted that the time resolution of the acquisitions did not allow to observe any difference in velocity between the 5 mm and the 10 mm cases, in fact, both the corresponding plasma plumes reached the substrate in the first acquisition. A reduction of the PV from 15 kV to 10 kV was also found to induce a similar effect, leading to a reduction of the ionization front velocity from 2 x 10^8 cm/s to 2.5 x 10^7 cm/s. The values of the average dissipated power calculated from voltage and current waveforms recorded during the tests are also reported in Figure 3.6; the dissipated power increases as the distance between the source and the liquid target is reduced or as the PV is increased (e.g. for the 15 kV, 10 cm case the dissipated power results nearly four times higher than for the 10 kV, 10 cm condition)..

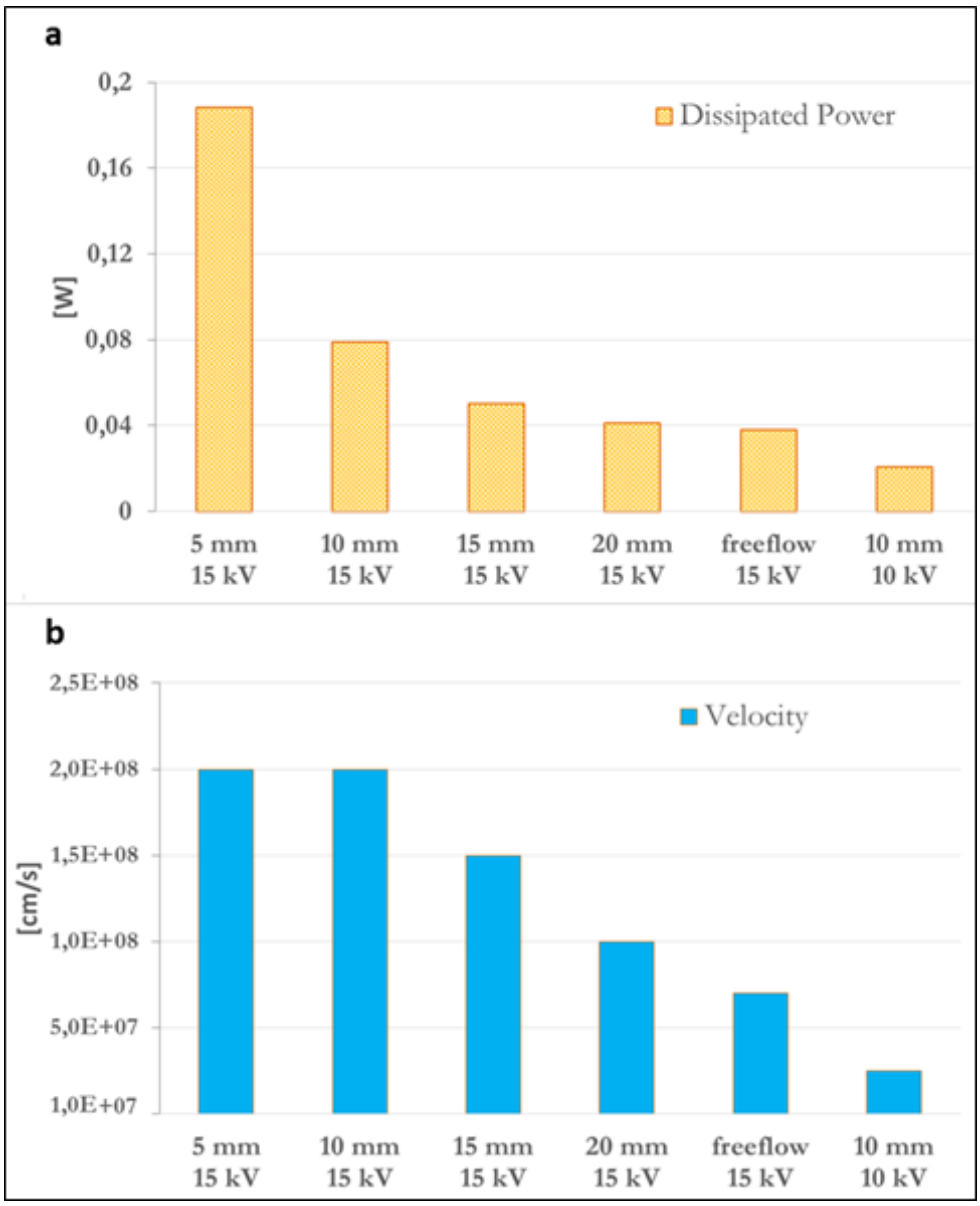

Figure 3.6 Average dissipated power (a) and ionization front velocity (b) of the jet source operating at 125 HZ (PRF) for different gap distances and PV.

3.5 Time resolved investigation of flow regime through Schlieren technique

Figure 3.7 presents results for the Schlieren high speed imaging of the plasma jet plume, generated at 125 HZ (PRF) and 15 kV (PV), impinging on the liquid substrate for different gap distances. Schlieren diagnostic is a qualitative technique, the black and white zones observed in the gas flow correspond to variations of the refractive index gradient due to density gradients between air rich and helium rich regions. In Figure 3.7 a sequence of selected frame is presented for each case. The first frame (0 ms) of each sequence captures the whole plasma discharge as the exposure of the high speed camera is 5 us while the entire plasma emission lasts less than 1 us. The time values reported on each frame are indicative of the time lapse between the acquisition of the first frame and the following one.

Interestingly, in the first frame the He gas flow results completely laminar in all cases; the He effluent expands from the source nozzle into open air forming a confined helium column along to the jet axis . The He then flows above the water surface radially outward from the stagnation point directly under the jet nozzle. Thus, from the first frame of each sequence it could be inferred that the plasma discharge doesn't affect directly the helium gas flow in a discernible way. Nonetheless, a significant modification of the He flow is evidenced in the following frames, therefore several tens of microsecond after the plasma was terminated.

The alteration of the He flow appears after 0.25 ms in the form of a transient turbulent structure across the effluent. The turbulent front coming outside the nozzle is visible only for the cases at 5, 10 and 15 mm and propagates downstream with a velocity similar for these cases and close to the one of the gas flow (~60 m/s). After this transient turbulent structure reaches the liquid surface several eddies are generated around the point of impact. This turbulent structure then move above the liquid surface away from the source axis.

Turbulent fronts appear also in the cases with 20 mm gap and free flow condition, initiating at a distance of 10 mm from the nozzle (1.13 ms after the discharge) and propagating with a velocity similar to the gas flow velocity. In all cases a laminar flow is finally re-established before the next discharge is generated (8 ms period for PRF 125 Hz).

Another detail visible in all the cases with the liquid substrate is the presence of a dimple, caused by the pressure applied by the He flow, on the water surface. As highlighted in Figure 3.8 for the case at 5 mm gap, the depth of the dimple is maximum when the He flow is laminar (e.g. during the plasma discharge); shortly after the turbulent front impact on the liquid surface (approximately 0.50-0.75 ms after the discharge) the dimple start reducing till it reaches its minimum (approximately 2.125 ms after the discharge). Then the dimple depth increases again under the pressure of the re-established laminar flow.

Time resolved plasma emission structures for different PV and PRF for the case at 10 mm gap are shown in Figure 3.9. Similarly to what observed in the ICCD acquisitions, also Schlieren frames present results nearly unaffected by a variation of the peak repetition frequency between 125 Hz and 50 Hz. On the other hand, the dynamic and intensity of the turbulent front generated after the plasma discharge is strongly affected by the peak voltage: reducing the peak voltage to 10 kV no turbulent front is visible until several milliseconds after the discharge, when some eddies are generated over the liquid surface.

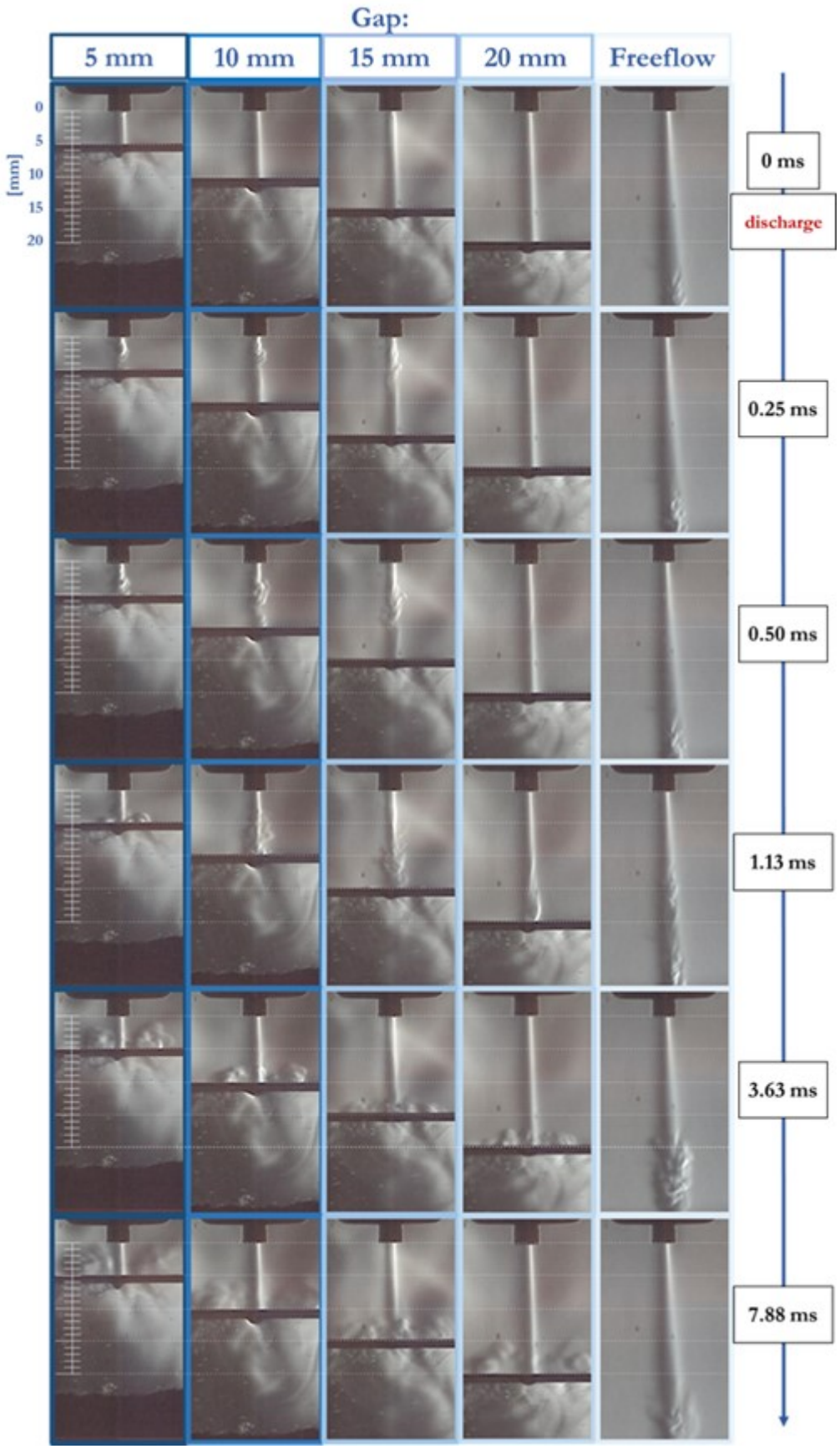

Figure 3.7 Time resolved Schlieren images of the plasma jet plume, generated at 125 HZ (PRF) and 15 kV (PV), impinging on the liquid substrate for different gap distances. The reported time values are indicative of the time lapse between the plasma discharge and the corresponding acquisition of the high speed camera.

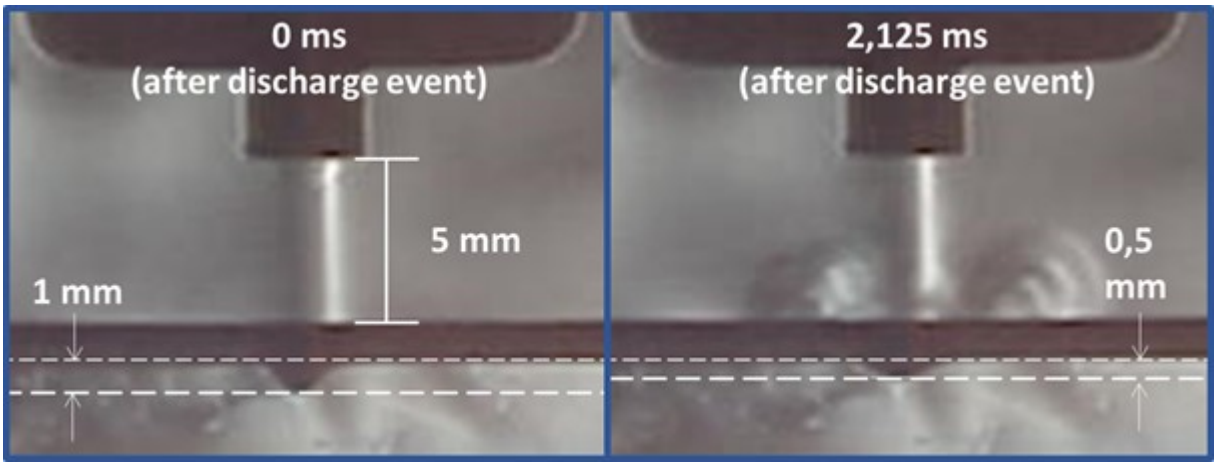

Figure 3.8 Time resolved Schlieren images of the plasma jet plume, generated at 125 HZ (PRF) and 15 kV (PV), impinging on the liquid substrate for different gap distances. The time values reported aside are indicative of the time lapse between the plasma discharge and the corresponding acquisition of the high speed camera.

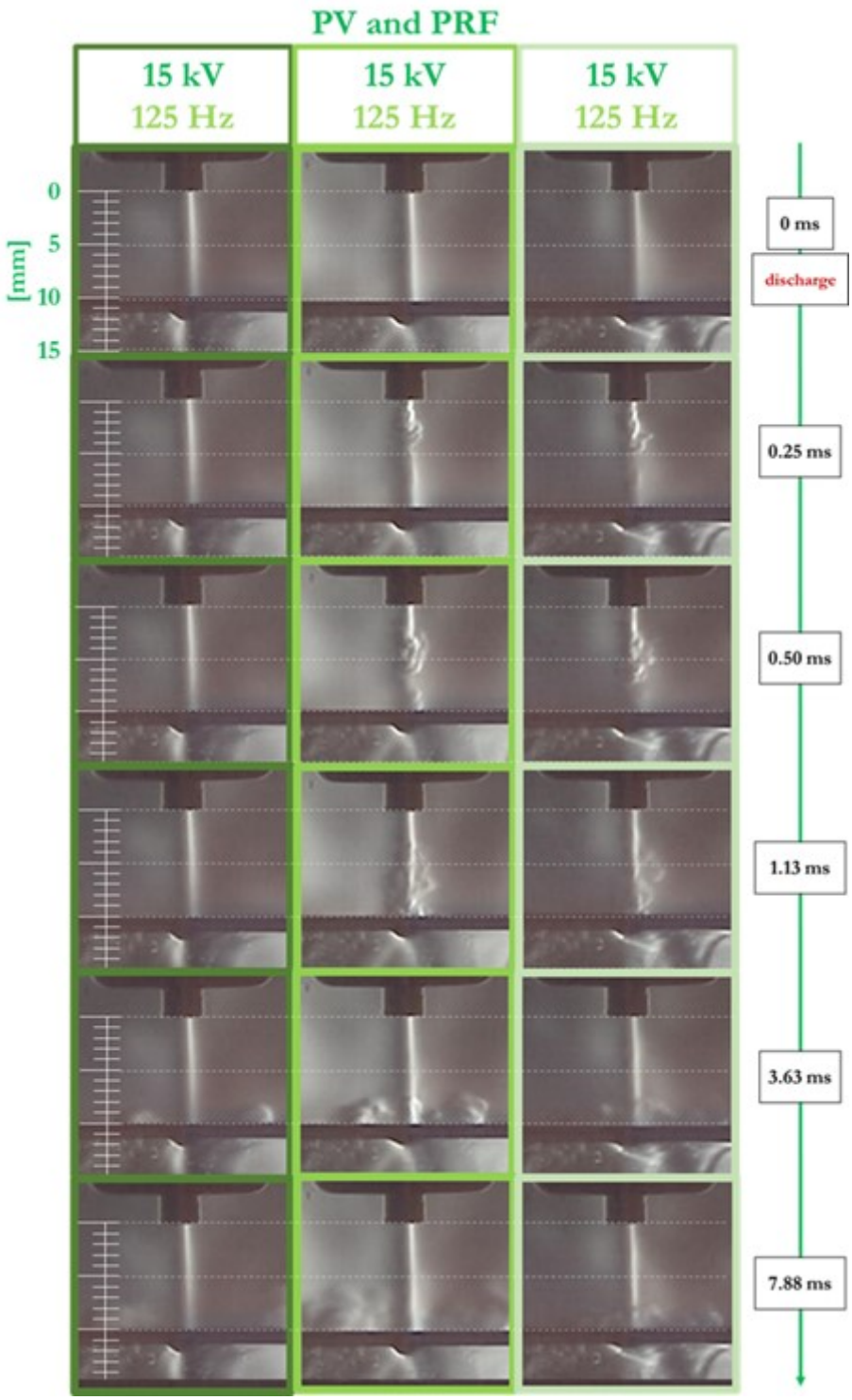

Figure 3.9 Time resolved Schlieren images of the plasma jet plume, generated at different PRF and PV, impinging on the liquid substrate at 10 mm gap distances. The reported time values are indicative of the time lapse between the plasma discharge and the corresponding acquisition of the high speed camera.

3.6 Discussion on plasma-substrate complex interaction

The results presented in the previous section highlight a strong influence of the liquid substrate on different parameters including discharge behaviour (velocity of propagation, emission intensity, morphology, etc…) and gas flow turbulences. These parameters in turns influence each other potentially increasing the effect of the presence of the substrate. For clarity reasons, the discussion of previous results has been divided by argument here in the following:

3.6.1 Discharge morphology, emission and velocity in the presence of a liquid substrate

Focusing on ICCD we observed that the presence of a substrate significantly affects the ionizing wave velocity. For example comparing the case in free flow with the one at 15 mm gap we have an increase in velocity from $7x10^7$ cm/s to $1,5x10^8$ cm/s. This trend is in agreement with the computational results reported by Kushner *et al.* in two recent papers [3,10] where they investigated a plasma source-substrate configuration very similar to our (single electrode APPJ, 1.6 mm nozzle diameter, 4 slm He, 7,5 mm distance to substrate). They investigated the APPJ incident on several surfaces, including one with high values of permittivity representative of liquid water (the case with $\varepsilon = 80$), and reported on how the presence of a substrate can promote a faster, more intense, ionization wave that leads to the formation of a more conductive channel between the high voltage electrode and the target surface. This is confirmed in our ICCD results where the free flow case present an ionization wave much slower and with a lower emission intensity than all the cases with the liquid substrate. Moreover, the velocity and emission intensity of the ionization wave increase as the gap is decreased.
Referring to the literature we can assume that for our plasma source configuration the electric field presents an axial component that enables the plasma to intersect with the liquid surface [16]. It is reasonable to assume that in our case the presence of the liquid substrate results in a higher electric field in the gap. This effect increases as the distance between the high voltage electrode and the substrate is reduced. Therefore, as observed in the ICCD acquisitions, the smaller the electrode-to-dielectric gap the earlier the ionization wave will strikes the surface in virtue of both the reduced distance and the higher propagation velocity.
The hypothesis that the effect of the substrate is mainly conveyed by the electric field in the gap between the source and the substrate is confirmed also by the comparison between the case at 15 kV and 10 kV PV (Figure 3.5). The emission intensity of the discharge and the ionization wave velocity are strongly reduced with the decrease of the applied peak voltage in a similar way as observed when the substrate distance is increased. Concerning the discharge emission and ionization wave velocity the effect of reducing the gap distance results in some way similar to the effect of increasing the peak voltage applied to the high voltage electrode, which is reasonable if we assume that both parameters contribute to increase the electric field in the gap. We can summarise that in general, the speed of the ionization wave, plasma luminous emission and the electric field in the gap all increase when the substrate distance is reduced.

In the case of the smaller gap (5 mm) the ionization wave reaches, the liquid surface earlier than the other cases both in virtue of is greater propagation velocity and the shorter distance. Once the ionization wave impact on the surface the capacitance of the surface is charged and the propagation of a surface ionizing wave is favoured. The charging of the surface layer of the liquid is due to the long relaxation time of the low-conductivity water [10]. The solvation of electrons into water and charge exchange from positive ions with water molecules, occurs on a ps to ns timescale. The low mobility of these charged species in the water confines the transferred charge to the surface of the water for the relatively short duration of the discharge. Other substrate, with different electrical characteristics, would induce probably very

different propagation of the plasma across the surface. Due to the low E/N value the plasma does not self-sustain inside the liquid and instead spreads on the surface of the liquid as the surface charges. Is worth noticing that the He flow from the surface after impinging on the water surface propagates radially over the liquid producing a thin helium layer where the discharge propagation is more favoured than in the surrounding air. This phenomenon is clearly visible in the ICCD acquisition in Fig 3.3 where light emission form the surface ionization wave are visible for the 5 mm case from 15 to 45 ns. The ionization wave apparently spreads across the surface. The formation of a visible surface ionization wave is not detected for other cases than the one at 5 mm gap. For all the cases, when the ionization wave impacts the water surface, only a small fluence of electrons has reached the surface and there is a little charging of the surface. The charging of the surface continues to occur in the following instant and strongly depends on the duration of the discharge. A possible explanation of the different behaviour of the 5 mm case is that in the other cases the ionization wave requires more time to reach the liquid surface, therefore, the time lapse between the moment of the strike and the end of the high voltage pulse is reduced. This reduced time lapse is probably not sufficient to grant enough charging of the capacitance of the surface. In turn, the limited surface charging of the dielectric can not produce a sufficiently high horizontal components of the electric field to sustain the formation of a SIW. Being the capacitance of the substrate identical in all cases the RC time constant for charging the surface is the same. What changes is the time available for the charging, that depends on the time required by the ionization front to reach the surface, that in turn depends on the gap distance. This difference can lead to significant effect for applications purposes. For example for the 5 mm case where the plasma spread over the liquid surface we can guess that a larger density of hydroxyl radical (OH) is produced adjacent to the water by the plasma interacting with the evaporating water vapour. The absence of the spreading of the plasma on the liquid in most of the cases significantly reduces the inventory of OH available. Photolysis of the water molecules in the liquid substrate also result much more significant when the plasma spreads over the surface [10].

It is worth mentioning that for the case at 20 mm the discharge remains in contact with the substrate for a very short time lapse (less than 20 ns) and that its emission in proximity of the surface is generally of lower intensity than near the nozzle. Consequently, the plasma plume generated by the source appears as not touching the liquid when observed by the naked eye or standard cameras (results not presented). This highlights the importance of ICCD observation of the phenomenon because, as observed by Kushner and colleagues [10], significantly different results for the reactive species composition in the liquid are observed whether the plasma is touching or not-touching the liquid. The same is expected for the electric field sensed by the substrate that is of particular relevance in the case of living tissues.

3.6.2 Substrate effect on gas flow and transient turbulent structure generation

In a gas jet with a circular cross-section such as studied in this work, the initial conditions at the nozzle exit determine the flow dynamics in the downstream region [17–19]. The Reynolds number (Equation 1) is considered as one of determining factors of these conditions. As reported in PAPER I, in our configuration the Reynolds number of the jet without plasma ignition is estimated to be 570 Re. According to Ungate *et al.* [20] if the Reynolds number falls inside a transition range (between 500 and 1000) the jet would become unstable at certain distance from the nozzle. For a configuration similar to our, the onset of the turbulence is expected to occur at about $50r_0$ from the outlet, where r_0 is the jet radius [10,21]. This is in agreement with the Schlieren acquisitions for the free flow case where it is observable a laminar flow up to about 25 mm away from the nozzle where a turbulent transition takes place.

According to Schlieren acquisitions, for the examined cases, it may be assumed that the presence of the liquid substrate does not affect the characteristic of the flow at the nozzle when the plasma is not ignited. Being the maximum investigated gap distance (20 mm) shorter than the distance for the onset of a turbulent transition, in our study the He flow between the source outlet and the substrate results completely laminar. When the liquid substrate is present, the He flow that impacts on its surface, generating a dimple, is deflected and start to propagate across the liquid surface away from the source axis. Is worth mentioning that the propagation of the He flow over the liquid surface is not visible in the acquisitions because of the presence of the water meniscus at the quartz wall that shadow the region few millimeters above the surface.

According to Kotsovinos [22] the Richardson number (Ri) expresses the ratio of potential to kinetic energy and as such reflects the influence of buoyancy on the flow.

Equation 1

$$Ri = \frac{gD(\rho_{air}-\rho_{He})}{V^2\rho_{air}}$$

From the definition of the Ri (Equation 1) where υ is the gas velocity; D is the characteristic length; g is the gravitational acceleration; ϱ_{∞} and ϱ_{gas} are the gas density of the surrounding and the core zone, respectively [23,24], we can esteem for our configuration a Richardson number of approximatively $1x10^{-5}$. As reported by Kotsovinos, being our Ri<<1 we can assume that buoyancy has a negligible effect on the flow for the region from the exit of the quartz tube to the onset of the turbulent transition. This result is in agreement with that found by Bruggeman *et al.* [25] even if for a slightly different APPJ configuration.

Very interestingly, after the plasma is ignited, a transient turbulent structure coming from the source outlet is observed to propagate downstream the He flow. Anyway, differently from what one may expect no modification of the gas flow is visible when the plasma discharge takes place (0 ms in Schlieren acquisitions, Figure 3.7). Apparently, the ionization wave and the formation of a conductive channel on a nanosecond time scale do not affect the gas property in such a way that it results visible by Schlieren technique. What is detected is a transient turbulent structure that propagates outside the nozzle 0.25 ms after the plasma discharge. The turbulent structure propagates downstream the He flow with a velocity compatible with that of the He flow and therefor much lower than that of the ionization front. The observed transient turbulent structure correlate well with those observed by Bruggeman *et al.* [25], even if of smaller dimension. We may assume, as for their case, that this turbulent structure is linked to an increase in the gas temperature that increases the gas velocity. The turbulence is obviously a consequence of the discharge but the mechanism is someway more complex than the direct heating of the ionized gas by the ionization process. The intensity of the turbulent structure results affected by the gap distance and the PV and therefore we may assume that it is driven by the plasma generation and therefore affected by the characteristics of the discharge generating the instability.

The results lead us to believe that the turbulence is due to a heating effect of the high voltage electrode on the surrounding He gas inside the plasma source. The high voltage electrode is sharply heated by Joule effect during the short plasma discharge. The electrode surface in turns then heats the surrounding gas, that, increasing in temperature varies its density. The less dense and faster moving flow from the nozzle interacts with the slower moving flow downstream, forming turbulent structures that propagate downstream the effluent. According to this explanation, the magnitude of the alteration should be proportional to the amount of heat released by the electrode. This in turn is related to the characteristics of the plasma discharge that are, as observed before, influenced by the presence and the distance of the liquid substrate. Increasing gas heating would lead to greater density variations and earlier perturbation development in the jet. This statement is supported by the observation that increasing the gap the average dissipated power reduce and the intensity of the flow instability reduces as well. In fact, in Schlieren

acquisitions the turbulent front is clearly visible outside the nozzle only for the cases with 5 and 10. For the case with 15 mm gap the turbulent flow is more difficult to discern near the nozzle while for the case with 20 mm gap and the free flow one the turbulent front is detected only 15 mm away from the nozzle. Probably in this region, the difference between the He flow and the surrounding air velocity is such that small variations like those induced by the discharge in these two configurations are sufficient to induce a turbulent regime transition. Near the nozzle the He flow velocity is supposedly higher and a greater variation is necessary to induce a visible effect in the flow regime.

The hypothesis is further supported also by the comparison between the cases at 10 and 15 kV PV which have a dissipated power of 0,08 W and 0,02 W respectively. No sensible variation in the He flow during the discharge is observed in both cases. Anyway, while in the 15 kV case after 0.25 ms a distinct turbulent front is visible at the outlet of the source in the 10 kV case no visible alteration of the flow is observed. The only sign of alteration of the gas flow for the 10 kV case is observed after the heated volume of He has hit the substrate. At 3.63 ms (Figure 3.9) the formation of turbulent structures is clearly visible on the surface of the liquid. The position and timing of the turbulent structures on the liquid surface is similar for both 10 kV and 15 kV. The fact that the instability result visible only later in the case at lower PV is probably to attribute to a minor alteration of the gas flow velocity that becomes relevant only after the flow velocity is reduced after the impact on the substrate.

The identification of gas heating as a possible key mechanism leading to the velocity increase of the gas and the reduction of the laminar length in APPJ has been previously advanced in some works [26,27] [PAPER I and II] as also the correlation between the average dissipated power and the effects on the flow dynamics [25]. Anyway, this probably the first work where a complete temporal decoupling between the plasma discharge phenomenon and the induced modification of the gas flow is observed. The effect of ion momentum transfer that is still debated as a possible cause of acceleration of the velocity of the gas flow in APPJs can be excluded in our case. A necessary condition for this effect to be important is in fact the occurrence of zones with space charge separation, that in the *Plasma Jet*, can be achieved only in the ionization fronts. If the effect of the ion drag would be important compared to thermal effects, one should observe some obvious flow regime distortion when the plasma is ignited, which is not the case in our configuration. Moreover the occurrence of the transient turbulent structure downstream the He flow follows a millisecond time scale that is absolutely compatible with a thermodynamic effect.

3.6.3 Effect of peak voltage (PV) and pulse repetition frequency (PRF) in the presence of a liquid substrate

ICCD and Schlieren result showed how a higher PV induces a higher plasma emission and a faster ionization wave that in turn lead to a more significant alteration of the gas flow. Achieved results support the hypothesis that one of the main effect of the substrate is an alteration of the electric field in the gap between the high voltage electrode and the liquid surface. The effect of increasing the gap distance results similar in some way to the effect of reducing the peak voltage applied to the high voltage electrode. This observation underline the importance of considering the substrate-source distance as a non-negligible parameter because its influence on plasma discharge characteristic is of considerable relevance.

It has been observed that the characteristics of the plasma discharge and of the transient turbulent structure generated are not directly affected by the PRF. It should be noted anyway that the range of frequencies investigated here is such as the laminar flow regime is re-established in the time lapse between one pulse and the following. Indeed, each ionization wave see an ideally unperturbed helium channel. The results of this study are therefore applicable to conditions of initial laminar flow with PRF of less

than few kHz where the plasma activated gas and heat induced turbulent front flow out of the effluent volume between two consecutive pulses.

Another effect, that may become relevant at higher PRF than those here investigated, is the gap distance variation due to the dimple relaxation. The dimple is an alteration of the liquid surface present even when the plasma is not ignited as is due to the pressure applied by the He flow on the liquid surface. Anyway, as can be observe in Schlieren acquisition, and highlighted in Figure 3.8 the dimple depth variates because of the impact of the transient turbulent structure induced by the plasma discharge. The dimple variation should not be regarded as a minor effect as it actually modify the source-surface distance and therefor may influence the electric voltage in the gap if during its relaxation a second plasma discharge were to ignite. This occurrence is driven by the PRF and therefor may lead, in the presence of a liquid substrate, to an indirect effect of the PRF on the plasma discharge electrical characteristics. Especially for the cases where the dimple depth variation is comparable to the gap distance these effect too should not be neglected (ex. the 5 mm case where the dimple variation 0,5 mm is about 10% of the gap distance).

3.7 References

[1] E. Robert, V. Sarron, T. Darny, D. Riès, S. Dozias, J. Fontane, L. Joly, and J.-M. Pouvesle, "Rare gas flow structuration in plasma jet experiments," Plasma Sources Sci. Technol., vol. 23, no. 1, p. 012003, 2014.

[2] O. Guaitella and a Sobota, "The impingement of a kHz helium atmospheric pressure plasma jet on a dielectric surface," J. Phys. D. Appl. Phys., vol. 48, no. 25, p. 255202, 2015.

[3] S. a. Norberg, E. Johnsen, and M. J. Kushner, "Helium atmospheric pressure plasma jets touching dielectric and metal surfaces," J. Appl. Phys., vol. 118, no. 1, p. 013301, 2015.

[4] D. Breden and L. L. Raja, "Computational study of the interaction of cold atmospheric helium plasma jets with surfaces," Plasma Sources Sci. Technol., vol. 23, no. 6, p. 065020, 2014.

[5] P. Lukes, E. Dolezalova, I. Sisrova, and M. Clupek, "Aqueous-phase chemistry and bactericidal effects from an air discharge plasma in contact with water: evidence for the formation of peroxynitrite through a pseudo-second-order post-discharge reaction of H 2 O 2 and HNO 2," Plasma Sources Sci. Technol., vol. 23, no. 1, p. 015019, 2014.

[6] R. Laurita, D. Barbieri, M. Gherardi, V. Colombo, and P. Lukes, "Chemical analysis of reactive species and antimicrobial activity of water treated by nanosecond pulsed DBD air plasma," Clin. Plasma Med., vol. 3, no. 2, pp. 53–61, 2015.

[7] K. Wende, P. Williams, J. Dalluge, W. Van Gaens, H. Aboubakr, J. Bischof, T. von Woedtke, S. M. Goyal, K.-D. Weltmann, A. Bogaerts, K. Masur, and P. J. Bruggeman, "Identification of the biologically active liquid chemistry induced by a nonthermal atmospheric pressure plasma jet," Biointerphases, vol. 10, no. 2, p. 029518, 2015.

[8] H. Jablonowski and T. von Woedtke, "Research on plasma medicine-relevant plasma-liquid interaction: What happened in the past five years?," Clin. Plasma Med., vol. 3, no. 2, pp. 42–52, 2015.

[9] R. Rhoades and D. Bell, Medical Phisiology: Principles for Clinical Medicine. 2012.

[10] S. a Norberg, W. Tian, E. Johnsen, and M. J. Kushner, "Atmospheric pressure plasma jets interacting with liquid covered tissue: touching and not-touching the liquid," J. Phys. D. Appl. Phys., vol. 47, no. 47, p. 475203, 2014.

[11] A. Liguori, E. Traldi, E. Toccaceli, R. Laurita, A. Pollicino, M. L. Focarete, V. Colombo, and M. Gherardi, "Co-Deposition of Plasma-Polymerized Polyacrylic Acid and Silver Nanoparticles for the Production of Nanocomposite Coatings Using a Non-Equilibrium Atmospheric Pressure Plasma Jet," Plasma Process. Polym., p. n/a–n/a, Oct. 2015.

[12] R. Laurita, M. Zaccaria, M. Gherardi, D. Fabiani, A. Merlettini, A. Pollicino, M. L. Focarete, and V. Colombo, "Plasma Processing of Electrospun Li-Ion Battery Separators to Improve Electrolyte Uptake," Plasma Process. Polym., vol. 13, no. 1, pp. 124–133, Jan. 2016.

[13] A. Liguori, A. Pollicino, A. Stancampiano, F. Tarterini, M. L. Focarete, V. Colombo, and M. Gherardi, "Deposition of Plasma-Polymerized Polyacrylic Acid Coatings by a Non-Equilibrium Atmospheric Pressure Nanopulsed Plasma Jet," Plasma Process. Polym., vol. 13, no. 3, pp. 375–386, 2016.

[14] D. Riès, G. Dilecce, E. Robert, P. F. Ambrico, S. Dozias, and J.-M. Pouvesle, "LIF and fast imaging plasma jet characterization relevant for NTP biomedical applications," J. Phys. D. Appl. Phys., vol. 47, no. 27, p. 275401, 2014.

[15] P. Lukes, E. Dolezalova, I. Sisrova, and M. Clupek, "Aqueous-phase chemistry and bactericidal effects from an air discharge plasma in contact with water: evidence for the formation of peroxynitrite through a pseudo-second-order post-discharge reaction of H 2 O 2 and HNO 2," Plasma Sources Sci. Technol., vol. 23, no. 1, p. 015019, 2014.

[16] J. L. Walsh and M. G. Kong, "Contrasting characteristics of linear-field and cross-field atmospheric plasma jets," Appl. Phys. Lett., vol. 93, no. 11, p. 111501, 2008.

[17] X. Grandchamp and A. Van Hirtum, "Near Field Round Jet Flow Downstream from an Abrupt Contraction Nozzle with Tube Extension," Flow, Turbul. Combust., vol. 90, no. 1, pp. 95–119, Jan. 2013.

[18] V. V. Kozlov, G. R. Grek, A. V. Dovgal, and Y. A. Litvinenko, "Stability of Subsonic Jet Flows," J. Flow Control. Meas. & Vis., vol. 01, no. 03, pp. 94–101, 2013.

[19] Y. A. Litvinenko, G. R. Grek, G. V. Kozlov, A. M. Sorokin, and M. V. Litvinenko, "Development of a free round jet at different conditions at the nozzle exit under an acoustic action," in Progress in Flight Physics, 2012, pp. 429–448.

[20] C. Ungate, D. Harleman, and G. Jirka, "Stability and mixing of submerged turbulent jets at low Reynolds numbers," Energy Lab. Rep., 1975.

[21] F. J. Armenio Vincenzo, Geurts Bernard, "Direct and Large-Eddy Simulation VII," in Direct and Large-Eddy Simulation VII: Proceedings of the Seventh International ERCOFTAC Workshop on Direct and Large-Eddy Simulation, held at the University of Trieste, September 8-10, 2008, 2010, p. 646.

[22] N. E. Kotsovinos, "A study of the entrainment and turbulence in a plane buoyant jet," 1975.

[23] H. Petersen, "The properties of helium: density, specific heats, viscosity, and thermal conducdivity at pressures from 1 to 100 bar and from room temperatur," 6 jellerups Boghandel, no. 224, pp. 1–42, 1970.

[24] R. S. Davis, "Equation for the Determination of the Density of Moist Air (1981/91)," Metrologia, vol. 29, no. 1, pp. 67–70, Jan. 1992.

[25] S. Zhang, a Sobota, E. M. van Veldhuizen, and P. J. Bruggeman, "Gas flow characteristics of a time modulated APPJ: the effect of gas heating on flow dynamics," J. Phys. D. Appl. Phys., vol. 48, no. 1, p. 015203, 2015.

[26] J.-S. Oh, O. T. Olabanji, C. Hale, R. Mariani, K. Kontis, and J. W. Bradley, "Imaging gas and plasma interactions in the surface-chemical modification of polymers using micro-plasma jets," J. Phys. D. Appl. Phys., vol. 44, no. 15, p. 155206, 2011.

[27] M. Ghasemi, P. Olszewski, J. W. Bradley, and J. L. Walsh, "Interaction of multiple plasma plumes in an atmospheric pressure plasma jet array," J. Phys. D. Appl. Phys., vol. 46, no. 5, p. 052001, 2013.

CHAPTER 4
NON-EQUILIBRIUM ATMOSPHERIC PRESSURE PLASMAS FOR BIOMEDICAL APPLICATIONS

4.1 Literature overview

The last century has witnessed many advances in the medical field that have contributed to increase the life expectancy by over 30 years [1,2]. Despite this huge progress, medicine is still facing considerable and increasing challenges. The aging of population, unhealthy lifestyles, degenerative diseases and multidrug resistant bacteria are causing increasing needs in the health care sector worldwide [3–8]. This situation makes it necessary to find innovative, effective, and less expensive ways for medical therapy and has prompted significant investments in various research fields for the development of new technologies. Plasma technology, especially at atmospheric pressure, is a relatively newcomer to the biomedical field even though its first application can be dated back to the late 19th century when Siemens developed plasma discharges in order to create ozone to clean biologically contaminated water [9–11]. Starting from early studies at low pressure in the '70s-'80s of the last century [12,13], plasma research has recently evolved at a rapid pace and extended in many biomedical applications [14]. Space uniform and well controlled CAP have become a reality in the last decades and their potential to provide breakthrough solutions to challenging medical problems has been proved by the work conducted at several major universities, research centers and hospitals around the world [14]. CAP can be directly used to promote wound healing and to treat skin, and dental diseases [14,15]. It has also proven to be promising for the treatment of blood and different forms of cancer [14,15]. Plasma has been proved to be able to disinfect different surfaces including living tissues, deactivate dangerous drug resistant pathogens including those in food and drinks, and stop serious bleeding without damaging healthy tissue.

Early applications of plasma for health care date back to the middle of the late 19th century, when the term *Plasma Medicine* has not been coined yet, and emerge from the popularity of electrotherapy. First experimental approaches to therapeutic plasma applications include, apart from Siemens ozone generation, carbon arc lamps to treat high blood pressure and electrotherapeutic devices such as the Violet Ray devices [16]. After a latent period, in the second half of the 20th century plasma was again investigated and used to improve the biocompatibility or biofunctionality of materials, which are supposed to be in direct contact with biological systems [17]. Medical materials or devices that can be treated or produced using plasma technology range from medical implants, catheters and in general materials in direct short-term or permanent contact with living tissue, up to laboratory disposals for cell cultivation, diagnostic tools or scaffolds for tissue engineering [16]. Because most of these devices are made from synthetic polymers, that are usually thermosensitive materials, cold plasmas close to room temperature are generally necessary for such treatments.

Apart from functionalization of materials, another very important field of plasma application closely related to plasma treatment of surfaces is the use of plasmas for the bio-decontamination of materials or devices. The trend to replace glass and steel with polymeric materials in medical devices resulted in an urgent need of sterilization procedures that are no longer based on heat and high temperatures. The first mention of the use of plasma as a sterilizing agent is found in a patent by Menashi in 1968 [18], where an apparatus is described in which a pulsed RF field is used to create an argon plasma at atmospheric pressure. As reported by several studies, the steadily increasing percentage of microorganisms exhibiting resistance to multiple antibiotics pose a serious threat to public health and new bactericidal agents are in great demand [8,19–21]. CAP is regarded as a promising candidate for combating drug resistant infections as no development of resistance against plasma treatment has yet been reported [19,20]. Nowadays, several research groups and companies are working on the development of atmospheric pressure plasma sources to sterilize and bio-decontaminate medical materials and devices as well as for general applications in the field of hygiene [22–26]. Despite strong research efforts, at present, there is only one commercially available system for the decontamination of medical materials based on atmospheric pressure plasma technology, the TipCharger, a device for cleaning pipette-like fluid delivery systems [16,27].
Within the field of plasma biomedical applications, the term *Plasma Medicine* is usually adopted in reference to the plasma treatment of living cells, tissues, and organs [16]. Some of the earlier applications of plasma in medicine relied mainly on the thermal effects of plasma. Starting indeed from the 1970s, atmospheric pressure thermal Ar plasmas are now commonly adopted to assist surgery as an efficient alternative to conventional electrocauterization [14,28,29]. Hot plasma is also being employed to cut tissue [29] although the exact mechanism by which this cutting occurs remains unclear. Heat delivered by plasma has also been investigated recently for cosmetic application in skin rejuvenation and regeneration [30,31].

A well-established area of medical application of thermal atmospheric pressure plasma jets is the electrosurgical method of argon plasma coagulation (APC, also sometimes called argon beam coagulation) that adopts argon discharges for tissue coagulation (Erbe Elektromedizin GmbH Tübigen, Germany; www.erbe-med.com). In Ar plasma coagulation, highly conductive plasma replaced the metal contacts in order to pass current through tissue avoiding the difficulties with tissue adhesion. Another electrosurgical technique based on plasma application is the so called *coblation* ("cool ablation"; ArthroCare Corp., Austin, TX, USA; www.arthrocare.de) where a compact bipolar electrode system is immersed in a conductive medium. The highly localized plasma created between the electrodes generates ions, reactive atoms or molecules, as well as electromagnetic radiation, able to break organic molecules and therefore induce ablation of tissues. In this way, a controlled non-heat driven ablation can be performed without tissue necrosis. A third example of commercially available plasma based medical device is the *PlasmaJet* (Plasma Surgical, Inc., Roswell, GA, USA; www.plasmasurgical.com), which is based on a bipolar electrode system with low argon flow used to cut or coagulate tissue. Even if these techniques are closely related to the plasma sources studied in this dissertation for therapeutic applications (Chapter 4 sections 4.2-4.5), their operation is mostly based on heat transfer and on a destructive plasma interaction with the living tissue.

Plasma effects not based on heat transfer are the main focus of more recent research on applications of plasma in medicine. These effects are so interesting and promising because tunable for various sub-lethal purposes such as wound healing [32,33], cell detachment [34,35], genetic transfection [14,36,37] and others. Moreover, non-thermal effects can be selective in achieving a desired result for a small part of a living tissue while having little effect on the surrounding tissue. Significant progress on the molecular mechanisms of plasma-cells interaction has only been made in the past decade [32]. The role of oxidants and antioxidants has increasingly been pinpointed in recent redox biological work [38–40]. Also, an ever increasing body of information is available on controlling and tuning the plasma and its characteristics to induce specific biological responses [41–43]; for example targeting to the interaction of a specific plasma component (e.g. UV radiations, specific RNS or ROS molecules) with the living cells in order to promote

either the stimulation or inhibition of cellular functions. From data available in the literature it is possible to summarize some of the plasma effects induced on mammalian cells or biochemical pathways that have been discovered. Plasma was found to potentially influence:

- cell migration
- cell proliferation
- angiogenesis
- detachment of cells from matrices
- expression of cell surface proteins (ex. integrins, cadherins,)
- detachment of cells from cell clusters
- DNA integrity
- apoptosis induction/inactivation of cancer cells
- reversible cell membrane permeabilization
- blood coagulation
- gene transfection

Recently, first efforts to systematize mechanisms of plasma–cell interactions have been made based mainly on indirect evidence and analogies [16,44] nevertheless details of this interaction are still elusive at the moment. One reason for this situation is the fact that, despite CAP medical research is only a few years old, published results have been achieved using a broad spectrum of different atmospheric pressure plasma sources with a very limited comparability. Plasma sources strongly differ from each other making it challenging to summarize or even compare results from different types of sources from a biological or physical point of view. Nevertheless, plasma treatments can be fit into two major categories: direct and indirect treatment. In direct plasma treatment, the plasma comes into direct contact with the treated tissue, which therefore plays the role of one of the plasma source electrodes. The treated tissue, usually grounded or at floating potential, being in contact with the plasma may be cross by some current in the form of either a small conduction current, displacement current, or both. In indirect plasma treatment, the plasma does not come into direct contact with the target and the treatment effect is mostly conveyed by uncharged atoms and molecules diffusing outside the plasma region. In this case, a small or null flux of charged particles reaches the target surface while active uncharged species are typically delivered to the surface via a flow of gas crossing the plasma region. Another kind of treatment that is raising more and more attention in the scientific community is the one mediated by a so-called *plasma activated medium* (PAM). When a liquid solution, usually water or cell culture medium, is treated with plasma, chemical reactions initiate in PAM and continue even after the plasma discharge is switched off and in the absence of any external energy source [45]. These reactions usually involve the presence of long-lived reactive species transferred from the discharge into the liquid and may induce significant biological effects on living organisms.
In conclusion, is worth mentioning how approaching plasma biomedical applications results in a real challenge being this an interdisciplinary topic that embrace not only physics and engineering but also medicine and biology. While an understanding of the mechanisms by which CAP interacts with living systems has begun to emerge only recently, a significant number of works and review papers have appeared since the late 2000s [10,14,16,19,20,46–52].

During my research, in the context of *Plasma Medicine*, I had the privilege and pleasure to collaborate with different life scientists from various domains. More precisely I had the opportunity to work with: Prof. Lia Rimondini and Dr. Andrea Cochis of the Department of Health Sciences of the University of Piemonte Orientale (UPO) concerning the study of the antibacterial effect of CAP for the decontamination of soft reline palatal obturators (Paragraph 4.3); Prof. Carmela Fimognari and Dr. Eleonora Turrini of the Department for Life Quality Studies of the Alma Mater Studiorum - Università di Bologna concerning the study of the plasma treatment of lymphoma cells to promote cell death and cell-cycle arrest (Paragraph 4.4); Dr. Riccardo Tonini and Dr. Diletta Forgione dental practitioner of the University of Brescia concerning the study of the application of an atmospheric pressure DBD plasma jet for the enhancement of the adhesion of dental restorations (Paragraph 4.5).

4.2 Design and characterization of a DBD plasma source for living tissue treatment

The plasma source adopted for the biomedical applications presented in the following paragraphs and adopted in PAPER VI and VII, is a particular DBD, named *DBD-Rod: a* picture and a schematic are presented in Figure 4.1. The source architecture is based on the "wand" source presented by Friedman *et al.* in a paper on plasma application for blood coagulation and tissue sterilization [48]. In our configuration, the plasma source consists of a cylindrical brass electrode, with a 10 mm diameter, having a semispherical tip, with curvature radius of approximatively 5 mm. The electrode is covered with a 1 mm thick dielectric: usually borosilicate glass, but that can be substituted by other dielectric materials as will be explained in the following. A large number of AC power supplies can drive this plasma source and some examples will be presented in the following paragraph for specific applications. The plasma source dimension and geometry allow its use for the direct treatment of cells in culture multiwell plates (24 wells or larger) and for the treatment of small samples (ex. soft reline specimens, Paragraph 4.3).
As already mentioned in the introduction of this chapter, in biomedical application the safety and controllability of novel plasma sources is an important issue. For example, 40 °C is regarded as the limit temperature that cells can withstand without the occurrence of thermal effects and damage. If properly operated, CAP sources can deliver the desired reactive species to a biological sample without significantly increase its temperature.

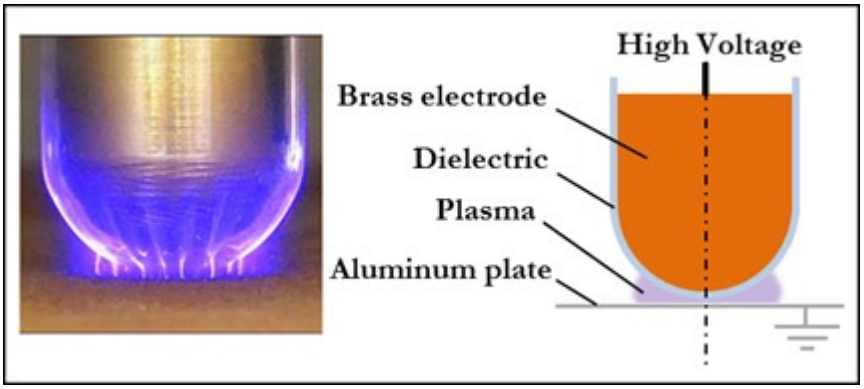

Figure 4.1 *DBD-Rod* discharge on a grounded plate (left) and schematic (right)

In order to attain uniform treatments and avoid localized temperature peaks, a diffused plasma condition is generally desirable for applications on living tissues. During the development of the *DBD-Rod* source two different dielectric materials, borosilicate glass and polystyrene, were tested as dielectric barrier. Powering the *DBD-Rod* with a commercial nanopulse generator (FID FPG 20-1NMK) the influence of the dielectric material on the characteristics of the generated plasma and on the temperature reached by the dielectric surface were studied by means of an high speed (HS) camera (NAC-GX3, 1000 fps, 1 ms shutter) and fiber optic temperature sensors (Opsens, see PAPER II). The *DBD-Rod* was operated in contact with a grounded aluminum plate acting as counter electrode (Figure 4.1 right). The temperature reached by the dielectric surface after different operating times and for different applied peak voltages is reported in Figure 4.2. Up to 4 s, there is no substantial difference in the temperature reached by the two dielectric materials. For longer operating times (8 and 16 s) the borosilicate glass reaches temperatures above 40 °C when 25kV and 29 kV peak voltages are applied (). With polystyrene instead the temperature remains below 40°C up to 8 s. Longer treatment times were not achievable with this dielectric because of a partial melting and deformation of the material itself.

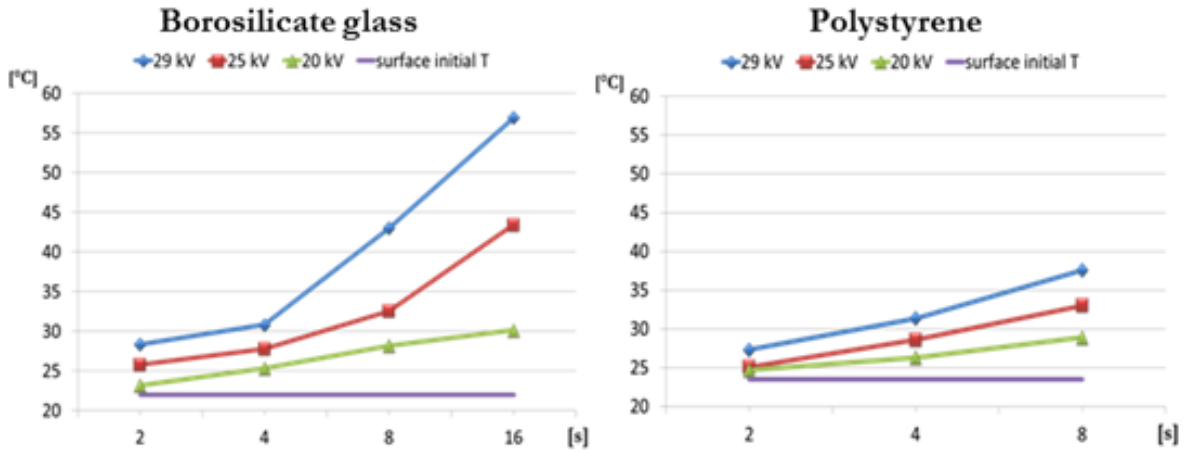

Figure 4.2 *DBD-Rod* dielectric surface temperature over treatment time for different dielectric materials (borosilicate glass and polystyrene) and applied peak voltages (20kV, 25 kV, 29 kV)

The characteristics of the plasma discharge in different configurations was also investigated by HS imaging. The investigation was performed both setting the plasma source in vertical position and tilted with respect to the grounded substrate. The configuration schematic is presented in Figure 4.3 together with some representative frames for the conditions at 25 kV. Independently of the tilt angle, the cases with the polystyrene dielectric layer produced a far less luminous and voluminous plasma discharge if compared with the equivalent case with borosilicate glass dielectric. This is most probably due to the lower relative permittivity of polystyrene (ε_r=~2,4) compared to the one of borosilicate glass (ε_r=~4,6) [53]. Due to the source hemispherical tip a mix of a diffuse plasma condition (near the point of contact with the substrate) or a partially filamentary one (few millimeters away from the point of contact) can be seen for the borosilicate case. Interestingly no substantial differences were observed between the vertical and tilted settings for both dielectric materials.
After this preliminary investigation, borosilicate glass was selected over polystyrene because in virtue of the more intense plasma discharge and the longer operating times achievable without structural damages.

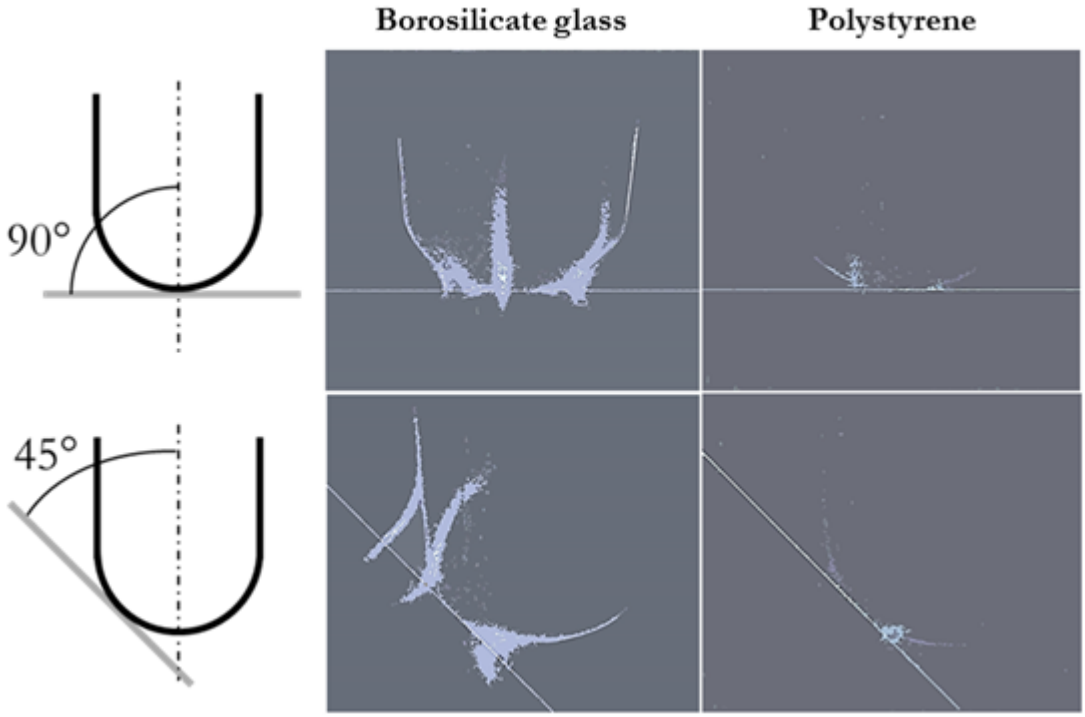

Figure 4.3 *DBD-Rod* discharge for different tilt angles and dielectric materials.

4.3 Antibacterial effect of non-equilibrium atmospheric plasma for the decontamination of soft reline palatal obturators

Traditionally, the decontamination or treatment of non-living objects like metals, plastics, fabrics, and other surfaces have been carried out either by temperature (i.e., autoclaves), liquid or gaseous chemistry (i.e., by ethylene oxide, ozone, chlorine, etc.), or at reduced pressure by non-equilibrium plasmas [14].
As it may be expected, all these techniques have their own limits and may result inappropriate for specific materials or applications. Conventional methods based on the use of antimicrobial agents [21] have been already demonstrated to be often ineffective against bacteria in biofilm form; therefore, the ability to destroy these living organisms is critical and the development of an alternative technique is demanded. CAP potentially offers a good alternative to conventional antimicrobial approaches, thanks to its characteristic blend of several and synergic biologically active agents; namely, ultra-violet radiation, and particles as neutral or excited atoms and molecules, negative and positive ions, free radicals and free electrons [46]. It has been proposed that charged particles and electric field associated with CAP can affect the cell membrane causing electrostatic disruption or at least permeabilization for a very short time [54]. As a consequence, plasma-derived ROS/RNS molecules can penetrate the cell membrane [55] inducing further chemical reactions inside the cytoplasm and leading to the oxidization of cellular proteins and microbial DNA [56]. In this connection, Park *et al.* reported about the possibility to induce disruption *of B. subtilis*, *E. coli*, *P. aeruginosa* and *S. typhimirium* with 20 s of exposure to a microwave-induced Ar plasma at atmospheric pressure [57]. Interestingly, some literature results report the effective use of plasma for biofilm disinfection or inactivation [58–61]. In a study by Joaquin *et al.* [62] on the effects of plasma on living biofilm-forming bacterial cells, is suggested that bacteria go through sequential physiological and morphological changes before becoming inactivated and that longer treatment times are necessary to ensure a complete inactivation of bacteria in biofilm than in planktonic state. The possibility to maintain substrate temperatures acceptable for living tissue and thermo-sensitive materials enables to extend plasma decontamination to these kind of substrates.
During my Ph.D. I had the opportunity to investigate the effects of CAP treatment for the decontamination of a particular type of prosthesis for oral tissue substitution. The results presented in this paragraph 4.3, have been submitted for publication on international journal (see PAPER VII). This part of my research has been possible only thanks to the collaboration with the group of Prof. Lia Rimondini of the Department of Health Sciences of the University of Piemonte Orientale (UPO). Her group took care of the preparation and contamination of the samples and of all biological assays while on my side I designed, realized and operated the plasma source setup for the treatment of the samples.

4.3.1 Literature overview

Malignant tumors involving the upper gum, palate and oral sinus accounts for 1-5% of malignant neoplasms of head and neck [63]. Most of these carcinomas are deeply invasive because late diagnosed. In these cases, the treatment of choice is surgical deep resections including palate- and maxillectomy, followed by reconstructive approaches. However, when the breach is wide, patients are required to temporary or definitively wear custom-made removable palatal obturators, to replace the lacking tissues and to restore masticatory, deglutition and speech functions as well as to improve cosmetic appearance [63]. Among the large number of materials suitable for this purpose, soft reline holds a relevant position since it is easily moldable and possesses, thanks to its sponge-like return, the mechanical characteristics required to sustain the typical values of the compressive oral forces. Soft reline oral palatal obturators are quite expensive because of the sophistication of the raw material and the custom-made production process. An eventual implant failure might be severely resource- and time- consuming. Severe bacteria biofilm contamination of the device is one of the major causes of failure of prosthetic rehabilitations. Therefore, the research of preventive and therapeutic approaches to counteract the formation of biofilm or remove it once formed are mandatory for clinical success [64–67].

In this study, the effectiveness of two plasma sources in the treatment of soft reline oral shutters to prevent biofilm adhesion and achieve biofilm decontamination is reported. The potential of the plasma in preventing biofilm adhesion was evaluated by contaminating with 24 hours old biofilm sterile specimens previously exposed to plasma treatment, while the efficacy in reducing bacteria viability was tested treating with specimens previously contaminated with 90 min (early) and 24 hours (mature) old biofilm. Two bacterial strains were chosen: *Streptococcus mutans* and *Aggregatibacter actinomycetemcomitans*, being strongly related to biofilm formation in the oral cavity. Finally, since palatal obturators are designed to replace resected tissues and come into contact with the healthy one, the viability of human primary cells cultivated directly onto the surface of plasma treated specimens has been investigated.

4.3.2 Plasma treatment of soft reline specimens

For this study, two dielectric barrier discharge (DBD) plasma sources were tested. One of the sources is the *DBD-Rod*, already presented in detail in paragraph 4.2, while the other is a planar DBD named *DBD-Plate* (described in detail in PAPER VII). A picture of both plasma sources during operation is presented in Figure 4.4. This dissertation will focus only on the results achieved with the *DBD-Rod* source, while the complete set of results, including those for the *DBD-Plate* source, can be found in PAPER VII, together with details on the experimental procedure, including biological protocols..
In this work, the *DBD-Rod* was powered by a generator producing high-voltage quasi-sinusoidal pulses having peak voltages of 15.4 kV, frequency of 40 kHz, pulse duration of 250 μs and pulse repetition frequency of 1000Hz. The distance between the dielectric surface and the grounded plate where soft reline specimens were placed during treatments was kept constant and equal to 3 mm. Soft reline was prepared following the manufacturer's instructions, afterwards, the polymer was cut in order to realize square specimens (5 mm per side) with a thickness of 2 mm. The specimens were treated for different times (30 s, 60 s, 120 s) to draw conclusions on the dependency of antibacterial effect over treatment time.

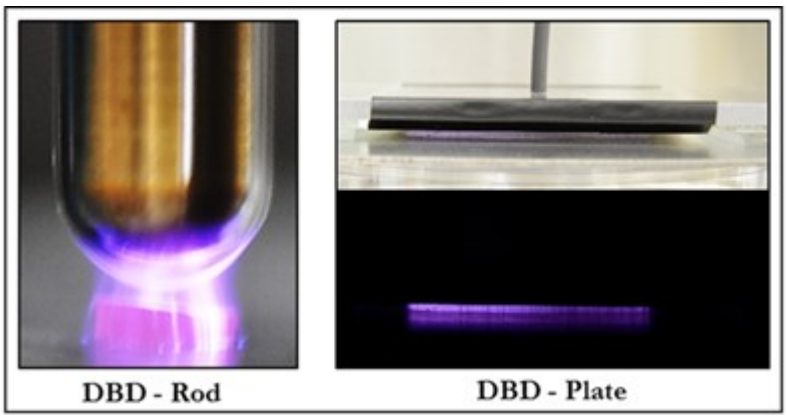

Figure 4.4 *DBD-Rod* (left) and *DBD-Plate* (right) during operation.

4.3.3 Evaluation of plasma reduction of bacteria adhesion

As shown in Figure 4.5 the *DBD-Rod* was found to be effective in preventing bacteria adhesion for both tested bacterial strains when used to treat soft reline palatal obturators before bacterial contamination. The CFUs counts highlighted that on plasma treated samples the CFU number was approximately 2 logs lower than the one registered on untreated control (CNT) ($p<0.05$, indicated by #), as reported in Figure 4.5 b-c (left histograms). Moreover, as shown in Figure 4.5 b-c (right histograms), also the bacteria viability evaluated on the soft reline palatal obturators resulted to be affected by plasma treatment, since a loss of bacteria viability of 40-60% was found for plasma treated samples with respects to the untreated ones ($p<0.05$, indicated by *).

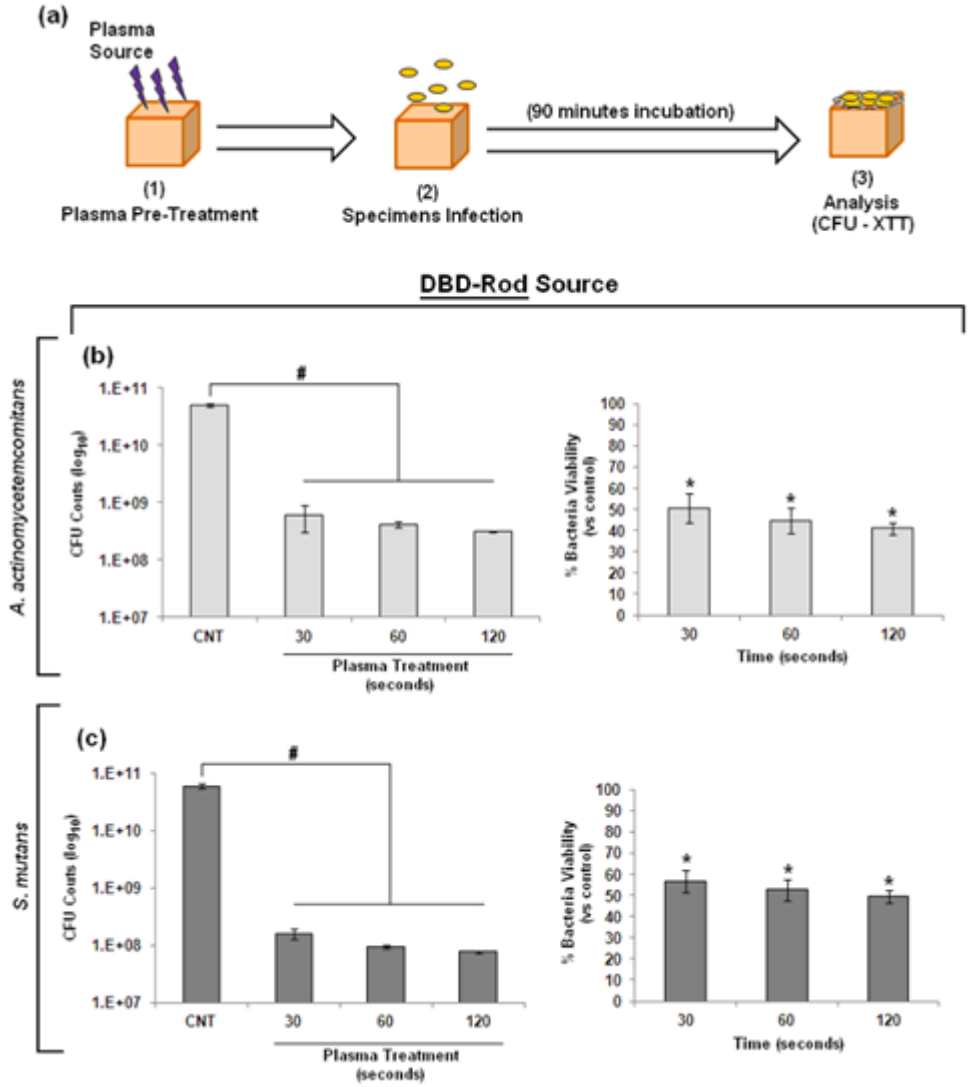

Figure 4.5 Schematic representation of the experimental protocol (a); assessment of the capability of *DBD-Rod* plasma source in affecting *A. actinomycetemcomitans* (b) and *S. mutans* (c) adhesion, by means of CFUs counts (left histograms) and evaluation of bacteria viability (right histograms). Results were statistically significant in comparison with untreated controls (CNT) for both CFUs ($p<0.05$, indicated by the #) and viability assessed by XTT ($p<0.05$, indicated by the *). Bars represent mean values and standard deviations [PAPER VII]

4.3.4 Evaluation of plasma activity in decontaminating early and mature biofilm

Plasma treatment of previously infected specimens (schematized in Figure 4.6a and Figure 4.7a) led to a significant decrease of CFU number and bacteria viability for both early and mature biofilm. As expected and observed comparing Figure 4.6 and Figure 4.7, plasma treatment is more effective on early biofilm than on mature one.

In fact, for the early biofilm case, the *DBD-Rod* induced at least a 3 Logs reduction of the CFUs number (left histograms) and a 40-60% loss in terms of bacteria viability (right histograms), for both tested bacterial strains. All the results obtained for plasma treated specimens were statistically significant in comparison to untreated controls ($p<0.05$, indicated by the # for CFUs counts and by the * for viability assay).

Significant results were also obtained for specimens infected by mature biofilm (Figure 4.7), even though the inhibition values resulted to be lower than the one obtained in the case of early biofilm. In fact, for the two considered biofilm formers, plasma treatment was able to induce 2 Logs reduction of the CFUs number (Figure 4.7 left histograms) and 20-40% loss in terms of bacteria viability (Figure 4.7 right histograms). Also in this case results were statistically significant in comparison to untreated controls ($p<0.05$, indicated by the # for CFUs counts and by the * for viability assay).

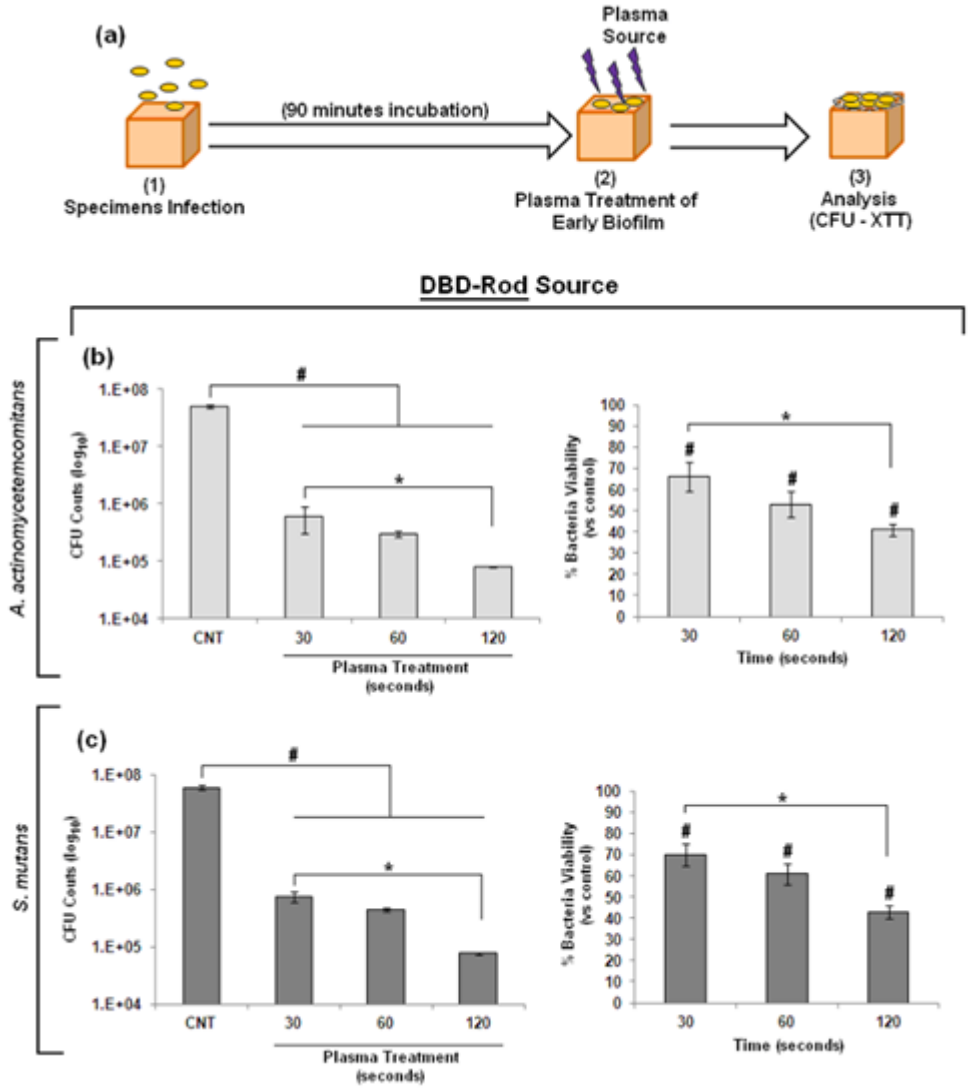

Figure 4.6 Schematic representation of the experimental protocol (a); assessment of the effectiveness of *DBD-Rod* plasma source in decontaminating *A. actinomycetemcomitans* (b) and *S. mutans* (c) early biofilm, by means of CFUs counts (left histograms) and evaluation of bacteria viability (right histograms). Results were statistically significant in comparison with untreated controls (CNT) for both CFUs ($p<0.05$, indicated by the #) and viability ($p<0.05$, indicated by the *). Bars represent means and standard deviations. [PAPER VII]

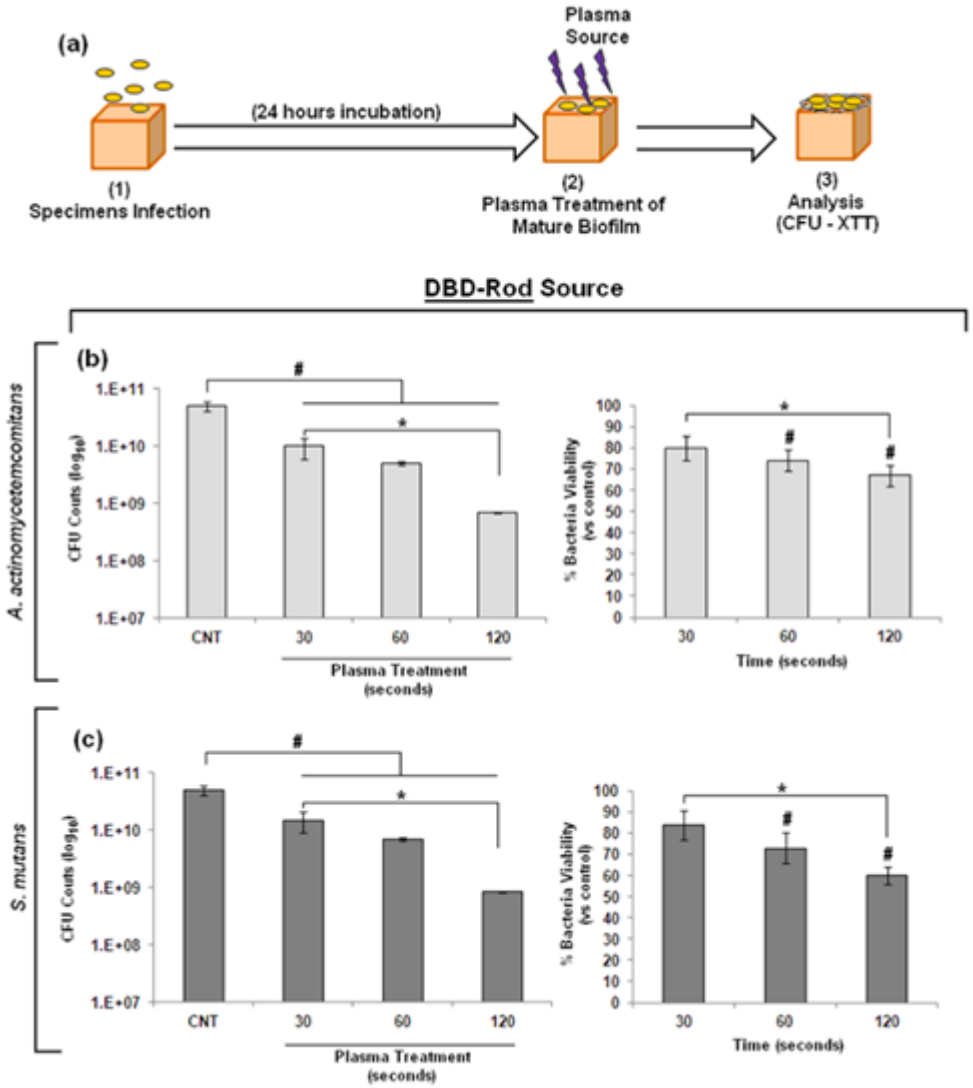

Figure 4.7 Schematic representation of the experimental protocol (a); assessment of the effectiveness of *DBD-Rod* plasma source in decontaminating *A. actinomycetemcomitans* (b) and *S. mutans* (c) mature biofilm, by means of CFUs counts (left histograms) and evaluation of bacteria viability (right histograms). Results were statistically significant in comparison with untreated controls (CNT) for both CFUs ($p<0.05$, indicated by the #) and viability ($p<0.05$, indicated by the *). Bars represent means and standard deviations. [PAPER VII]

4.3.5 Assessment of cytocompatibility of plasma treated soft reline specimens

Cytocompatibility of untreated soft reline specimens was evaluated against pooled primary human gingival fibroblasts (HGFs) and skin keratinocytes (HEKs). Results showed that both HEKs and HGFs were able to grow onto the specimens surface and no difference ($p>0.05$) with respect to the polystyrene control was observed, as reported in Figure 4.8. The same procedure was repeated for reline specimens subjected to plasma treatment performed under the same operating conditions implemented for bacterial decontamination tests. Results confirmed that plasma treatment of soft reline specimens did not affect their cytocompatibility; in fact, an almost insignificant, when compared to the controls (polystyrene and polymer, $p>0.05$), decrease of the eukaryotic cells viability ratio was registered only after 120 seconds plasma treatment. Furthermore, also the visual observation confirmed that, after 24 hour of cultivation,

morphology, spread and density of both HEKs (Figure 4.8 b) and HGFs (Figure 4.8 d) cultured onto treated specimens were comparable with those of eukaryotic cells cultured on both the controls.

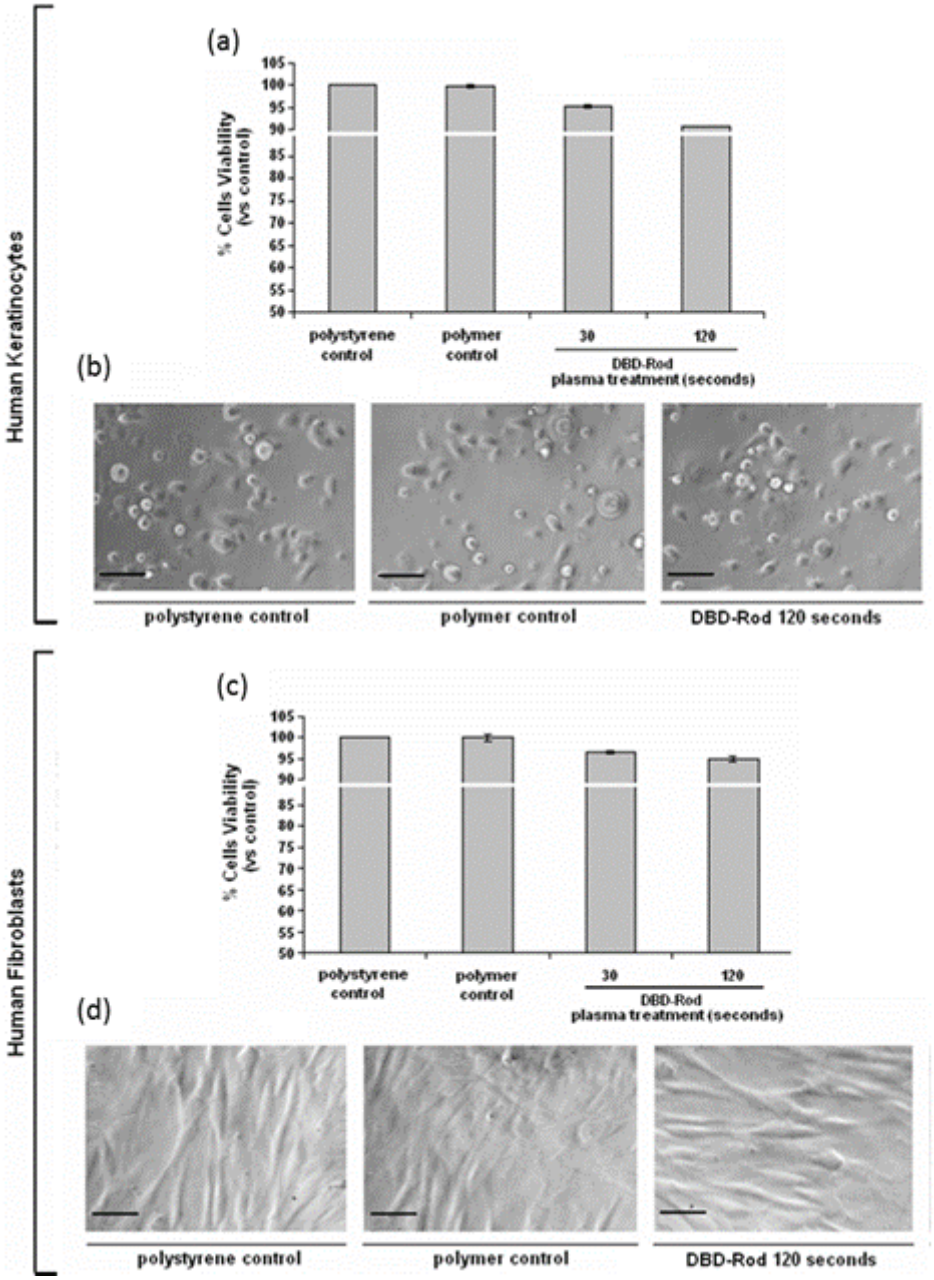

Figure 4.8 Assessment of cyotocompatibility of soft reline specimens treated by the *DBD-Rod* plasma source, by means of the evaluation of eukaryotic cell viability and visual observation. The viability and morphology of HEKs (upper panel) and HGFs (lower panel) grown onto plasma treated specimens were comparable towards controls cultivated onto untreated reline (polymer control) and polystyrene wells (polystyrene control). No statistically significant differences ($p>0.05$) were detected between treated and control groups. [PAPER VII]

4.3.6 Conclusions on plasma antibacterial treatment of soft reline palatal obturators

The decontamination of soft reline palatal obturators, worn as a replacement of lacking soft tissues by patients who suffered from oronasal communication, represents a challenge for clinicians [68]. In fact, in most cases, due to the inefficacy of conventional methods in reducing the microbial load, the removal and substitution of contaminated implants are required; this procedure is expensive and time consuming because each obturator needs a custom-made molding procedure in order to fit with patients' tissue defects. Since the bacterial and fungal biofilm contamination is the most recognized cause of prosthetic stomatitis [69] and, in case of immunocompromised patients also a potentially life-threatening condition [70], innovative methods able to affect biofilm adhesion and reduce bacterial load onto soft reline palatal obturators are strongly demanded. The obtained results highlighted the feasibility to employ CAP to achieve this goal. CAP pre-treatment of soft reline surface can reduce later bacterial contamination. Moreover, CAP achieved very promising results in the decontamination of early biofilm. On mature biofilm, the bacterial load reduction was less pronounced but still relevant. Results also confirmed that plasma treatment of soft reline specimens did not affect their cytocompatibility or mechanical properties. Concluding, the results achieved during this research in collaboration with the group of prof. Rimondini show that the direct application of cold atmospheric plasma represents a suitable procedure able to significantly reduce bacterial contamination, even in a single short time treatment, and to prevent bacteria adhesion on sterile soft reline specimens. Considering the preliminary in vitro data, even if more *in vitro* and *in vivo* studies are still necessary, it is possible to state that CAP can be considered as a very promising solution for soft reline obturators decontamination.

4.4 Plasma treatment of lymphoma cells to promote cell death and cell-cycle arrest

4.4.1 Literature overview

Despite improvements in survival rates, cancer is still the second leading cause of death in Western countries [71]. While the rapidly expanding knowledge of cancer pathogenesis at the molecular level is providing new targets for drug discovery and development, the multiple genetic and molecular alterations involving transformation, dysregulation of apoptosis, proliferation, invasion, angiogenesis and metastasis make cancer an extremely complex disease [52,72]. Currently, the treatment of cancer largely revolves around chemotherapy, sometimes in combination with new therapeutic approaches under investigation. Despite the development of multiple new agents, antitumor therapies are strongly limited by the low therapeutic index of most of the adopted drugs and by the development of chemoresistance. In particular, the onset of chemoresistance frequently hampers the successful treatment of cancer either at the initial presentation or following primary or subsequent relapses [73]; while relapse continues to be the most common cause of death [74]. Thus, cancer remains a formidable therapeutic challenge that requires the identification and the development of novel agents for the treatment of this disease.
CAPs are encountering increasing interest as a novel anti-tumor treatment, since they provide a blend of physical and chemical components which was demonstrated to exert anti-tumor effects by some pioneering work both on *in vivo* and *in vitro* models [75,76]. However, the mechanism of plasma-cell interaction is still not completely understood, as well as the selectivity associated to the various plasma generated species. Gweon *et al.* [77] considered reactive oxygen species (ROS) responsible for the dissociation of integrin and the consequent detachment of human liver cancer cells (SK-HEP-1). Ishaq *et al.* [78] demonstrated that plasma treatment induced apoptosis in melanoma cells and, differently from the previous works, focused their attention on intracellular ROS levels. Song *et al.* [79], through the use of ROS scavengers, demonstrated how CAP induced increases in extracellular nitric oxide (NO) did not affect P53-mutated cancer cell viability, while intracellular ROS increased under CAP exposure and

induced apoptotic cell death. On the other hand, Volotskova *et al.* [80] demonstrated that plasma treatment enhances the oxidative stress of cells in the S phase of the cell cycle. Interestingly, recent studies [81] have reported that plasma not only affects cancer cells when they are directly exposed to it or suspended in the culture medium being treated, but also when they are subject to indirect treatment, being suspended in a medium that was previously treated and activated by plasma. Tanaka *et al.* [82] demonstrated that, when treated by plasma activated medium, glioblastoma human brain tumor cells were induced to undergo apoptosis, through AKT down-regulation; moreover, they also demonstrated *in vitro* and *in vivo* that plasma-activated medium has an anti-tumor effect on chemo-resistant epithelial ovarian carcinoma cells [83]. Fridman *et al.* [84] proposed a completely different approach suggesting the plasma stimulation of the immune system to trigger localized immunogenic cell death. These observations together with the rapidly expanding knowledge of cancer biology have fueled a growing interest in exploiting CAP as an interesting strategy in the oncological field endowed with the potential of shifting the current paradigm of cancer treatment and enabling the transformation of cancer treatment technologies.

4.4.2 Non-equilibrium plasma application on lymphoma cells

During my Ph.D. I had the opportunity to investigate the effects of plasma treatment on lymphoma cells. The results here presented, have been published in the form of PAPER VI. This part of my research has been possible only thanks to the collaboration with the group of prof. Carmela Fimognari of the Department for Life Quality Studies of the Alma Mater Studiorum - Università di Bologna. Her group took care of the lymphoma cell samples preparation and of all biological assays while on my side I designed, realized and operated the plasma source setup for the treatment of the samples and effectuated the characterization of both the plasma discharge and the plasma treated culture medium.
In the work, we focused on the fundamental mechanisms of plasma interaction with cancer cells, investigating cell viability, proliferation and cell-cycle distribution of L5178Y lymphoma cells treated by the *DBD-Rod* plasma source. Plasma direct treatment was performed for two different sets of operating conditions differing for treatment time and gap width between the tip of the plasma source and the culture medium surface; the differences between the plasma discharges generated in various operating conditions were highlighted and analyzed through ICCD and high speed (HS) imaging. Flow cytometry was employed to evaluate cell viability at 6 h, 24 h and 48 h after plasma treatment, as well as to analyze cell-cycle distribution after cell culture for 24 h and 48 h. Finally, a comparison of the effects on cancer cells of the exposure to a previously plasma treated culture medium instead of being directly exposed to the plasma, and the semi-quantitative measurement of nitrites, nitrates and peroxides in the plasma treated medium were carried out to support the analysis of the observed cell response to plasma exposure.

4.4.3 Plasma treatment of lymphoma cells

Plasma treatment of lymphoma cells was performed either in direct and indirect configuration, as schematically presented in Figure 4.4. In direct configuration, 5 x 105 cells in 1 mL complete medium were seeded in a monolayer through centrifugation and directly exposed to plasma treatment in a 24 wells plate. During the experiments, the *DBD-Rod* was driven by a unipolar nanosecond (5 ns rise time) high voltage generator (already described in paragraph 4.2) at 20 kV PV and 500 Hz PRF. Two different sets of operating conditions have been considered: in the first case (T1), a 60 s treatment was performed keeping a 1.25 mm distance between the tip of the plasma source and the surface of the liquid medium (gap); in the second case (T2), a 120 s treatment was performed setting the gap at 2.50 mm. These two sets of operating conditions were selected after a series of preliminary tests based on cell viability assays. The selected operating conditions resulted in a significant reduction of cell viability, but still higher than

50% (normalized to the cell viability of untreated cells), necessary to perform the cell proliferation experiments.
In indirect configuration, 1 mL of complete medium not containing lymphoma cells was exposed to plasma treatment in a 24 wells plate; 500 000 lymphoma cells were added to the medium immediately after that. A comparison of the effects of direct and indirect treatments was carried out at PV 20 kV, PRF 500 Hz and gap 1.25 mm for various treatment times (30 s, 45 s, 60 s, 90 s and 120 s).

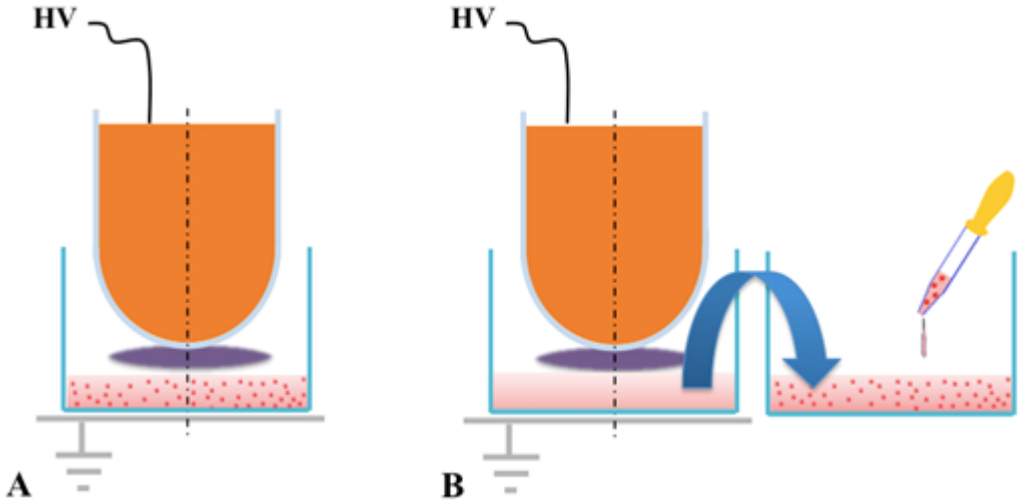

Figure 4.4 *DBD-Rod* plasma treatment of lymphoma cells: A) direct treatment setup; B) indirect treatment setup. [PAPER VI]

4.4.4 High Speed Imaging and ICCD imaging of the plasma discharge

A qualitative investigation of the temporal evolution of the plasma discharge in contact with the cell culture medium (DMEM) was performed by means of High Speed and ICCD camera. For practical and safety reasons the culture medium did not contained lymphoma cells during the experimental tests concerning the characterization of the plasma discharge and the plasma treated culture medium; apart from that all operating conditions were identical to those adopted for biological tests.
The reported HS images (Figure 4.5) immediately highlight the effect of a variation of gap width, and thus of electrical field in the gap, on the plasma discharge aspect; for the smallest gap width (T1), the discharge appears characterized by several microdischarges located close to the tip of the plasma source. In this case, for the longest exposure time (100 fps image), a faint glow appears in the gap region and a larger number of filaments are observed with respect to the image taken at 500 fps, as a consequence of the accumulation of the plasma emissions associated to 5 subsequent high voltage pulses; the comparison between images taken at 100 fps and 500 fps highlights also that during subsequent pulses, for the selected operating conditions, the microdischarges form in different locations, with no significant memory effect observed [26]; possibly as a consequence of the adopted value of PRF and the liquid surface acting as a second electrode [85].
When the gap between the plasma source and the culture medium surface is larger (T2), the plasma discharge appears completely different from the previous case, being characterized by a single filament located at the tip of plasma source, where the gap is the smallest and the electric field is the highest. The single filament has a funnel-like shape, which appears broader at the upper electrode (due to charge distribution and electric field distortion at the dielectric surface) and more collimated close to the culture medium surface; moreover, in case T2 images taken at different exposure times seem to show that filament produced during successive pulses are formed always in the same position, along the axis of the plasma source.

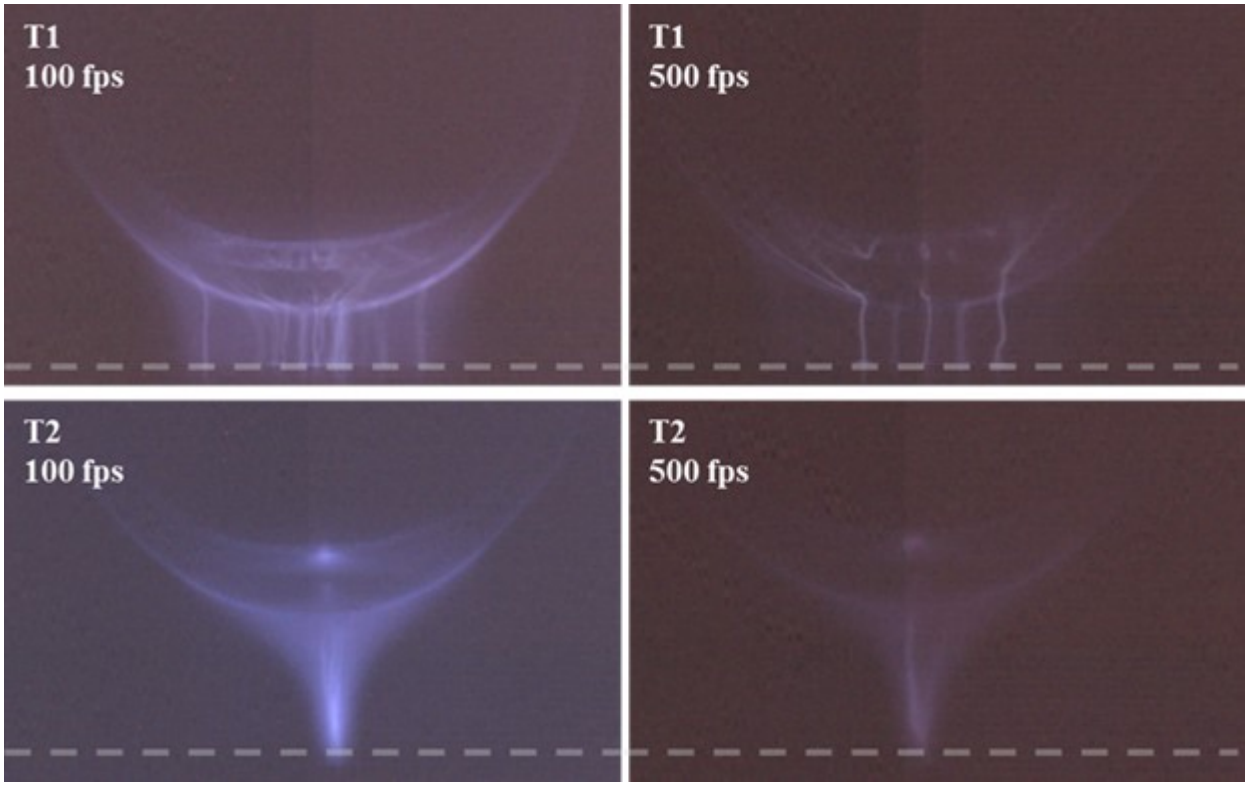

Figure 4.5 HS images of the plasma discharge during the treatment of culture medium (the dashed line indicates the culture medium surface) for both selected operating configurations (top: T1, bottom: T2). Acquisitions were realized at two different frame rates (left: 100 fps, right 500 fps). [PAPER VI]

ICCD imaging, being characterized by exposure times of a few nanoseconds, allowing for the investigation of the plasma behavior with greater time resolution than HS images, was here used to study the temporal evolution of a single discharge event. Assuming the repeatability of the plasma discharge (verified comparing three different acquisition) it was possible to analyze the discharge evolution along the voltage pulse by mean of the iCCD camera even acquiring only one acquisition per voltage pulse. . In our experiments, the exposure time was set at 3 ns (gate time) and the voltage pulse was scanned with time steps of 1 ns, obtained progressively increasing the trigger delay time.

In Figure 4.6, eight subsequent frames representing plasma evolution are shown for each operating condition (T1 and T2); for clarity purposes, the gate opening of the first (1, colored in green) and last acquisitions (8, colored in red) are plotted against the recorded voltage waveform in Figure 4.7 following the methodology already presented in Chapter 2 for the APPJ source. From ICCD acquisitions, the discharge structures for T1 and T2 cases turn out to be more similar to each other than previously observed by means of HS imaging. In both cases, the first plasma luminous emission appears almost at the same time, corresponding to the initial part of the voltage ramp; moreover, the third frame, collected in correspondence of the maximum peak voltage, is the most luminous both for T1 and T2. Most interestingly, a multi-filamentary structure is observed in both operating conditions; while this behavior was already observed by means of HS imaging in T1 conditions, only a single filament could be seen for the T2 case in HS images. This is probably due to the fact that in HS imaging acquisition no light signal intensification is applied; therefore the signal of short living or low emitting microdischarges could be shadowed by the presence of a longer living or higher emitting microdischarge.

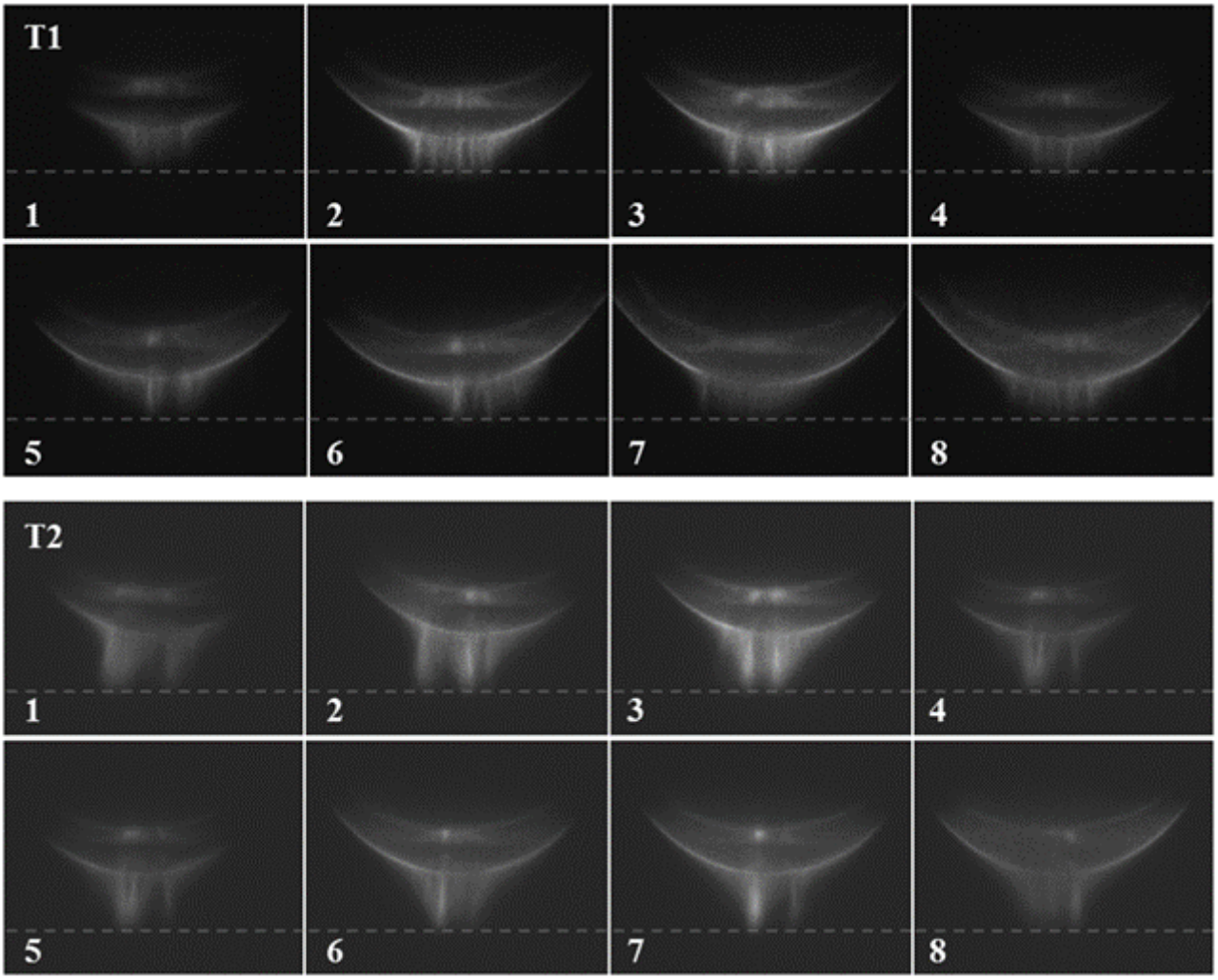

Figure 4.6 ICCD images depicting the temporal evolution along the voltage pulse of the plasma discharge formed in contact with 1 ml of culture medium (the dashed line indicates the culture medium surface), for both operating configurations adopted for cancer cell treatment (T1, T2). The start of each acquisition (3 ns exposure) is delayed of 1 ns with respect to the previous one. [PAPER VI]

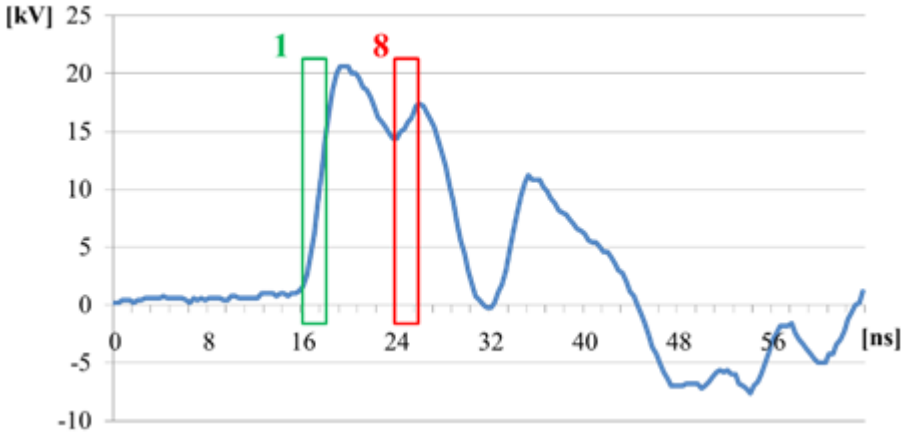

Figure 4.7 Measured voltage waveform with superimposed exposure gates for the first (1, green) and last (8, red) ICCD frames. [PAPER VI]

4.4.5 Studies of cell viability, proliferation and cell-cycle progression following direct or indirect plasma treatment

Results in Figure 4.8 a significant decrease in cell viability 48 h after a direct plasma treatment. The effect is more pronounced after 120 s of exposure at 2.5 mm of distance than after 60 s at 1.25 mm. Furthermore, cold plasma affected cells proliferation both 24 h and 48 h after the exposure (Figure 4.9). The highest effect was observed also in this case for the exposure condition at 2.50 mm for 120 s.
24 h after the treatment, it was also possible to observe an accumulation of cells in G2/M phase (cell cycle checkpoint important to ensure DNA repairing before entering mitotic phase [86]) for both exposure conditions, as showed in Figure 4.10A. 48 h after plasma exposure, the accumulation of cells in G2/M phase was statistically significant for the exposure condition 2.50 mm, 120 s (52.2% cells vs 42.8% of untreated cells) (Figure 4.10B).
Based on these results, the cell-cycle arrest appears reversible for the 60 s and 1.25 mm condition; indeed, in that condition, an accumulation of G2-cells is observed 24 h after plasma treatment but not 48-h post-treatment. This means that cells can overcome the plasma-induced cell-cycle arrest and start proliferating. The 120 s and 2.50 mm condition is able to induce a stronger antiproliferative effect, from which cells is not able to recover; in this case, we can conclude that the cell-cycle arrest induced by plasma is irreversible.
Taken together, these results demonstrate that the growth inhibition of lymphoma cells induced by plasma treatment is imputable to cell death and cell-cycle arrest in which G2 accumulation is a key event. The simultaneous appearance of G2 block and cell death suggests that cell death is a primary direct effect of plasma treatment, and not a secondary effect due to the cells' inability to overcome growth arrest and proceed through the cell cycle.

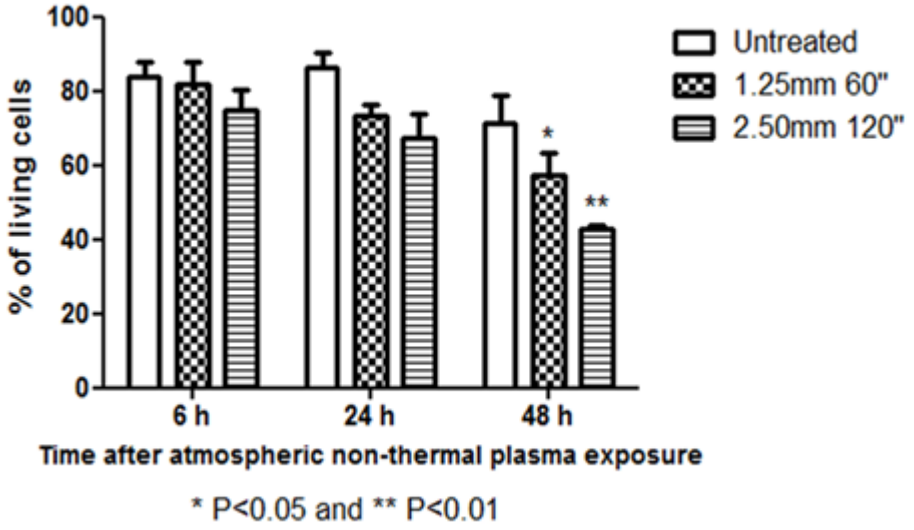

Figure 4.8. % of living cells after 6h , 24 h and 48 h from direct CAP exposure. [PAPER VI]

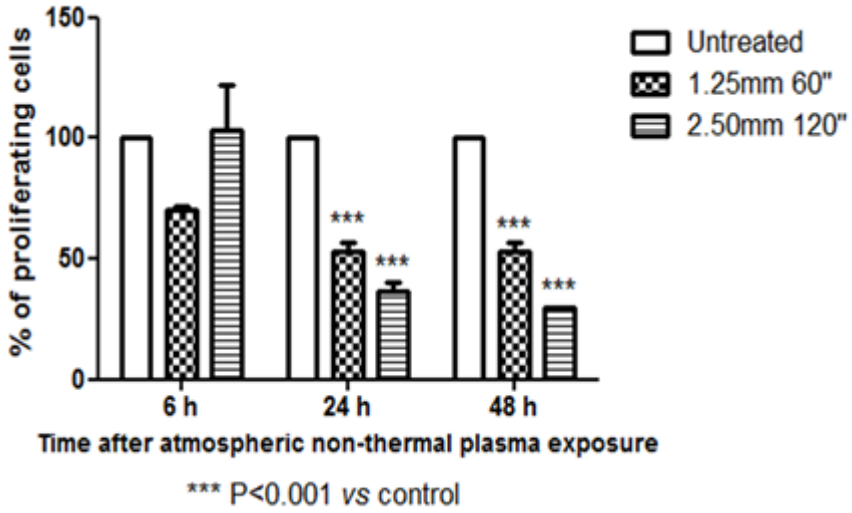

Figure 4.9. % of proliferating cells after 6 h, 24 h and 48 h from direct CAP exposure. [PAPER VI]

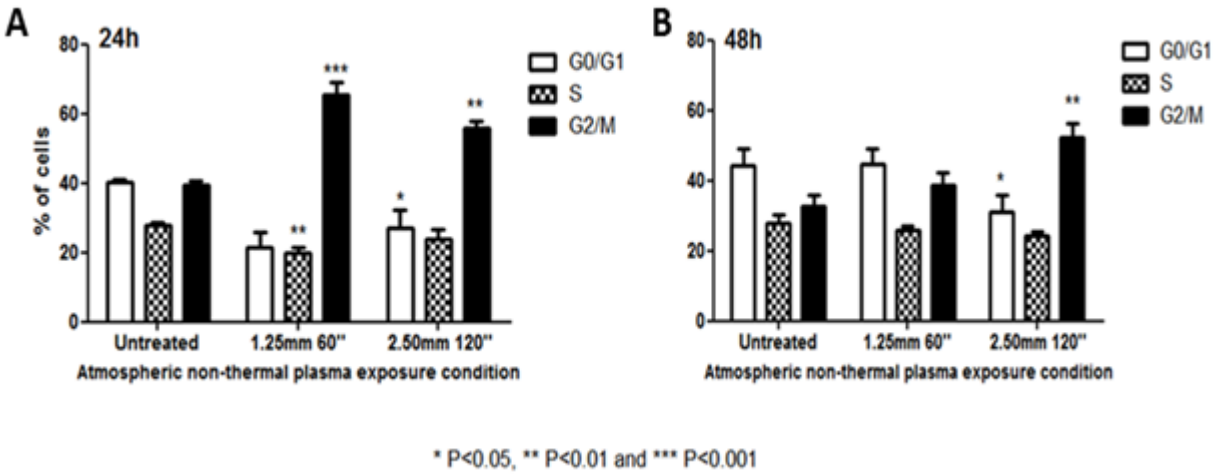

Figure 4.10. Cell-cycle distribution after 24 h (A) and 48 h (B) from CAP exposure. [PAPER VI]

Comparative results of direct and indirect treatment are presented in Figure 4.11, showing that the longer the treatment time (from 30 s to 120 s) and the culture time after plasma treatment (6 h, 24 h and 48 h), the higher the reduction in cell viability; no relevant difference can be observed between direct and indirect treatment results. No significant differences between the direct and indirect treatment were also observed with a gap of 2.50 mm(data not shown). This suggests that the chemistry induced by plasma treatment in the culture medium plays the leading role in plasma reduction of cancer cells viability; similar considerations were previously reported by Vandamme *et al.*[87] and Mohades *et al.* [88], who compared the effects of direct and indirect treatment on glioblastoma U87MG and SCaBER bladder cancer cells, respectively.

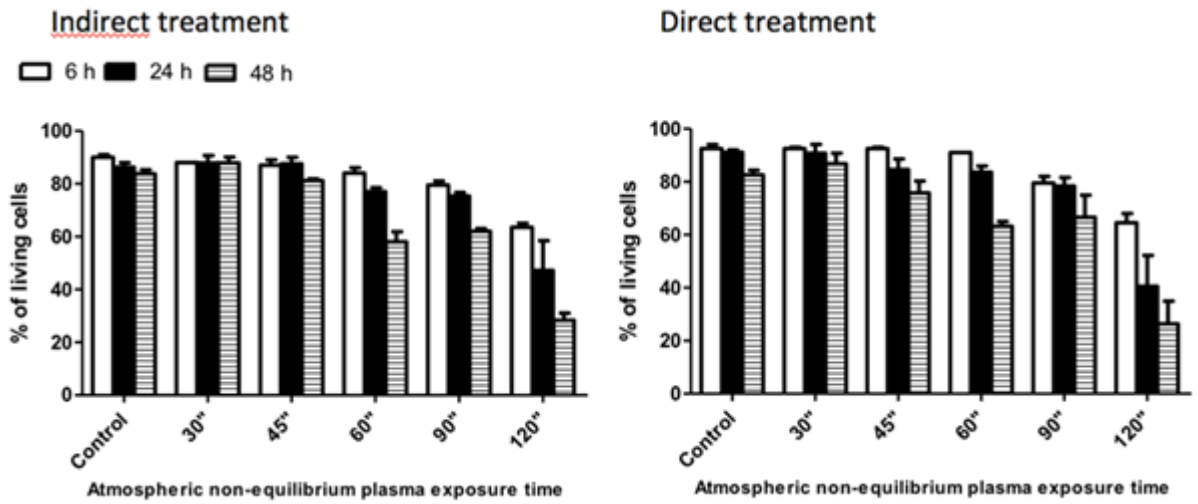

Figure 4.11 % of living cells after direct and indirect plasma treatment for different treatment times. Data were collected 6 h, 24 h and 48 h after cells were added toCAP CAP treated medium (indirect treatment) or 6 h, 24 h, 48 h afterCAP CAP exposure of cells (direct treatment). Operating conditions: PV 20 kV, PRF 500 Hz and gap 1.25 mm. [PAPER VI]

4.4.6 Measurement of reactive species in cell culture medium after plasma exposure

Results for the concentration of NO_2^-, NO_3^- and H_2O_2 produced in 1 mL of complete cell culture medium after plasma treatment, semi-quantitatively measured by means of analytic strips, are reported in Table 4.1. Results refer to treatments carried out in the same operating conditions (T1 and T2) adopted for the studies of cell viability, proliferation and cell-cycle progression; moreover, also results for plasma treatment performed with gap width 1.25 mm and treatment time 120 s, which was shown in Figure 4.10 to induce the lowest cell viability among the tested treatments, are presented for comparison and discussion.

Table 4.1 Nitrite, nitrate and peroxide concentrations in the as is and plasma treated cell culture medium. All treatments were performed at PV 20 kV and PRF 500.

Operating conditions	NO_2^- (mg/L)	NO_3^- (mg/L)	H_2O_2 (mg/L)
Untreated	0	0	0
Gap 1.25 mm, treatment time 60 s (T1)	5 - 10	100 - 250	3 - 10
Gap 2.5 mm, treatment time 120 s (T2)	5 - 10	100 - 250	3 - 10
Gap 1.25 mm, treatment time 120 s	10 - 20	100 - 250	3 - 10

For the cases T1 and T2, the measured concentration of all reactive species fell in the same range; since viability, proliferation and cell-cycle progression tests have shown different results for conditions T1 and T2, we would have to conclude that the limited sensitivity of the analytic strips prevents us from drawing further conclusions on the relative importance of the various reactive species on the modulation of cell

response to plasma exposure. Despite this limited sensitivity, a significantly higher nitrite concentration with respect to the T1 and T2 treatments was measured for the case with a 1.25 mm gap and for 120 s, while nitrate and peroxide concentrations were measured in the same range. Nitrites were previously suggested to possibly have a significant role in plasma oncology [89] and to be linked to the reduction of cell viability after plasma treatment [90,91]; accordingly, we measured the highest concentration of nitrites for the case inducing the highest reduction of cell viability: considering only the 48 h culture times, the treatment performed with a 1.25 mm gap and for 120 s resulted in a percentage of viable cell of 26%, while T1 and T2 resulted in percentages of 57.3% and 43%, respectively.

4.4.7 Conclusions on plasma treatment of lymphoma cells

CAP is a new auspicious candidate in cancer treatment and has encountered a great interest since its potential to exert anti-tumor effects was initially reported [92–94]. Beside few pioneering studies [75,87], plasma-cell interaction mechanisms are still mostly unsolved and thus are an extremely relevant subject of current cutting edge researches [95,79]. With the aim to contribute to garner knowledge on the fundamental aspects of plasma interactions with cancers cells, the effects of plasma treatment on the viability, proliferation and cell-cycle distribution of L5178Y TK+/- clone (3.7.2C) cells of mouse lymphoma have been presented in this study. Plasma treatment was shown to significantly reduce cell proliferation and to induce a statistically significant accumulation of cells in G2/M phase.
Furthermore, results for direct and indirect treatment were compared: no differences were observed, suggesting that the leading role in plasma treatment of cancer cells is played by the reactive species produced in the culture medium. Measurement of nitrites, nitrates and peroxides highlighted the production of significant concentrations of reactive species in the culture medium after plasma treatment hinting at a connection between nitrite concentration and the reduction of cell viability, supporting data and speculations presented in other works [90,91]. Future activities will be focused on a more detailed identification and quantification of the reactive species produced by plasma treatment in the culture medium and in the investigation of their role in the mechanisms of plasma interaction with cancer cells.

4.5 Atmospheric pressure DBD plasma jet for the enhancement of the adhesion of dental materials

This section of the dissertation focuses on the application of CAP in the field of dentistry for the enhancement of the bonding strength of adhesive restoration systems. The results here presented have been achieved thanks to the collaboration with two expert dental practitioners from the University of Brescia: Riccardo Tonini and Diletta Forgione. They provided the teeth samples, took care of the teeth conditioning and the standard restoration procedures and materials. Their experience was important through all the phases of the study including the design of experiments and data analysis.

4.5.1 Literature overview

The need for better adhesive performances for dental restoration systems has prompted the research of innovative tools and therapies. A possible alternative to conventional strategies that has been suggested in recent years and that is attracting considerable interest, is the use of CAP. Eva Stoffles may be regarded as the first to introduce the idea of a possible therapeutic use of plasma in dentistry in 2002 [96,97] and since then several studies have investigated such a possibility. Most of these works are reported in two useful review papers from Cha and Park [9] and Wang *et al.* [98]. Among the many dental applications of CAP reported in the literature we can find: modification of implants surfaces to improve osteointegration [99,100], cleaning of dental instruments and implants [101,102], enhancing of self-etch adhesive polymerization [103], tooth bleaching [104,105] and root canal disinfection in endodontic treatment [106–108]. Concerning the enhancement of adhesive qualities of dental restorations, few studies already demonstrated the potential of CAP pretreatment on feldspathic ceramics [109,110], enamel, dentin and composites [111–117]. The application of plasma in dentistry showed several unique advantages over conventional approaches, like the ability to easily penetrate in small and irregular root canal recesses (Figure 4.12), so avoiding the using of potentially dangerous chemicals (ex. sodium hypochlorite) [106]. With every new study, the adoption of CAP in standard dental procedures appears more and more near. Nevertheless, the use of plasma sources with limited potential for translation into real endodontic practice (due to size limitations or geometrical characteristics) combined with the absence of fundamental studies on the effect of CAP when incorporated into actual bonding procedures [98], highlights a lack in the current state of the art.
The present study aims to partially fill this gap, investigating the use of a source based on the *Plasma Gun* architecture [118,119] in a realistic endodontic procedure for the medical treatment of root canals. Push-out test results here presented demonstrate that a few minutes of plasma treatment can greatly improve the dentin-adhesive interface mechanical properties along the whole length of the root canal. The contact angle measurements support the hypothesis that the effect is driven by a plasma induced increase in dentin wettability. Moreover, the *Plasma Gun* (PG) adopted in this study was specifically designed for dental applications and can be realistically handheld and used in endodontic practice. The potential of this plasma source as a multipurpose dental device exploitable in realistic endodontic procedures is demonstrated by this study and another one, conducted in parallel, where the efficacy of the PG also in the decontamination of tooth root canals is proven [106].

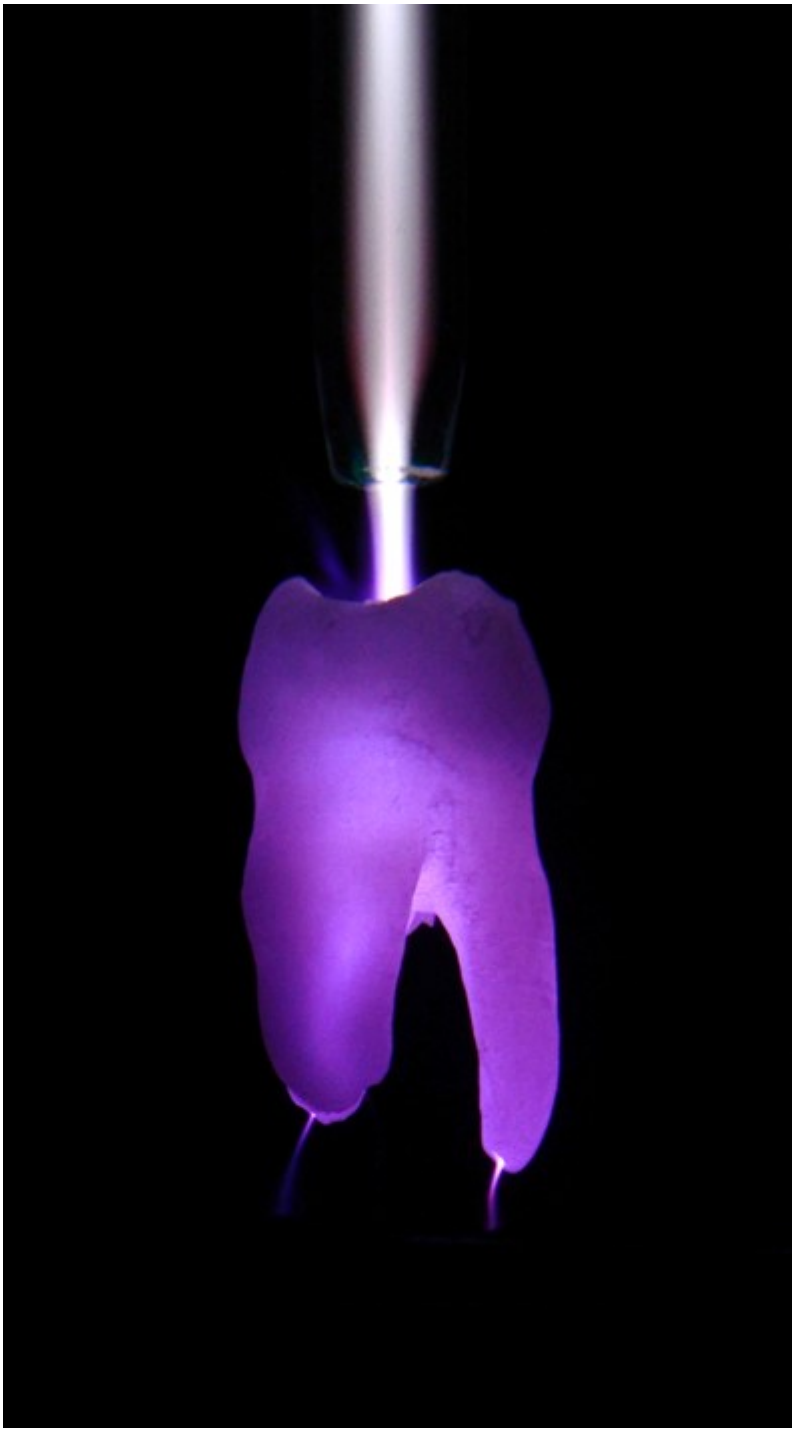

Figure 4.12 PG plume propagating inside a molar tooth model, standardized shaping the root canal by means of a conventional endodontic procedure. Plasma can be seen propagating outside tooth artificial apical openings

4.5.2 Materials and methods

Tooth sample preparation for push-out test.

Sixty monoradicular human teeth, extracted for periodontal diseases, with straight roots and regular single canals were selected for this study. Teeth were stored in 0.1% thymol solution at 4°C and used within 3 months following extraction. The crown was sectioned off at the cemento-enamel junction using a water-cooled diamond blade on a cutting machine (Isomet, Buhler, Lake Bluff, NY, USA) to expose the root canal. The first 8 mm of the canal were shaped to a regular diameter of 1,6 mm by means of a cylindrical diamond bur (Komet 837/016, Brasseler, Lemgo, D). The teeth were then embedded in epoxy resin cylinders (Silaex) using a custom molding system. The mold was designed to ensure the alignment of the root canal along the cylinder axis. As later described, this enabled an accurate alignment of the specimens during the push-out tests. After curing of the epoxy resin, the mold was opened and the samples were randomly distributed into 6 groups and conditioned with different type of dentin pre-treatment: three control group subjected to standard procedures (G1, G3, G5) and three experimental groups subjected to modified procedure that included plasma treatment (G2, G4, G6). Two different solutions were adopted as chelating agent: 17% EDTA and 1% IP6 (phytic acid). The specific conditioning protocol adopted for each group prior toadhesive and cement application is reported in Table 4.2.

Group	Dentin pretreatment
1	No dentin pretreatment
2	Plasma treatment (180 s)
3	EDTA (60 s)
4	EDTA (60 s) + plasma treatment (180 s)
5	IP6 (60 s)
6	IP6 (60 s) + plasma treatment (180 s)

Table 4.2 Dentin pretreatment protocol applied to each group after root canal shaping and prior to adhesive and cement application. Application time of each step is reported within brackets.

For all groups, after dentin pre-treatment , the canal was dried with paper point and the application of the self-etching adhesive system (Clearfil SE Bond 2 (CSE)) and of the post luting cement (Clearfil DC Core Plus) were performed, following manufacturers' instructions. Disposable plastic endodontic tips were used to inject luting material. Following light curing of the cement, specimens were stored for 24 h in water at 37°C. After water storage, accordingly to Gagliani *et al.* [120], the roots were sectioned transversally by means of a diamond saw irrigated with water. Tooth section 2.0 mm-thick were obtained from coronal and medial portions of the root canal as schematically described in Figure 4.13. The coronal and medial sections were respectively cut 1 and 4 mm apically from the cementoenamel junction. Thanks to the molding system procedure, root canal sections are found at the center of the circular specimens independently of the tooth irregular shape, allowing the accurate positioning of the specimens in the push-out testing machine.

Tooth sample preparation for contact angle measurements

Forty human third molars were used for this analysis. Teeth were stored at 4°C in a solution of 0,1% thymol for no longer than 3 months after extraction. Teeth were cut transversely to the long axis of the toot using a cutting machine (Isomet, Buhler, Lake Bluff, NY, USA) with water-cooling. A first cut, in the occlusal third of the crown, was aimed to eliminate occlusal enamel, while the second cut was performed 1 mm above the cement-enamel junction. Finally, dentin discs were 3 mm thick. Specimens obtained were finally polished using 600-grit SiC papers and randomly divided in eight groups.

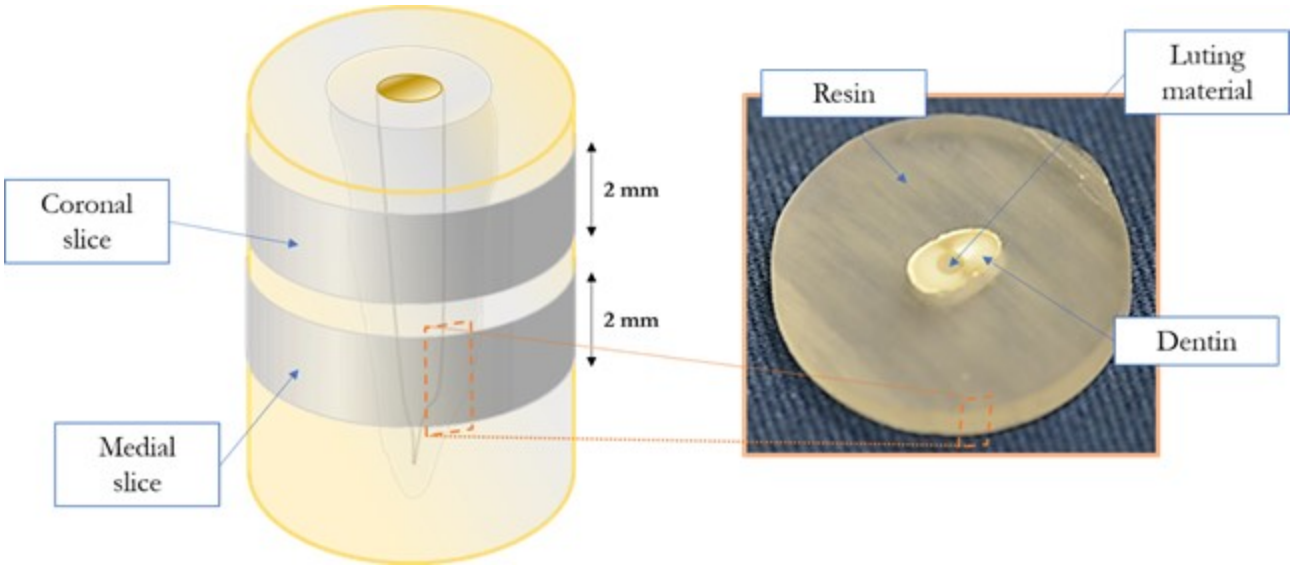

Figure 4.13 Tooth coronal and medial section specimens for pushout test.

Cold plasma treatment and experimental setup

The plasma source adopted in this work is the PG already described in detail in Chapter 2 and in a work on the decontamination of tooth root canals [106]. A picture of the PG nozzle in a real oral environment is presented in Figure 4.14. For this study the PG is driven by a micro-sinusoidal pulses HV generator (frequency and duty cycle were kept constant at 22 kHz and 7,5% respectively) with a fixed pulse repetition frequency of 100 Hz. For all experiments, the PG was operated with 15 kV of applied peak voltage with a He flow of 3 slpm. Voltage and current were monitored by means of high voltage (Tektronix P6015A) and current (Pearson 6585) probes connected to an oscilloscope (Tektronix DPO 40034). A simple description of the experimental setup used for the root canal treatments is shown in Figure 4.15. The gap distance between the PG outlet and the tooth specimens was fixed at 2 mm. In the experimental tests regarding the wettability increase of the dentin surface, different plasma treatment times were investigated (30, 60, 120 and 180 seconds) while all tooth specimens for the pushout tests were plasma exposed for 180 seconds.

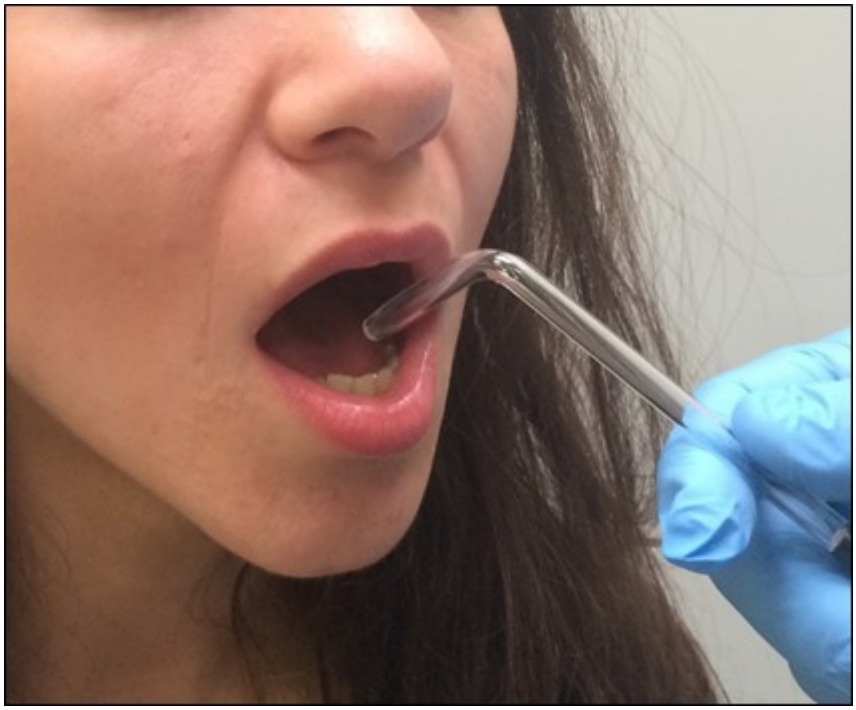

Figure 4.14 Comparison of the PG device geometry and dimension with a realistic oral environment

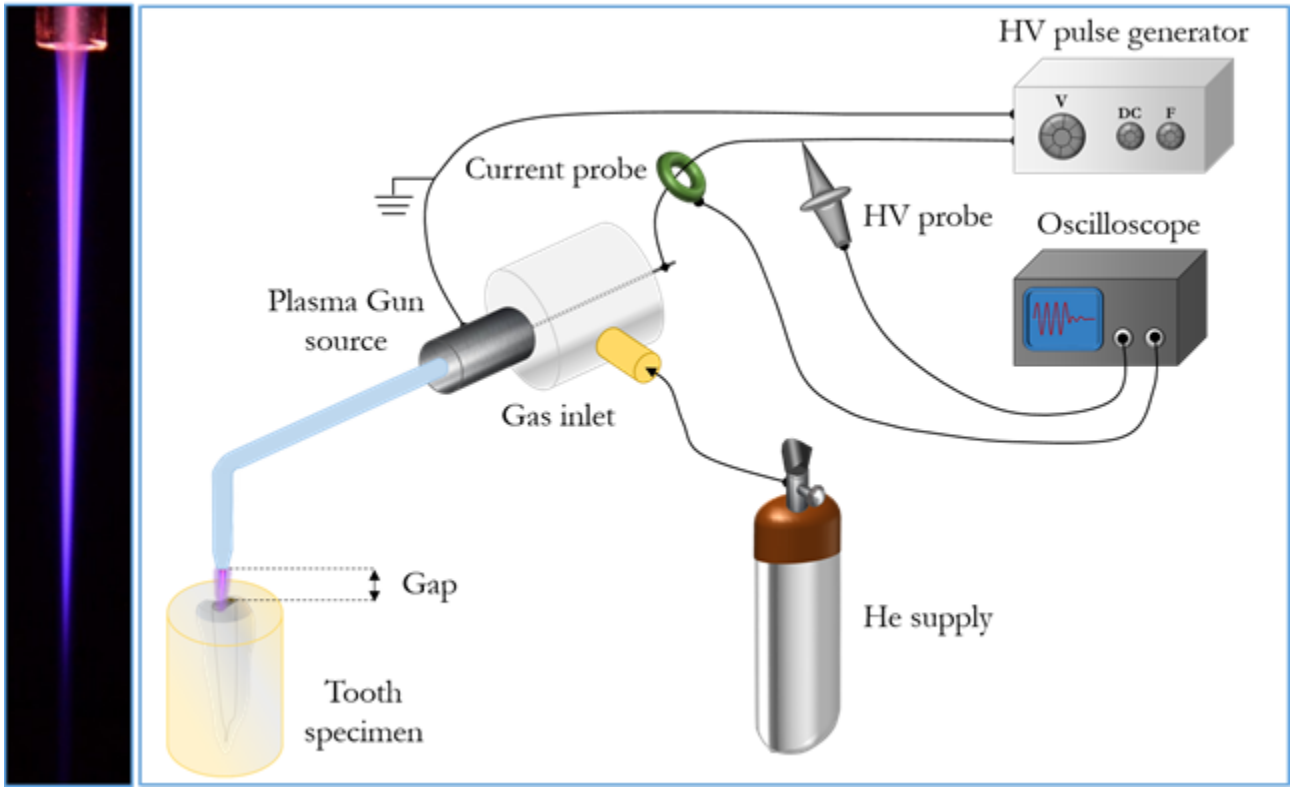

Figure 4.15 Experimental setup adopted during the plasma treatments (right side) and a plasma plume produced by PG in free flow condition (left side).

Pushout tests

The push-out test [121,120,122] evaluates bond strength between luting material and root dentin. A representative photo of push-out test is reported in Figure 4.16. The tests were performed using a universal testing machine (Instron model 8033, load cell HBM U2A 200 kg, MTS electronic Test Star IIs). The specimens were axially loaded on the cement section (Ø 1,6 mm) with a cylindrical metallic plunger (Ø 1,4 mm) at a cross-head speed of 0.5 mm/min. When dislodgement occurred, the maximum failure load was recorded in volts (V) and then converted into newton (N). For the final conversion into MPa the surface of the cement-dentin interface was esteemed from the height of each specimen measured with a digital calliper. Statistical analysis was performed applying one-variable analysis of variance (ANOVA) as post-hoc comparison at a significance level set at $p<0,05$.

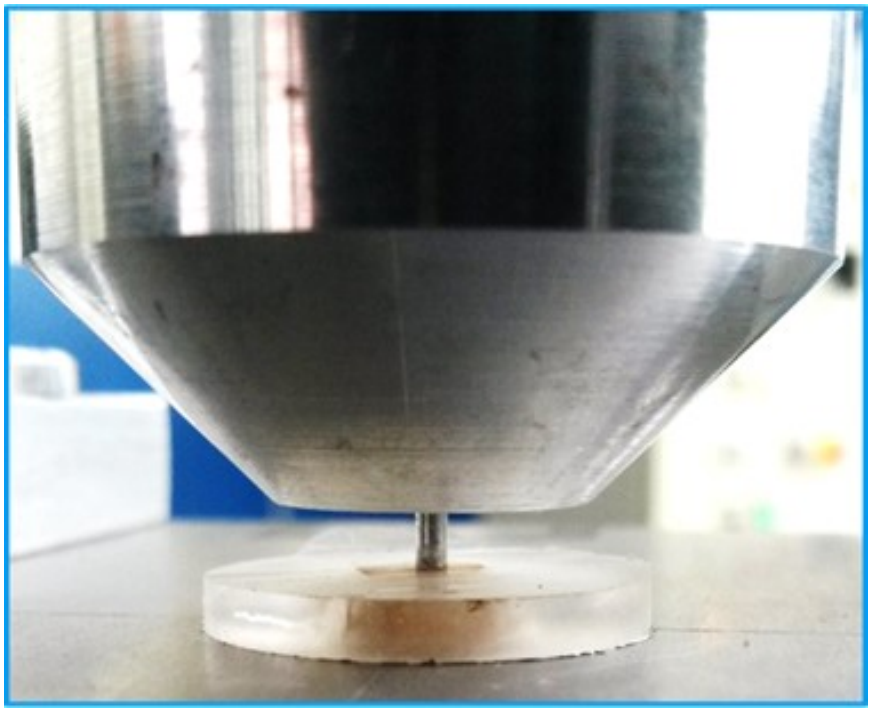

Figure 4.16 Picture of the push-out tests setup

Contact Angle (CA) measurements

CA measurements were performed to evaluate the activation of dentin surface as a result of different times of plasma exposure. Since in real practice adhesive liquids are used for the procedures, the analysis was carried out with both distillated water and adhesive droplets by means of a commercial Kruss Drop Shape Analysis System DSA 30, operated at room temperature. Using the instrument software, measurements of the static droplet CA was automated. The volume of the droplet placed over the dentin surface was fixed at 20 μl. Each measurement was run in triplicate and results are given as the average value and relative standard deviation.

4.5.3 *Results*

Pushout test

Figure 4.17 shows the mean bond strength and standard deviation of adhesives to dentin evaluated through pushout test. The data for coronal and medial sections are reported both separately and averaged. One-way ANOVA revealed that plasma treated specimens had a statistically significant increase, approximatively two times higher (~ 100%), in adhesive-denting bonding strength for the cases that included the use of an etching reagent, being it EDTA (p=0,0001) or IP6 (p=0,0018). No significant difference is observed between the plasma group pre-treated with EDTA or IP6, suggesting that the efficacy of plasma treatment is independent of the chelating agent nature. Moreover, the plasma induced enhancement of the bonding strength is achieved along the whole length of the canal system since results are not influenced by the section position (coronal or medial). Differently from these results, specimens that where not etched with EDTA or IP6 show no statistically significantly (p=0,56) variation induced by the plasma treatment.

	Mean bonding strength			% Improvement		
	Coronal	Medial	Average	Coronal	Medial	Average
No pre-treatment	26,3 ± 9,3	32,7 ± 10,5	**29,5 ± 10,0**	6%	-18%	No difference
Plasma	27,9 ± 11,6	26,7 ± 5,0	**27,3 ± 8,5**			
EDTA	22,3 ± 9,1	31,5 ±9,2	**26,9 ± 10,0**	131%	87%	**+ 104%**
EDTA + Plasma	51,5 ± 19,4	58,8 ± 20,3	**54,8 ± 19,2**			
IP6	28,8 ± 15,2	25,1 ± 13,4	**27,1 ± 13,9**	82%	114%	**+ 96%**
IP6 + Plasma	52,5 ± 18,6	53,8 ± 24,0	**53,2 ± 20,8**			

Figure 4.17 Mean bond strength of self-etching adhesives to dentin evaluated through pushout test. Last column reports the average improvement in bonding strength due to plasma application with respect to untreated control.

Surface contact angle assessment

The surface wettability results are presented in Figure 4.18. The water contact angle on the dentin surface is reduced with increasing plasma treatment duration. The contact angle of a drop of water on the un-treated dentin surface was 69,8 ± 14,3°. The treatment time investigated for the push-out tests is found to be in an asymptotic range where a minimum constant angle (<10°) is achieved.
Since in the real practice the adhesive liquid is used for the procedure the contact angle measurements were performed also using this liquid. Results of these tests are presented in Figure 4.19. Also in this case, a very small contact angle is reached for a treatment equal to that adopted for push-out tests (180s). Plasma treatment not only contributed to a significant decrease of the adhesive contact angle but also in reducing the data dispersion, meaning that the natural differences between teeth were partially levelled by the process.

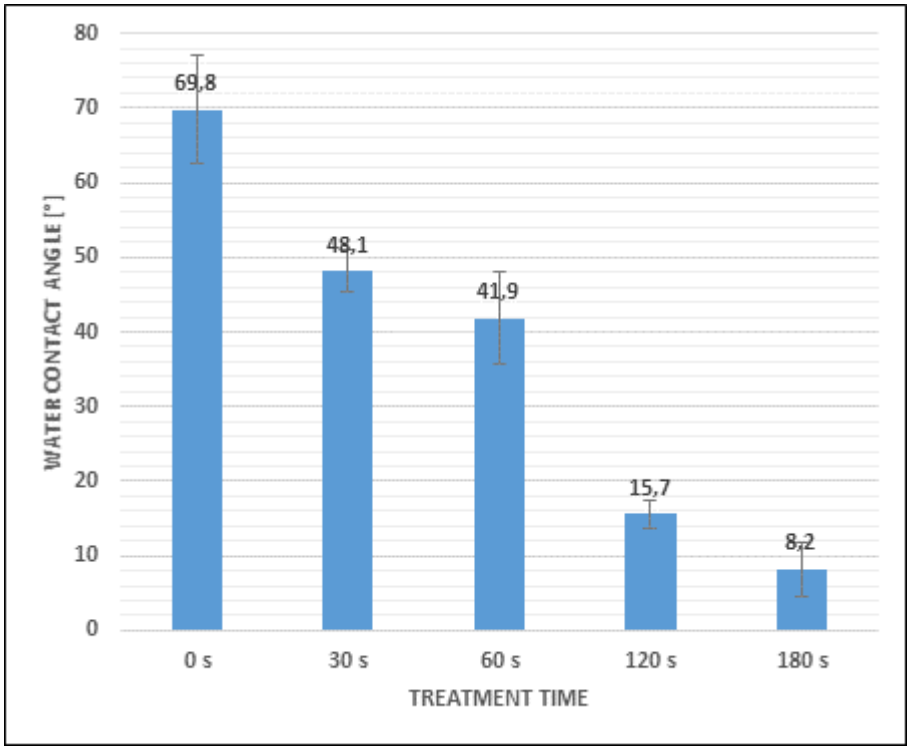

Figure 4.18 Water contact angle values of dentin slices as a function of exposure time to PG treatment.

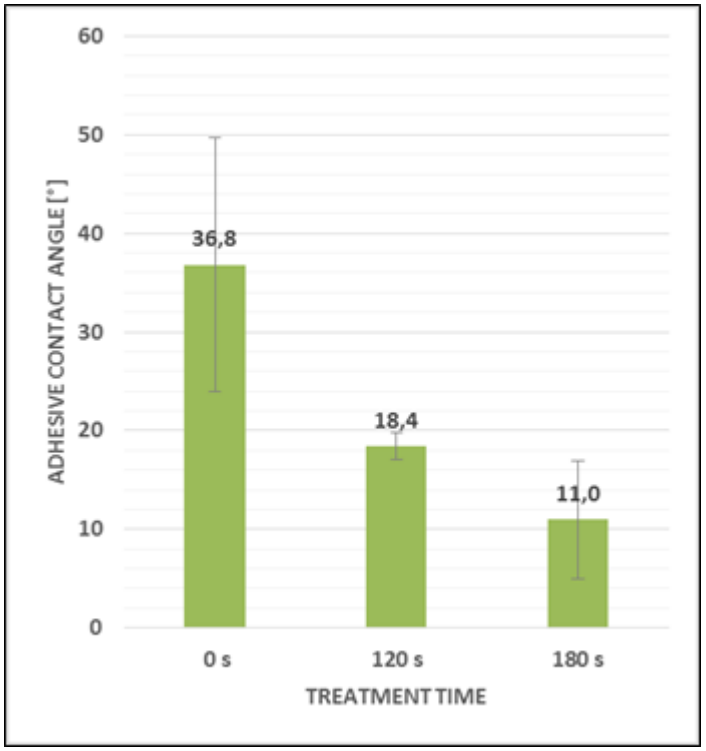

Figure 4.19 Adhesive contact angle values of dentin slices as a function of exposure time to PG treatment.

4.5.4 *Discussion*

The present study demonstrates bonding strength improvement following the introduction of CAP application in a conventional dental restoration endodontic procedure. Results were obtained with a handheld plasma device (*Plasma Gun*) having a compact size that can be comfortably operated by dental practitioners in clinics.

Push-out results clearly showed an extremely significant enhancement of the dentin-composite interface mean bonding strength as a consequence of plasma dentin pre-treatment. The results report an improvement of adhesion strength of approximatively +100% when plasma was applied on the root canal dentin after chelating agent application. Recorded data indicate that this effect does not dependent on the nature of the chelating agent as very similar values were achieved both for EDTA and IP6.

The absolute values obtained both for control samples are slightly lower than those reported by other studies for the same adhesive system tested by means of microtensile bond strength test (μMBS) instead of push-out [117]. Nevertheless, the mean bond strength percentage increase of plasma treated specimens over untreated control results higher than those found in literature (~25-65%) for various plasma sources (Ar plasma brush [111,113,116], Kin-Pen [117], He DBD-jet [114]).

To achieve a satisfying adhesion the bonding solution must come into close contact with the substrate to facilitate molecular interaction and allow both micromechanical entanglement and chemical absorption [123]. Shallow depth of penetration is a major drawback of mild self-etching adhesive like the Clearfil SE Bond adopted in this study [116]. Relatively short resin tags (infiltrations of adhesive resin inside dentine tubules) are normally obtained in correspondence of dentin tubules [124,125]. As already reported in other studies [114,116,117], plasma treatment of dentine may help the adhesive to penetrate into dentin and dentinal tubules and form a thicker hybrid layer and longer resin tags. The drastic improvement of the adhesive-dentin interface bonding strength observed in our case can be reasonably attributed to an increase in adhesive penetration in dental tubules that strongly enhances the interface quality.

The hypothesis is supported by contact angle measurements where a significant increase of the wettability is induced by plasma treatment. As expected by the literature [114,116,117], the water contact angle of the dentin surface decreases with increasing plasma treatment duration, down to values characteristic of highly hydrophilic surfaces (<10°) after 180s of treatment. In our study we also directly demonstrated the enhanced spreading of the adhesive liquid induced by the plasma treatment measuring the adhesive contact angle on the treated dentin surface.

The contact angle value depends on chemical composition and surface roughness. As reported by Chen *et al.* [126] a dentin surface morphology change is unlikely the result of exposure to CAP. This suggests that the enhancement in the spreading of the adhesive is mostly due to a chemical modification of the dentin surface induced by forming new oxygen-containing groups (ex. -OH, -OOH), and in general by the grafting of new polar functionalities, onto the dentin surface [126,127]. Since the PG was supplied with high purity helium gas, the oxygen most probably comes from ambient air diffusion into the plasma plume, which once excited can form highly reactive oxygen species that then react with the dentin surface [126].

After root canal shaping the dentine surface is usually covered by an unstable layer of microcrystalline and organic particle debris known as "smear layer" [99]. This layer, hard to remove if not by applying chelating agents such as EDTA or IP6 [99], can prevent the penetration of adhesive liquid into dentine tubules and therefore the achieving of high adhesive-dentin bonding strength. As reported in the work of Dong *et al.* [116], the plasma treatment of dentin surface alone does not grant removal of the smear layer. Thus, the plasma enhancement of adhesive penetration into tubules may by nullified by the presence of the smear layer. This assumption is confirmed both by our results and those by Hirata *et al.* [117], where no significant differences in the adhesive bonding strength of control and plasma treated specimens were found when no chelating agents were adopted. Tubules size, orientation, surface area and water content of dentin can vary from location to location in the tooth [111]. Partially in contrast with the literature [111], in this case the effectiveness of plasma treatment in enhancing the adhesive bonding strength does not vary significantly along the root canal length. It may be assumed that in our

case the plasma plume, is able to penetrate into the root canal recesses and dentin tubules, in this way activating the entire root canal surface.

4.5.5 *Conclusions on plasma enhancement of adhesion of dental materials*

Numerous research papers have been published providing evidences of efficacy and advantages of CAP technology in the field of dentistry, attracting considerable attention. Nevertheless, the literature is somehow lacking with respect to plasma overall effect when introduced in actual dental procedures. In this study, the feasibility of adopting CAP technology to increase adhesive-dentin surface bonding strength and reduce root canal restoration failure has been demonstrated showing how the simple addition of a 180 s plasma treatment to a conventional procedures can lead to approximatively the doubling of the mean bonding strength along the entire root canal length.
The experimental results obtained from this study, combined with those already published in a previous work [106], demonstrate the *Plasma Gun* device may be a feasible option for obtaining an enhancement of dental adhesive systems and an effective root canal decontamination. Even if future clinical *in vivo* studies are still required, the future of dental plasma devices appears day by day more certain.

4.6 References

[1] D. Cutler, A. Deaton, and A. Lleras-Muney, "The Determinants of Mortality," Cambridge, MA, Jan. 2006.

[2] J. D. Howell, "Technology in the Hospital: Transforming Patient Care in the Early Twentieth Century," Nat. Med., vol. 2, no. 4, p. 479, 1996.

[3] A.-P. Magiorakos, A. Srinivasan, R. B. Carey, Y. Carmeli, M. E. Falagas, C. G. Giske, S. Harbarth, J. F. Hindler, G. Kahlmeter, B. Olsson-Liljequist, D. L. Paterson, L. B. Rice, J. Stelling, M. J. Struelens, A. Vatopoulos, J. T. Weber, and D. L. Monnet, "Multidrug-resistant, extensively drug-resistant and pandrug-resistant bacteria: an international expert proposal for interim standard definitions for acquired resistance," Clin. Microbiol. Infect., vol. 18, no. 3, pp. 268–281, Mar. 2012.

[4] S. Stewart, "Heart failure and the aging population: an increasing burden in the 21st century?," Heart, vol. 89, no. 1, pp. 49–53, Jan. 2003.

[5] S. M. F. Pluijm, M. Visser, M. T. E. Puts, M. G. Dik, B. W. M. Schalk, N. M. van Schoor, L. A. Schaap, R. J. Bosscher, and D. J. H. Deeg, "Unhealthy lifestyles during the life course: association with physical decline in late life," Aging Clin. Exp. Res., vol. 19, no. 1, pp. 75–83, Feb. 2007.

[6] Y. Li, S. H. Ley, D. K. Tobias, S. E. Chiuve, T. J. VanderWeele, J. W. Rich-Edwards, G. C. Curhan, W. C. Willett, J. E. Manson, F. B. Hu, and L. Qi, "Birth weight and later life adherence to unhealthy lifestyles in predicting type 2 diabetes: prospective cohort study," BMJ, p. h3672, Jul. 2015.

[7] D. C. Wallace, "A Mitochondrial Paradigm of Metabolic and Degenerative Diseases, Aging, and Cancer: A Dawn for Evolutionary Medicine," Annu. Rev. Genet., vol. 39, no. 1, pp. 359–407, Dec. 2005.

[8] L. Diaz Högberg, K. Weist, C. Suetens, J. Griskeviciene, D. Monnet, and O. Heuer, "Annual epidemiological report."

[9] S. Cha and Y.-S. Park, "Plasma in dentistry," Clin. Plasma Med., vol. 2, pp. 1–7, 2014.

[10] R. Tiede, J. Hirschberg, G. Daeschlein, T. von Woedtke, W. Vioel, and S. Emmert, "Plasma Applications: A Dermatological View," Contrib. to Plasma Phys., vol. 54, no. 2, pp. 118–130, 2014.

[11] Z. B. Guzel-Seydim, A. K. Greene, and A. C. Seydim, "Use of ozone in the food industry," LWT - Food Science and Technology, vol. 37, no. 4. pp. 453–460, 2004.

[12] Y. Haque and B. D. Ratner, "Preparation and properties of plasma-deposited films with surface energies varying over a wide range," J. Appl. Polym. Sci., vol. 32, no. 4, pp. 4369–4381, Sep. 1986.

[13] B. D. Ratner, A. Chilkoti, and G. P. Lopez, Plasma deposition and treatment for biomaterial applications. Academic Press inc., 1990.

[14] G. Fridman, G. Friedman, A. Gutsol, A. B. Shekhter, V. N. Vasilets, and A. Fridman, "Applied plasma medicine," Plasma Process. Polym., vol. 5, no. 6, pp. 503–533, 2008.

[15] J. Han, "Review of Major Directions in Non-Equilibrium Atmospheric Plasma Treatments in Medical, Biological, and Bioengineering Applications," Plasma Med., vol. 3, no. 3, pp. 175–243, 2013.

[16] T. von Woedtke, S. Reuter, K. Masur, and K.-D. Weltmann, "Plasmas for medicine," Phys. Rep., vol. 530, no. 4, pp. 291–320, Sep. 2013.

[17] R. d'Agostino, P. Favia, C. Oehr, and M. R. Wertheimer, "Low-Temperature Plasma Processing of Materials: Past, Present, and Future," Plasma Process. Polym., vol. 2, no. 1, pp. 7–15, 2005.

[18] Menashi Wilson, "Treatment of surfaces," US3383163 A, 1968.

[19] J. H. Park, N. Kumar, D. H. Park, M. Yusupov, E. C. Neyts, C. C. W. Verlackt, A. Bogaerts, M. H. Kang, H. S. Uhm, E. H. Choi, and P. Attri, "A comparative study for the inactivation of multidrug resistance bacteria using dielectric barrier discharge and nano-second pulsed plasma.," Sci. Rep., vol. 5, no. April, p. 13849, 2015.

[20] J. L. Zimmermann, T. Shimizu, H.-U. Schmidt, Y.-F. Li, G. E. Morfill, and G. Isbary, "Test for bacterial resistance build-up against plasma treatment," New J. Phys., vol. 14, no. 7, p. 073037, Jul. 2012.

[21] F. Perez, A. M. Hujer, K. M. Hujer, B. K. Decker, P. N. Rather, and R. A. Bonomo, "Global Challenge of Multidrug-Resistant Acinetobacter baumannii," Antimicrob. Agents Chemother., vol. 51, no. 10, pp. 3471–3484, Oct. 2007.

[22] M. K. Boudam, M. Moisan, B. Saoudi, C. Popovici, N. Gherardi, and F. Massines, "Bacterial spore inactivation by atmospheric-pressure plasmas in the presence or absence of UV photons as obtained with the same gas mixture," J. Phys. D. Appl. Phys., vol. 39, no. 16, pp. 3494–3507, Aug. 2006.

[23] X. T. Deng, J. J. Shi, H. L. Chen, and M. G. Kong, "Protein destruction by atmospheric pressure glow discharges," Appl. Phys. Lett., vol. 90, no. 1, p. 013903, 2007.

[24] M. Moreau, N. Orange, and M. G. J. Feuilloley, "Non-thermal plasma technologies: New tools for bio-decontamination," Biotechnol. Adv., vol. 26, no. 6, pp. 610–617, 2008.

[25] M. Laroussi, "Nonthermal decontamination of biological media by atmospheric-pressure plasmas: Review, analysis, and prospects," IEEE Trans. Plasma Sci., vol. 30, no. 4 I, pp. 1409–1415, 2002.

[26] K.-D. Weltmann, R. Brandenburg, T. von Woedtke, J. Ehlbeck, R. Foest, M. Stieber, and E. Kindel, "Antimicrobial treatment of heat sensitive products by miniaturized atmospheric pressure plasma jets (APPJs)," J. Phys. D. Appl. Phys., vol. 41, no. 19, p. 194008, 2008.

[27] P. Hensley, "TipCharger®, A Breakthrough Wash Technology," J. Assoc. Lab. Autom., vol. 7, no. 1, pp. 64–65, Feb. 2002.

[28] S. Iseni, "Laser diagnostics of an Ar atmospheric pressure plasma jet for biomedical applications Diagnostic laser d ' un jet plasma froid d ' argon à la pression atmosphérique pour les applications biomédicales Dissertation présentée pour l ' obtention du titre de," 2016.

[29] A. Fridman and G. Friedman, Plasma Medicine. Wiley-VCH, 2013.

[30] M. A. Bogle, K. A. Arndt, and J. S. Dover, "Evaluation of Plasma Skin Regeneration Technology in Low-Energy Full-Facial Rejuvenation," Arch. Dermatol., vol. 143, no. 2, Feb. 2007.

[31] M. L. Elsaie and J. N. Kammer, "Evaluation of plasma skin regeneration technology for cutaneous remodeling," J. Cosmet. Dermatol., vol. 7, no. 4, pp. 309–311, Dec. 2008.

[32] S. Bekeschus, A. Schmidt, K.-D. Weltmann, and T. von Woedtke, "The plasma jet kINPen – A powerful tool for wound healing," Clin. Plasma Med., pp. 1–10, 2016.

[33] J.-H. Lee, E.-H. Choi, K.-M. Kim, and K.-N. Kim, "Effect of non-thermal air atmospheric pressure plasma jet treatment on gingival wound healing," J. Phys. D. Appl. Phys., vol. 49, no. 7, p. 075402, 2016.

[34] I. E. Kieft, D. Darios, A. J. M. Roks, and E. Stoffels, "Plasma treatment of mammalian vascular cells: A quantitative description," IEEE Trans. Plasma Sci., vol. 33, no. 2 II, pp. 771–775, 2005.

[35] E. Stoffels, I. E. Kieft, R. E. J. Sladek, E. P. Van Der Laan, and M. Steinbuch, "Plasma needle for in vivo medical treatment : recent developments," Plasma Sources Sci. Technol., vol. 15, pp. 169–180, 2006.

[36] S. Coulombe, V. Léveillé, S. Yonson, and R. L. Leask, "Miniature atmospheric pressure glow discharge torch (APGD-t) for local biomedical applications," Pure Appl. Chem., vol. 78, no. 6, Jan. 2006.

[37] Y. Sakai, V. Khajoee, Y. Ogawa, K. Kusuhara, Y. Katayama, and T. Hara, "A novel transfection method for mammalian cells using gas plasma," J. Biotechnol., vol. 121, no. 3, pp. 299–308, 2006.

[38] D. B. Graves, "Oxy-nitroso shielding burst model of cold atmospheric plasma therapeutics," Clin. Plasma Med., vol. 2, no. 2, pp. 38–49, 2014.

[39] N. Kaushik, N. Kumar, C. H. Kim, N. K. Kaushik, and E. H. Choi, "Dielectric Barrier Discharge Plasma Efficiently Delivers an Apoptotic Response in Human Monocytic Lymphoma," Plasma Process. Polym., vol. 11, no. 12, pp. 1175–1187, Dec. 2014.

[40] T. Bjarnsholt, P. Ø. Jensen, M. Burmølle, M. Hentzer, J. A. J. Haagensen, H. P. Hougen, H. Calum, K. G. Madsen, C. Moser, S. Molin, N. Høiby, and M. Givskov, "Pseudomonas aeruginosa tolerance to tobramycin, hydrogen peroxide and polymorphonuclear leukocytes is quorum-sensing dependent.," Microbiology, vol. 151, no. Pt 2, pp. 373–83, Feb. 2005.

[41] X. Cheng, J. Sherman, W. Murphy, E. Ratovitski, J. Canady, and M. Keidar, "The Effect of Tuning Cold Plasma Composition on Glioblastoma Cell Viability," PLoS One, vol. 9, no. 5, p. e98652, May 2014.

[42] J.-W. Lackmann, S. Schneider, E. Edengeiser, F. Jarzina, S. Brinckmann, E. Steinborn, M. Havenith, J. Benedikt, and J. E. Bandow, "Photons and particles emitted from cold atmospheric-pressure plasma inactivate bacteria and biomolecules independently and synergistically," J. R. Soc. Interface, vol. 10, no. 89, pp. 20130591–20130591, Sep. 2013.

[43] S. Samukawa, M. Hori, S. Rauf, K. Tachibana, P. Bruggeman, G. Kroesen, J. C. Whitehead, A. B. Murphy, A. F. Gutsol, S. Starikovskaia, U. Kortshagen, J.-P. Boeuf, T. J. Sommerer, M. J. Kushner, U. Czarnetzki, and N. Mason, "The 2012 Plasma Roadmap," J. Phys. D Appl. Phys. J. Phys. D Appl. Phys, vol. 45, no. 45, pp. 253001–253001, 2012.

[44] D. Dobrynin, G. Fridman, G. Friedman, and A. Fridman, "Physical and biological mechanisms of direct plasma interaction with living tissue," New J. Phys., vol. 11, 2009.

[45] P. Lukes, E. Dolezalova, I. Sisrova, and M. Clupek, "Aqueous-phase chemistry and bactericidal effects from an air discharge plasma in contact with water: evidence for the formation of peroxynitrite through a pseudo-second-order post-discharge reaction of H 2 O 2 and HNO 2," Plasma Sources Sci. Technol., vol. 23, no. 1, p. 015019, 2014.

[46] M. G. Kong, G. Kroesen, G. Morfill, T. Nosenko, T. Shimizu, J. Van Dijk, and J. L. Zimmermann, "Plasma medicine: An introductory review," New J. Phys., vol. 11, 2009.

[47] K.-D. Weltmann and T. von Woedtke, "Basic requirements for plasma sources in medicine," Eur. Phys. J. Appl. Phys., vol. 55, no. 1, p. 13807, 2011.

[48] G. Fridman, M. Peddinghaus, M. Balasubramanian, H. Ayan, A. Fridman, A. Gutsol, and A. Brooks, "Blood Coagulation and Living Tissue Sterilization by Floating-Electrode Dielectric Barrier Discharge in Air," Plasma Chem. Plasma Process., vol. 26, no. 4, pp. 425–442, Aug. 2006.

[49] H. Jablonowski and T. von Woedtke, "Research on plasma medicine-relevant plasma-liquid interaction: What happened in the past five years?," Clin. Plasma Med., vol. 3, no. 2, pp. 42–52, 2015.

[50] C. Hirt, A. Papadimitropoulos, M. G. Muraro, V. Mele, E. Panopoulos, E. Cremonesi, R. Ivanek, E. Schultz-Thater, R. A. Droeser, C. Mengus, M. Heberer, D. Oertli, G. Iezzi, P. Zajac, S. Eppenberger-Castori, L. Tornillo, L. Terracciano, I. Martin, and G. C. Spagnoli, "Bioreactor-engineered cancer tissue-like structures mimic phenotypes, gene expression profiles and drug resistance patterns observed 'in vivo,'" Biomaterials, vol. 62, pp. 138–146, 2015.

[51] D. B. Graves, "The emerging role of reactive oxygen and nitrogen species in redox biology and some implications for plasma applications to medicine and biology," J. Phys. D. Appl. Phys., vol. 45, no. 26, p. 263001, 2012.

[52] M. Keidar, R. Walk, a Shashurin, P. Srinivasan, a Sandler, S. Dasgupta, R. Ravi, R. Guerrero-Preston, and B. Trink, "Cold plasma selectivity and the possibility of a paradigm shift in cancer therapy.," Br. J. Cancer, vol. 105, no. 9, pp. 1295–301, 2011.

[53] L. F. Chen, C. K. Ong, C. P. Neo, V. V. Varadan, and V. K. Varadan, Microwave Electronics: Measurement and Materials Characterization. Wiley, 2004.

[54] G. Isbary, J. L. Zimmermann, T. Shimizu, G. E. Morfill, A. Mitra, H. M. Thomas, T. G. Klampfl, J. Koeritzer, V. Boxhammer, J. Schlegel, and W. Stolz, "Reasons Why We Need Cold Atmospheric Plasmas in Bacteria-Related Diseases in Medicine," Plasma Med., vol. 2, no. 1–3, pp. 85–96, 2012.

[55] R. Pompl, F. Jamitzky, T. Shimizu, B. Steffes, W. Bunk, H.-U. Schmidt, M. Georgi, K. Ramrath, W. Stolz, R. W. Stark, T. Urayama, S. Fujii, and G. E. Morfill, "The effect of low-temperature plasma on bacteria as observed by repeated AFM imaging," New J. Phys., vol. 11, no. 11, p. 115023, Nov. 2009.

[56] D. Dobrynin, G. Friedman, A. Fridman, and A. Starikovskiy, "Inactivation of bacteria using dc corona discharge: role of ions and humidity," New J. Phys., vol. 13, no. 10, p. 103033, Oct. 2011.

[57] B. J. Park, D. H. Lee, J.-C. Park, I.-S. Lee, K.-Y. Lee, S. O. Hyun, M.-S. Chun, and K.-H. Chung, "Sterilization using a microwave-induced argon plasma system at atmospheric pressure," Phys. Plasmas, vol. 10, no. 11, p. 4539, 2003.

[58] M. Y. Alkawareek, Q. T. Algwari, G. Laverty, S. P. Gorman, W. G. Graham, D. O'Connell, and B. F. Gilmore, "Eradication of Pseudomonas aeruginosa Biofilms by Atmospheric Pressure Non-Thermal Plasma," PLoS One, vol. 7, no. 8, p. e44289, Aug. 2012.

[59] F. Marchal, H. Robert, N. Merbahi, C. Fontagné-Faucher, M. Yousfi, C. E. Romain, O. Eichwald, C. Rondel, and B. Gabriel, "Inactivation of Gram-positive biofilms by low-temperature plasma jet at atmospheric pressure," J. Phys. D. Appl. Phys., vol. 45, no. 34, p. 345202, Aug. 2012.

[60] L. Taghizadeh, G. Brackman, A. Nikiforov, J. van der Mullen, C. Leys, and T. Coenye, "Inactivation of Biofilms Using a Low Power Atmospheric Pressure Argon Plasma Jet; the Role of Entrained Nitrogen," Plasma Process. Polym., vol. 12, no. 1, pp. 75–81, 2015.

[61] S. Ermolaeva, A. F. Varfolomeev, M. Y. Chernukha, D. S. Yurov, M. M. Vasiliev, A. a. Kaminskaya, M. M. Moisenovich, J. M. Romanova, A. N. Murashev, I. I. Selezneva, T. Shimizu, E. V. Sysolyatina, I. a. Shaginyan, O. F. Petrov, E. I. Mayevsky, V. E. Fortov, G. E. Morfill, B. S. Naroditsky, and A. L. Gintsburg, "Bactericidal effects of non-thermal argon plasma in vitro, in biofilms and in the animal model of infected wounds," J. Med. Microbiol., vol. 60, no. 1, pp. 75–83, 2011.

[62] J. C. Joaquin, C. Kwan, N. Abramzon, K. Vandervoort, and G. Brelles-Marino, "Is gas-discharge plasma a new solution to the old problem of biofilm inactivation?," Microbiology, vol. 155, no. 3, pp. 724–732, Mar. 2009.

[63] G. Tirelli, R. Rizzo, M. Biasotto, R. Di Lenarda, B. Argenti, A. Gatto, and F. Bullo, Obturator prostheses following palatal resection: clinical cases., vol. 30, no. 1. 2010, pp. 33–39.

[64] F. Song, H. Koo, and D. Ren, "Effects of Material Properties on Bacterial Adhesion and Biofilm Formation," J. Dent. Res., pp. 1–8, 2015.

[65] S. L. Percival, L. Suleman, C. Vuotto, and G. Donelli, "Healthcare-associated infections, medical devices and biofilms: risk, tolerance and control," J. Med. Microbiol., vol. 64, no. Pt_4, pp. 323–334, Apr. 2015.

[66] C. J. Crnich and P. Drinka, "Medical Device-Associated Infections in the Long-Term Care Setting," Infectious Disease Clinics of North America, vol. 26, no. 1. pp. 143–164, 2012.

[67] W. Heuer, C. Elter, A. Demling, A. Neumann, S. Suerbaum, M. Hannig, T. Heidenblut, F. W. Bach, and M. Stiesch-Scholz, "Analysis of early biofilm formation on oral implants in man," J. Oral Rehabil., vol. 34, no. 5, pp. 377–382, 2007.

[68] M. C. Goiato, D. M. dos Santos, A. Moreno, J. F. Santiago, M. F. Haddad, A. A. Pesqueira, and G. I. Miyahara, "Prosthetic Treatments for Patients With Oronasal Communication," J. Craniofac. Surg., vol. 22, no. 4, pp. 1445–1447, Jul. 2011.

[69] B. C. Webb, C. J. Thomas, M. D. P. Willcox, D. W. S. Harty, and K. W. Knox, "Candida-associated denture stomatitis. Aetiology and management: A review. Part 3. Treatment of oral candidosis," Aust. Dent. J., vol. 43, no. 3, pp. 244–249, Aug. 1998.

[70] D. J. Miller, "Diagnosis and management of Candida and other fungal infections of the head and neck," Curr. Infect. Dis. Rep., vol. 4, no. 3, pp. 194–200, May 2002.

[71] A. Jemal, R. Siegel, J. Xu, and E. Ward, "Cancer statistics, 2010," CA Cancer J Clin, vol. 60, no. 5, pp. 277–300, 2010.

[72] D. Hanahan and R. a Weinberg, "the hallmark of cancer," Cell, vol. 60, pp. 319–326, 2000.

[73] A. Arcangeli, S. Pillozzi, and A. Becchetti, "Targeting Ion Channels in Leukemias: A New Challenge for Treatment," Curr. Med. Chem., vol. 19, no. 5, pp. 683–696, 2012.

[74] J. E. Karp, D. D. Ross, W. Yang, M. L. Tidwell, Y. Wei, J. Greer, D. L. Mann, T. Nakanishi, J. J. Wright, and A. D. Colevas, "Timed sequential therapy of acute leukemia with flavopiridol: in vitro model for a phase I clinical trial," Clin Cancer Res, vol. 9, no. 1, pp. 307–315, 2003.

[75] M. Keidar, R. Walk, a Shashurin, P. Srinivasan, a Sandler, S. Dasgupta, R. Ravi, R. Guerrero-Preston, and B. Trink, "Cold plasma selectivity and the possibility of a paradigm shift in cancer therapy.," Br. J. Cancer, vol. 105, no. 9, pp. 1295–301, 2011.

[76] M. Vandamme, E. Robert, S. Pesnel, E. Barbosa, S. Dozias, J. Sobilo, S. Lerondel, A. Le Pape, and J. M. Pouvesle, "Antitumor effect of plasma treatment on u87 glioma xenografts: Preliminary results," Plasma Process. Polym., vol. 7, no. 3–4, pp. 264–273, 2010.

[77] B. Gweon, M. Kim, D. Bee Kim, D. Kim, H. Kim, H. Jung, J. H. Shin, and W. Choe, "Differential responses of human liver cancer and normal cells to atmospheric pressure plasma," Applied Physics Letters, vol. 99, no. 6. 2011.

[78] M. Ishaq, S. Kumar, H. Varinli, Z. J. Han, A. E. Rider, M. D. M. Evans, A. B. Murphy, and K. Ostrikov, "Atmospheric gas plasma-induced ROS production activates TNF-ASK1 pathway for the induction of melanoma cancer cell apoptosis," Mol. Biol. Cell, vol. 25, no. 9, pp. 1523–1531, May 2014.

[79] Y. Ma, C. S. Ha, S. W. Hwang, H. J. Lee, G. C. Kim, K.-W. Lee, and K. Song, "Non-Thermal Atmospheric Pressure Plasma Preferentially Induces Apoptosis in p53-Mutated Cancer Cells by Activating ROS Stress-Response Pathways," PLoS One, vol. 9, no. 4, p. e91947, Apr. 2014.

[80] O. Volotskova, T. S. Hawley, M. a Stepp, and M. Keidar, "Targeting the cancer cell cycle by cold atmospheric plasma.," Sci. Rep., vol. 2, p. 636, 2012.

[81] T. Adachi, H. Tanaka, S. Nonomura, H. Hara, S. Kondo, and M. Hori, "Plasma-activated medium induces A549 cell injury via a spiral apoptotic cascade involving the mitochondrial–nuclear network," Free Radic. Biol. Med., vol. 79, pp. 28–44, 2015.

[82] H. Tanaka, M. Mizuno, K. Ishikawa, K. Nakamura, H. Kajiyama, H. Kano, F. Kikkawa, and M. Hori, "Plasma-Activated Medium Selectively Kills Glioblastoma Brain Tumor Cells by Down-Regulating a Survival Signaling Molecule, AKT Kinase," Plasma Med., vol. 1, no. 3–4, pp. 265–277, 2011.

[83] F. Utsumi, H. Kajiyama, K. Nakamura, H. Tanaka, M. Mizuno, K. Ishikawa, H. Kondo, H. Kano, M. Hori, and F. Kikkawa, "Effect of indirect nonequilibrium atmospheric pressure plasma on anti-proliferative activity against chronic chemo-resistant ovarian cancer cells in vitro and in vivo," PLoS One, vol. 8, no. 12, p. e81576, 2013.

[84] V. Miller, A. Lin, and A. Fridman, "Why Target Immune Cells for Plasma Treatment of Cancer," Plasma Chem. Plasma Process., 2015.

[85] A. Wilson, D. Staack, T. Farouk, A. Gutsol, A. Fridman, and B. Farouk, "Self-rotating dc atmospheric-pressure discharge over a water-surface electrode: regimes of operation," Plasma Sources Sci. Technol., vol. 17, no. 4, p. 045001, Nov. 2008.

[86] A. R. Cuddihy and M. J. O'Connell, "Cell-cycle responses to DNA damage in G2," Int. Rev. Cytol., vol. 222, pp. 99–140, 2003.

[87] M. Vandamme, E. Robert, S. Lerondel, V. Sarron, D. Ries, S. Dozias, J. Sobilo, D. Gosset, C. Kieda, B. Legrain, J.-M. Pouvesle, and A. Le Pape, "ROS implication in a new antitumor strategy based on non thermal plasma.," Int. J. Cancer, 2011.

[88] S. Mohades, N. Barekzi, and M. Laroussi, "Efficacy of Low Temperature Plasma against SCaBER Cancer Cells," Plasma Process. Polym., vol. 11, no. 12, pp. 1150–1155, Dec. 2014.

[89] D. B. Graves, "Reactive Species from Cold Atmospheric Plasma: Implications for Cancer Therapy," Plasma Process. Polym., vol. 11, no. 12, pp. 1120–1127, Dec. 2014.

[90] A. R. Gibson, H. O. McCarthy, A. A. Ali, D. O'Connell, and W. G. Graham, "Interactions of a Non-Thermal Atmospheric Pressure Plasma Effluent with PC-3 Prostate Cancer Cells," Plasma Process. Polym., vol. 11, no. 12, pp. 1142–1149, Dec. 2014.

[91] J. Liebmann, J. Scherer, N. Bibinov, P. Rajasekaran, R. Kovacs, R. Gesche, P. Awakowicz, and V. Kolb-Bachofen, "Biological effects of nitric oxide generated by an atmospheric pressure gas-plasma on human skin cells," Nitric Oxide, vol. 24, no. 1, pp. 8–16, 2011.

[92] G. Fridman, A. Shereshevsky, M. M. Jost, A. D. Brooks, A. Fridman, A. Gutsol, V. Vasilets, and G. Friedman, "Floating electrode dielectric barrier discharge plasma in air promoting apoptotic behavior in Melanoma skin cancer cell lines," Plasma Chem. Plasma Process., vol. 27, no. 2, pp. 163–176, 2007.

[93] X. Yan, Z. Xiong, F. Zou, S. Zhao, X. Lu, G. Yang, G. He, and K. K. Ostrikov, "Plasma-Induced Death of HepG2 Cancer Cells: Intracellular Effects of Reactive Species," Plasma Process. Polym., vol. 9, no. 1, pp. 59–66, Jan. 2012.

[94] S. Kalghatgi, C. Kelly, E. Cerchar, and J. Azizkhan-Clifford, "Selectivity of Non-Thermal Atmospheric-Pressure Microsecond-Pulsed Dielectric Barrier Discharge Plasma Induced Apoptosis in Tumor Cells over Healthy Cells," Plasma Med., vol. 1, no. 3–4, pp. 249–263, 2011.

[95] N. Kaushik, N. Kumar, C. H. Kim, N. K. Kaushik, and E. H. Choi, "Dielectric Barrier Discharge Plasma Efficiently Delivers an Apoptotic Response in Human Monocytic Lymphoma," Plasma Process. Polym., vol. 11, no. 12, pp. 1175–1187, Dec. 2014.

[96] E. Stoffels, a J. Flikweert, W. W. Stoffels, and G. M. W. Kroesen, "Plasma needle: a non-destructive atmospheric plasma source for fine surface treatment of (bio)materials," Plasma Sources Sci. Technol., vol. 11, pp. 383–388, 2002.

[97] R. E. J. Sladek, E. Stoffels, R. Walraven, P. J. a. Tielbeek, and R. a. Koolhoven, "Plasma treatment of dental cavities: a feasibility study," IEEE Trans. Plasma Sci., vol. 32, no. 4, pp. 2002–2005, 2004.

[98] Y. Liu, Q. Liu, Q. S. Yu, and Y. Wang, "Nonthermal Atmospheric Plasmas in Dental Restoration," J. Dent. Res., 2016.

[99] G. Giro, N. Tovar, L. Witek, C. Marin, N. R. F. Silva, E. A. Bonfante, and P. G. Coelho, "Osseointegration assessment of chairside argon-based nonthermal plasma-treated Ca-P coated dental implants," J. Biomed. Mater. Res. - Part A, vol. 101 A, no. 1, pp. 98–103, 2013.

[100] K. Duske, I. Koban, E. Kindel, K. Schröder, B. Nebe, B. Holtfreter, L. Jablonowski, K. D. Weltmann, and T. Kocher, "Atmospheric plasma enhances wettability and cell spreading on dental implant metals," J. Clin. Periodontol., vol. 39, no. 4, pp. 400–407, 2012.

[101] A. G. Whittaker, E. M. Graham, R. L. Baxter, A. C. Jones, P. R. Richardson, G. Meek, G. A. Campbell, A. Aitken, and H. C. Baxter, "Plasma cleaning of dental instruments," J. Hosp. Infect., vol. 56, no. 1, pp. 37–41, 2004.

[102] I. Koban, B. Holtfreter, N. O. Hübner, R. Matthes, R. Sietmann, E. Kindel, K. D. Weltmann, A. Welk, A. Kramer, and T. Kocher, "Antimicrobial efficacy of non-thermal plasma in comparison to chlorhexidine against dental biofilms on titanium discs in vitro - Proof of principle experiment," J. Clin. Periodontol., vol. 38, no. 10, pp. 956–965, 2011.

[103] M. Chen, Y. Zhang, X. Yao, H. Li, Q. Yu, and Y. Wang, "Effect of a non-thermal, atmospheric-pressure, plasma brush on conversion of model self-etch adhesive formulations compared to conventional photo-polymerization," Dent. Mater., vol. 28, no. 12, pp. 1232–1239, 2012.

[104] J. K. Park, S. H. Nam, H. C. Kwon, A. A. H. Mohamed, J. K. Lee, and G. C. Kim, "Feasibility of nonthermal atmospheric pressure plasma for intracoronal bleaching," Int. Endod. J., vol. 44, no. 2, pp. 170–175, 2011.

[105] H. W. Lee, G. J. Kim, J. M. Kim, J. K. Park, J. K. Lee, and G. C. Kim, "Tooth Bleaching with Nonthermal Atmospheric Pressure Plasma," J. Endod., vol. 35, no. 4, pp. 587–591, 2009.

[106] E. Simoncelli, D. Barbieri, R. Laurita, A. Liguori, A. Stancampiano, L. Viola, R. Tonini, M. Gherardi, and V. Colombo, "Preliminary investigation of the antibacterial efficacy of a handheld Plasma Gun source for endodontic procedures," Clin. Plasma Med., vol. 3, no. 2, pp. 77–86, 2015.

[107] Z. Xiong, Y. Cao, X. Lu, and T. Du, "Plasmas in Tooth Root Canal," Science (80-.)., vol. 39, no. 11, pp. 1–2, 2011.

[108] X. Lu, Y. Cao, P. Yang, Q. Xiong, Z. Xiong, Y. Xian, and Y. Pan, "An RC plasma device for sterilization of root canal of teeth," IEEE Trans. Plasma Sci., vol. 37, no. 5, pp. 668–673, 2009.

[109] B.-H. Cho, G.-J. Han, K.-H. Oh, S.-N. Chung, and B.-H. Chun, "The effect of plasma polymer coating using atmospheric-pressure glow discharge on the shear bond strength of composite resin to ceramic," J. Mater. Sci., vol. 46, no. 8, pp. 2755–2763, 2011.

[110] G. B. Valverde, P. G. Coelho, M. N. Janal, F. C. Lorenzoni, R. M. Carvalho, V. P. Thompson, K. D. Weltemann, and N. R. F. A. Silva, "Surface characterisation and bonding of Y-TZP following non-thermal plasma treatment," J. Dent., vol. 41, no. 1, pp. 51–59, 2013.

[111] A. C. Ritts, H. Li, Q. Yu, C. Xu, X. Yao, L. Hong, and Y. Wang, "Dentin surface treatment using a non-thermal argon plasma brush for interfacial bonding improvement in composite restoration," Eur. J. Oral Sci., vol. 118, no. 5, pp. 510–516, 2010.

[112] L. Zhao, Y. Wang, L. Jin, M. Qin, X. Li, A. Wang, and C. Song, "Decomposition of Hydrogen Sulfide in Non-Thermal Plasma Aided by Supported CdS and ZnS Semiconductors Contents :," 2013.

[113] X. Dong, A. C. Ritts, C. Staller, Q. Yu, M. Chen, and Y. Wang, "Evaluation of plasma treatment effects on improving adhesive-dentin bonding by using the same tooth controls and varying cross-sectional surface areas," Eur. J. Oral Sci., vol. 121, no. 4, pp. 355–362, 2013.

[114] G. J. Han, J. H. Kim, S. N. Chung, B. H. Chun, C. K. Kim, D. G. Seo, H. H. Son, and B. H. Cho, "Effects of non-thermal atmospheric pressure pulsed plasma on the adhesion and durability of resin composite to dentin," Eur. J. Oral Sci., vol. 122, no. 6, pp. 417–423, 2014.

[115] X. Dong, M. Chen, Y. Wang, and Q. Yu, "A mechanistic study of plasma treatment effects on demineralized dentin surfaces for improved adhesive/dentin interface bonding," Clin. Plasma Med., vol. 2, no. 1, pp. 11–16, 2014.

[116] X. Dong, H. Li, M. Chen, Y. Wang, and Q. Yu, "Plasma treatment of dentin surfaces for improving self-etching adhesive/dentin interface bonding," Clin. Plasma Med., vol. 3, no. 1, pp. 10–16, 2015.

[117] R. Hirata, H. Teixeira, A. Paula, A. Ayres, L. S. Machado, / Paulo, G. Coelho, / Van, P. Thompson, and M. Giannini, "Long-term Adhesion Study of Self-Etching Systems to Plasma-Treated Dentin," vol. 17, no. JUNE, 2015.

[118] E. Robert, V. Sarron, D. Riès, S. Dozias, M. Vandamme, and J.-M. Pouvesle, "Characterization of pulsed atmospheric-pressure plasma streams (PAPS) generated by a plasma gun," Plasma Sources Sci. Technol., vol. 21, no. 3, p. 034017, 2012.

[119] E. Robert, M. Vandamme, L. Brullé, S. Lerondel, a. Le Pape, V. Sarron, D. Riès, T. Darny, S. Dozias, G. Collet, C. Kieda, and J. M. Pouvesle, "Perspectives of endoscopic plasma applications," Clin. Plasma Med., vol. 1, no. 2, pp. 8–16, 2013.

[120] L. Boschian Pest, G. Cavalli, P. Bertani, and M. Gagliani, "Adhesive post-endodontic restorations with fiber posts: Push-out tests and SEM observations," Dent. Mater., vol. 18, no. 8, pp. 596–602, 2002.

[121] T. M. Haller B,Thull R, Klaiber B, "An extrusion test for determination of bond strength to dentin," J Dent Res, 1991.

[122] J. Cheylan, N. Eid, and M. Degrange, "Adherence of different luting agents using a push-out method," in Proceedings of the 35th Annual IADR/CED Meeting, 1999.

[123] D. R. Beech, "Adhesion to teeth: principles and mechanisms," in Biocompatibility of dental materials, vol. 2, CRC Press Boca Raton, FL, 1982, p. 95.

[124] U. Lohbauer, S. A. Nikolaenko, A. Petschelt, and R. Frankenberger, "Resin tags do not contribute to dentin adhesion in self-etching adhesives.," J. Adhes. Dent., vol. 10, no. 2, pp. 97–103, Feb. 2008.

[125] L. Giachetti, F. Bertini, and D. Scaminaci Russo, "Investigation into the nature of dentin resin tags: a scanning electron microscopic morphological analysis of demineralized bonded dentin.," J. Prosthet. Dent., vol. 92, no. 3, pp. 233–8, Sep. 2004.

[126] M. Chen, Y. Zhang, M. Sky Driver, A. N. Caruso, Q. Yu, and Y. Wang, "Surface modification of several dental substrates by non-thermal, atmospheric plasma brush," Dent. Mater., vol. 29, no. 8, pp. 871–880, 2013.

[127] I. Koban, K. Duske, L. Jablonowski, K. Schröder, B. Nebe, R. Sietmann, K. D. Weltmann, N. O. Hübner, A. Kramer, and T. Kocher, "Atmospheric plasma enhances wettability and osteoblast spreading on dentin in vitro: Proof-of-principle," Plasma Process. Polym., vol. 8, no. 10, pp. 975–982, 2011.

CHAPTER 5
CONCLUDING REMARKS

5.1 Concluding remarks

Since the pioneer works in the late '90s, a vast amount of studies were conducted in the emerging field of CAP applications. In spite of the huge research efforts made by the scientific community, new publications routinely bring new questions and highlight new aspects that need to be clarified and be taken into account. This is because of the novelty of the field and the ample variety of plasma devices and applications. To my personal opinion, this is also what makes this emerging research field so stimulating and interesting.

In this dissertation, I tried to summarize my Ph.D. research, which focused on many different aspects that in some way reflect those that are the research paths in the field of non-equilibrium atmospheric plasma. The characterization of atmospheric plasma devices through several diagnostic approach is, since the beginning, an extremely important aspect of plasma technology. Everyday more and more light is shed on the fundamental mechanisms driving plasma generation and propagation. In Chapter 2, my research efforts in the characterization of a single electrode APPJ expanding freely in atmosphere were presented along with the detailed description of the methodology developed for the ICCD analysis of plasma discharges driven by sub-microsecond voltage pulses. These results were published through the years and can be found in their final form in PAPER I, II, III, IV, V. Still unpublished are the results concerning the influence of a liquid substrate on the discharge characteristics presented in Chapter 3

Finally, some of the plasma applications that I have investigated during my Ph.D. studies are summarized in Chapter 4. The applications here reported concern the medical field which is probably the most investigated and promising field of application for non-equilibrium plasmas. The applications reported in this dissertation included bacterial decontamination of prosthesis, anticancer potential of plasma and adhesion enhancement for dental restorations. The presented results support the feasibility of these plasma applications and help in the understanding of some of their governing mechanisms.

Concluding, future work possibilities are nearly limitless in this emerging field. Many directions of future work exist and only a few of them can be foreseen at the moment. Concerning the plasma characterization through diagnostic techniques an obvious direction is increasing the time, space and spectral resolutions of the presented techniques. Another important aspect for future studies could be increasing our control over surrounding atmosphere and target sample characteristics as their influence over the plasma processes can not be neglected. Concerning plasma application in the medical field, the development of new plasma devices, easy to handle and intrinsically safe is a necessary step for the

expansion of this field. Studies concerning the adoption of plasma treatment in realistic medical procedure are required and should be the aim of future works.
The road to see cold atmospheric plasma technology pervading our daily life is still long. Nevertheless, we are advancing fast and at increasing speed. The future of plasma technology is hardly questionable but much work still remains to be done to complete the task. I hope that with my research I contributed adding a little piece to the completion of this common effort.

CHAPTER 6
ORIGINAL PUBLICATIONS

5 Original publications

This thesis is based on the following peer-reviewed articles published in international scientific journals:

Paper I:

Boselli M, Colombo V, Ghedini E, Gherardi M, Laurita R, Liguori A, Sanibondi P, Stancampiano A (2014). Schlieren high-speed imaging of a nanosecond pulsed atmospheric pressure non-equilibrium plasma jet. *Plasma Chemistry and Plasma Processing*, *34*(4), 853–869.
doi: 10.1007/s11090-014-9537-1

Paper II:

Boselli, M., Colombo, V., Gherardi, M., Laurita, R., Liguori, A., Sanibondi, P., Simoncelli E, Stancampiano, A. (2015). Characterization of a Cold Atmospheric Pressure Plasma Jet Device Driven by Nanosecond Voltage Pulses, *IEEE Transactions on Plasma Science 43*(3), 713–725.
doi: 10.1109/TPS.2014.2381854

Paper III:

Stancampiano A, Gherardi, M., Puač, N., Marić, D., Malović, G., Colombo, V., & Petrović, Z. L. (2015). Practical and theoretical considerations on the use of ICCD imaging for the characterization of non-equilibrium plasmas. *Plasma Sources Science and Technology*, *24*(6), 064004.
doi: 10.1088/0963-0252/24/6/064004

Paper IV:

Bianconi, S., Cavrini, F., Colombo, V., Gherardi, M., Laurita, R., Liguori, A., Sanibondi P, Stancampiano, A. (2014). iCCD Imaging of the Transition From Uncoupled to Coupled Mode in a Plasma Source for Biomedical and Materials Treatment Applications, *IEEE Transactions on Plasma Science 42*(10), 2746–2747.
doi: 10.1109/TPS.2014.2321012

Paper V:

Boselli, M., Colombo, V., Ghedini, E., Gherardi, M., Laurita, R., Liguori, A., Sanibondi P, Stancampiano, A. (2014). High-speed multi-imaging of repetitive unipolar nanosecond-pulsed DBDs. *IEEE Transactions on Plasma Science*, *42*(10), 2744–2745.
doi: 10.1109/TPS.2014.2330954

Paper VI:

Gherardi, M., Turrini, E., Laurita, R., De Gianni, E., Ferruzzi, L., Liguori, A., Stancampiano A, Colombo V, Fimognari, C. (2015). Atmospheric Non-Equilibrium Plasma Promotes Cell Death and Cell-Cycle Arrest in a Lymphoma Cell Line. *Plasma Processes and Polymers*,
doi: 10.1002/ppap.201500033

Paper VII:

Stancampiano A, Cochis A, Liguori A, Laurita, R., Azzimonti B, Sorrentino R, Varoni E, Petri M, Colombo V, Gherardi, M., Rimondini L, Cold atmospheric plasma treatment affects early bacterial adhesion and decontamination of soft reline palatal obturators. *Submitted to Journal of Biomedical Materials Research: Part B - Applied Biomaterials 2016*

* The authors name in Paper I, II, IV, V are in alphabetical order. In these papers, SA contributed designing and realizing the experiment, analysing the results and writing the manuscript.

6.1 Paper I

Schlieren high-speed imaging of a nanosecond pulsed atmospheric pressure non-equilibrium plasma jet[a]

DOI: 10.1007/s11090-014-9537-1

Plasma Chem Plasma Process (2014) 34:853–869
DOI 10.1007/s11090-014-9537-1

ORIGINAL PAPER

Schlieren High-Speed Imaging of a Nanosecond Pulsed Atmospheric Pressure Non-equilibrium Plasma Jet

M. Boselli · V. Colombo · E. Ghedini · M. Gherardi · R. Laurita · A. Liguori · P. Sanibondi · A. Stancampiano

Received: 23 January 2014 / Accepted: 24 February 2014 / Published online: 8 March 2014

Abstract The fluid-dynamic characterization by means of Schlieren high-speed imaging of the effluent region of a single electrode plasma jet is presented. The plasma source is powered by a high-voltage generator producing pulses with nanosecond rise time. Time evolution of fluctuations generated in a free flow regime and when the jet is impinging on substrates of different geometries (plain substrates, Petri dishes, etc.) and materials (metal, dielectric covered metal, polystyrene) has been investigated. Plasma ignition causes fluid-dynamic instabilities moving in the direction of the jet flow and correlated with the high-voltage pulses: for low pulse repetition frequency (PRF) (<125 Hz), the movement of the turbulent front between two voltage pulses can be tracked, whereas for higher PRF (1,000 Hz) the flow is completely characterized by turbulent eddies in the effluent region, without relevant changes between subsequent voltage pulses. When the jet is impinging on a substrate, turbulent fronts propagate over the surface starting from the gas impinging zone.

Keywords Atmospheric pressure non-equilibrium plasma · Schlieren · High-speed imaging

Electronic supplementary material The online version of this article (doi:10.1007/s11090-014-9537-1) contains supplementary material, which is available to authorized users.

M. Boselli · V. Colombo · E. Ghedini
Industrial Research Centre for Advanced Mechanics and Materials (C.I.R.I.-M.A.M.), Alma Mater Studiorum-Università di Bologna, Via Saragozza 8, 40123 Bologna, Italy

V. Colombo (✉) · E. Ghedini · M. Gherardi · R. Laurita · A. Liguori · P. Sanibondi · A. Stancampiano
Department of Industrial Engineering (DIN), Alma Mater Studiorum-Università di Bologna, Via Saragozza 8, 40123 Bologna, Italy
e-mail: vittorio.colombo@unibo.it

Introduction

Non-thermal atmospheric pressure plasma jets are rapidly gaining importance as tools for plasma processing of various types of materials because they are environmentally friendly, easy to handle and economical. The possible applications involving the use of plasma jets include thin film deposition [1], surface modification [2], wound treatment [3], sterilization [4] and nanoadditives dispersion enhancement [5]; all subjects of particular importance in the field of plasma medicine. Because of the complexity of plasma interaction with biological and thermo-sensitive materials, diagnostic analysis is unavoidable to evaluate process feasibility and to develop plasma sources optimized for specific applications. Integrated approaches relying not only the effectiveness of the plasma treatment, but also the characterization of plasma sources, are required in order to promote a multi-step optimization of the process. Consequently, the scientific community has dedicated large efforts to characterize different plasma sources for biomedical applications and to identify the most suitable diagnostic techniques [6–12].

In this work, the characterization of the outflow of a novel plasma jet device developed in our laboratory and driven by high-voltage pulses with nanosecond rise time has been carried out using a high-speed Schlieren imaging technique.

The plasma jet is a single electrode plasma jet suitable for the treatment of different substrates such as metals, polymers, glasses and biological materials (Fig. 1) [13]. The source has two separate gas inlets that can be fed with two different gases at the same time in order to control the composition of the plasma for the production of reactive species (ROS or RNS) or for polymerization; the primary gas is usually Ar, He or air, while the secondary one is generally O_2, N_2, air or a gas-phase monomer. In this work, since the flow rate of the secondary gas is usually much lower than that of the primary, the fluid-dynamics at the outflow has been investigated only for cases with no secondary gas. The plasma jet can be driven by different voltage waveforms, such as repetitive pulses with nanosecond or microsecond rise time or sinusoidal, triangular, square and sawtooth waveforms and it has been previously shown that this parameter strongly affects the effectiveness of the treatment [5]. In particular, in this paper only results for the plasma source driven by high-voltage pulses with nanosecond rise time will be presented.

Low speed imaging is widely adopted in the characterization of non-thermal plasma sources since it enables to identify the macroscopic aspect of the plasma discharge and to have an estimate of the length of the jet [14, 15]. Conventional low speed imaging however has a limited efficacy for the description of fluid-dynamic phenomena. A qualitative and very effective study of the fluid-dynamic behavior of a jet can be generally conducted by Schlieren imaging, which has been applied in this work to investigate fluid-dynamic instabilities, turbulence front propagation and the relative length of laminar and turbulent regions of the plasma jet. Schlieren photography has already been used to investigate turbulence in the plasma generated by different plasma jet sources: as an example, Bradley et al. used Schlieren photography to investigate laminar and turbulent flows of a microjet generated in He on a polystyrene surface and also to determine the length of laminar and turbulent flow regions [2, 16]. However, the works presented in literature are based on acquisitions made using common photographic cameras associated with Schlieren technique and do not allow to study the time evolution of the turbulent phenomena.

The novelty of this work is based on the use of a diagnostic setup based on the Schlieren technique coupled with a high-speed imaging camera to visualize the time evolution of the turbulence in the outflow of a plasma jet powered by a high-voltage generator with nanosecond rise time.

Fig. 1 Nanosecond pulsed plasma jet operating in Ar (*left*) and He (*right*)

High-speed Schlieren imaging was used to investigate the effects of mass flow rate (Q), peak voltage (PV) and pulse repetition frequency (PRF) on the fluid-dynamics of a plasma jet propagating in the surrounding air (free flow jet) and to analyze, for the case of plasma jet impinging on a surface, the propagation of the turbulent front over substrates of different materials.

Experimental and Diagnostic Apparatus

Nanosecond Pulsed Plasma Jet

The plasma source used in this work is a single electrode plasma jet [17] developed in our laboratory and previously reported in [18]; a schematic of the source is presented in Fig. 2. The high voltage single electrode is a 19.5 mm long stainless steel sharpened metallic needle with a diameter of 0.3 mm; the electrode protrudes from a quartz capillary (outer diameter of 1 mm) by 3 mm. A peculiarity of this source is the possibility of operating with two different gas supplies at the same time. The case, made of DELRIN, presents two gas inlets to introduce a primary gas sustaining the plasma (Ar, He, Air) and to separately inject a secondary gas (O_2, N_2, gas-phase monomer). The primary gas is injected through a 12-hole (0.3 mm diameter) diffuser aimed at ensuring a uniform and laminar distribution of the primary gas flow along the electrode, while the secondary gas can be introduced through twelve 0.3 mm holes, tilted with respect to the plasma jet axis. The gas is ejected through a 1 mm orifice. Figure 3 shows the differences in jet length and radial diffusion in the surrounding air between Ar and He plasma jets at the same operating conditions. The primary gas used in this work is helium (He) with a mass flow rate (Q) of 1, 3 and 5 slpm, whereas no secondary gas was employed. In these conditions the Reynolds number of the jet without plasma ignition is estimated to be 170, 500 and 840, respectively. The plasma source is driven by a commercial pulse generator (FID GmbH—FPG 20-1NMK) producing high voltage pulses with a slew rate of few kV/ns, a PV of 7–20 kV into a 100–200 Ω load impedance and a maximum PRF of 1,000 Hz. A typical voltage waveforms applied to the plasma source during operation is presented in Fig. 4.

High-Speed Schlieren Imaging Setup

The behaviour of the plasma jet was investigated through a Schlieren imaging setup in a Z configuration (Fig. 5) composed of a 450 W ozone free xenon lamp (Newport-Oriel 66355 Simplicity Arc Source), a slit and an iris diaphragm, two parabolic mirrors with a focal

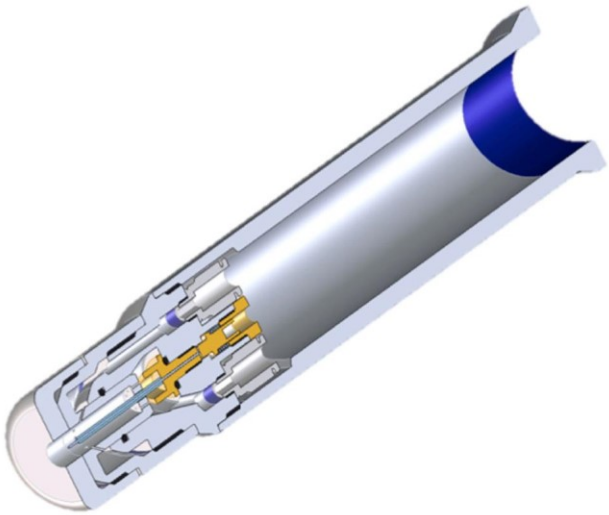

Fig. 2 Three dimensional cross-section representation of the plasma source adopted in the experiments [18]

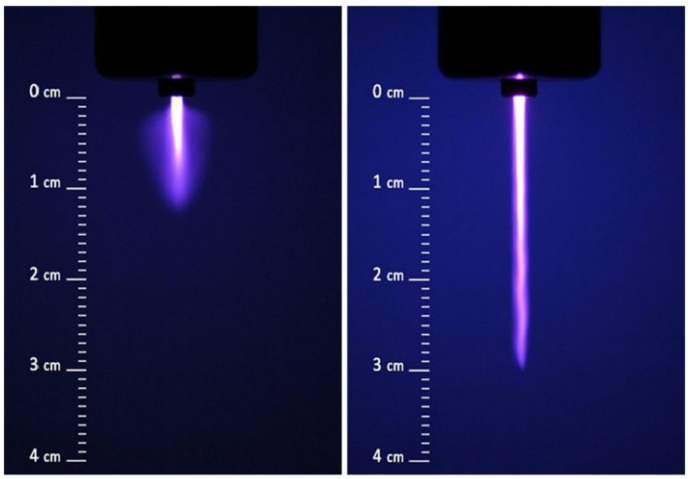

Fig. 3 Low speed imaging of the plasma jet operating in Ar (*left*) and He (*right*). PV = 17 kV, PRF = 1 kHz and mass flow rate = 3 slpm [18]

length of 1 m, a knife edge positioned vertically and a high-speed camera that records the Schlieren image [1].

The plasma jet has been positioned in the middle of the optical path between the two parabolic mirrors, with a vertically downward direction. A first high-speed camera (Memrecam K3R-NAC Image Technology), with a setup of 4,000 fps and 1/50,000 s shutter time, has been used to visualize the turbulent region of the plasma jet [results presented in "Plasma Jet with No Substrate (Free Flow Jet)" section], whereas a second high-speed camera (Memrecam GX-3-NAC Image Technology), operating at 4,000 fps and 1/200,000 s shutter time, has been used to study the behaviour of an impinging plasma jet on different substrates (results presented in "Plasma Jet Impinging on Grounded Metallic Substrate", "Effects of Dielectric Layer Covering the Metallic Substrate", "Plasma Jet Impinging on a Petri Dish"

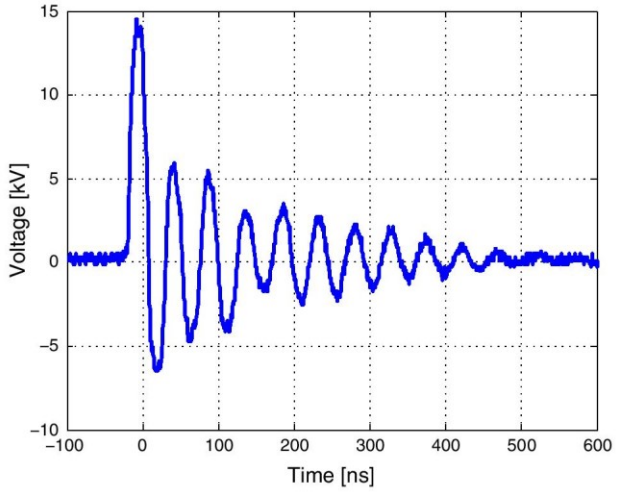

Fig. 4 Typical voltage waveform applied to the plasma source during operation in with the following conditions: PV = 14 kV, PRF = 1,000 Hz and He mass flow rate = 3 slpm

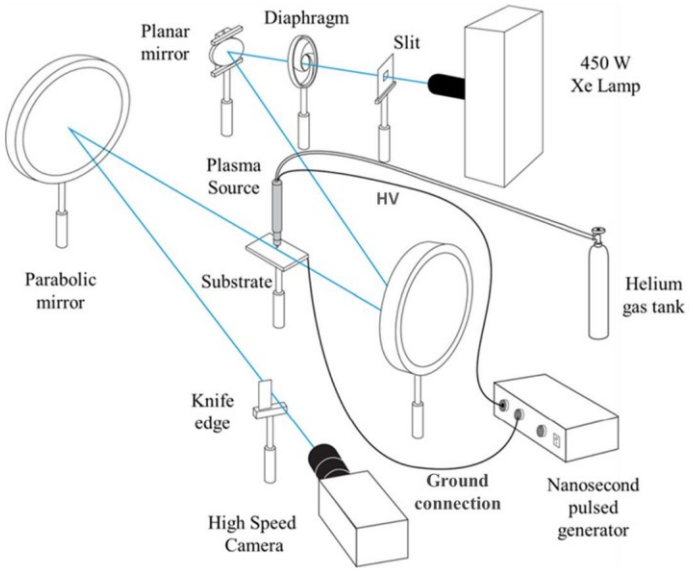

Fig. 5 Experimental setup for high-speed Schlieren imaging in an impinging configuration

sections). Since the duration of the high-voltage pulse driving the plasma source is <500 ns and the time span for each high-speed camera frame is 0.25 ms, during the voltage pulse only one frame is recorded, which has been labelled with t = 0 ms.

Free Flow Jet and Impinging Configurations

The plasma jet outflow has been investigated for different substrates and for the case with no substrate. The latter configuration was defined as "free flow jet" as the jet outflow was

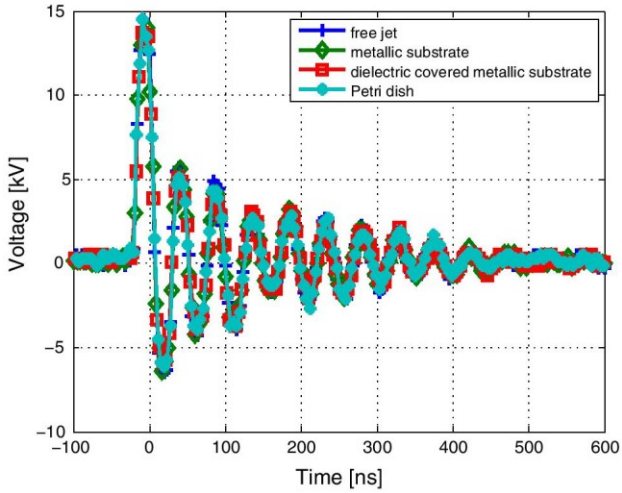

Fig. 6 Comparison of the applied voltage waveform for the plasma source operating with PV = 14 kV, PRF = 1,000 Hz and a He mass flow rate of 3 slpm when impinging on different substrates at a distance on 1.8 cm

allowed to expand freely in the surrounding ambient air. In all the other cases, the jet outflow was impinging on a substrate posed at 1.8 cm from the outlet. Three different substrates have been tested: a grounded metallic substrate made of anodized aluminium, the same grounded metallic substrate covered with a dielectric layer (PVC tape 0,15 mm thickness) and a polystyrene Petri dish (D × H 1 × 4 cm) which is a typical substrate adopted in biomedical studies. As shown in Fig. 6, for the operating conditions adopted in this paper the substrate characteristics have negligible effects on the voltage waveform applied to the electrode.

Results and Discussion

Even though the random behavior of the turbulent flow induces every acquisition set to be slightly different from any other, the overall phenomenon can be described in a repeatable way selecting frames among a wide range of results obtained for different operating conditions, varying PV, PRF, mass flow rate of the primary gas and eventual substrate materials.

A set of different plasma jet images taken with conventional camera with a few seconds of exposure time (low speed imaging) are presented for different flow rates (Fig. 7). A flow rate increase from 1 to 3 He slpm causes a length increase in the plasma plume, whereas a further increase up to 5 slpm results in a turbulent behavior of the plume, due to the increased shear force between the high velocity jet and the surrounding stagnant air, that leads to a shortening of the visible plasma plume. According to Colombo et al. [19], a jet is completely laminar for Reynolds numbers below 500. This is the case for the plasma jet presented in this work when operated with a flow rate of 1 and 3 slpm of He, corresponding to a Reynolds number of 170 and 500, respectively. When the flow rate is increased to 5 slpm, the Reynolds number falls inside a transition range (between 500 and 1,000) in which the jet becomes unstable at a certain distance from the nozzle.

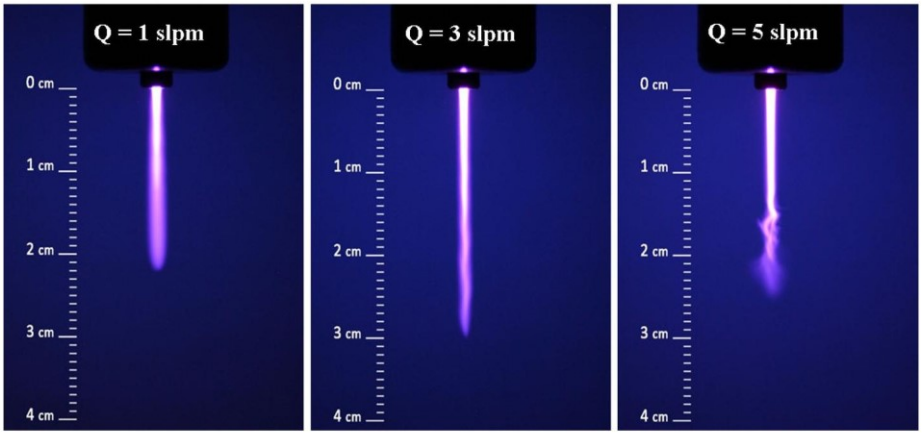

Fig. 7 Low speed imaging of plasma jets generated with PRF = 1 kHz, PV = 17 kV and He mass flow rate = 1, 3 and 5 slpm, respectively

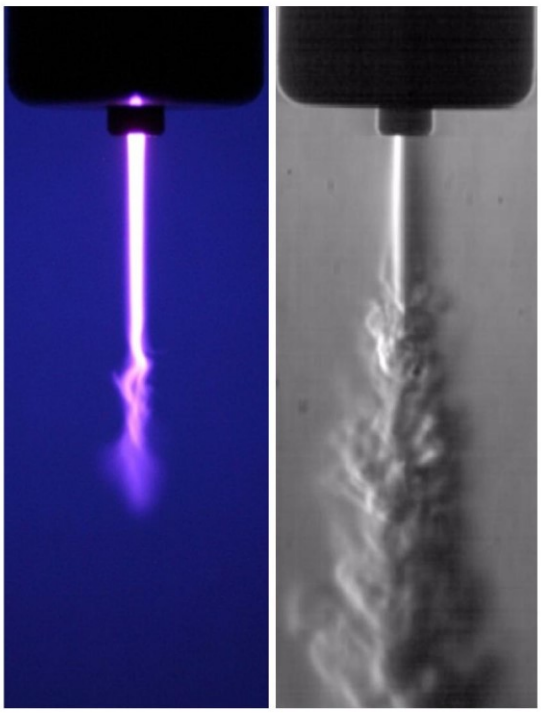

Fig. 8 Conventional low speed imaging (*left*) and high speed Schlieren imaging (*right*) of a He plasma jet with PV = 17 kV, PRF = 1 kHz and mass flow rate = 5 slpm

A direct comparison between conventional and Schlieren frames of a plasma jet in the same operating conditions is presented in Fig. 8. The complete propagation of plasma jet in the surrounding air, the effective length of the laminar region and the structure of the eddies of the turbulent zone can be observed in Schlieren frames, whereas they can not be seen in conventional photography.

Plasma Jet with No Substrate (Free Flow Jet)

In this subsection, the fluid-dynamics of the plasma jet is evaluated in free flow conditions.

In Fig. 9 selected frames that highlight the effects of plasma ignition on the fluid-dynamic structure of the jet are reported. For the cases with no plasma ignition (Fig. 9a) a transition from laminar to turbulent flow is observed when the mass flow rate is increased from 3 to 5 slpm. In particular, the 3 slpm case shows a completely laminar behaviour in the acquired area, whereas in the 5 slpm case the effluent flow is characterized by a first laminar zone 1.5 cm long followed by an unstable zone with many visible eddies, due to the turbulent mixing of He with the surrounding air.

When plasma is ignited fluid-dynamic instabilities are visible also for 3 slpm, while for the 5 slpm case a length decrease of the laminar region from 1.5 to 0.5 cm is evinced, as shown in Fig. 9b.

In Fig. 10, selected frames for the case with PV = 20 kV, PRF = 83.3 Hz and a He mass flow rate of 3 slpm are presented to highlight the temporal evolution of the plasma jet fluid-dynamics in the time span of two voltage pulses, which occur at t = 0 ms and t = 12 ms. At 0.5 ms before the voltage pulse, the jet is mostly laminar. After 1.5 ms from the voltage pulse, a turbulent front is observed which propagates in the downstream region of the plasma jet (see frames at t = 2.5, 5 and 7.5 ms). The observed turbulent front propagation is similar for each voltage pulse: in the frame acquired at t = 14.5 ms, which correspond to a delay of 2.5 ms after the second voltage pulse, the fluid-dynamic structure of the plasma jet is similar to that of the frame at 2.5 ms, with the formation of a turbulent front 1.5 cm downstream the nozzle.

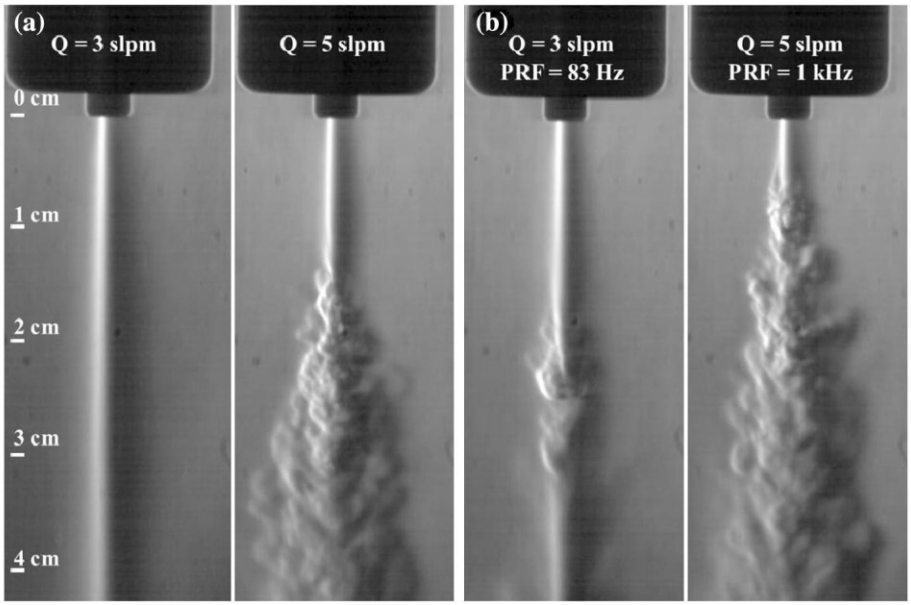

Fig. 9 Schlieren imaging of effluent fluid-dynamics at two values of mass flow rate without plasma generation (**a**) and with plasma ignition (PV = 20 kV) in two different operative conditions (**b**)

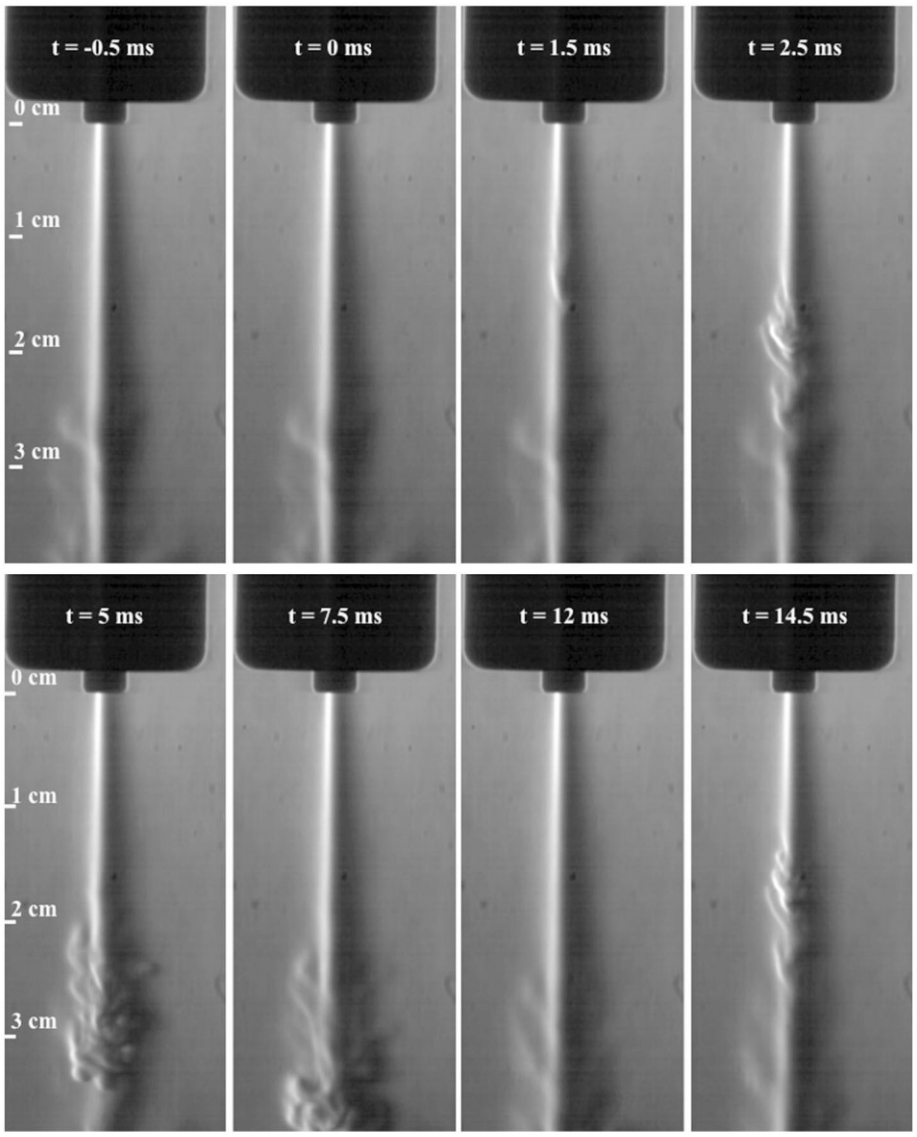

Fig. 10 Schlieren imaging of the plasma jet evolution between two voltage pulses, at t = 0 ms and t = 12 ms. PV = 20 kV, PRF = 83.3 Hz and He mass flow rate = 3 slpm (Online resource 1)

The propagation velocity of the turbulent front along the laminar region was estimated, by analysing the high-speed Schlieren acquisitions, to be about 60 m/s, which is close to the mean gas velocity.

For a plasma jet generated with PV = 20 kV, PRF = 125 Hz and He mass flow rate = 5 slpm, the fluid-dynamic structure 0.25 ms before the voltage pulse (t = − 0.25 ms) is characterized by a laminar zone that propagates 2 cm downstream the nozzle, followed by a turbulent zone (see Fig. 11). During voltage pulse (starting at t = 0 ms), the formation of a turbulent front inside the laminar region can be observed,

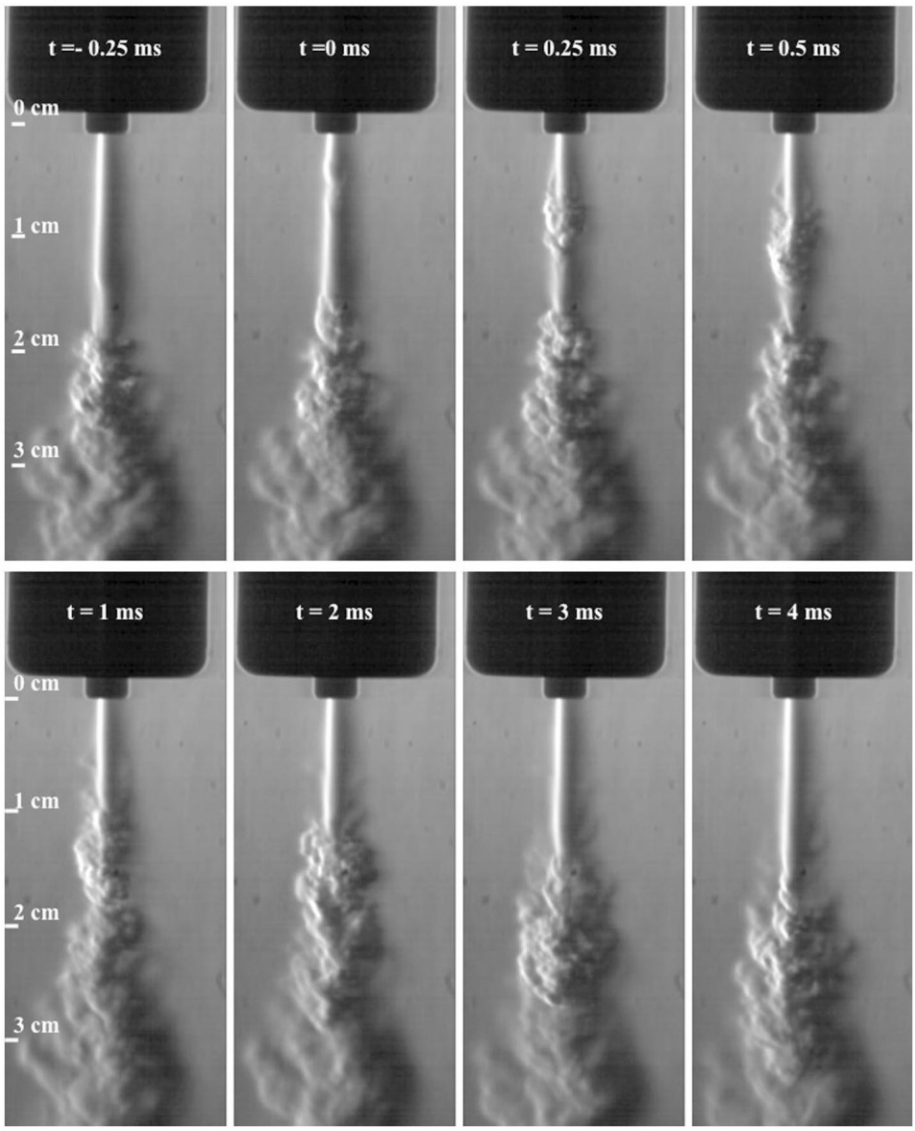

Fig. 11 Schlieren imaging of the plasma jet fluid-dynamics during a voltage pulse, starting at t = 0 ms. PV = 20 kV, PRF = 125 Hz, and He mass flow rate = 5 slpm (Online resource 2)

with no significant change downstream the turbulent zone. The growth and the propagation of the turbulent front can be tracked in the frame sequence from t = 0.25 ms to t = 4 ms, where relevant changes in both the laminar and turbulent regions can be appreciated.

With a PRF of 1,000 Hz, the time required for the turbulent front to travel along the laminar region (around 1 ms) becomes comparable with the period between voltage pulses (1 ms); in this case, no turbulent front propagation can be observed between voltage pulses: as can be seen in Fig. 12, the Schlieren acquisitions of the jet before (t = − 0.25 ms) and after (t = 0.25 ms) the voltage pulse, which occurs at t = 0 ms, are very

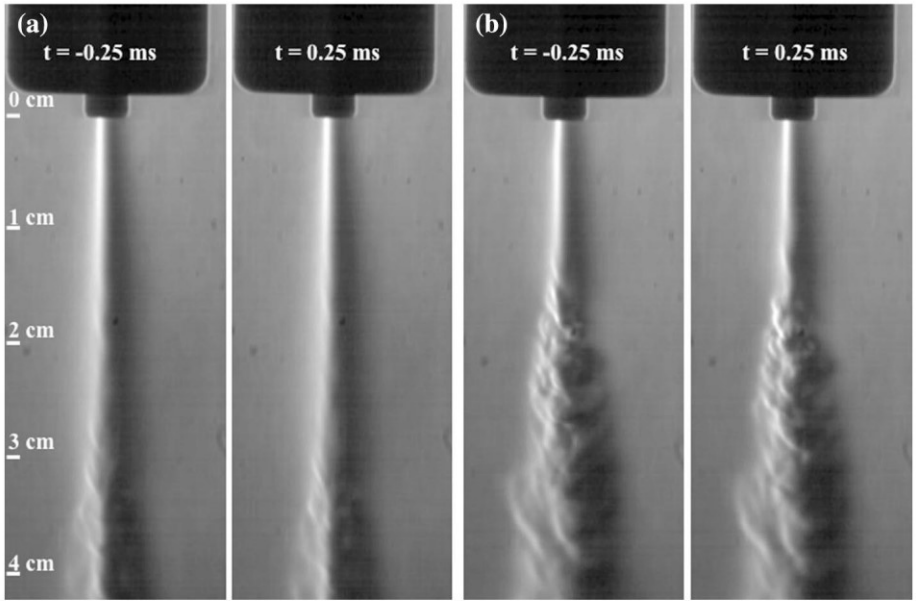

Fig. 12 Schlieren imaging of the plasma jet fluid-dynamics with PV = 14 kV (**a**) and 20 kV (**b**). PRF = 1 kHz, He mass flow rate = 3 slpm. Voltage pulse at t = 0 ms (Online resource 3)

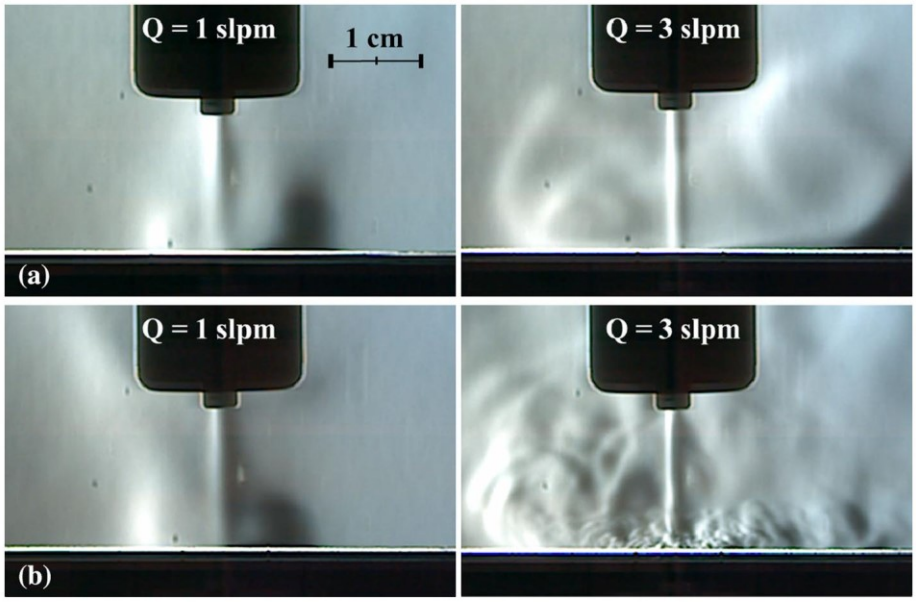

Fig. 13 Schlieren imaging of a jet impinging on a metallic substrate without (**a**) and with (**b**) plasma ignition. He mass flow rate set at 1 (*left*) and 3 slpm (*right*). PV = 14 kV and PRF = 1 kHz

similar to one another. The effects of the PV on the plasma jet evolution at high repetition frequency are highlighted in Fig. 12a, b. The increase of the PV from 14 (Fig. 12a) to 20 kV (Fig. 12b) causes a shortening of the laminar region from 3 to 1.5 cm. Comparing

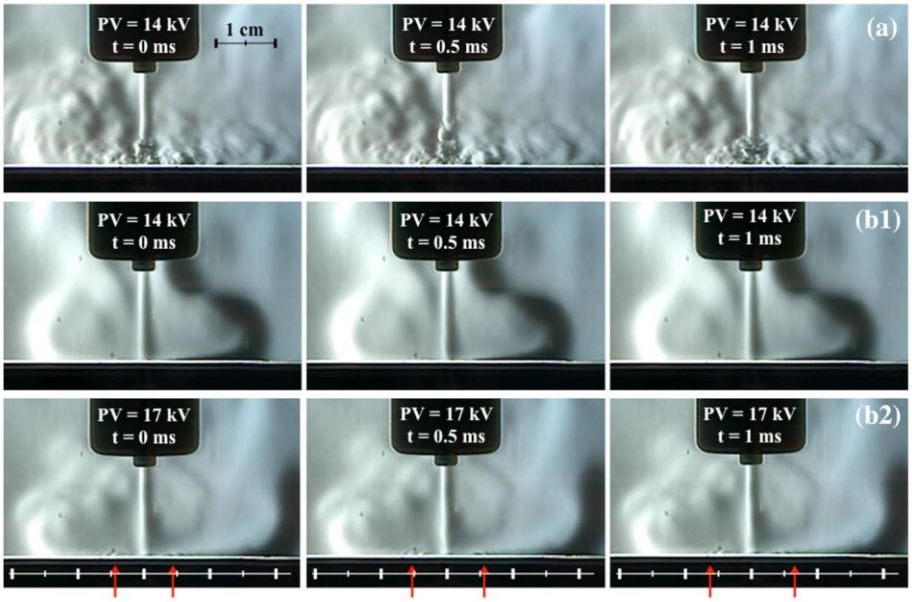

Fig. 15 Schlieren imaging of the plasma jet fluid-dynamics without (**a**) and with (**b1**, **b2**) a layer of dielectric material on the surface of a metallic substrate. PV at 14 (**a**, **b1**) and 17 kV (**b2**), He mass flow rate = 3 slpm, PRF = 1 kHz. Turbulent wave fronts are tracked by *arrows*. Voltage pulse at t = 0 ms (Online resource 5)

substrate is visible. The turbulent wave front becomes visible 1 ms after the voltage pulse and it propagates along substrate surface; after 3 ms the turbulent wave front has propagated 0.75 cm from the jet axis.

Effects of Dielectric Layer Covering the Metallic Substrate

To evaluate the influence of the material of the substrate on the fluid-dynamic characteristics of the plasma jet at the impinging region, Schlieren frames at 0, 0.5 and 1 ms after the voltage pulse are presented for a metallic substrate (Fig. 15a) and a metallic substrate covered with an insulating layer (Fig. 15b1, b2). A drastic reduction in turbulent behaviour of the plasma jet at the impinging region can be observed passing from a metallic to a dielectric substrate. For the cases with dielectric substrate, the flow is almost laminar and the time scale of fluid-dynamic instabilities is much longer (several ms) than for the cases with turbulent behaviour (<1 ms): for this reason, frames at 0, 0.5 and 1 ms after the voltage pulse acquired during the same recording are very similar to one another (Fig. 15b1). However, with a higher PV (17 kV) the occurrence of turbulent wave fronts with a time scale of <1 ms is observed also for the case with plasma jet impinging on the dielectric covered substrate (Fig. 15b2).

Plasma Jet Impinging on a Petri Dish

Schlieren frames of the plasma jet impinging on a Petri dish have been reported in Fig. 16 for two different He mass flow rates (3 and 5 slpm, left and right columns respectively),

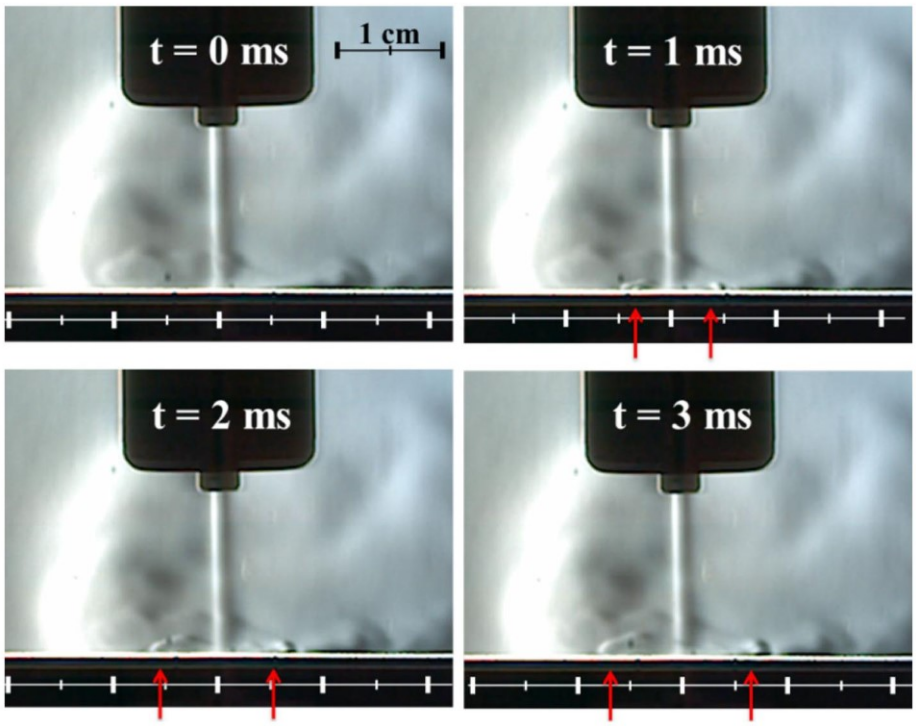

Fig. 14 Propagation of turbulent wave fronts (see *arrows*) induced by a plasma jet impinging on a metallic substrate. PV = 14 kV, PRF = 125 Hz, He mass flow rate = 3 slpm. Voltage pulse at t = 0 ms (Online resource 4)

different time frames in the same operating conditions, no relevant differences for the laminar region length are notable in the plasma jet fluid-dynamic structure before and after the pulse, contrary to what was observed for lower PRF (see Figs. 10, 11).

From the comparison between Fig. 9a (He jet with flow rate at 3 slpm but with no plasma ignition) and Fig. 12, it can be seen that plasma ignition with PRF at 1,000 Hz induces the onset of a turbulent behaviour in the tail of the jet.

Plasma Jet Impinging on Grounded Metallic Substrate

The effects of plasma ignition on the fluid-dynamic behaviour of He gas jet impinging on a metallic substrate is highlighted in Fig. 13. For a mass flow rate of 1 slpm no great difference in the impinging region can be observed comparing the jet without and with plasma ignition (PV = 14 kV, PRF = 1,000 Hz). In both cases no relevant turbulence can be observed. For a He mass flow rate of 3 slpm, a slight turbulent behaviour in the external fringes for the case with no plasma can be observed, mainly due to the buoyancy effect of He. More relevant fluid-dynamic instabilities can be seen in the impinging region when plasma is ignited.

Reducing the PRF to 125 Hz (PV = 14 kV, He mass flow rate = 3 slpm), it is possible to track the propagation of a turbulent wave front along the substrate surface (see Fig. 14). At t = 0 ms, corresponding to the voltage pulse, no turbulent front over the metallic

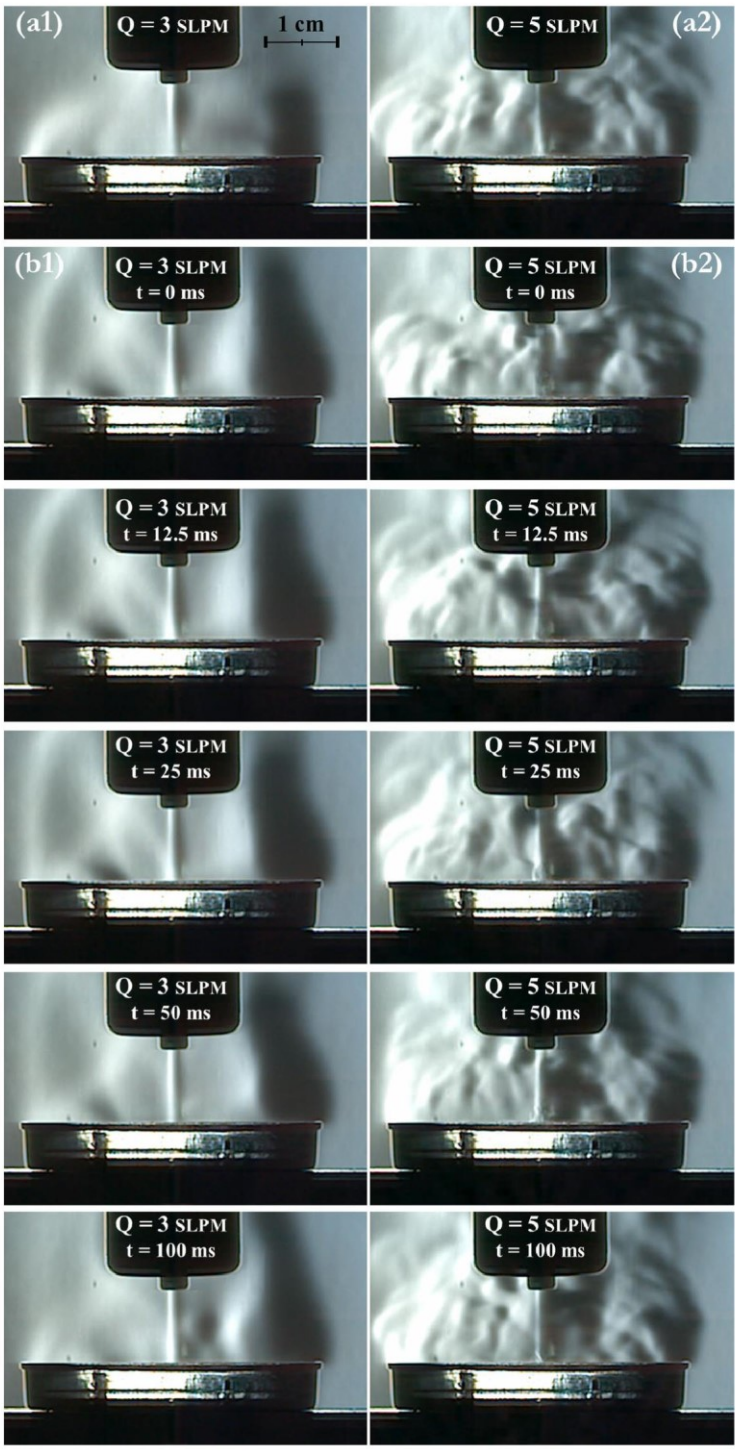
(a1)
Q = 3 SLPM
1 cm
Q = 5 SLPM
(a2)
(b1)
Q = 3 SLPM
t = 0 ms
Q = 5 SLPM
t = 0 ms
(b2)
Q = 3 SLPM
t = 12.5 ms
Q = 5 SLPM
t = 12.5 ms
Q = 3 SLPM
t = 25 ms
Q = 5 SLPM
t = 25 ms
Q = 3 SLPM
t = 50 ms
Q = 5 SLPM
t = 50 ms
Q = 3 SLPM
t = 100 ms
Q = 5 SLPM
t = 100 ms

◀ **Fig. 16** Schlieren imaging of the fluid-dynamics of a jet impinging on a petri dish with He mass flow rate of 3 (**a1**, **b1**) and 5 slpm (**a2**, **b2**) without (**a1**, **a2**) and with plasma ignition (**b1**, **b2**). PV = 14 kV, PRF = 1 kHz (Online resource 6)

with and without plasma ignition. In these conditions, the helium flow impinges on the Petri dish and it is subsequently directed upward mainly as a consequence of the buoyancy effect and of the presence of the Petri walls that obstruct the sideway gas flow. For the case with no plasma ignition, since the Schlieren frames at different time steps were very similar to one another, only one frame has been reported in Fig. 16a1, a2. With plasma ignition, for the case at 3 slpm a flow motion can be seen in the region outside the plasma jet on a time scale of few hundreds ms (see Fig. 16b1); with a flow rate of 5 slpm (see Fig. 16b2), a fluid-dynamic instability can be seen in the jet region in frames at t = 0 ms and t = 25 ms, which is characterized by a time scale of <1 ms, whereas turbulence in the surrounding atmosphere above the Petri dish is characterized by a time scale of tens of ms.

Discussion

The results presented in "Results and Discussion" section have shown that plasma ignition triggers the formation of a turbulent front which propagates along the jet; also, the onset of turbulence induces the reduction of the jet laminar region when the period between subsequent voltage pulses is comparable with time required for the turbulent front to propagate along the laminar region of the jet (about 1 ms).

A reduction of the laminar region length due to plasma ignition has been already observed for other plasma jets driven by AC voltage waveforms and nanosecond pulses [16, 20, 21].

The mechanism responsible for the formation of a turbulent front in correspondence of the high-voltage pulse is still poorly understood; possible mechanisms include gas heating, local pressure increase, variation of transport properties of gas or momentum transfer between ions and neutrals. Gas heating during the voltage pulse can induce the reduction of gas density, which in turn results in a localized increase of gas velocity; a pressure peak can also take place near the powered electrode during the voltage pulse as a consequence of local ionization, with a subsequent increase of jet velocity; also, the variation of the transport properties of gas (especially viscosity) in presence of ionized species during the pulse can result in a gradient of gas velocity and in the formation of a turbulent front; finally, when the structure of the plasma jet is characterized by plasma bullets, which are travelling with a velocity of several km/s [17], turbulence onset can be linked to momentum transfer between ions and neutrals.

For dielectric barrier plasma jets [21] it has been concluded that the key mechanism leading to reduction of the laminar region after plasma ignition is gas heating, which in turn induces an increase in gas velocity.

In our experiments it was possible to measure the propagation velocity of the turbulent front, which has been found to be in the same order of magnitude as gas velocity (between 20 and 100 m/s). For this reason, in our plasma jet we can exclude a correlation between turbulent front propagation and the generation of plasma bullets. However, further investigations are needed to understand the relative importance of the suggested mechanisms.

Results in "Results and Discussion" section have shown that, for the cases with jet directed towards a substrate, a turbulent front is propagating along substrate surface

starting from the jet impinging point; this effect is more pronounced in the case of a metallic substrate with respect to the case with a dielectric covered metallic substrate. Indeed, since the adopted plasma source is a single electrode plasma jet, the substrate acts as a counter electrode and in the case of dielectric covered substrate the current is self-limited by charge deposition on the dielectric surface; this induces a less intense discharge with respect to the case with bare grounded electrode and consequently less intense turbulence in the jet.

Conclusions

The fluid-dynamic behaviour of a single electrode non-equilibrium plasma source driven by high voltage pulses with nanosecond rise time at atmospheric pressure has been characterized with a high-speed Schlieren imaging technique. This study is a first step in a multi-stage integrated approach that relies on diagnostics and experiments for the tailoring of the plasma source to specific applications, among which also biomedical ones.

The use of high-speed Schlieren technique has allowed us to observe several phenomena for the first time. Plasma ignition causes fluid-dynamic instabilities that are moving in the direction of the jet flow and are correlated with the high-voltage pulses: for low PRF (<125 Hz) it is possible to track the movement of the turbulent front between two voltage pulses, whereas for higher PRF (1,000 Hz) the flow is completely characterized by turbulent eddies in the effluent region without relevant changes between the voltage pulses.

Moreover, fluid-dynamic characteristics of the plasma jet at the impinging region for metallic and insulating substrates and the turbulent propagation front have been observed. Turbulent eddies, more visible with the metallic substrate than with the insulating one, propagate over the surface starting from the gas impinging zone.

The results presented in this paper will serve as a basis for the design, optimization and analysis of plasma processes for treatment of biological and biocompatible materials, in which the plasma jet can be used as a source of chemical reactive species, whose generation and transport can be strongly influenced by turbulence.

Acknowledgments This work was partially supported by FP7 COST Action MP1101 "Biomedical Applications of Atmospheric Pressure Plasma Technology" and FP7 COST Action TD1208 "Electrical discharges with liquids for future applications". The contribution of Silvano Dallavalle for the design of the plasma source is acknowledged.

References

1. Ito Y, Urabe K, Takano N, Tachibana K (2008) Appl Phys Express 1:067009
2. Olabanji OT, Bradley JW (2012) Plasma Process Polym 9:929–936
3. Nastuta AV, Topala I, Grigoras C, Pohoata V, Popa G (2011) J Phys D Appl Phys 44:105204
4. Fridman G, Friedman G, Gutsol A, Shekhter AB, Vasilets VN, Fridman A (2008) Plasma Process Polym 5:503–533
5. Colombo V, Fabiani D, Focarete ML, Ghedini E, Gherardi M, Gualandi C, Laurita R, Sanibondi P, Zaccaria M (2013). In: Proceedings of the 11th IEEE international conference on solid dielectrics—ICSD 11, Bologna, Italy, June 30–July 4, 2013
6. Weltmann KD, Kindel E, Brandenburg R, Meyer C, Bussiahn R, Wilke C, von Woedtke T (2009) Contrib Plasma Phys 49:631–640
7. O'Neill FT, Twomey B, Law VJ, Milosavljevic V, Kong M, Anghel SD, Dowling D (2012) IEEE Trans Plasma Sci 40:2994–3002

8. Deng XL, Nikiforov AY, Vanraes P, Leys C (2013) J Appl Phys 113:023305
9. Xiong Q, Nikiforov AY, Li L, Vanraes P, Britun N, Snyders R, Lu XP, Leys C (2012) Eur Phys J D 66:281
10. Hong Y, Lu N, Pan J, Li J, Wu Y, Shang KF (2013) J Electrost 71:93–101
11. van Gessel AFH, Hrycak B, Jasinski M, Mizeraczyk J, van der Mullen JJAM, Bruggeman PJ (2013) J Phys D Appl Phys 46:095201
12. Xiong Q, Nikiforov AY, Gonzalez MA, Leys C, Lu XP (2013) Plasma Sources Sci Technol 22:015011
13. Boselli M, Colombo V, Ghedini E, Gherardi M, Laurita R, Liguori A, Marani F, Sanibondi P, Stancampiano A (2013). In: Proceedings of 21st international symposium on plasma chemistry—ISPC21, Cairns, Australia, 4–9 August 2013
14. Shao T, Long K, Zhang C, Yan P, Zhang S (2008) J Phys D Appl Phys 41:215203
15. Ayan H, Fridman G, Gutsol AF, Vasilets VN, Fridman A, Friedman G (2008) IEEE Trans Plasma Sci 36:504–508
16. Oh JS, Olabanji OT, Hale C, Mariani R, Kontis K, Bradley JW (2011) J Phys D Appl Phys 44:155206
17. Lu X, Laroussi M, Puech V (2012) Plasma Sources Sci Technol 21:034005
18. Colombo V, Fabiani D, Focarete ML, Gherardi M, Gualandi C, Laurita R, Zaccaria M (2014) Plasma Process Polym. doi:10.1002/ppap.201300141
19. Ungate CD, Harleman DR, Jirka GH (1975) Stability and mixing of submerged turbulent jets at low Reynolds numbers, MIT Energy Lab
20. Folletto M, Douat C, Fontane J, Joly L, Pitchford L, Puech V (2013). In: Proceedings of 31th international conference on phenomena in ionized gases—ICPIG, Granada, Spain, 14–19 July 2013
21. Ghasemi M, Olszewski P, Bradley JW, Walsh JL (2013) J Phys D Appl Phys 46:052001

6.2 Paper II

Characterization of a Cold Atmospheric Pressure Plasma Jet Device Driven by Nanosecond Voltage Pulses

DOI: 10.1109/TPS.2014.

Characterization of a Cold Atmospheric Pressure Plasma Jet Device Driven by Nanosecond Voltage Pulses

Marco Boselli, Vittorio Colombo, Matteo Gherardi, Romolo Laurita, Anna Liguori, Paolo Sanibondi, Emanuele Simoncelli, and Augusto Stancampiano

***Abstract*— The structure, fluid-dynamic behavior, temperature, and radiation emission of a cold atmospheric pressure plasma jet driven by high-voltage pulses with rise time and duration of a few nanoseconds have been investigated. Intensified charge-coupled device (iCCD) imaging revealed that the discharge starts when voltage values of 5–10 kV are reached on the rising front of the applied voltage pulse; the discharge then propagates downstream the source outlet with a velocity around 10^7–10^8 cm/s. Light emission was observed to increase and decrease periodically and repetitively during discharge propagation. The structure of the plasma plume presents a single front or either several branched subfronts, depending on the operating conditions; merging results of investigations by means of Schlieren and iCCD imaging suggests that branching of the discharge front occurs in spatial regions where the flow is turbulent. By means of optical emission spectroscopy, discharge emission was observed in the ultraviolet-visible (UV-VIS) spectral range (N_2, N_2^+, OH, and NO emission bands); total UV irradiance was lower than 1 μW/cm^2 even at short distances from the device outlet (<15 mm). Plasma plume temperature does not exceed 45 °C for all the tested operating conditions and values close to ambient temperature were measured around 10 mm downstream the source outlet.**

***Index Terms*— Cold atmospheric pressure plasma jets (APPJs), plasma diagnostics, material and biomedical applications.**

I. Introduction

IN RECENT years, nonequilibrium atmospheric pressure plasma jets (APPJs) have been raising a significant interest because of their broad range of applications, among which the decontamination and sterilization of surfaces [1], [2], surface modification of polymers [3]–[5], thin film deposition [6], [7], and nanomaterials fabrication and modification [8]–[12]. Moreover, APPJs are widely investigated for plasma-assisted medical therapies: starting with the pioneering works from [13], APPJs have been evaluated for numerous applications at the forefront of research, ranging from blood coagulation and chronic wound remediation to cancer treatment [14]–[27].

One of the reasons of the diffuse interest toward APPJs is their versatility, granted by the diverse possible combinations of driving power supply, gas employed, and source architecture [28]; among this ample number of plasma sources, APPJs notable for their scientific and historical relevance, characteristic architecture, or extensive application are the plasma needle [29], the plasma gun [30], the plasma pencil [31], the kINPen [32], the plasma jet array or *Gatling machine gun-like* plasma jet [33], [34], and the plasma jet with the porous alumina layer between anode and cathode developed in [35].

Several studies have been devoted to the investigation of physical and chemical phenomena taking place in the discharge generated by APPJs [32], [36]–[42]. A particular attention in APPJs characterization has been dedicated to discharge structure since the first works reporting on the observation of plasma bullets [43]–[45], whose fundamental aspects are still debated within the international scientific community; indeed, a new theory was recently introduced along with a new nomenclature (pulsed atmospheric-pressure plasma streams) [46], [47]. An extensive review on the theoretical and experimental studies on plasma bullets has been published earlier this year [48].

In this paper, the characterization of a single electrode (SE) plasma jet driven by voltage pulses with nanosecond rise time and pulse duration in the order of few tens of nanoseconds is presented. The plasma source, developed by the authors, was previously adopted for the treatment of polymer solutions to increase nanoparticle dispersion [49] and to improve the electrospinnability of poly (L-lactic acid) for the production of high quality solvent free nanofibrous scaffolds for biomedical applications [50], [51]; moreover, the plasma jet has been previously investigated in terms of fluid-dynamic behavior and it has been shown that turbulent or laminar regimes can be obtained changing the operating conditions of the plasma source [52]. Here, we present a deeper characterization of the APPJ device, exploiting a set of techniques to get deeper insights on the correlation between the plasma structure and fluid-dynamic behavior of the jet (by means of iCCD and

Manuscript received June 30, 2014; revised October 14, 2014; accepted December 8, 2014. Date of publication January 1, 2015; date of current version March 6, 2015. This work was supported in part by European Cooperation in Science and Technology (COST) Action through the Project entitled Biomedical Applications of Atmospheric Pressure Plasma Technology under Grant MP1101, in part by COST Action through the Project entitled Electrical Discharges With Liquids for Future Applications under Grant TD1208, and in part by the Alma Mater Studiorum-Università di Bologna through the University Fundings For Basic Research entitled Plasmat.

The authors are with the Department of Industrial Engineering and Industrial Research Centre for Advanced Mechanics and Materials, Alma Mater Studiorum-Università di Bologna, via Saragozza 8, Bologna 40123, Italy (e-mail: vittorio.colombo@unibo.it).

Color versions of one or more of the figures in this paper are available online at http://ieeexplore.ieee.org.

Digital Object Identifier 10.1109/TPS.2014.2381854

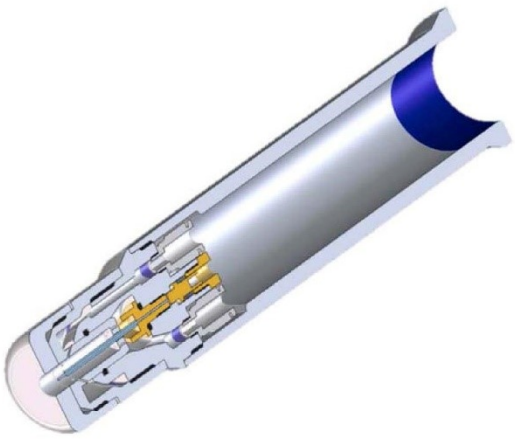

Fig. 1. 3-D cross-sectional representation of the plasma source adopted in the experiments [50].

high-speed Schlieren imaging) and to assess the compatibility of the plasma jet for the treatment of thermosensible materials and for biomedical applications (by means of temperature measurements, optical emission spectroscopy, and UV absolute radiometry).

II. Experimental Setup

A. Cold Atmospheric Pressure Plasma Jet Source

The plasma source adopted in this paper is a SE plasma jet developed in our laboratory and previously reported in [49]–[52]. A schematic of the plasma source is shown in Fig. 1. The high-voltage SE is a 19.5 mm long stainless steel sharpened metallic needle with a diameter of 0.3 mm; the electrode protrudes from a quartz capillary (outer diameter of 1 mm) by 3 mm. In this source, a primary gas [Ar, helium (He), and air] is introduced for sustaining the plasma, whereas a secondary gas (O_2, N_2, gas-phase monomer) can be introduced when required in specific applications. The primary gas is injected through a 12-hole (0.3 mm diameter) diffuser aimed at ensuring a uniform and laminar flow along the electrode and at sustaining the plasma discharge, while the secondary gas is introduced in the discharge region downstream the electrode tip through twelve 0.3 mm holes, tilted with respect to the plasma source axis. The plasma is ejected through a 1 mm orifice [50], [52]. In this paper, the primary gas used is He, whereas no secondary gas was employed.

The plasma source is driven by a commercial pulse generator (FID GmbH—FPG 20–1NMK) producing high-voltage pulses with a slew rate of few kilovoltages per nanosecond, a pulse duration around 30 ns, a peak voltage (PV) of 7–20 kV, and an energy per pulse of 50 mJ at maximum voltage amplitude into a 100–200 Ω load impedance with a maximum pulse repetition frequency (PRF) of 1000 Hz.

B. iCCD Imaging

Temporal evolution of the plasma discharge has been investigated by means of an iCCD camera (Princeton Instruments PIMAX3). A pulse generator (BNC 575 digital pulse/delay generator) has been used to synchronize the generator, the oscilloscope (Tektronix DPO 40034), and the iCCD camera. Two configurations of the iCCD camera have been adopted: in the first configuration, several sequential frames at time steps of 0.25 ns and with an exposure time of 3 ns [50 accumulations collected on the charge coupled device (CCD) sensor for each frame] have been acquired to track the temporal evolution of the plasma discharge during the high-voltage pulse; in the second configuration, a single frame with exposure time of 35 ns covering the entire voltage pulse has been acquired with the aim of comparing the discharge structure and the fluid-dynamic behavior of the jet, which has been observed through Schlieren imaging.

C. Schlieren Imaging

A Schlieren imaging setup in a Z-configuration [52] has been adopted to visualize refractive-index gradients generated in the region downstream the plasma source outlet by the plasma gas mixing with the surrounding ambient air. The imaging setup is composed of a 450 W ozone free xenon lamp (Newport-Oriel 66355 Simplicity Arc Source), a slit and an iris diaphragm, two parabolic mirrors with a focal length of 1 m, a knife edge positioned vertically, and a high-speed camera (Memrecam K3R-NAC Image Technology, operated at 4000 frames/s and 1/50 000-s shutter time) that records the Schlieren image. The plasma jet has been positioned in the middle of the optical path between the two parabolic mirrors, as shown in Fig. 2.

D. Temperature Measurements

Plasma jet temperature has been measured by means of a fiber optic temperature sensor (OPSENS OTP-M) with a calibration range of 20 °C–60 °C, a resolution of 0.01 °C, an accuracy of 0.15 °C, and a response time of less than 1 s.

The fiber optic sensor head has a cylindrical shape with a radius of 1.2 mm and a length of 7 mm. During measurement, the sensor head was positioned coaxially with the source orifice. A second fiber optic sensor was employed to monitor the room temperature during the measurements. Fiber optic sensors have been chosen for measurements because they are immune from electromagnetic interferences [53] and they only slightly affect the discharge because of the small diameter and the dielectric properties of the sensor head.

E. Optical Emission Spectroscopy

An iCCD camera (PIMAX3, Princeton Instruments) mounted on a 500 mm spectrometer (Acton SP2500i, Princeton Instruments) has been adopted to collect spatially resolved optical emission spectra in the UV, VIS and near infrared (NIR) regions. Details of the experimental setup can be found in [50]. Measurements have been performed using a lens with 30 mm focal length and a 20 μm slit width to collect spectra in the region extending from the source outlet to 15 mm downstream, with a spatial resolution of 0.1 mm and a spectral resolution of 0.17 nm. Exposure time has been set at 20 μs and for each spectrum a set of 50 accumulations has been collected on the CCD sensor.

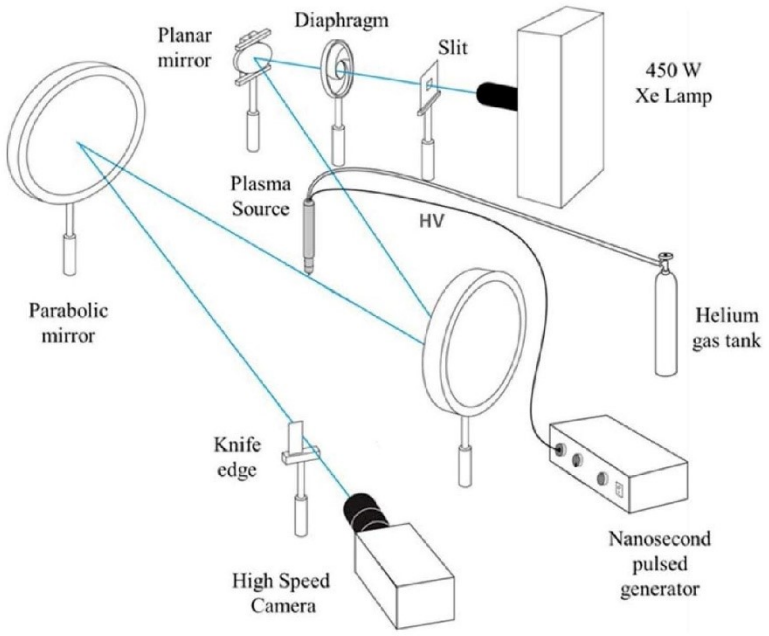

Fig. 2. Experimental setup for high-speed Schlieren imaging of the plasma jet.

F. UV Irradiance Measurement

UV irradiance has been measured using the UV power meter Hamamatsu C9536/H9535-222 (measurement range of 0.001–200 mW/cm^2, high spectral response in the range 150–350 nm). The sensor head, covered with a quartz disk to avoid direct exposure to the plasma jet, has been positioned downstream the plasma source outlet. The protecting quartz disk (thickness = 0.5 mm and diameter = 35 mm) is characterized by an integral UV transmission of 93% across the sensor spectral range. The sensitive part of the UV power meter was centered on the axis of the source orifice so that the plasma plume was directly impinging on the protective quartz disk. Measurements have been carried out at different axial distances from the source outlet.

III. Results

A. Structure of the Plasma Discharge

The structure of the plasma jet and its evolution in time have been investigated for two different sets of operating conditions, inducing strongly different plasma characteristics: in the first case, PV, PRF, and mass flow rate were set to 17 kV, 1000 Hz and 2 SLPM of He respectively; in the second case, the PV and mass flow rate were increased to 25 kV and 3 SLPM of He, respectively.

The iCCD camera has been set to scan the voltage pulse with an exposure time of 3 ns. The iCCD gate opening for the first recorded frame of each scan was set at the start of the voltage pulse and subsequent frames were recorded at fixed time steps of 0.25 ns; therefore, two consecutive frames overlap for 2.75 ns.

For the first case, a sequence of representative frames is shown in Fig. 3, where the time values reported on top of each frame are indicative of the time lapse between the start of the voltage pulse and the corresponding opening of the iCCD gate. For the sake of clarity, the exposures of the most relevant frames depicted in Fig. 3 are reported, together with the high-voltage pulse waveform, in Fig. 4.

The plasma plume appears 5 ns after the start of the voltage rise, which corresponds to a voltage in the range 5–10 kV, and it can be observed in all the subsequent frames taken during the voltage pulse. Nevertheless, its intensity and extension seem to fluctuate during the high-voltage pulse. For example, from the frame starting at 5 to the one at 9.75 ns, both the intensity and the length of the plasma plume increase up to a maximum reached at 6.75 ns and then they start to decrease. A similar behavior can be observed every 5 ns: from 10 to 15 ns, from 15 to 20 ns, and from 20 to 25 ns. To the best of the authors' knowledge, this fluctuating behavior has never been reported in the literature before.

Considering only the brightest frame in each fluctuation (6.75, 11.75, 16.75, and 21.75 ns), a progressive elongation of the plasma plume is clearly visible. As it can be observed in the frames reported in Fig. 3 with a chromatic scale modified to enhance the light emissions with lower intensity, the propagating plasma front remains connected to the plasma source by a VIS channel even in the frames in which the plasma plume is characterized by weaker intensity. This structure,

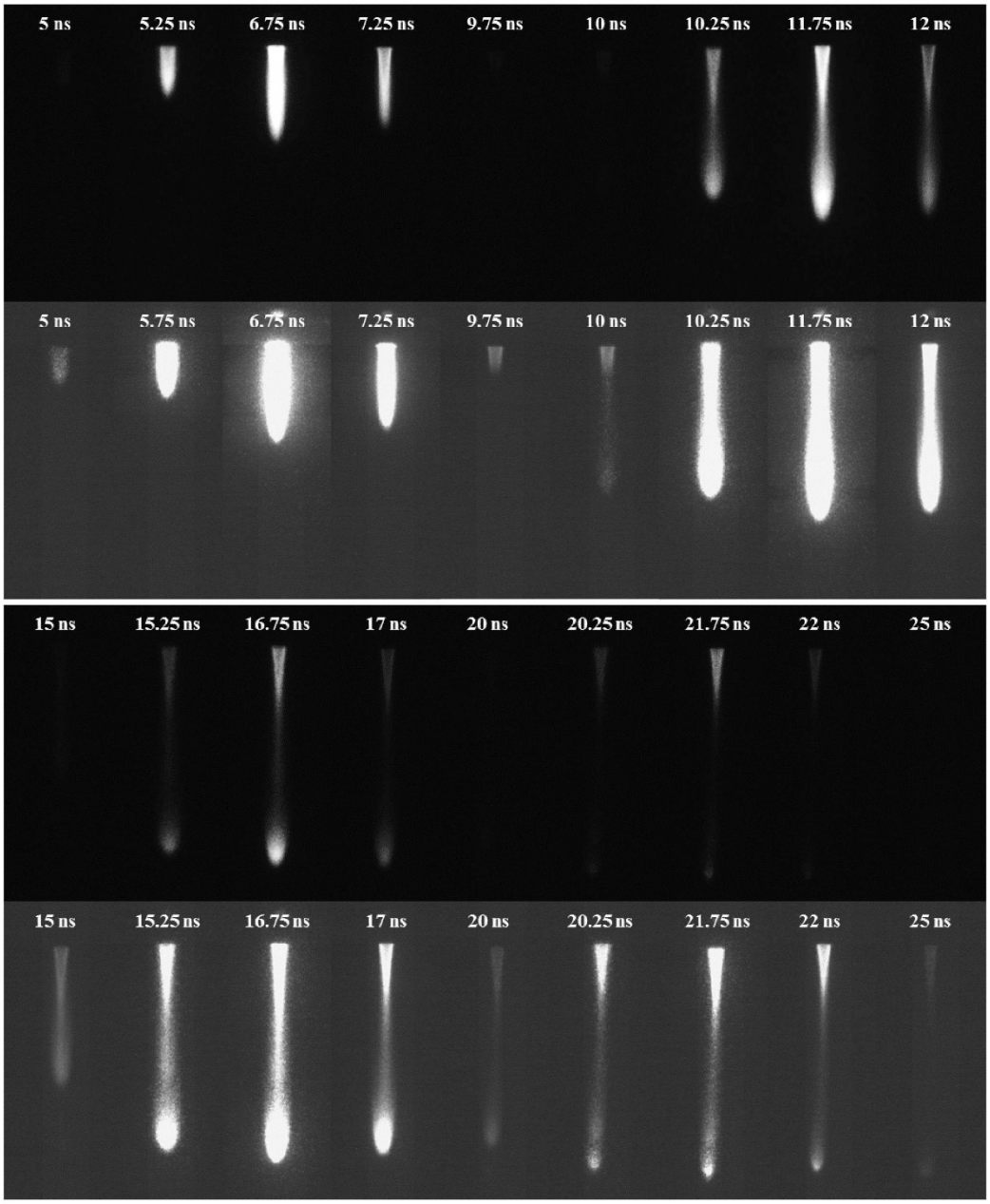

Fig. 3. iCCD frames (3 ns exposure time, 50 accumulations) for the case with 17 kV (PV), 1000 Hz (PRF), and 2 SLPM of He as working gas. Two different chromatic scales were adopted to make all the frames clearly visible (top—higher intensity scale and bottom—low intensity scale). The time values reported on top of each frame are indicative of the time lapse between the start of the voltage pulse and the corresponding opening of the iCCD gate.

characterized by a moving front connected to the source, is similar to what already reported in the literature for other plasma jet sources [54]–[56].

By tracking the temporal evolution of the plasma plume, it is possible to estimate the velocity of the front propagation. The obtained values are in the order of 10^8 cm/s during the

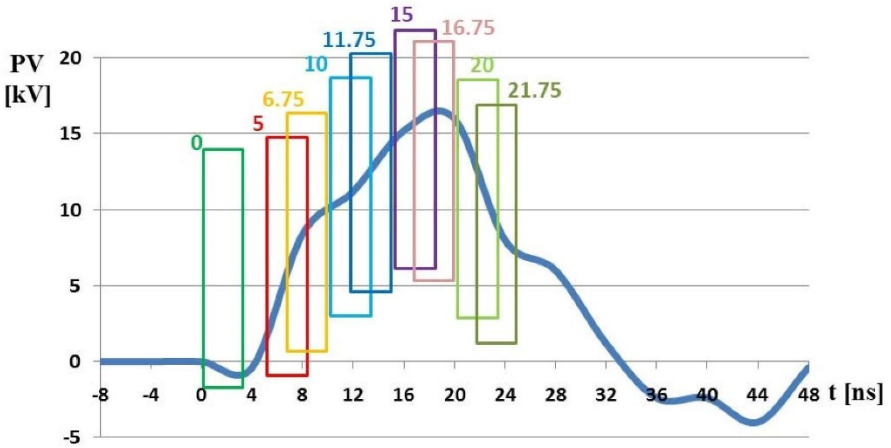

Fig. 4. Voltage waveform for the case with 17 kV (PV), 1000 Hz (PRF), and 2 SLPM of He as working gas with superimposed exposures for relevant iCCD frames. The time values reported on top of each exposure are indicative of the time lapse between the start of the voltage pulse and the corresponding opening of the iCCD gate.

first acquired frames (from 5 to 7.25 ns) and the velocity is reduced to 5×10^7 cm/s when the PV is reached. Similar values have been reported for other plasma jet sources driven by voltage pulses with nanosecond rise time [30], [57], [58].

A similar analysis has been conducted for the second case and results are reported in Figs. 5 and 6. In this case too, it is possible to observe a fluctuation of both the intensity and the length of the plasma plume with a period (5 ns) similar to that observed in the first case. Nevertheless, the structure of the plasma evolves in a sensibly different way. While in the first case, only one front can be observed in the plasma jet, in the second case, the final part of the plasma jet is at first distorted (frames at 11 and 11.25 ns in Fig. 5) and then branched in several fronts connected to the plasma source by converging tails characterized by weaker emission (frames at 16 and 16.25 ns).

A behavior of the plasma front similar to the one observed at instants 11 and 11.25 ns has been observed in [59] and described as snake-like mode. This aspect, as well as the subsequent branching of the plasma jet front, is probably related to hydrodynamic instabilities of the He gas flow, which result in turbulent mixing of He species with the surrounding ambient air; as the plasma discharge is propagating preferentially in regions with high He concentration [60], the turbulent mixing of He and surrounding air can induce several pathways for the plasma discharge, resulting in branching of the plasma jet front. To investigate the correlation between the gas flow instabilities and discharge structure, further investigations exploiting Schlieren imaging have been conducted and the results are presented in the following paragraph.

B. Influence of Jet's Fluid Dynamics on Discharge Structure

Schlieren high-speed recordings of the fluid-dynamic behavior of the plasma jet and iCCD images of the discharge structure have been acquired for the different operating conditions of the plasma source. The He flow rate has been kept fixed at 3 SLPM while the PV and the PRF have been changed in the range 17–30 kV and 125–1000 Hz, respectively.

Since the duration of the high-voltage pulse driving the plasma source is less than the time span of each Schlieren high-speed camera frame (0.25 ms at 4000 frames/s), the fluid-dynamic phenomena occurring during the voltage pulse are observed in a single frame. This frame has been reported in Fig. 7 for different operating conditions of the plasma source together with the corresponding iCCD acquisition performed with an exposure window of 35 ns to collect light emitted during the whole high-voltage pulse.

From Schlieren images, it can be noted that the flow at the source outlet is almost laminar (Reynolds number is approximately 500 for the plasma source operated with 3 SLPM of He) while fluid-dynamic instabilities can be observed in a more downstream position. With increasing PRF (from 125 to 1000 Hz), the length of the laminar region becomes shorter and fluid-dynamic instabilities of higher intensity can be observed. With PV increasing from 17 to 30 kV, the same trend is observed, but the effect is weaker in comparison with the change in PRF.

From iCCD images, it can be noted that the length of the plasma plume is increased as the PV is increased, whereas with increasing PRF, the plasma plume length is generally reduced.

From the comparison of Schlieren frames and iCCD images, a clear correspondence between fluid-dynamic instabilities and branching of the plasma plume can be observed. The ending part of the plasma plume becomes branched in the cases in which the operating conditions induce the plasma plume to propagate into the spatial region where the flow is turbulent. This phenomenon is mostly evident for the cases with highest PV (30 kV), which are characterized by a longer plasma plume that can penetrate the regions with higher intensity of fluid-dynamics instabilities. It should be noted that the branching of the plasma plume appears in correspondence of the region where the transition from laminar to turbulent flow is observed.

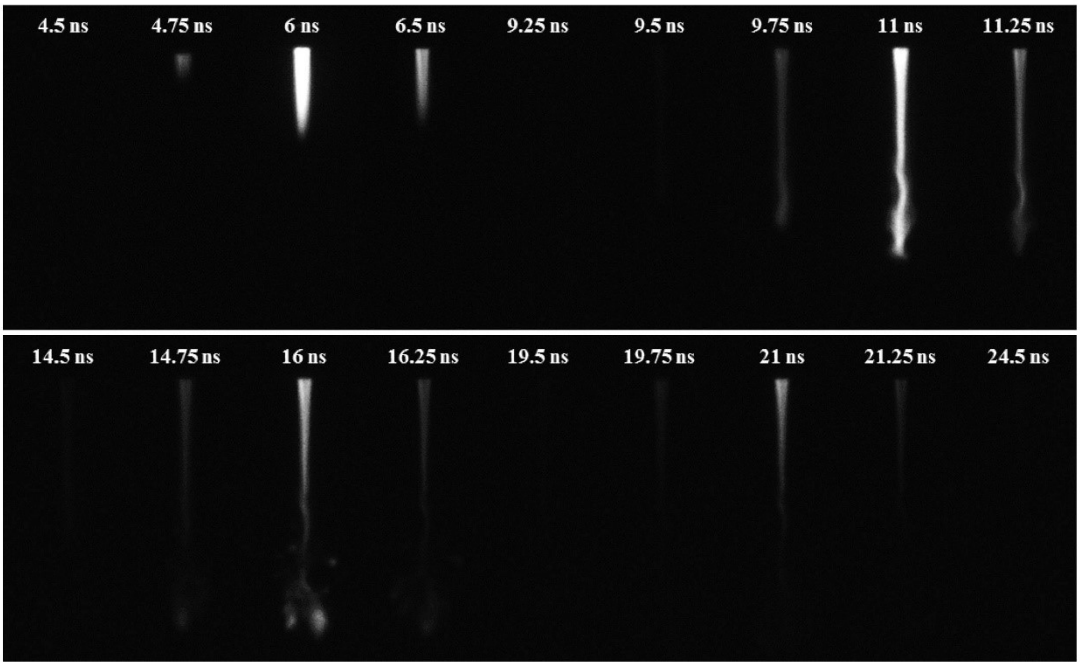

Fig. 5. iCCD frames (3 ns exposure time, 50 accumulations) for the case with 25 kV (PV), 1000 Hz (PRF), and 3 SLPM of He as working gas. The time values reported on top of each frame are indicative of the time lapse between the start of the voltage pulse and the corresponding opening of the iCCD gate.

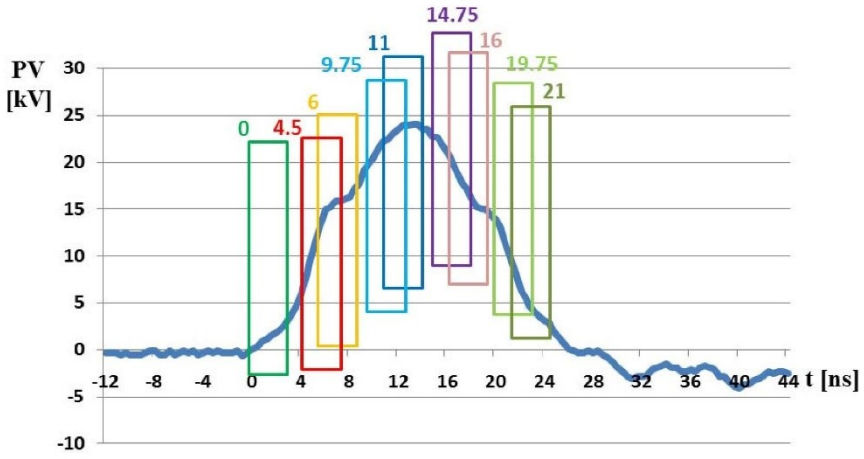

Fig. 6. Voltage waveform for the case with 25 kV (PV), 1000 Hz (PRF), and 3 SLPM of He as working gas with superimposed exposures for relevant iCCD frames. The time values reported on top of each exposure are indicative of the time lapse between the start of the voltage pulse and the corresponding opening of the iCCD gate.

On the contrary, in the cases with lowest PV (17 kV), the plasma plume is propagating in the laminar region only and no branching of the front is observed.

These results support the idea that fluid-dynamic instabilities of the jet induce a turbulent mixing of He and the surrounding air and, consequently, the formation of more than one preferential pathways through which the plasma plume can propagate, resulting in branching of the plasma front.

C. Gas Temperature in the Plasma Jet

Plasma jet temperature has been measured during operation with a PRF varying between 125 and 1000 Hz, PV in the range 17–25 kV, and He flow rate at 1 or 3 SLPM.

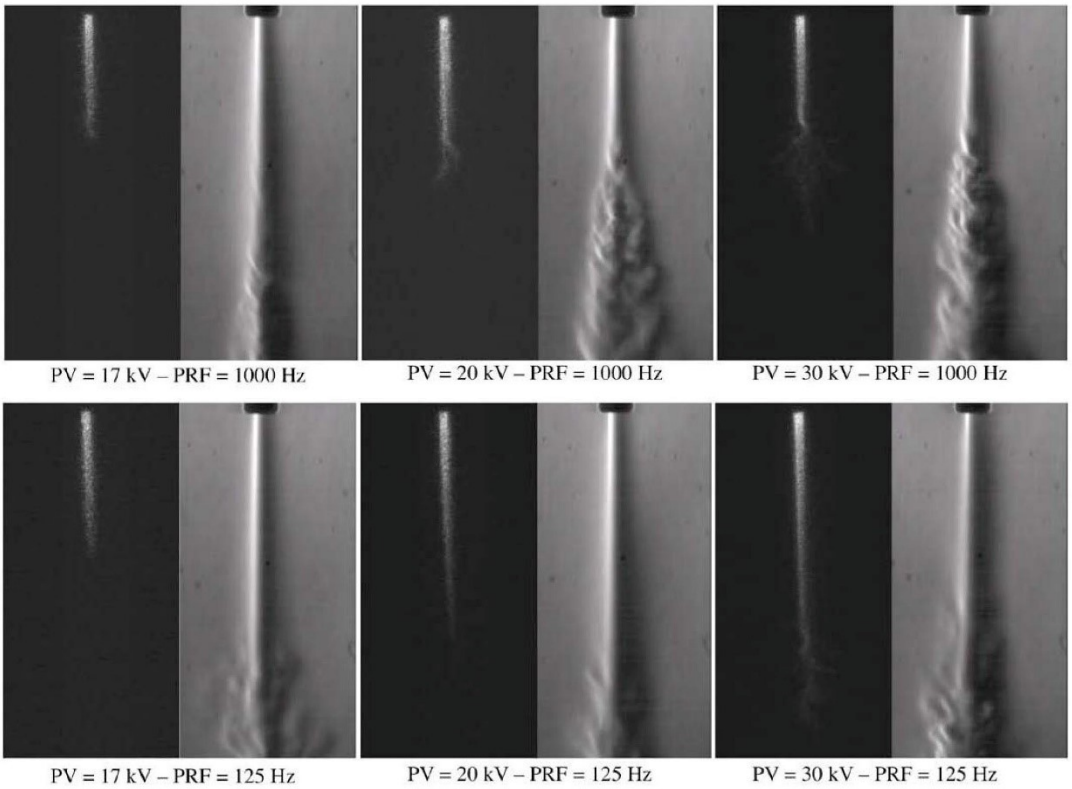

Fig. 7. Comparison of synchronized (left) iCCD and (right) Schlieren acquisitions of the plasma jet for different values of PV (17, 20, and 30 kV) and PRF (125 and 1000 Hz). Flow rate set at 3 SLPM of He for all cases.

Axial temperature profiles (with the axial position defined as the distance measured from the sensor tip to the source outlet; so axial position = 0 mm corresponds to the source outlet) are presented for four different operative conditions with a fixed PRF of 125 and 1000 Hz in Figs. 8 and 9, respectively. Three different measurements have been carried out for each operating condition.

It should be noted that in all the investigated cases, the maximum gas temperature measured by means of fiber optic sensor in the region downstream the source outlet is lower than 45 °C.

For the cases with PRF = 125 Hz (Fig. 8), the temperature is lower than 40 °C. In particular, in the cases with a flow rate of 1 SLPM, the maximum temperature is reached in the region close to the source outlet and a steep decrease of the temperature is observed at 6 and 12 mm downstream plasma source tip for the cases with PV at 17 and 25 kV, respectively. With a higher flow rate (3 SLPM of He), the temperature profile is almost uniform along the axis and the peak value is close to room temperature.

An increase of PRF up to 1000 Hz, as shown in Fig. 9, induces an increase of the plasma temperature in the zone closest to the plasma tip, reaching a maximum temperature of 45 °C for the case with highest peak voltage and lowest flow rate. For the case with 1 SLPM of He, when the plasma is driven by a PV of 25 kV, a drastic drop of temperature is observed 10 mm downstream the plasma source, while a smoother decrease is observed for lower applied voltage. For a higher flow rate (3 SLPM of He), a flatter temperature profile is registered with respect to the cases with flow rate at 1 SLPM of He) with values close to the ambient temperature.

D. Optical Emission Spectroscopy and UV Irradiance Measurements

Optical emission spectra in the UV–VIS–NIR regions as a function of both the wavelength and the distance from the source outlet are shown in Fig. 10 for the plasma jet operated with a PV of 20 kV, a PRF of 125 Hz, and a He gas flow rate of 3 SLPM.

Optical radiation is emitted mainly in the UV-VIS region, where bands of excited molecular nitrogen (second positive system of N_2) can be found between 280 and 450 nm, together with OH radicals in the Ultraviolet B region at 307 nm. Emission from the first negative system of N_2^+ is detected

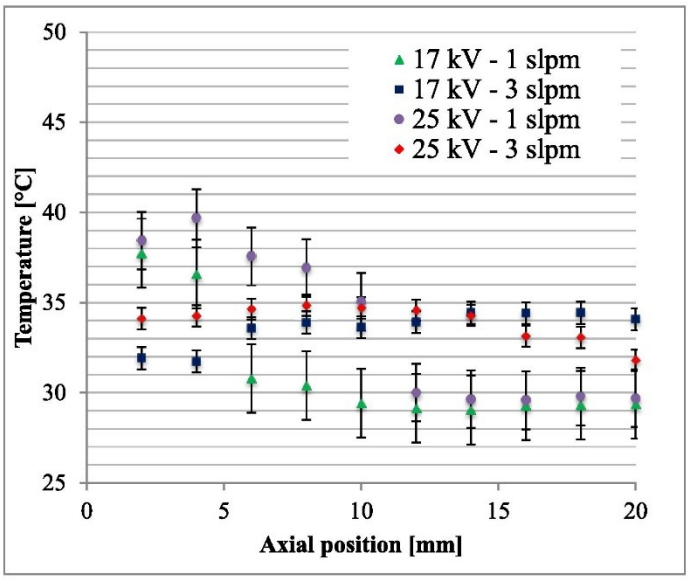

Fig. 8. Axial temperature profile of the plasma jet at constant PRF (125 Hz) for different values of PV (17 and 25 kV) and He flow rate (1 and 3 SLPM). Room temperature during measurements around 29 °C. Axial position = 0 mm corresponds to the source outlet.

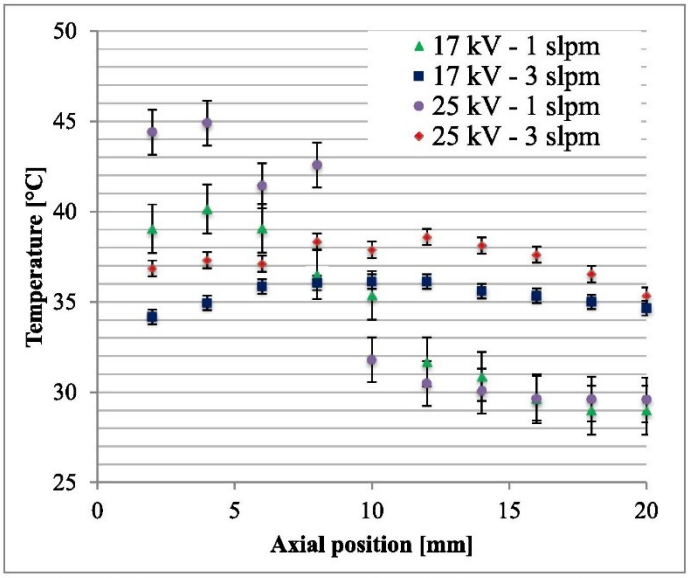

Fig. 9. Axial temperature profile of the plasma jet at constant PRF (1 kHz) for different values of PV (17 and 25 kV) and He flow rate (1 and 3 SLPM). Room temperature during measurements: around 29 °C. Axial position = 0 mm corresponds to the source outlet.

at 391, 427, and 470 nm. A faint emission in the UVC region between 250 and 280 nm due to NO radicals was also observed.

In VIS-NIR, only a few lines of He and O and the second-order diffractions of N_2 and N_2^+ systems can be observed. He lines were registered at 501, 587, 667, and 706 nm. Emission of atomic oxygen was observed at 777 nm. Spectral bands observed between 675 and 760 nm are generated by second-order diffractions of the monochromator and are related to N_2 emission bands.

As the plasma gas is He, at the axial position corresponding to the outlet of the plasma source, only the emission from He lines is observed. At higher distance from the source outlet, the surrounding air is diffusing into the plasma gas and the

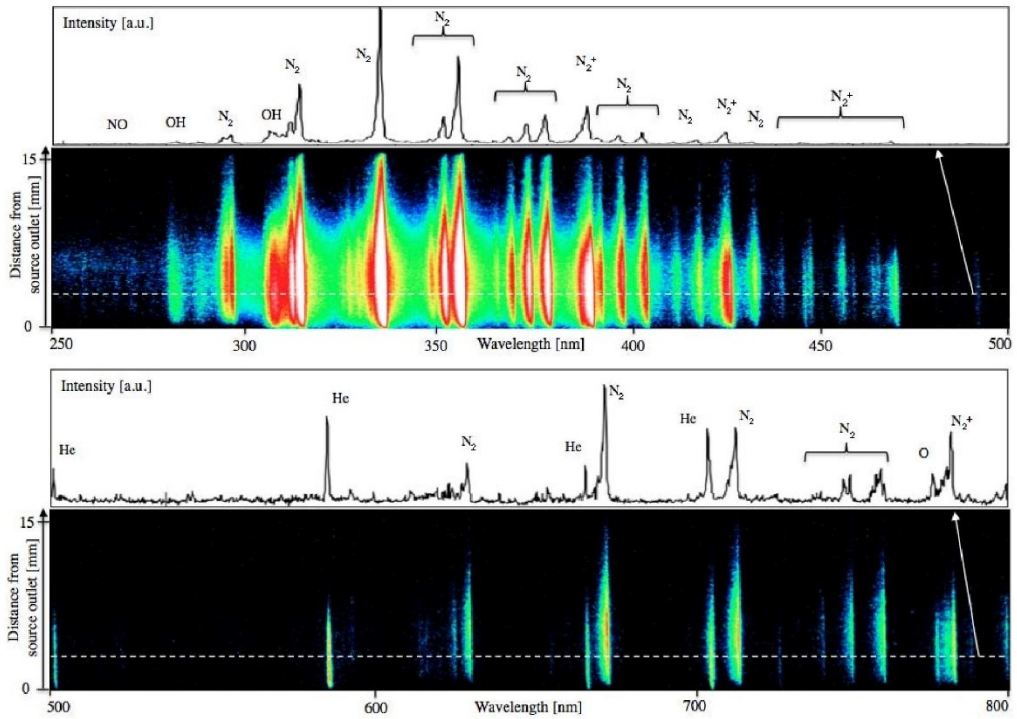

Fig. 10. Optical emission spectra in (top) UV-VIS and (bottom) VIS-NIR range as a function of both the wavelength and the distance from the source outlet. Plasma jet operated with PV = 20 kV, PRF = 125 Hz, and He flow rate = 3 SLPM.

emission bands of excited N_2, OH, and NO can be observed, which are characterized by maximum intensity positioned approximately at 6 mm downstream the source outlet. This can be explained as the emission intensity of these bands depends on: 1) the concentration of ground state molecules and 2) the rate of molecule excitation; while the concentration of ground state molecules increases the further from the source outlet, as a consequence of an increasing mole fraction of air due to diffusion into the plasma gas, the rate of molecule excitation decreases the further from the outlet, because of the decrease of the local electric field intensity (being the plasma source of the SE type with a virtual grounded electrode) and because the electron concentration decreases as a consequence of the increasing mole fraction of air. The opposite trends expected for these two parameters can be appointed as responsible for the maximum emission intensity to be at a certain distance from source outlet, which we experimentally determined to be 6 mm, for the considered operating conditions. Similar considerations and results have been previously presented in a computational analysis of a He/O_2 plasma jet flowed into humid air [61].

A qualitatively similar emission spectrum can be observed also for other investigated operating conditions.

The intensity of emission increases for higher values of PV and He gas flow rate, as shown in Fig. 11, where the relative intensities of selected emission bands of OH, N_2, N_2^+, and emission lines of O and He are reported.

The effect of PV increase can be explained in terms of the higher local electric field produced in the plasma plume which, in turn, produces a higher electron concentration that enhances the production of excited species and radiation emission.

Meanwhile, increasing He flow rate (for operating conditions that results in an almost laminar flow in the emitting region, as shown in Fig. 7) was previously shown to result in a lower mole fraction of ambient air in the plasma plume region [48], [62], that can lead to higher local electron concentration [61], which can explain the observed higher emission intensity from excited species.

The effect of He flow rate on the emission intensities from He lines and N_2 bands is further highlighted in Fig. 12. An increase of He flow rate is there shown to result in a higher emission intensity from He species, which extends over a longer region downstream the plasma jet orifice (significant values of emission intensity are measured up to 5 mm downstream for the 1 SLPM case and up to 10 mm for the 3 SLPM case); this enhanced emission intensity can be related to the lower diffusion of air in the plasma region that allows for an increase of electron concentration, He mole fraction in the plume region and, as a consequence, of excited He atoms. A higher He flow rate is also shown to cause

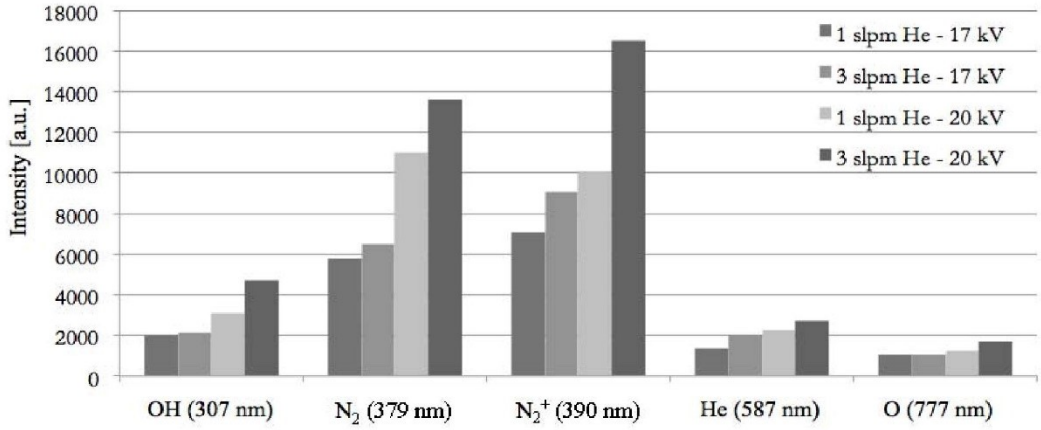

Fig. 11. Relative emission intensity of selected spectral atomic lines and molecular bands for the plasma jet operated with PRF = 125 Hz for different values of PV (17 and 20 kV) and He flow rate (1 and 3 SLPM). For each emission line and band, the value corresponding to the maximum intensity has been reported.

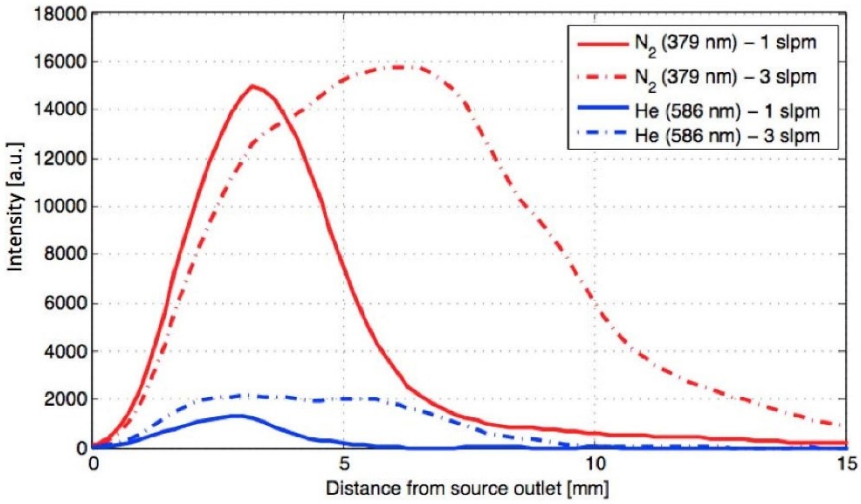

Fig. 12. Relative emission intensity of N_2 molecular band at 379 nm and He atomic line at 586 nm as a function of distance from the plasma source outlet for PRF = 125 Hz, PV = 20 kV, and He flow rate (1 and 3 SLPM).

a higher N_2 peak emission intensity and a significant N_2 emission is observed much further from the source outlet; this can be appointed again to the lower diffusion of air in the plasma region, which results in an increase of electron concentration and, thus, of the N_2 excitation rate. Moreover, the peak of N_2 emission intensity was found to be located further away from the torch outlet in the case with 3 SLPM; indeed, while the higher He flow rate reduces air diffusion in the plasma region and allows for higher electron concentration, it also reduces the mole fraction of ground state N_2 available for excitation in the plasma at a fixed axial position. Therefore, at the same distance from the source outlet where the peak emission intensity was located for the case with 1 SLPM of He (distance of 3 mm), a higher electron concentration and a lower mole fraction of ground state N_2 molecules are expected for the case of 3 SLPM of He, which results in a lower emission intensity. For the latter case, the N_2 peak emission intensity is observed further downstream (distance of 6 mm), where the diffusion of air in the plasma region has enabled the buildup of ground state N_2 mole molecules to be excited, but still has not excessively dampened the electron concentration; at this same axial position, a much lower N_2 emission intensity is observed for the case with 1 SLPM of He, as the higher diffusion of air results in a higher air mole fraction and a faster decrease of electron concentration.

The influence of different operating parameters on the total irradiance in the UV range of the plasma plume has been indirectly evaluated measuring the distance at which an

TABLE I
UV IRRADIANCE MEASUREMENTS FOR DIFFERENT PLASMA JET OPERATING CONDITIONS

Plasma gas flow rate	Pulse repetition frequency	Peak voltage	Distance from source outlet at which UV irradiance = 1 μW/cm^2
1 slpm He	83 Hz	17 kV	<3 mm
1 slpm He	83 Hz	20 kV	<3 mm
3 slpm He	83 Hz	17 kV	<3 mm
3 slpm He	83 Hz	20 kV	9 mm
3 slpm He	125 Hz	17 kV	7.5 mm
3 slpm He	125 Hz	20 kV	12 mm
3 slpm He	1000 Hz	20 kV	15 mm

irradiance of 1 μW/cm^2 can be detected using a UV power meter: the higher is the distance at which UV irradiance = 1 μW/cm^2, the higher is the plasma total UV irradiance. Several plasma operating conditions were tested adjusting He mass flow rate, PV, and PRF.

Results reported in Table I highlight that the plasma UV irradiance increases for higher values of PV, PRF, and gas flow rate.

For a mass flow rate of 1 SLPM of He and low values of both PRF (83 Hz) and PV (17 kV), a UV irradiance of 1 μW/cm^2 can be detected only at a distance of less than 3 mm. Independently increasing the flow rate to 3 SLPM of He, or the PV to 20 kV, no relevant change in UV irradiance can be noticed. By increasing both parameters at the same time, irradiance of 1 μW/cm^2 is reached already 9 mm downstream the source outlet. With flow rate fixed at 3 SLPM of He, increasing the PRF from 83 to 125 Hz results in a higher UV emission (UV irradiance of 1 μW/cm^2 reached at 7.5 and 12 mm for PV set at 17 and 20 kV, respectively).

For the highest flow rate, PV and PRF considered (3 SLPM of He, 20 kV, and 1000 Hz, respectively), the irradiance of 1 μW/cm^2 has been obtained for a distance of 15 mm.

A similar analysis of UV radiation has been carried out by different groups for other plasma sources usually adopted for biomedical applications [32], [63]–[65], with the aim of selecting operating conditions that result in UV irradiances compatible with biomedical treatments. The values obtained for our plasma jet are below those reported in the literature for these plasma sources, which range between 10 and 1000 μW/cm^2.

IV. CONCLUSION

The discharge generated by an APPJ developed by the authors and driven by high-voltage pulses with rise time and duration of a few nanoseconds has been investigated. The plasma plume is characterized by a front propagating with a velocity close to the values reported for plasma bullets (10^7-10^8 cm/s) [30], [57], [58]. The plume presents a single front or several branched subfronts depending on the operating conditions. The comparison of results from Schlieren and iCCD imaging suggests that branching of the plasma jet front occurs in spatial regions where the flow is turbulent. A possible explanation of plume branching is that turbulent mixing of plasma gas and ambient air creates several randomly changing preferential paths characterized by high concentration of He through which the discharge front tends to propagate. It was also observed that the temporal evolution of the plasma plume during the discharge presents oscillations both in light emission intensity and plume length. This phenomenon needs to be further investigated by future studies.

It has been shown that, for a discharge generated in He, the plasma plume is mainly emitting in the UV-VIS range with a spectrum characterized by N_2, N_2^+, NO, and OH spectral bands as a consequence of mixing with ambient air. The achieved results suggest that both electrical parameters of the generator (PV and PRF) affect the plasma UV component. However, for the operating conditions considered in this paper, the values obtained for the UV irradiance are compatible with biomedical applications.

Axial temperature profiles confirm that the plasma source driven by nanosecond pulses can generate a plasma jet with temperature compatible with heat-sensitive materials, including biological substrates.

The presented results provide some fundamental understanding of the characteristics and behavior of the discharge generated by an APPJ driven by nanosecond voltage pulses; this can support the development of a wide range of applications such as surface functionalization, thin film deposition, electrospinning of polymers, and nanoadditive dispersion in polymer solutions.

REFERENCES

[1] K. D. Weltmann *et al.*, "Antimicrobial treatment of heat sensitive products by miniaturized atmospheric pressure plasma jets (APPJs)," *J. Phys. D, Appl. Phys.*, vol. 41, no. 19, pp. 194008–194014, Sep. 2008.

[2] J. Shen *et al.*, "Sterilization of *Bacillus subtilis* spores using an atmospheric plasma jet with argon and oxygen mixture gas," *Appl. Phys. Exp.*, vol. 5, no. 3, p. 036201, Feb. 2012.

[3] U. Lommatzsch, D. Pasedag, A. Baalmann, G. Ellinghorst, and H.-E. Wagner, "Atmospheric pressure plasma jet treatment of polyethylene surfaces for adhesion improvement," *Plasma Process. Polym.*, vol. 4, no. 1 pp. S1041–S1045, Apr. 2007.

[4] C. Cheng, Z. Liye, and R.-J. Zhan, "Surface modification of polymer fibre by the new atmospheric pressure cold plasma jet," *Surf. Coat. Technol.*, vol. 200, no. 24, pp. 6659–6665, Aug. 2006.

[5] E. J. Szili, S. A. Al-Bataineh, P. M. Bryant, R. D. Short, J. W. Bradley, and D. A. Steele, "Controlling the spatial distribution of polymer surface treatment using atmospheric-pressure microplasma jets," *Plasma Process. Polym.*, vol. 8, no. 1, pp. 38–50, Jan. 2011.

[6] X. Deng *et al.*, "Engineering of composite organosilicon thin films with embedded silver nanoparticles via atmospheric pressure plasma process for antibacterial activity," *Plasma Process. Polym.*, vol. 11, no. 10, pp. 921–930, 2014.

[7] H. Fakhouri, D. B. Salem, O. Carton, J. Pulpytel, and F. Arefi-Khonsari, "Highly efficient photocatalytic TiO_2 coatings deposited by open air atmospheric pressure plasma jet with aerosolized TTIP precursor," *J. Phys. D, Appl. Phys.*, vol. 47, no. 26, pp. 265301–265312, Jun. 2014.

[8] D. Mariotti and M. Sankaran, "Perspectives on atmospheric-pressure plasmas for nanofabrication," *J. Phys. D, Appl. Phys.*, vol. 44, no. 17, pp. 174023–174031, Apr. 2011.

[9] D. Mariotti, J. Patel, V. Svrcek, and P. Maguire, "Plasma–liquid interactions at atmospheric pressure for nanomaterials synthesis and surface engineering," *Plasma Process. Polym.*, vol. 9, nos. 11–12, pp. 1074–1085, Dec. 2012.

[10] S. Mitra, V. Svrcek, D. Mariotti, T. Velusamy, K. Matsubara, and M. Kondo, "Microplasma-induce liquid chemistry for stabilizing of silicon nanocrystals optical properties in water," *Plasma Process. Polym.*, vol. 11, no. 2, pp. 158–163, Feb. 2014.

[11] S. W. Lee, D. Liang, X. P. A. Gao, and R. M. Sankaran, "Direct writing of metal nanoparticles by localized plasma electrochemical reduction of metal cations in polymer films," *Adv. Funct. Mater.*, vol. 21, no. 11, pp. 2155–2161, Jun. 2011.

[12] S. W. Lee, C. Mattevi, M. Chhowalla, and R. M. Sankaran, "Plasma-assisted reduction of graphene oxide at low temperature and atmospheric pressure for flexible conductor applications," *J. Phys. Chem. Lett.*, vol. 3, no. 6, pp. 772–777, Feb. 2012.

[13] I. E. Kieft, M. Kurdi, and E. Stoffels, "Reattachment and apoptosis after plasma-needle treatment of cultured cells," *IEEE Trans. Plasma Sci.*, vol. 34, no. 4, pp. 1331–1336, Aug. 2006.

[14] G. Fridman *et al.*, "Blood coagulation and living tissue sterilization by floating-electrode dielectric barrier discharge in air," *Plasma Chem. Plasma Process.*, vol. 26, no. 4, pp. 425–442, Aug. 2006.

[15] G. Fridman, G. Friedman, A. Gutsol, A. B. Shekhter, V. N. Vasilets, and A. Fridman, "Applied plasma medicine," *Plasma Process. Polym.*, vol. 5, no. 6, pp. 503–533, Aug. 2008.

[16] G.-C. Kim, H. J. Lee, and C.-H. Shon, "The effects of a micro plasma on melanoma (G361) cancer cells," *J. Korean Phys. Soc.*, vol. 54, no. 2, pp. 628–632, 2009.

[17] C.-H. Kim *et al.*, "Induction of cell growth arrest by atmospheric non-thermal plasma in colorectal cancer cells," *J. Biotechnol.*, vol. 150, no. 4, pp. 530–538, Dec. 2010.

[18] M. Keidar *et al.*, "Cold plasma selectivity and the possibility of a paradigm shift in cancer therapy," *Brit. J. Cancer*, vol. 105, no. 9, pp. 1295–1301, 2011.

[19] H. Kurita *et al.*, "Single-molecule measurement of strand breaks on large DNA induced by atmospheric pressure plasma jet," *Appl. Phys. Lett.*, vol. 99, no. 19, p. 191504, 2011.

[20] X. Yan *et al.*, "Plasma-induced death of HepG2 cancer cells: Intracellular effects of reactive species," *Plasma Process. Polym.*, vol. 9, no. 1, pp. 59–66, Jan. 2012.

[21] J. Huang *et al.*, "Dielectric barrier discharge plasma in Ar/O_2 promoting apoptosis behavior in A549 cancer cells," *Appl. Phys. Lett.*, vol. 99, no. 25, p. 253701, 2011.

[22] H. M. Joh, S. J. Kim, T. H. Chung, and S. H. Leem, "Reactive oxygen species-related plasma effects on the apoptosis of human bladder cancer cells in atmospheric pressure pulsed plasma jets," *Appl. Phys. Lett.*, vol. 101, no. 5, p. 053703, 2012.

[23] O. Volotskova, T. S. Hawley, M. A. Stepp, and M. Keidar, "Targeting the cancer cell cycle by cold atmospheric plasma," *Sci. Rep.*, vol. 2, no. 636, pp. 636–645, Sep. 2012.

[24] J. F. Kolb, A. M. Mattson, C. M. Edelblute, X. Hao, M. A. Malik, and L. C. Heller, "Cold DC-operated air plasma jet for the inactivation of infectious microorganisms," *IEEE Trans. Plasma Sci.*, vol. 40, no. 11, pp. 3007–3026, Nov. 2012.

[25] R. Jijie, C. Luca, V. Pohoata, and I. Topala, "Effects of atmospheric-pressure plasma jet on pepsin structure and function," *IEEE Trans. Plasma Sci.*, vol. 40, no. 11, pp. 2980–2985, Nov. 2012.

[26] S. Zhao *et al.*, "Combined effect of N-acetylcysteine (NAC) and plasma on proliferation of HepG2 cells," *IEEE Trans. Plasma Sci.*, vol. 40, no. 9, pp. 2179–2184, Sep. 2012.

[27] L. Brulle *et al.*, "Effects of a non thermal plasma treatment alone or in combination with gemcitabine in a MIA PaCa2-luc orthotopic pancreatic carcinoma model," *PLoS ONE*, vol. 7, p. e52653, Dec. 2012.

[28] X. Lu, M. Laroussi, and V. Puech, "On atmospheric-pressure non-equilibrium plasma jets and plasma bullets," *Plasma Sour. Sci. Technol.*, vol. 21, no. 3, p. 034005, Apr. 2012.

[29] E. Stoffels, A. J. Flikweert, W. W. Stoffels, and G. M. W. Kroesen, "Plasma needle: A non-destructive atmospheric plasma source for fine surface treatment of (bio)materials," *Plasma Sour. Sci. Technol.*, vol. 11, no. 4, pp. 383–388, Aug. 2002.

[30] E. Robert *et al.*, "Experimental study of a compact nanosecond plasma gun," *Plasma Process. Polym.*, vol. 6, no. 12, pp. 795–802, Dec. 2009.

[31] M. Laroussi and X. Lu, "Room-temperature atmospheric pressure plasma plume for biomedical applications," *Appl. Phys. Lett.*, vol. 87, no. 11, p. 113902, 2005.

[32] K.-D. Weltmann *et al.*, "Atmospheric pressure plasma jet for medical therapy: Plasma parameters and risk estimation," *Contrib. Plasma Phys.*, vol. 49, no. 9, pp. 631–640, Nov. 2009.

[33] J. Y. Kim, J. Ballato, and S.-O. Kim, "Intense and energetic atmospheric pressure plasma jet arrays," *Plasma Process. Polym.*, vol. 9, no. 3, pp. 253–260, Mar. 2012.

[34] S. Bianconi *et al.*, "iCCD imaging of the transition from uncoupled to coupled mode in a plasma source for biomedical and materials treatment applications," *IEEE Trans. Plasma Sci.*, vol. 42, no. 10, pp. 2746–2747, Oct. 2014.

[35] K. Kim, G. Kim, Y. C. Hong, and S. S. Yang, "A cold micro plasma jet device suitable for bio-medical applications," *Microelectron. Eng.*, vol. 87, nos. 5–8, pp. 1177–1180, May/Aug. 2010.

[36] F. T. O'Neill *et al.*, "Generation of active species in a large atmospheric-pressure plasma jet," *IEEE Trans. Plasma Sci.*, vol. 40, no. 11, pp. 2994–3002, Nov. 2012.

[37] X. L. Deng, A. Y. Nikiforov, P. Vanraes, and C. Leys, "Direct current plasma jet at atmospheric pressure operating in nitrogen and air," *J. Appl. Phys.*, vol. 13, no. 2, p. 023305, 2013.

[38] Q. Xiong *et al.*, "Absolute OH density determination by laser induced fluorescence spectroscopy in an atmospheric pressure RF plasma jet," *Eur. Phys. J. D*, vol. 66, p. 281, Nov. 2012.

[39] Y. Hong, N. Lu, J. Pan, J. Li, Y. Wu, and K. F. Shang, "Characteristic study of cold atmospheric argon plasma jets with rod-tube/tube high voltage electrode," *J. Electrostatics*, vol. 71, no. 2, pp. 93–111, Apr. 2013.

[40] A. F. H. van Gessel, B. Hrycak, M. Jasinski, J. Mizeraczyk, J. J. A. M. van der Mullen, and P. J. Bruggeman, "Temperature and NO density measurements by LIF and OES on an atmospheric pressure plasma jet," *J. Phys. D, Appl. Phys.*, vol. 46, no. 9, p. 095201, 2013.

[41] Q. Xiong, A. Y. Nikiforov, M. A. Gonzalez, C. Leys, and X. P. Lu, "Characterization of an atmospheric helium plasma jet by relative and absolute optical emission spectroscopy," *Plasma Sour. Sci. Technol.*, vol. 22, no. 1, p. 015011, Dec. 2013.

[42] E. Karakas and M. Laroussi, "Experimental studies on the plasma bullet propagation and its inhibition," *J. Appl. Phys.*, vol. 108, no. 6, p. 063305, 2012.

[43] M. Teschke, J. Kedzierski, E. G. Finantu-Dinu, D. Korzec, and J. Engemann, "High-speed photographs of a dielectric barrier atmospheric pressure plasma jet," *IEEE Trans. Plasma Sci.*, vol. 33, no. 2, pp. 310–311, Apr. 2005.

[44] X. Lu and M. Laroussi, "Dynamics of an atmospheric pressure plasma plume generated by submicrosecond voltage pulses," *J. Appl. Phys.*, vol. 100, no. 6, p. 063302, 2006.

[45] C. Cachoncinlle, R. Viladrosa, E. Robert, J.-M. Pouvesle, A. Khacef, and S. Dozias, "Transient plasma ball generation system at long distance," U.S. Patent 8 482 206 B2, Jul. 9, 2013.

[46] E. Robert, V. Sarron, D. Ries, S. Dozias, M. Vandamme, and J. M. Pouvesle, "Characterization of pulsed atmospheric-pressure plasma streams (PAPS) generated by a plasma gun," *Plasma Sour. Sci. Technol.*, vol. 21, no. 3, p. 034017, May 2012.

[47] Z. Xiong, E. Robert, V. Sarron, J.-M. Pouvesle, and M. J. Kushner, "Dynamics of ionization wave splitting and merging of atmospheric-pressure plasmas in branched dielectric tubes and channels," *J. Phys. D, Appl. Phys.*, vol. 45, no. 7, pp. 275201–275220, Jun. 2012.

[48] X. Lu, G. V. Naidis, M. Laroussi, and K. Ostrikov, "Guided ionization waves: Theory and experiments," *Phys. Rep.*, vol. 540, no. 3, pp. 123–166, Jul. 2014.

[49] D. Fabiani *et al.*, "Plasma assisted nanoparticle dispersion in polymeric solutions for the production of electrospun lithium battery separators," in *Proc. IEEE Int. Conf. Solid Dielectr. (ICSD)*, Bologna, Italy, Jun./Jul. 2013, pp. 718–721.

[50] V. Colombo *et al.*, "Atmospheric pressure non-equilibrium plasma treatment to improve the electrospinnability of poly(L-lactic acid) polymeric solution," *Plasma Process. Polym.*, vol. 11, no. 3, pp. 247–255, Mar. 2014.

[51] D. Fabiani *et al.*, "Study of the effect of atmospheric pressure plasma treatment on electrospinnability of poly-L-lactic acid solutions: Voltage waveform effect," in *Proc. IEEE Int. Conf. Solid Dielectr. (ICSD)*, Bologna, Italy, Jun./Jul. 2013, pp. 358–361.

[52] M. Boselli *et al.*, "Schlieren high-speed imaging of a nanosecond pulsed atmospheric pressure non-equilibrium plasma jet," *Plasma Chem. Plasma Process.*, vol. 34, no. 4, pp. 853–869, Jul. 2014.

[53] M. R. Wertheimer, B. Saoud, M. Ahlawat, and R. Kashyap, "Accurate in-situ gas temperature measurements in dielectric barrier discharges at atmospheric pressure," *J. Appl. Phys*, vol. 100, no. 20, p. 201112, 2012.

[54] A. Shashurin, M. N. Shneider, and M. Keidar, "Measurements of streamer head potential and conductivity of streamer column in cold non-equilibrium atmospheric plasmas," *Plasma Sour. Sci. Technol.*, vol. 21, no. 3, p. 034006, 2012.

[55] Y. Xian *et al.*, "From short pulses to short breaks: Exotic plasma bullets via residual electron control," *Sci. Rep.*, vol. 3, Apr. 2013, Art. ID 1599.

[56] C. Jiang, M. T. Chen, and M. A. Gundersen, "Polarity-induced asymmetric effects of nanosecond pulsed plasma jets," *J. Phys. D, Appl. Phys.*, vol. 42, no. 23, p. 232002, Nov. 2009.

[57] J. P. Boeuf, L. L. Yang, and L. C. Pitchford, "Dynamics of a guided streamer ('plasma bullet') in a helium jet in air at atmospheric pressure," *J. Phys. D, Appl. Phys.*, vol. 46, no. 1, pp. 015201–0152014, 2013.
[58] S. Wu, H. Xu, X. Lu, and Y. Pan, "Effect of pulse rising time of pulse dc voltage on atmospheric pressure non-equilibrium plasma," *Plasma Process. Polym.*, vol. 10, no. 2, pp. 136–140, Feb. 2013.
[59] S. Wu, Z. Wang, Q. Huang, X. Tan, X. Lu, and K. Ostrikov, "Atmospheric-pressure plasma jets: Effect of gas flow, active species, and snake-like bullet propagation," *Phys. Plasmas*, vol. 20, no. 2, p. 023503, Feb. 2013.
[60] R. Xiong, Q. Xiong, A. Y. Nikiforov, P. Vanraes, and C. Leys, "Influence of helium mole fraction distribution on the properties of cold atmospheric pressure helium plasma jets," *J. Appl. Phys.*, vol. 112, no. 3, p. 033305, 2012.
[61] N. Y. Babaeva and M. J. Kushner, "Interaction of multiple atmospheric-pressure micro-plasma jets in small arrays: He/O_2 into humid air," *Plasma Sour. Sci. Technol.*, vol. 23, no. 1, p. 015007, Jan. 2014.
[62] Y. Sakiyama and D. B. Graves, "Neutral gas flow and ring-shaped emission profile in non-thermal RF-excited plasma needle discharge at atmospheric pressure," *Plasma Sour. Sci. Technol.*, vol. 18, no. 2, p. 025022, Mar. 2009.
[63] D. Dobrynin, K. Arjunan, A. Fridman, G. Friedman, and A. M. Clyne, "Direct and controllable nitric oxide delivery into biological media and living cells by a pin-to-hole spark discharge (PHD) plasma," *J. Phys. D, Appl. Phys.*, vol. 44, no. 7, p. 075201, Jan. 2011.
[64] T. G. Klampfl *et al.*, "Cold atmospheric air plasma sterilization against spores and other microorganisms of clinical interest," *Appl. Environ. Microbiol.*, vol. 78, no. 15, pp. 5077–5082, May 2012.
[65] T. Shimizu *et al.*, "Characterization of microwave plasma torch for decontamination," *Plasma Process. Polym.*, vol. 5, no. 6, pp. 577–582, Aug. 2008.

Marco Boselli was born in Italy in 1983. He received the master's degree in energy engineering from the Alma Mater Studiorum-Università di Bologna, Bologna, Italy, in 2009, with a focus on industrial applications of thermal plasmas.

He has been a Researcher in modeling and diagnostics on metal cutting and welding plasma processes with the Interdepartmental Center for Industrial Research-Advanced Applications in Mechanical Engineering and Materials Technology, Alma Mater Studiorum-Università di Bologna, since 2011.

Vittorio Colombo was born in Italy in 1961. He received the master's degree in nuclear engineering and the Ph.D. degree in energetics from the Politecnico di Turin, Turin, Italy, in 1986 and 1990, respectively.

He was with the Nuclear Reactor Physics Group, Politecnico di Turin, as a Researcher, from 1990 to 1992. Since 1992, he has been with the Faculty of Engineering, Alma Mater Studiorum-Università di Bologna, Bologna, Italy, where he has been a Full Professor of Industrial Applications of Plasmas with the Department of Industrial Engineering since 2000. Since 2010, he has been a member of the Interdepartmental Center for Industrial Research-Advanced Applications in Mechanical Engineering and Materials Technology with the Alma Mater Studiorum-Università di Bologna.

Matteo Gherardi was born in Italy in 1985. He received the master's degree in energy engineering from the Alma Mater Studiorum-Università di Bologna, Bologna, Italy, in 2009, and the Ph.D. degree in industrial applications of plasmas from the Department of Industrial Engineering, Alma Mater Studiorum-Università di Bologna, in 2013.

He has been a Post-Doctoral Researcher with the Alma Mater Studiorum-Università di Bologna since 2013. His current research interests include plasma assisted nanoparticle synthesis and plasma biomedical applications.

Romolo Laurita was born in Italy in 1986. He received the master's degree in energy engineering from the Alma Mater Studiorum-Università di Bologna, Bologna, Italy, in 2011, where he is currently pursuing the Ph.D. degree in industrial applications of plasmas.

His current research interests include design and characterization of atmospheric pressure nonthermal plasma sources for biomedical applications.

Anna Liguori was born in Italy in 1989. She received the master's degree in energy engineering from the Alma Mater Studiorum-Università di Bologna, Bologna, Italy, in 2012, where she is currently pursuing the Ph.D. degree in industrial applications of plasmas. Her master's degree thesis was on characterization of atmospheric cold plasma sources for scaffold biocompatibilzation.

Paolo Sanibondi was born in Italy in 1983. He received the master's degree in energy engineering from the Alma Mater Studiorum-Università di Bologna, Bologna, Italy, in 2007, and the Ph.D. degree in industrial applications of thermal plasmas from the Department of Mechanical Engineering, Alma Mater Studiorum-Università di Bologna, in 2011.

He has been a Post-Doctoral Researcher with the Alma Mater Studiorum-Università di Bologna, since 2011, where he is involved in plasma modeling and diagnostics.

Emanuele Simoncelli was born in Italy in 1990. He received the master's degree in energy engineering from the Alma Mater Studiorum-Università di Bologna, Bologna, Italy, in 2014, where he is currently pursuing the Ph.D. degree in industrial applications of plasmas.

Augusto Stancampiano was born in Italy in 1987. He received the master's degree in energy engineering from the Alma Mater Studiorum-Università di Bologna, Bologna, Italy, in 2012, where he is currently pursuing the Ph.D. degree in industrial applications of plasmas. His master's degree thesis was on the characterization of atmospheric cold plasma sources and their possible applications in the functionalization of polylactic acid films.

6.3 Paper III

Practical and theoretical considerations on the use of ICCD imaging for the characterization of non-equilibrium plasmas

DOI: 10.1088/0963-0252/24/6/064004

IOP Publishing Plasma Sources Science and Technology
Plasma Sources Sci. Technol. **24** (2015) 064004 (17pp) doi:10.1088/0963-0252/24/6/064004

Practical and theoretical considerations on the use of ICCD imaging for the characterization of non-equilibrium plasmas

Matteo Gherardi[1,2,4], Nevena Puač[3,4], Dragana Marić[3,4], Augusto Stancampiano[1,4], Gordana Malović[3], Vittorio Colombo[1,2] and Zoran Lj Petrović[3]

[1] Department of Industrial Engineering (D.I.N.), Alma Mater Studiorum-Università di Bologna, Via Saragozza 8, 40123 Bologna, Italy
[2] Industrial Research Centre for Advanced Mechanics and Materials (C.I.R.I.-M.A.M.), Alma Mater Studiorum-Università di Bologna, Via Saragozza 8, 40123 Bologna, Italy
[3] Institute of Physics, Unversity of Belgrade, Pregrevica 118, 11080 Belgrade, Serbia

E-mail: Vittorio.colombo@unibo.it and zoran@ipb.ac.rs

Received 3 July 2015, revised 10 September 2015
Accepted for publication 11 September 2015
Published 14 October 2015

Abstract

Over the past decade the use of ICCD cameras as a means for characterizing non-equilibrium plasmas has been steadily increasing. Due to their high sensitivity and high speed gateability, ICCD cameras enable time-resolved studies of the anatomy and, when adopted in conjunction with filters, monochromators, spectrometers or laser systems, time-resolved investigation of physical and chemical properties of non-equilibrium plasma discharges. This paper is meant as an introduction to ICCD technology and its use as a plasma diagnostic technique, discussing the experimental problems typically associated with its use and providing the readers with practical examples and suggestions on how to address them. In particular, the issues of ICCD camera synchronization with the voltage pulse driving the plasma discharge and of investigating small volume discharges are addressed, focusing mainly on the case of non-equilibrium atmospheric pressure plasma jets. Finally, a possible way to achieve absolute calibration of plasma discharge emission is presented and discussed. A wide range of data, mostly unpublished, is provided here to illustrate the points.

Keywords: ICCD imaging, best practices, non-equilibrium plasmas, plasma jets, spatial profiles of emission, temporal profiles of emission

(Some figures may appear in colour only in the online journal)

1. Introduction

A charge coupled device (CCD) is a semiconductor architecture whose operation is based on the movement of electrical charge through storage areas until the area where manipulation with the collected charge can be performed. The three basic functions of the device are: charge collection, charge transfer and conversion of collected charge into a measurable parameter (usually voltage). The initial concept of the operation of CCD device was given by Boyle and Smith [1]. When an image intensifier is mounted in front of the CCD this makes intensified charge coupled device (ICCD). An ICCD consists of photocathode, microchannel plate (MCP) and phosphor screen. The image intensifier can be connected to the CCD either by a fiberoptic bundle or a relay lens. The sensitivity of the ICCD camera is mainly determined by the photocathode responsivity. Nowadays, photocathodes of GenII (multialkali photocathode) and GenIII (GaAs photocathode) are used in most of the ICCD cameras. The main advantage of ICCD cameras, beside high sensitivity, is high speed gateability. Due to their construction, ICCD cameras can enable shutter times of the order of picoseconds.

The advancement from presenting drawings of the observations, taking photographs [2–4], scanning by a photomultiplier

[4] These authors contributed equally to this work.

(plus the slits and associated optics) [5], using a sensitive security camera (CCD) [6] (with procedure to grab frames and digitize them taken from the Bose Einstein condensation experiment [7]) to the fully developed ICCD, was not only gradual, but also necessary as new options opened with each step. In earlier times, temporal development was achieved by boxcar integrators combined with photomultipliers (PM) [5] with a number of limitations, one being that it did not allow the time-resolved recording of a 2D picture; a special technique allowing both temporal and spatial recording consisted of a system of a PM with slits and the time resolution achieved by triggering of detection as has been done in pulsed Time of Flight swarm experiments [8], with the limitation that this technique could be applied only to repetitive processes with a very small jitter.

In principle, ICCD can be compared to photomultipliers. While sensitivity of photomultipliers is normally greater, the speed and parallel storage of the entire image are essential features providing ICCDs with a distinct advantage in most applications. Moreover, ICCD allows generating animated sequences of still shots that can track most physical processes throughout their development; this feature has proved to be critical and has been exploited in numerous time-resolved studies of the anatomy of plasma discharges whereby one may detect whether the discharge is stable or oscillating or randomly changing position and shape [9–19].

In this paper we shall discuss several examples of the use of ICCD for detection of mainly atmospheric and high pressure non-equilibrium plasmas. Through those examples we shall try to illustrate some of the problems that have to be overcome in implementation of ICCD diagnostics.

Lately, plasma jets are becoming the main focus of several studies because of their wide range of applications, spanning from materials treatment [20–30] to sterilisation and plasma-assisted medical therapies [31–45] enabled by an ample versatility by virtue of the diverse possible combinations of driving power supply, gas employed, physic behind the formation and propagation of the discharge and source architecture [15, 46–52]. The need for fundamental understanding of the physics of plasma jets and of their complex interaction with various materials (e.g. biological materials, liquids, etc.), required for the optimisation of plasma jet assisted processes of practical use, has prompted the scientific community to thoroughly investigate these plasma discharges by means of a diversity of diagnostic techniques [50, 53–58].

ICCD cameras have been relied on extensively for the investigation of plasma jets and several characteristics of plasma jets have been discovered using this technology; as an example, plasma jets seen as a continuous plasma flow by the human eye were recently revealed, by means of fast imaging systems, to be often composed of the sequences of fast moving discrete luminous clusters also known either as pulsed atmospheric pressure streamers (PAPS) or the plasma 'bullets' [9, 59–62]. Moreover, other features of these moving ionization fronts or streamer fronts and the discharge as a whole have been detected by ICCD. Modern intensified charge coupled device cameras (ICCD cameras) with down to nanosecond expositions were adopted to record PAPS speeds of several kilometers per second or even higher by using freeze frame detection and careful triggering at numerous points during the phase between subsequent plasma formations (repeating voltage pulses or high frequency sinusoidal field); the speed is several orders of magnitude higher than the speed of the feed gas, usually helium or argon, and the same phenomenon is observed for various input voltage waveforms, polarities and electrode configurations [9, 59, 60, 63]. Introducing a transparent yet conductive material as the electrodes [9, 63] enabled scientists to follow the entire temporal and spatial development of the discharge; thus, what seemed like an uncorrelated emergence of the PAPS at the edge of the plasma jet glass tube actually is a continuous development all the way from the inception of the discharge at the inner edge of the instantaneous cathode. Importantly, the glow behind the ionization front is weak and ionization front inside the tube is much weaker than the glow observed once the PAPS leaves the glass tube while the speed of the front increases by a large amount. Experimental investigation by Puač *et al* of a helium plasma jet with transparent electrodes by using ICCD camera with Nikkor 50 mm lens showed two types of radial emission profiles [63]: when plasma travels through the electrode region the 'ring-shape' profile (*wall hugging* according to Kushner and coworkers [64]) is observed inside the tube, in the inter-electrode region the maximum of emission is observed along the axis of the tube and in the region of mixing of helium with the ambient air authors reported the highest emissions with formation of what appears to be a PAPS. Simulations by Naidis also confirm the existence of these two profiles [65]. It is obvious that the propagation of the plasma in contact with the dielectric surface and in the open space exhibits distinctive properties that can be exploited for biomedical applications [66].

All above mentioned features of the plasma jets at atmospheric pressure have been and could only be detected by ICCDs. Our ability to do so critically depends on the characteristics of the adopted ICCD cameras, among which the time resolution, that is required to match the speed of the observed phenomenon (e.g. propagation speed of PAPS), and the dynamic range, that has to be large enough to record the entire plasma discharge at once; this is especially relevant for the case of plasma jets, typically characterized by a brighter region (PAPS head) as well as a weaker continuous region behind the ionization front (see figures 1 and 2 [14]—where we display some of the features and examples of the PAPS detection by ICCD). In addition, it is important to have good triggering to correctly investigate the temporal evolution of the plasma discharge, arranging single shot recording in continuous animated movies or freeze frame developments; this also allows integration of the signal over several pulses to investigate weaker regions of the plasma.

Both of the main ICCDs characteristics (sensitivity, high speed gating) can be further exploited coupling these systems with filters [67–72] and monochromators or spectrometers [73–75]. In particular, the use of bandpass optical filters coupled with ICCD cameras can enable, in principle, to perform space-, time- and wavelength-resolved spectral analysis of plasma discharges. As an example, Sands *et al* [70]

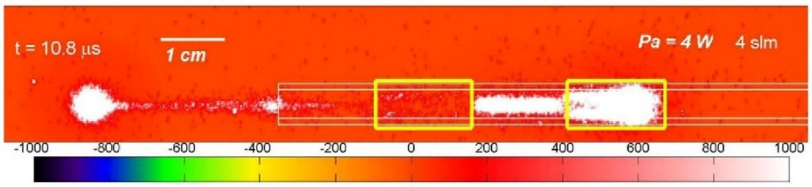

Figure 1. ICCD image of a PAPS. The image is overexposed in order to see the ionisation front (PAPS) and the continuous plasma tail behind. The PAPS is represented by the intense plasma 'ball' on the left hand side of the image. The scale (colorbar) is in arbitrary units. It is extended to negative values in order to get finer distribution of colors and clearer picture of the plasma tail. In the figure, the electrodes are marked by yellow rectangles. The powered electrode is closer to the end of the glass tube and the grounded one is further away. The glass tube is represented by white lines.

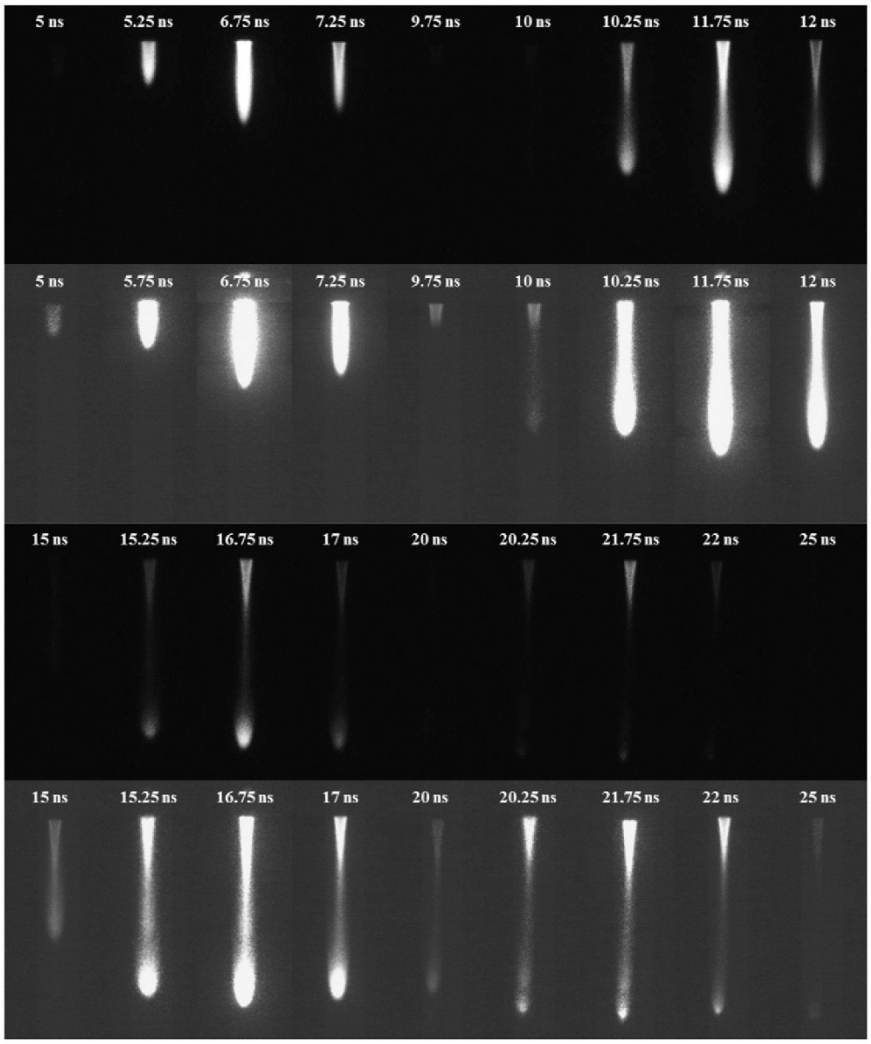

Figure 2. ICCD frames (3 ns exposure time, 50 accumulations, 0.25 ns of delay increase from one frame to the following) of a plasma jet driven by nanosecond pulses (17 kV, 1000 Hz, 2 slpm of He). Two different chromatic scales were adopted to make all the frames clearly visible (top: higher intensity scale, bottom: low intensity scale [14].

investigated the emission lines related to different excited species, such as Ar, He, N_2 and N^+, generated by an Ar/He plasma jet source filter, using filters transparent to specific wavelengths and acquiring images with very short gate times (5 ns); the wavelength filtered images revealed a not homogeneous structure of the PAPS and a plasma discharge characterized by an intense emission from Ar (750 nm) in the plasma ignition area between the two electrodes, while the ionization front appeared mainly related to excited He (389 nm) and N_2^+ (391 nm) emissions and the weakly ionized plasma channel that persists behind the propagating front to N_2 emission (337 nm). The same authors adopted a similar setup also to investigate a plasma jet with two crossed gas flows while impinging on an aluminum plate, this time focusing on the emission bands of excited N_2^+, CH, C_2, He and Ar to investigate the role of these species in the plasma discharge event [71]. Cha and colleagues [72] also reported on the use of a bandpass optical filter (330 nm $\pm$ 10 nm) to discern the N_2 ($C^3\ \Pi_u$–$B^3\Pi_g$) transition (337.1 nm) in a plasma jet used for plasma assisted combustion, while minimizing the interference from the chemiluminescence of the flame itself. It is also worth mentioning the work by Kong *et al* [76] where wavelength integrated and wavelength filtered ICCD images were compared to quantitatively evaluate the spatial uniformity of an array of seven plasma jets. Time-resolved spectral analysis of a plasma jet can also be performed coupling the ICCD with monochromators and/or spectrometers; as examples, this setup was adopted by Park *et al* [74] to acquire the optical emission spectrum of a jet propagating through an agarose gel channel and by Gucker *et al* [75] to investigate the spectra emitted by an rf plasma jet generated underwater. Furthermore, an innovative setup using two dispersion gratings and an ICCD camera was proposed by Xiong *et al* [77] to perform a time- and space-resolved analysis of the propagation in open air of the excited radicals produced in a plasma jet powered by sub-microsecond voltage pulses. It should be noticed that ICCD imaging may also add a new dimension of spatial and/or temporal resolution to laser [78–81] and x-ray induced fluorescence [82, 83] diagnostics; in this paper we have not covered topic as it is beyond the scope of the contribution and is beyond our expertise.

Finally, we would like to point out another very interesting application of ICCDs for the study of plasma jets proposed by Sobota and colleagues [84]; here an ICCD camera is used together with a BSO ($Bi_{12}SiO_{20}$) crystal and a 633 nm coherent light source to measure, through the Pockels technique, the electric field magnitude induced on a dielectric surface by an impinging plasma jet. In a recent work, Wu *et al* [85] also proposed a method relying on the use of an ICCD camera to detect the polarized radiation emitted by the interaction of two counter-propagating He plasma jets and esteem the produced electric field.

As a consequence of these features and their versatility, over the past decade ICCD cameras have become a standard tool in diagnostics of non-equilibrium discharges, especially at atmospheric pressure where small dimensions and fast developing phenomena can impede other diagnostic techniques. While fast imaging is valuable in revealing mechanisms of ignition and development of discharge, it is not always clear how to connect overall discharge behavior with elementary processes. As an example, in efforts to obtain elementary coefficients that may be employed in modeling and thereby explaining the pertinent physics of high pressure plasmas, one needs to perform quantitative comparisons, which are often best done by a simple (e.g. parallel plane) geometry and at low pressures. From the point of view of atmospheric pressure plasma diagnostics, it should be emphasized that ICCD technique was essential in studies of microdischarges—in interpretation of results and in exploring possibilities and limitations of applying the scaling laws to extend phenomenology and data on elementary processes from standard size discharges at low pressures to micrometer size discharges at high pressures. This technique has been used to establish a correct method to define scaling parameters in small dimensions [86] and to clarify some common misinterpretations of apparent failure of the Paschen law on the left hand side of the curve due to the long path breakdown [13]. Moreover, spatial profiles of emission from microdischarges were used to determine ionization coefficients [87], which were in good agreement with the standard data measured in standard size discharges [88], proving that low pressure measurements and scaling up to the atmospheric pressure may be the source of quantitative data of general importance. Finally, spatial profiles of emission acquired in low current diffuse Townsend discharge may yield some rates for elementary processes (ionization rate, drift velocity [87, 89]). The use of absolute calibration of spatial profiles provides an opportunity to obtain other coefficients and even some properties of surfaces. For example fast neutral excitation cross sections may be obtained from absolute emission close to the cathode, one may observe non-hydrodynamic (non-local) transport close to the cathode and one may normalize a number of inelastic processes of electrons in gases such as electronic and vibrational excitation [90, 91]. Those processes may be building blocks either as rates or as cross sections for plasma models and may be applied at all pressures having been confirmed at low pressures in well defined regimes and geometries.

Despite all the work done to date, the understanding of plasma jets physics and of the mechanisms of their interactions with target materials is still incomplete; for this reason, further investigations of these systems by using ICCD cameras, as well as other diagnostic techniques, is of the outmost importance. This paper is meant as an introduction to ICCD technology for the characterization of plasma jets and is mainly aimed at assisting novice users in approaching this diagnostic, providing the reader with practical examples and suggestions on how to address experimental problems and correctly setup the instrumentation; moreover, we hope the paper will stimulate the drive for standardization of the procedures adopted for ICCD diagnostics, facilitating the comparison between results coming from different groups using different plasma sources. The paper develops along three main topics, each associated to a specific problem that should be taken into account when adopting ICCDs as a diagnostic tool: synchronization of the camera with the voltage pulse driving the plasma discharge, the use of additional lenses with the camera to investigate

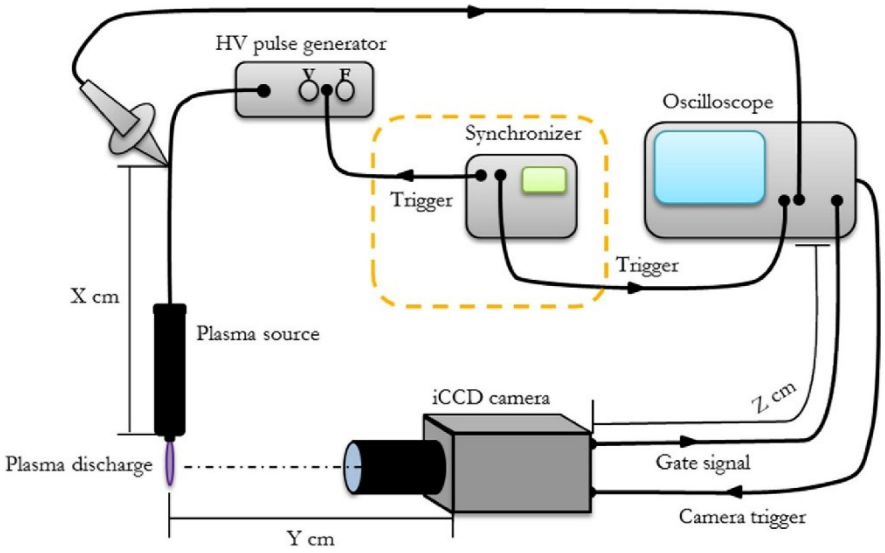

Figure 3. Experimental setup adopted for the ICCD imaging experiments reported in Paragraph 2. The delay generator (or synchronizer, circled in orange), which is used to synchronize the generator and the oscilloscope, was required only by the experiments with the nanopulse generator; for the tests with the micropulse generator this element was removed.

small volume discharges and the absolute calibration of the discharge emission. To highlight the best practices to be adopted when dealing with ICCD diagnostics, previously unpublished results will be presented together with a detailed description of the experimental setups for each of these topics.

2. Synchronization of the ICCD camera

We previously underlined the relevance of having good triggering to investigate the temporal evolution of plasma discharges; indeed, to achieve a properly time-resolved visualization of the discharge phenomenon it is extremely important that the gating of the camera sensor is correctly synchronised with the discharge event and, as a consequence, with the voltage pulse driving the plasma discharge. An important part for the correct gate setting is the evaluation of signal transmission delays, which include the delay related to cable transmission and the internal response time of instrumentations; these delays may greatly affect the accuracy of ICCD acquisitions, especially in the case of plasma jet sources excited by sub-microsecond pulses.

In the following parts of this paragraph, a series of best practices to realize a correct synchronization between the ICCD camera and the plasma discharge will be discussed; ICCD acquisitions of a plasma jet driven by microsecond pulses as well as nanosecond pulses will be presented and compared to show the effects of taking into account (best practice) or ignoring (bad practice) the signal delays for different excitation pulses.

2.1. Experimental setup

A schematic of the experimental setup adopted for the demonstration of the effects of considering or ignoring signal delays during ICCD imaging of a plasma jetis shown in figure 3. For the sake of clarity, we decided to adopt a setup as simple as possible, composed of only the essential elements (ICCD camera, plasma source, voltage probe, oscilloscope, pulse generator, synchronizer); in this way we hope to provide the reader with general guidelines and suggestions, easily transferable to more complex and specific configurations.

In this example the plasma discharge is produced by a single electrode plasma jet operated using He (99.999% pure) as working gas with a fixed flow rate of 3 slpm; an extended description of this plasma source can be found in [14, 30, 92]. The plasma source is here powered by two different high voltage generators; the first generator, in the following referred to as 'micropulse generator', is composed of a high voltage power amplifier (Trek model 30/20 A) connected to a function generator (Stanford Research model DS335, 3 MHz). This generator was used to produce a square waveform of 16 kV peak voltage (PV), 1000 Hz frequency (RF) and 80 μs rise time and pulse duration of 1 ms. The second power supply system is a commercial nanosecond pulser (FPG 20-1NMK, FID GmbH), in the following referred to as 'nanopulse generator', here used to produce a high voltage pulse of positive polarity with 17 kV PV, 500 Hz RF, 5 ns rise time and pulse duration of 35 ns.

Voltage waveforms were collected on the high voltage cable connecting the plasma source to the pulse generators with a high voltage passive probe (Tektronix P6015A) and registered by an oscilloscope (Tektronix DPO 40034, 350 MHz, 2.5 GSa s^{-1}). To investigate the plasma jet morphology and temporal evolution, an iCCD camera (Princeton Instruments PIMAX3, spectral response 180–900 nm) triggered by the same oscilloscope used to acquire the voltage waveform was adopted. During the tests with the nanopulse generator,

a delay generator (BNC 575 digital pulse/delay generator) was used to synchronize the generator and the oscilloscope, which in turn was used to trigger the ICCD camera. All TTL (Transistor-Transistor Logic) signals (from ICCD camera, oscilloscope and synchronizer) were transmitted by means of common coaxial cables with BNC connectors.

2.2. Estimate of signals delay for correct synchronisation

One of the key instruments to acquire temporally resolved images of the plasma discharge synchronized with the excitation waveform is the oscilloscope, which is used to monitor both the voltage waveform obtained by the high voltage probe and the gate signal generated by the ICCD camera. Since the gate signal is representative of the photocathode gating, thus of time interval during which the ICCD camera is acquiring frames, its accurate synchronization with the voltage waveform is required to perform a reliable time-resolved analysis of the plasma discharge. This can be achieved only if the delays between the aforementioned signals and their measurement and visualization on the oscilloscope are properly taken into account. In particular, for the excitation signal we should consider the cable delay from the high voltage electrode to the high voltage probe, the high voltage probe characteristic delay and the cable delay from the high voltage probe to the oscilloscope; on the other hand, for the case of the ICCD Gate signal we should take into account the delay related to light transmission from the plasma discharge to the ICCD sensor, the ICCD camera internal delay for gate signal generation and the cable delay from the ICCD camera output to the oscilloscope. A detailed description of each of these sources of delay is presented in the following paragraphs.

As a first step, a starting point (zero value, t_0) from which to calculate the delay of the two signals has to be defined; in the following, t_0 is taken as the instant when the high voltage excitation signal reaches the high voltage electrode where the ionization phenomenon takes place.

Considering first the delays on the side of the measurement of the excitation signal, we know that the excitation pulse will be recorded by the high voltage probe a certain time lapse before t_0, since the high voltage probe will be positioned at a certain distance from the high voltage electrode (X cm in figure 3). To estimate this delay, affected by the length of cable between the electrode and the voltage probe as well as by the cable characteristics, there are a few possibilities:

(a) referring to the delay characteristic (ns/m) provided by the cable supplier and calculating the effective delay over the cable length X;
(b) performing two acquisitions of the HV signal, with the probe positioned at two different distances from the HV electrode, and calculating the delay characteristic of the cable (ns/m) by measuring the delay between the two acquired signals. The delay is then calculated as before, multiplying the delay characteristic of the cable by the cable length X;
(c) measuring the real delay, by performing two acquisitions of the HV signal, one with the HV probe in the position that will be adopted during the diagnostic experiments (at a certain distance X from the HV electrode) and the other with the HV probe positioned on the position associated to t_0, which is the tip of the HV electrode in our case.

Among the three possibilities, the last should be preferred, but depending on the plasma source architecture the HV electrode could not be easily accessed; for the experiments described in this paragraph we relied on this method and measured a cable delay of 3.8 ns. Then, the characteristic delay of the high voltage probe has to be taken into account; for commercial probes, this data is typically reported in the datasheet and already comprises the delay associated to the cable delay from the high voltage probe to the oscilloscope. In the case of a Tektronix P6015A probe, which was used in our experiments, the supplier indicates an overall delay of 14.7 ns. Finally, to calculate the total delay for the excitation pulse reading, the cable delay from the HV electrode to the HV probe has to be subtracted from the characteristic delay of the probe. If the HV probe is positioned between the pulse generator and the source, the excitation signal is registered with a certain anticipation (equal to the cable delay time) with respect to the instant it reaches the HV electrode (previously defined as the starting point t_0), effectively reducing the total delay for the excitation pulse. Therefore, for the setup described in Paragraph 2.1 a total delay time on the side of the excitation pulse reading of 10.9 ns should be considered, introducing the corresponding adjustment in the channel of the oscilloscope dedicated to this measurement.

Similarly, the delays related to the gate signal of the ICCD camera can be estimated. Considering again as the starting point t_0 the instant when the HV excitation signal reaches the electrode, in this case the total delay, should take into account the delay related to light transmission from the plasma discharge to the ICCD sensor, the ICCD camera internal delay for gate signal generation and the cable delay from the ICCD camera output to the oscilloscope. On the contrary, the time interval between the instant t_0 and the instant when the plasma starts emitting is the result of the ionization avalanche and should not be compensated for the correct interpretation of the discharge event. Starting with the delay associated to the time required for the light signal to reach the camera sensor, its estimate can be done dividing the distance between the discharge region and the camera sensor (Y cm in figure 3) by the speed of light in the medium filling the gap (~299 700 km s^{-1} for ambient air); for a distance of $Y = 76$ cm, which we adopted in our experiments, the delay is 2.5 ns. The ICCD internal delay is associated to the delay between the actual intensifier photocathode gating and the generation of a corresponding electrical signal, which is the one transmitted to the oscilloscope for synchronization purposes; this delay is typically reported in the datasheet of the ICCD camera and for the case of a PIMAX3 is 5 ns. Finally, the delay associated with the transmission of the ICCD camera signal to the oscilloscope along a coaxial cable of a certain length (Z cm in figure 3) has to be evaluated, relying on the delay characteristic (ns/m) either provided by the cable supplier or measured in laboratory. In our case, for a coaxial cable of length $Z = 365$ cm the

measured delay was 18 ns. In conclusion, these delays have to be summed up to determine the total delay on the side of the ICCD gate signal, which for our setup resulted in a 25.5 ns delay to be introduced as an adjustment in the channel of the oscilloscope dedicated to this measurement.

2.3. Results for ICCD acquisitions considering or neglecting signals delay

Following the procedure described in the previous paragraph for setting the proper adjustments on the oscilloscope in order to compensate the delays, the voltage waveform and camera gate signal should be properly synchronized allowing the correct acquisition of time-resolved pictured and the proper interpretation of results; on the other hand, either failing to properly estimate the delays or neglecting the issue can lead to the misinterpretation of results due to incorrect synchronization. The higher the difference between the total delay on the side of the excitation pulse reading and the total delay on the side of the ICCD gate signal (14.6 ns in our setup) the greater can be the negative effect of neglecting or miscalculating the delays.

In order to clarify the issue, ICCD images obtained with the setup presented in figure 3 and adopting the 'best practice', thus taking delays into account and applying the appropriate adjustments to achieve good synchronization, or the 'bad practice', thus failing to take into account the aforementioned delays, are reported and compared in figure 4. In the experiments, different excitation pulses (microsecond and nanosecond pulses, as described earlier in Paragraph 2.1) and gate width were used to highlight the cases when the use of 'best practices' is mandatory for a correct time-resolved analysis of the plasma discharge. For each case, the acquired ICCD image and the corresponding voltage waveform, with over imposed gate signal (real or supposed, in the case of delays not considered), are reported in figure 4.

Results for the ICCD imaging of the plasma jet powered by the micropulsed generator are presented in the first two rows of figure 4; two different camera gates were chosen to visualize either one entire voltage pulse (gate 1 ms) or only the positive voltage rise (gate 80 μs). No accumulations were performed and each acquisition was repeated 30 times in order to verify the reproducibility of the phenomenon. As it is possible to observe, in both cases no significant difference can be observed between 'best practice' and 'bad practice' acquisitions, since the signal delay difference (14.6 ns) is at least three orders of magnitude smaller than the gate width.

On the contrary, when the plasma source is powered by a nanopulsed generator, the shorter pulses require the use of shorter camera gates, of the same order of magnitude of signal delay difference, and therefore a proper synchronization is required. In the third row of figure 4, 'best practice' and 'bad practice' acquisitions are reported for the camera gate set to extend over an entire voltage pulse (35 ns); even if the two plasma discharges are very similar. In the case of the 'bad practice' the plasma discharge is shorter and its emission intensity is slightly lower. The reported images are the result of 30 accumulations and the experiment has been repeated several times, therefore the reduction in the discharge length is unlikely to be due to random fluctuation in the electrical or fluid dynamic parameters, but has to be appointed to the incorrect synchronization between the gate timing and the excitation pulse. Indeed, in the 'bad practice' case the real camera gate (blue rectangle in figure 4) is shifted 14.6 ns earlier than the supposed camera gate (red rectangle in figure 4) and as a consequence the light emission related to the second half of the HV pulse was not recorded in this acquisition and is the reason of the observed differences.

This issue is even more pronounced when the gate width is further reduced to investigate the temporal evolution of the plasma jet during the HV pulse. In the last row of figure 4 a sequence of ICCD acquisitions (camera gate 10 ns and 30 accumulations) is shown, together with the recorded voltage waveforms with the camera gates super imposed; the ICCD gate opening for the first frame of each scan was set at t_0 and subsequent frames were recorded at fixed time steps (delays) of 10 ns. In the best practice case, the iCCD acquisitions show the formation of the plasma plume in the first 10 ns of the HV pulse, its increase in length along the entire voltage pulse duration and a maximum emission intensity in correspondence of the voltage peak; these results are in good agreement with other previously obtained for the same plasma source in similar operating conditions, but analysed with a different setup [14]. Instead, in the 'bad practice' case no light emission is observed in the first frame (first 10 ns of the HV pulse) and only a faint plasma discharge is discernible in the second one; considering the supposed camera gates (red rectangles in figure 4), these misleading results would suggest that the plasma is not generated during the entire HV rising front and that the highest emission intensity is not reached in correspondence of the HV peak. Indeed, if the real camera gates (blue rectangles in figure 4) are considered, it can be observed that the gate corresponding to the first frame is entirely located before the HV pulse and that the gate corresponding to the second frame overlaps only partially with the HV pulse, and this is in agreement with the corresponding ICCD images of the plasma discharge. In conclusion, failing to account for signal delays may lead to an unrealistic interpretation of the investigated phenomenon for the case of nanosecond pulsed excitation; this because the time scale of the signal delays and the camera gates usually adopted for these experiments are of the same order of magnitude (tens of nanoseconds).

Finally, the case of picosecond pulse excitation is worth mentioning: since here the duration of the investigated phenomenon is even shorter than the typical signal delays. Without proper synchronization the emission visualization may be impossible. A good example of plasma discharge visualization on a sub-nanosecond time scale is described in the work of Starikovskiy *et al* [93].

3. Using ICCD cameras with small volume discharges

Among the first non-equilibrium atmospheric pressure plasma sources investigated for biomedical applications, the plasma

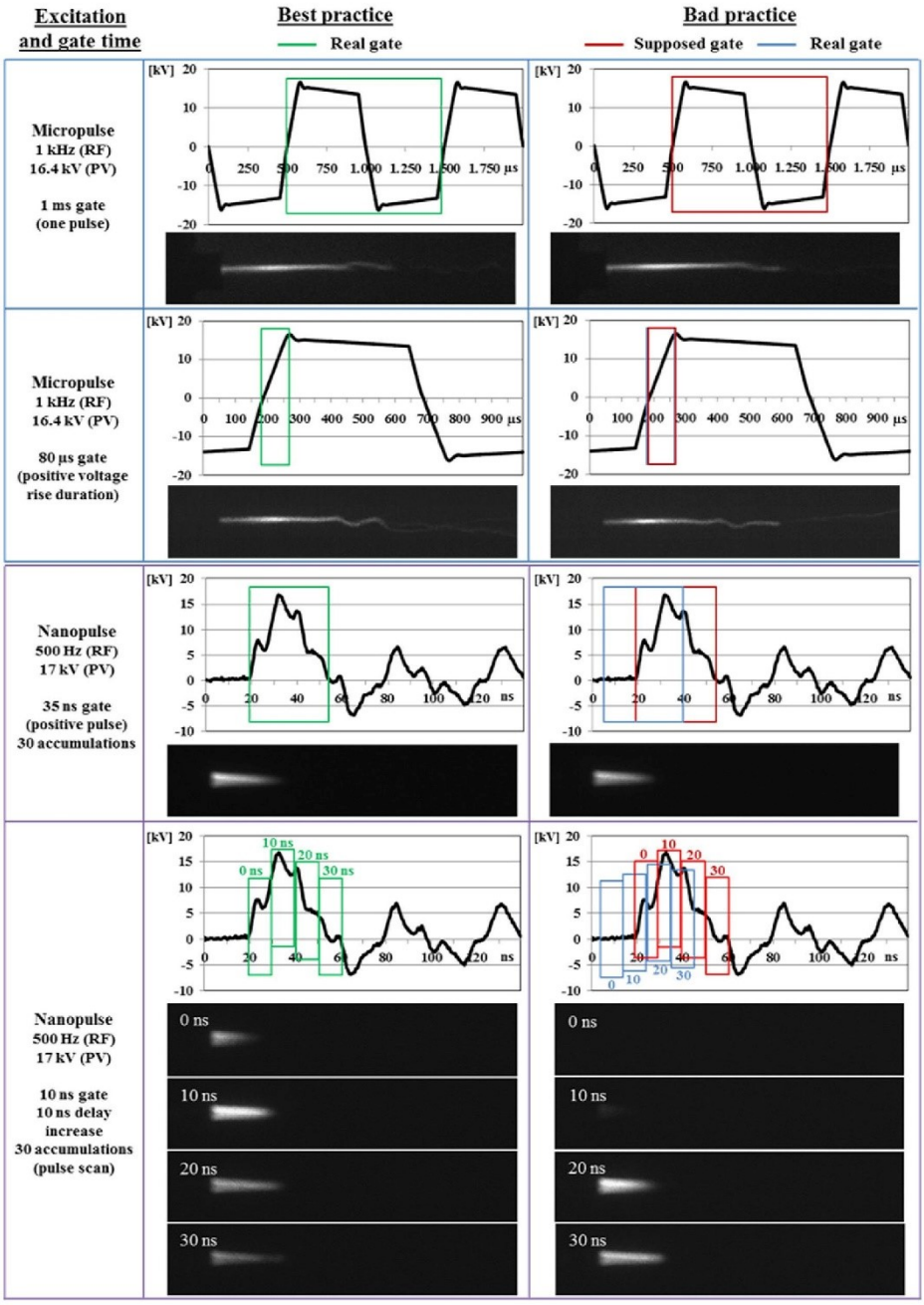

Figure 4. ICCD acquisition and voltage waveform for the plasma jet operated with micropulsed and nanopulsed generators. For each operating condition two different gate times were adopted and results obtained compensating signal delays ('Best practice') are compared with those obtained without delay compensation ('Bad practice'). Recorded ICCD gate are superimposed on the voltage waveform with green ('Best practice') and red ('Bad practice') rectangles. For the bad practice case, the real position (artificially compensating the delays) of the gates is shown in blue rectangles.

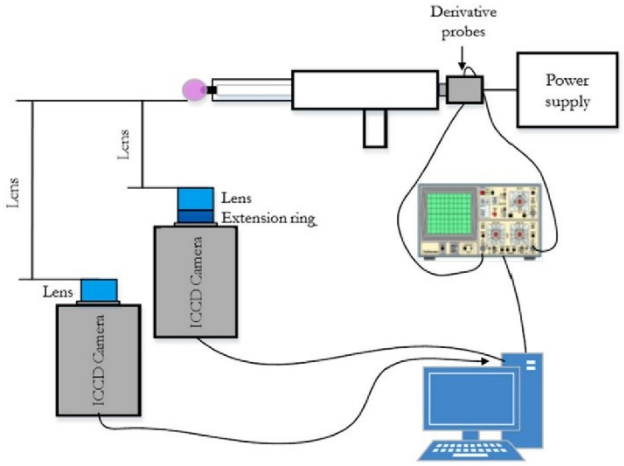

Figure 5. Schematic of experimental set-up. Introducing of the extension ring PN-11 before the Nikkor 105 mm f/2.8D lens reduced the focusing distance by half. Without the extension ring the focusing distance was $y = 0.41$ m and after adding the ring it was reduced to $x = 0.205$ m.

needle, originally described by [47], is a single-electrode plasma jet [46] characterized by a very small plasma discharge, whose dimension poses significant challenges to imaging diagnostics such as ICCD. In this paragraph we will discuss how to perform ICCD imaging of a small volume discharge, presenting results for a self-developed plasma needle, to some extent similar (but not identical) to the plasma needle introduced in [47]. Our plasma needle, described in greater detail in [94] is powered at 13.56 MHz and operated in a mixture of air and He. He flow rate was 100 sccm and was kept constant during all experiments with plasma needle. This flow rate is much smaller than the flow rates used in plasma jet devices having similar electrode geometry (wire as the central powered electrode) but operating at lower frequencies. The fact that our plasma needle device operates in MHz range enables to use smaller flows of the working gas (He). Also, with the electrical circuit constructed and tuned correctly, higher voltages can be obtained without the need for high power supply units and, therefore, plasma can be produced. The produced plasma discharge is non-aggressive, local, with small penetration depth and, at the same time, produces chemically active species at a low gas temperature; so far, we have used it very successfully in various treatments like sterilization of bacteria in form of suspensions and biofilms, treatment of plant calli, hPB-MSCstem cells, teeth surface, etc [95–98].

Due to the fact that this discharge is very small in volume (~mm^3) it is quite difficult to perform diagnostics by using ICCD camera without using of additional camera lenses and rings that will increase the resolution of the image. Here we have employed the ICCD camera Andor iStar DH720-18U-0. The camera has $18 \times 6.7\,mm^2$ active area that consists of 690×256 pixels. Minimum optical gate width is 2 ns. The minimum optical gate width is characteristics of the ICCD camera and is given by the manufacturer. In case of Fast ICCD cameras the minimum gate widths are in range of few ns and they enable the time resolved measurements with the discharges that operate in MHz range. When doing such a measurements one should take care about the jitter of the camera, i.e. how much the 'window' during which the camera is collecting signal is shifted with respect to the desired acquisition instant. In our case the camera jitter did not influence the results due to the long exposure time that was used. Images were obtained in integrated mode for exposure time of 5 ms. The spectral range of the photocathode is 180–850 nm. This range was limited to the visible part of emission spectra due to the fact that we had to use a camera lens made of standard optical glass. In addition to the camera lens (Nikkor 105 mm f/2.8D) we have used an additional extension ring (Nikon PN-11). The schematics of experimental set-up are given in figure 5. The extension ring Nikon PN-11 is the longest extension in singular use. An extension ring is an attachment that goes between camera body and the lens. Since this is not an optical element there is no lens inside the ring. Its main purpose is to get the lens further away from the focal plane. The practical point of this is that the minimum focusing distance gets smaller. Therefore with an extension ring you can get closer to the discharge i.e. reduce the focusing distance and increase the size of the obtained discharge image while still achieving excellent focus. This was necessary because dimensions of the discharge were of the order of few cubic millimeters and we wanted to obtain a larger image i.e. to have more pixels over the area of the discharge. The camera was positioned orthogonally to the needle tip so that we could record side-on images of the plasma.

Furthermore, we used two self-developed derivative probes [94, 99] to monitor the instantaneous voltage and current signals i.e. for obtaining power transmitted to the plasma, which can be used as a control parameter.

ICCD and U-I diagnostics were performed with a flat dielectric surface placed against the tip of the needle as a target. The needle was not additionally grounded. The plasma needle device was not additionally grounded. This is usually done

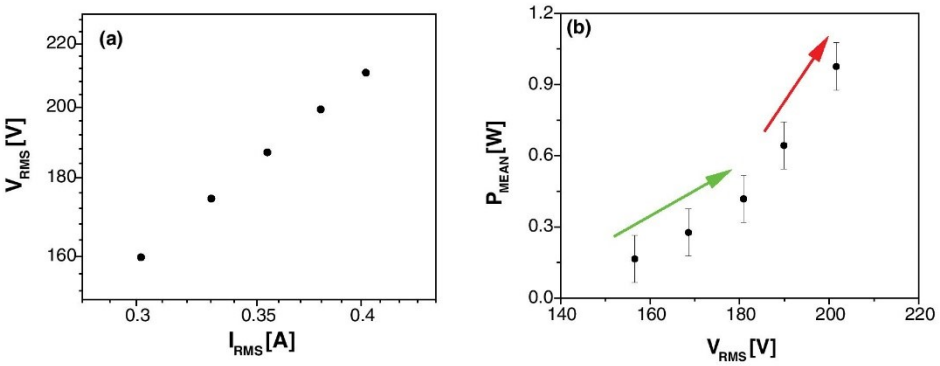

Figure 6. (a) V_{RMS}–I_{RMS} characteristic of the plasma needle discharge. (b) Mean power transmitted to the discharge. He flow rate was kept constant at 100 sccm. The distance between the plasma needle tip and the target was 1 mm. The green and red lines are given in the figure only to emphasize the voltages associated with the change in the plasma mode.

[46] by wrapping a copper ring around the glass tube and grounding it separately, thus providing a more stable field configuration and the flow of current. Distance between the tip of the plasma needle and the target was 1 mm.

3.1. OES and electrical measurements of plasma needle discharge

The instantaneous current and voltage signals were transferred from time to frequency domain (FFT—Fast Fourier Transform), changed according to the calibration curves and then transferred back to time domain (IFFT—Inverse Fast Fourier Transform) [99]. With this procedure we were able to calculate the instantaneous power, mean power transmitted to the plasma and voltage-current characteristics of the discharge.

In figure 6 V_{RMS}–I_{RMS} characteristic in this experiment is shown. RMS voltage and current values lie in the ranges of 160–220 V and 0.3–0.42 A, respectively. Values for the mean power lie in the range of 0.1–1 W (see figure 6(b)) and were suitable for plasma needle treatment of plant cells [94] and even living animal and human tissues, as no appreciable heating of the gas and substrate has been recorded. We can see that there is an increase in mean power with an increase of applied voltage. When the applied voltage is higher than 180 V the slope of the power versus voltage curve increases more rapidly and this can be seen in the change of the plasma behaviour. When the voltage is higher than 180 V, the plasma starts to spread towards the target. For power above 0.6 W, the plasma is covering the surface of the target and the mode changes from unipolar to bipolar. For easier recognition of the above mentioned processes, green and red arrowed lines are added to figure 6(b). The green one follows the increase of the power in the range where plasma is in unipolar mode and is shaped as a small ball positioned only one the tip of the needle. The red arrowed line follows the increase in power range where the plasma spreads towards the target and changes from unipolar to bipolar mode. If we take a look at the V-I characteristics the change in plasma behaviour is not that obvious. Only a small reduction in impedance can be observed.

On the other hand, with an ICCD camera the details of the discharge transition can be studied in much greater detail. ICCD camera was positioned side-on and we took single shots with the camera gate width set to 5 ms (i.e. averaged over many RF cycles). Before and after every set of measurements we took one single shot of the system while the discharge was off to check if the distance between the tip of the needle and dielectric target stayed unchanged during the measurements. For all measurements, background light (plasma not ignited) was subtracted from the total emission.

Emission intensities obtained while increasing power are shown in figure 7. We can see that with an increase of power, the volume of the discharge and the intensity of light emission increase. For lower powers, plasma was working in a unipolar mode, i.e. discharge was concentrated at the tip of the needle without expanding to target's surface (see figure 7). The plasma is formed on the tip of the needle in form of a 'ball- (sphere)' that surrounds the tip and spreads a little bit along the powered electrode. This spreading of the plasma is more pronounced with the increase of power transmitted to the plasma. It can be seen that the wire that we were using in the experiments was not completely flat at the tip and as a consequence plasma is slightly deformed. This unipolar mode corresponds to the 'corona' mode observed by Sakiyama and Graves [100]. In this mode discharge is concentrated at the tip of the needle and it does not reach the target's surface. In this case the surrounding air acts as the grounded electrode.

For the highest power given by RF power supply, the discharge abruptly spreads towards the dielectric surface that acts as a target. At this power, transition from 'unipolar' mode to what we call a 'bipolar' mode occurrs. One can see that in this (bipolar) mode a sheath is formed at the target's surface. This type of mode transition was also observed by Stoffels and co-workers and confirmed by simulations done by Sakiyama and Graves [100–102]. In these papers authors refer to mode transition as transitions from the corona mode (plasma is contained at the tip of the needle) to the glow mode (plasma spreads itself over the target's surface). In glow mode in addition to the intense ionisation in the vicinity of the needle, another ionization zone appears near the dielectric surface

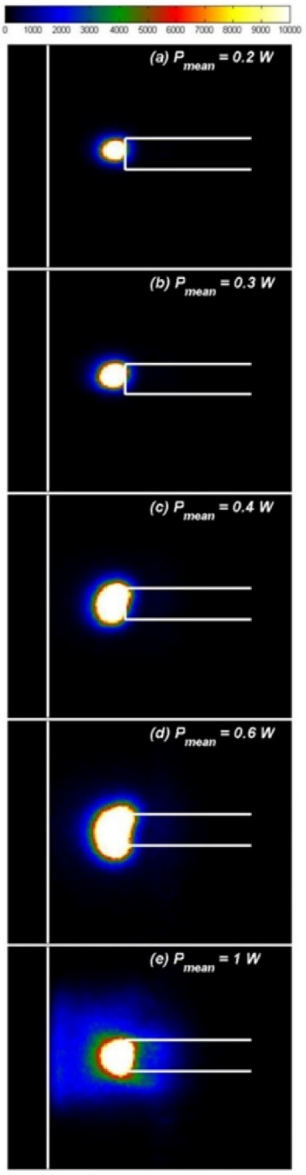

Figure 7. Emission intensities emitted from the discharge for different RMS voltages. Distance between tip of the needle and the target was 1 mm and He flow rate was 100 sccm. The saturation of the central part of the plasma is intentional as it allows us to observe the extension of plasma and the sheath.

(see figure 7(e)). Newly formed ionization zone spreads radially over the surface of the target.

If we look at figure 7 we can see that the discharge is not perfectly symmetrical around the needle tip. This displacement from the centre of the powered electrode can be explained by the fact that the wire that acts as the powered electrode is not perfectly flat. Also, discharge itself does not sustain a round shape at the tip of the needle, but with the power increase it changes its shape along vertical axis figures 7(c) and (d).

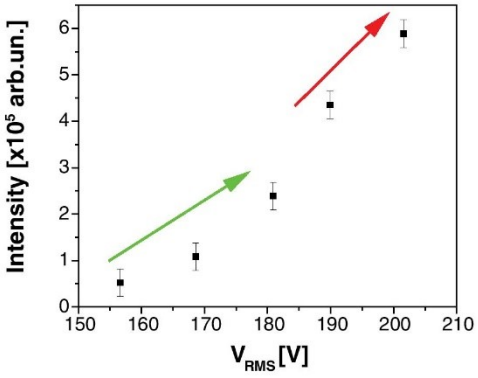

Figure 8. Integral emission intensity as function of root-mean-square voltage.

Integral emission intensity from the discharge as a function of the voltage (root-mean-square value) is shown in figure 8. We can see that the integral emission intensities increase with the applied voltage (i.e. transmitted power). The change from the unipolar to bipolar mode is clearly seen in the images taken by ICCD camera, represented in figure 7, and the same can be followed in figure 8. For lower powers the plasma is concentrated at the tip of the needle and spreads along the tip. Only when the transmitted power is 0.4 W the plasma covers the whole surface of the tip. In figure 8 (as well as 6(b)) this power range is highlighted by the green arrow. With an increase in the transmitted power (see figure 7(d)) plasma starts to spread towards the target. When reaching 1 W plasma is in bipolar mode and covers the surface of the target with the highest emission intensity still coming from the plasma covering the tip of the needle. This range of powers is represented in the figure 8 by the red arrowed line. The change in the regime of plasma operation is observed very weakly in the electrical diagnostics of the plasma, even weakly in the integral emission but is clearly shown in the ICCD images thus showing the importance and power of studying the anatomy of discharges as an indication of their operation.

For a better clarity of the mode transition horizontal and vertical profiles for RMS voltages are shown in figures 9 and 10, respectively. Profiles were obtained by summing image data in columns (horizontal profile) and rows (vertical profile). If we look at the horizontal profiles obtained from the images of the discharge (see figure 9) we can see both of the plasma needle modes.

For lower powers, the discharge is in corona mode, which means that it is localized at the tip of the needle. When the power is increased above 0.6 W (above 190 V) the discharge spreads itself towards the dielectric target. At the power of 1 W ($V_{RMS} = 200$ V), an observable sheath is created at the target (glow discharge mode-like). We can see in figure 9 that for 1 W emission intensity of the discharge increases 2 times in the area surrounding the tip of the needle compared to the

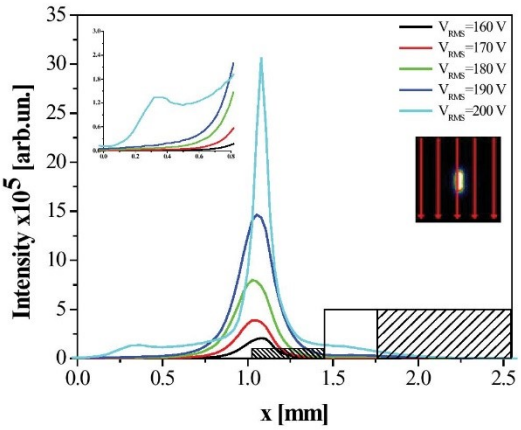

Figure 9. Horizontal profiles for different powers given by RF power supply. Integral intensities are obtained as a sum of the intensities along vertical axes of the discharge (see small image inserted in the graph).

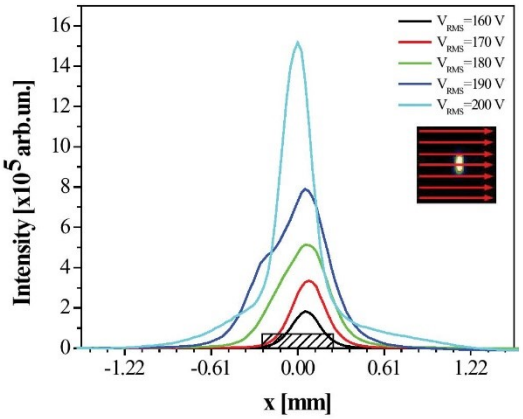

Figure 10. Vertical profiles for different powers given by RF power supply. Integral intensities are obtained as a sum of the intensities along horizontal axes (see small image inserted in the graph).

emission intensity for 0.6 W. In figure 9 the smaller graph represents enlarged area near the dielectric target. Sheath is observed through a significant increase in the emission near the dielectric surface. The emission intensity in this second ionization zone is about 10% of the intensity surrounding the tip of the needle. This value was obtained by integrating emission profiles in the area near target and around tip of the needle. Peak of emission is slightly shifted off the central axis due to the asymmetry of the tip (see figure 10). The discharge and therefore the profiles are shifted to one side (in this case—the right hand side). As mentioned before, this is probably due to the fact that the tip of the needle is not perfectly flat.

4. Diagnostics of low pressure discharges, scaling from low to high pressures, elementary processes and absolute calibration of discharge emission

ICCD was shown to be extremely useful for studies of the dc (and pulsed dc) breakdown and discharges at low pressures. The first advantage of ICCDs in the analysis of dc discharges is the short temporal gating that allows freeze frame recording of very fast processes, even on the time scales of few ns. Temporal development of the breakdown to investigate the avalanche, current growth, low current oscillations and transition between the modes were followed in [10, 103]. The second major advantage provided by ICCD is that through instantaneous recording of a 2D frame one may observe inhomogeneous behaviour and even more complex geometries [104, 105]. The use of transparent electrodes allowed studies of constrictions and radial profiles in general [6, 106, 107], thus enabling determination of the true current density [108] and testing of the scaling due to space charge effects [13, 109]. Apart from the time resolved tracking of the 2D discharge structure, low pressure studies of breakdown in simple geometries provide information on elementary processes and on transport of charged particles [87, 89]. For example, axial profiles of emission showed establishment of the non-local region close to the cathode where either no excitation exists or Franck Hertz like luminous (Holst Oosterhuis) layers exist in the development of the equilibration of the distribution function. The correction due to equilibration distance makes a large effect on the analysis of the Paschen curves and the resulting secondary yields [90]. At the same time equilibrium exponential growth of emission allows determination of the ionization coefficients [90, 110]. All of these can only be established by using spatial emission profiles i.e. ICCD.

Disadvantage of the ICCD technique is that the CCD detector does not measure an absolute emission, i.e. it does not give absolute data on excitation processes. As a consequence, it is difficult to relate recorded structure of the plasmas to the processes of electronic and vibrational excitation. The aim of this section is to address the two key issues in using the ICCD technique in diagnostic of atmospheric pressure discharges: how to extend the knowledge and results of the ICCD diagnostics, well established in low pressure discharges, to the atmospheric pressure plasmas in various geometries; and how to overcome a lack of information on absolute emission in measured signal.

4.1. Scaling from low to high pressures

Spatial profiles in low pressure regime and their agreement with the micro discharges [87] in principle produce data that are universally applicable and may even pose a possibility of a simpler absolute calibration of emission from atmospheric pressure plasmas in order to perform quantitative comparisons with models. Use of ICCD and a possibility to normalize the emission profiles are a key facility in that respect. In addition to scaling up to the atmospheric pressure, absolute emission

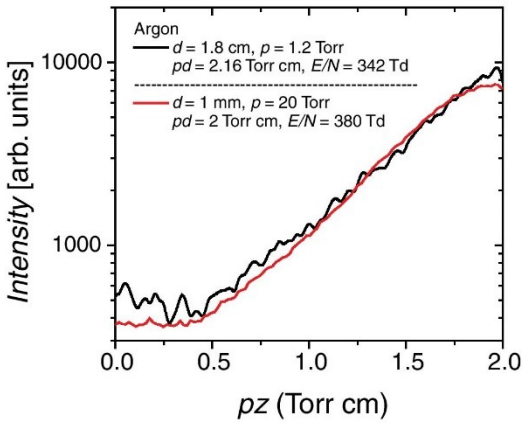

Figure 11. Comparison of axial profiles of emission from Townsend discharge, in millimeter size (data from figure 3 in [87] and centimeter size geometries. Emission intensities are acquired by an ICCD camera at similar *pd*. Measurements with exactly the same *pd* were not available, but the values are close enough for comparison. Distance from the cathode (z) is multiplied with pressure (p) to enable comparisons of emission profiles recorded at different electrode gaps.

comparisons may prove to be the source of quantitative data on rates and surface processes that are applicable universally.

As stated in the introduction, ICCD has been used to establish scaling to small dimensions [86] (high pressures) and to clarify the shape of the Paschen curve [13]. Emission profiles from standard size and microdischarges were used to obtain quantitative data for ionization coefficients [87, 88], which may be used generally under all conditions when locality of the electric field and reduced electric field (*E/N*: *E*—electric field, *N*—the gas number density) is valid.

As long as the standard *pd* (*p*—pressure; *d*—electrode gap) and j/p^2 (*j*—discharge current density) scaling laws are valid and relative emission intensities maintained, absolute calibration done at low pressures can be extended to smaller dimensions and higher pressures [86, 87]. Under the conditions where the discharge dimensions are within the order of magnitude of electron mean free path, it is critical to properly define scaling parameters, as it was shown in [13, 86]. Figure 11 illustrates that distribution of emission intensity remains the same in discharges at the same *pd*, with an order of magnitude difference in size (pressure). It should be noted here that emission intensity is the most sensitive property of discharge for comparison. Still, one has to be aware of limitations: processes, such as stepwise ionization, photoionization and three body collisions violate scaling. At very small electrode distances (<10 μm) even field emission can occur, which leads to drastic breakdown of scaling in the left-hand branch of Paschen curve [86].

4.2. A possible way to achieve absolute calibration of discharge emission

While emission intensity acquired by the ICCD camera can be put on a relative scale, it does not give direct information on absolute emission. Generally, systems with photomultipliers and precise optics that include slits defining accurately the solid angles may be calibrated using black body standards of emission [111]. Once signal (S_a) is measured, quantum efficiency ($Q(\lambda)$) and geometry factor (G) determined independently, the absolute emission coefficient (ε/N)can be produced as follows:

$$\frac{\varepsilon}{N} = \frac{S_a}{i}\frac{e}{Q(\lambda)G\Delta xN}\frac{A_j}{A_{ji}}\left[1+\frac{N}{A_j}k_q\right].$$

Here A_j and A_{ij} are Einstein's transition probabilities summed for the upper level and for a single transition respectively; N is the gas number density and i is the current (which at the anode is carried by electrons only). The term in brackets is due to quenching of excited states by collisions by the background gas (or impurities)—the so called Stern Volmer kinetics. Shortage of data for k_q is the principal limitation, but it may be bypassed by measurements at the same E/N and different pressures which is only possible in the non-selfsustained regime. Data for the quenching coefficient exist for most transitions of the basic gases such as Ar, N_2, H_2 even H_2O but are needed for higher excited levels and for gases such as CF_4, and other fluorocarbons, or more complex molecules.

Excitation coefficient is an integral of the electron energy distribution function and the excitation cross section as such can be predicted in calculations, thus allowing quantitative comparison between experiments and models. Using absolutely calibrated emission profiles would allow comparisons with numerical predictions at a much deeper and significant level. Absolute calibration may also be achieved by normalizing the measured data to the calculated excitation coefficient in the low current limit where one is assured that conditions for a steady state Townsend discharge are valid and thus transport and excitation kinetics are represented exactly (limited only by the accuracy of the available cross sections).

Absolute calibration of ICCD is not impossible, but is more difficult due to uncertainties in the depth of field and focus. In principle one could calibrate the ICCD by using the same setup as for photomultipliers and scanning it across the area of the detector, but defining the solid angle and integration volume would be more difficult in application to the plasma (unless collimators are being used). Thus, apart from giving a brief statement of how elementary processes may be obtained by using space time development of plasma, we shall discuss how absolute calibration may be achieved more easily by normalizing the profiles in the Townsend regime discharges first at low pressures and then by extrapolating to higher pressures using micro discharges. The normalization will then be valid for higher current discharges in different regimes provided that the relative sensitivity of the ICCD is maintained and recorded.

The procedure of normalization of the spatial emission profiles by using calculated excitation coefficients to produce absolute emission has been developed by Phelps many years ago for the system that used scanning photomultiplier and interference filters [112]. In principle, the procedure is the same for emission profiles recorded by ICCD camera. Typical characteristic of the Townsend regime of discharge is the

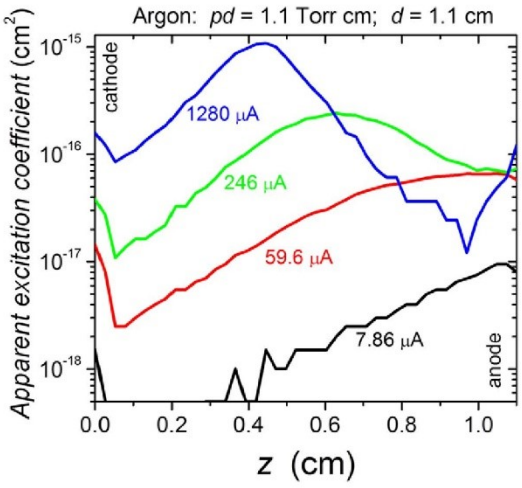

Figure 12. Axial emission profiles of a dc discharge in Argon with 1.1 cm gap [90]. The data have been normalized at the lowest current to the excitation coefficient of one of $2p_1$ level of Ar [114, 115] at the anode. Peaks at the cathode are due to the scattered light.

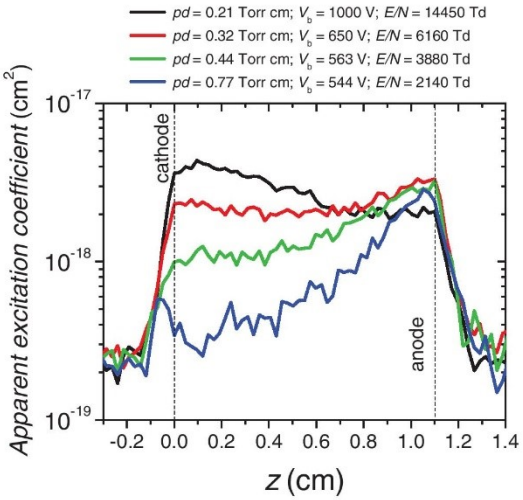

Figure 13. Axial profiles of Hα emission in Townsend regime in H_2O [120]—preliminary data. Results were normalized at the anode peak at 2140 Td based on MC calculation from standard available cross sections.

exponential growth of emission from the cathode to the anode at relatively low reduced electric fields (E/N). The emission signal is extrapolated to the anode, where it is assumed that total current is equal to the electron current. The anode signal is then normalized to the excitation coefficient for the particular transition, that can be obtained from the Boltzmann or Monte Carlo calculation (or from experimental measurements, if available). At the same time higher current emission profiles may be renormalized by the same scaling factor if relative intensities are well maintained. This has been done for profiles obtained in Ar by ICCD [90] as seen in figure 12. Practically, normalization of the profile in Townsend regime also puts all the distributions for other regimes on the absolute scale. In [109, 113], comparisons have been made between a series of measurements for a dc discharge and calculations based on a hybrid model. The relative profiles have been normalized to the calculated absolute profiles only for one spatial position and one current. All profiles, for four very distinct regimes of operation (Townsend low current diffuse regime ~8 μA; subnormal glow ~60 μA, normal glow ~250 μA and abnormal glow ~1.3 mA), came immediately to an excellent agreement based on the same scaling factor. This proves that relative magnitudes may be maintained very well in experiments using ICCD and also that there is a great value in quantitative comparisons between models and measurements.

The technique of normalization to calculate excitation coefficients has been used by Phelps to unfold a number of cross sections for electrons and even for fast neutrals in a wide range of gases [116–118]. In figure 13 we show measurements performed in water vapour [119] in the Townsend (low current diffuse) regime. We use an example of gas (H_2O) that attracts increasing attention due to a pressing need for elementary data for development and optimization of possible applications of atmospheric pressure plasmas. Measurements were done only at low currents in Townsend regime at different E/N from moderately high to the very high values. One can see that increasing E/N (as observed elsewhere for other gases) results in increasing cathode peak that has been shown to be due to fast neutrals (mainly fast H in hydrogen containing molecules). The peak due to the fast neutrals may be unrelated to electron excitation, but it is normalized by the same factor even when the electron induced peak close to the anode cannot be observed. Normalization was based on calculated excitation rate at the lowest E/N (standard cross sections were used) [120]. As this is a work in progress and provided here as an example of the technique we will not further discuss the details of calculations and magnitude of the results, just the opportunity provided by normalization of the spatial emission profiles provided by ICCD. In any case, as shown in figure 13, ICCD provides a unique opportunity to reveal the fast neutral excitation especially having in mind that fast neutrals have a large role in plasma etching (charging free plasma etching) and presumably similar effects on the living cells and biomaterials.

5. Conclusions

ICCD cameras, thanks to their high sensitivity and high speed gateability, are an extremely important tool to support the studies on non-equilibrium plasmas, enabling time-resolved analysis of their anatomy as well as of their physical and chemical characteristics. In this paper, properties and architecture of ICCD cameras is briefly discussed and an overview of relevant scientific publications adopting this technology for the characterization of non-equilibrium plasmas. We focus in particular on plasma jets. Moreover, practical examples and suggestions on how to address the experimental problems

typically encountered when using ICCD technology to characterize non-equilibrium plasmas at atmospheric pressure are given.

First, the problem of achieving a correct synchronization of the camera with the voltage pulse driving the plasma discharge is presented and the importance of accounting for signal transmission delays, including the delays related to cable transmission and the internal response time of instrumentations, is discussed; results of an experimental test case using a single electrode He plasma jet driven by microsecond pulses as well as nanosecond pulses taking into account (best practice) or ignoring (bad practice) the signal delays are given to support the discussion. Results show that either failing to properly estimate the delays or neglecting the issue can lead to the misinterpretation of results, especially in the case of submicrosecond pulsed excitation, since the time scale of the signal delays and the camera gates typically adopted for these experiments are of the same order of magnitude of the excitation signal.

Second, the challenges associated to ICCD imaging of very small volume plasma discharges are presented and discussed for the case of a plasma needle powered at 13.56 MHz, operated in a mixture of air and He and facing a flat dielectric surface; in the presented case the discharge volume is in the order of few mm^3, thus the use of additional camera lenses and extension rings is necessary to decrease the minimum focusing distance and to increase the resolution of the image. Voltage and current measurement during operation are presented together with captured ICCD images; two modes of operations were identified: unipolar/corona mode, with the discharge concentrated at the tip of the needle without expanding to target's surface, for lower powers and bipolar mode, with the discharge spreading towards and forming a sheath at the dielectric surface, for higher powers.

Finally, scaling laws are valuable for studies of high pressure/small volume discharges, as long as limitations of validity of scaling laws are clear. ICCD images are among the best ways to test the scaling such as *pd* (and other) in the extrapolation from low pressure to atmospheric pressure micro discharges. Any departure from the scaling may indicate incorrect operation or even an entrance of new physical processes. A possible way to extend the absolute calibration of the discharge emission achieved for a low pressure low current dc discharge to the case of micro discharges at high and close to atmospheric pressure is illustrated; preliminary results for the case of a water vapour discharge at different *E/N* values (from moderately high to very high) are presented to exemplify the interesting opportunities, provided by normalization of the spatial emission profiles captured by ICCD, for producing absolute data, allowing quantitative comparisons with theory and possible adjustments to the basic data.

Acknowledgments

This work was supported in part by European Cooperation in Science and Technology (COST) Action through the project entitled Biomedical Applications of Atmospheric Pressure Plasma Technology under Grant MP1101 and in part by COST Action through the project entitled Electrical Discharges With Liquids for Future Applications under Grant TD1208. The work of the group in Bologna is supported in part by the Alma Mater Studiorum—Università di Bologna through the University Fundings For Basic Research entitled Plasmat. The work of the group in Belgrade is supported in parts by the projects III41011 and ON171037 of the MPNTR-RS.

References

[1] Boyle W S and Smith G E 1970 *Bell Sys. Tech. J.* **49** 587–93
[2] Raether H 1964 *Electron Avalanches and Breakdown in Gases* (London: Butterworths)
[3] Ingold J H 1978 *Glow Discharges at dc and Low Frequencies: Anatomy of a Discharge in Gaseous Electronics* ed M N Hirsh and H J Oskam (New York: Academic) vol 1 p 19
[4] Druyvesteyn M J and Penning F M 1940 *Rev. Modern Phys.* **12** 87
[5] Jelenković B and Phelps A V 1999 *J. Appl. Phys.* **85** 7089
[6] Petrović Z Lj and Phelps A V 1997 *Phys. Rev.* E **56** 5920
[7] Anderson M H, Ensher J R, Matthews M R, Wieman C E and Cornell E A 1995 *Science* **269** 168
[8] Blevin H A, Fletcher J, Hunter S R and Marzec L M 1976 *J. Phys. D: Appl. Phys.* **9** 471
[9] Maletić D, Puač N, Selaković N, Lazović S, Malović G, Đorđević A and Petrović Z Lj 2015 *Plasma Sources Sci. Technol.* **24** 025006
[10] Marić D, Malović G and Petrović Z Lj 2009 *Plasma Sources Sci. Technol.* **18** 034009
[11] Wagenaars E, Bowden M D and Kroesen G M W 2007 *Phys. Rev. Lett.* **98** 075002
[12] Schaper L, Waskoenig J, Kong M G, Schulz-von der Gathen V and Gans T 2011 *IEEE Trans. Plasma Sci.* **39** 2370–1
[13] Marić D, Škoro N, Maguire P D, Mahony C M O, Malović G and Petrović Z Lj 2012 *Plasma Sources Sci. Technol.* **21** 035016
[14] Boselli M, Colombo V, Gherardi M, Laurita R, Liguori A, Sanibondi P, Simoncelli E and Stancampiano A 2015 *IEEE Trans. Plasma Sci.* **43** 713–25
[15] Bianconi S, Cavrini F, Colombo V, Gherardi M, Laurita R, Liguori A, Sanibondi P and Stancampiano A 2014 *IEEE Trans. Plasma Sci.* **42** 2746–2747
[16] Marinov I, Guaitella O, Rousseau A and Starikovskaia S M 2013 *J. Phys. D: Appl. Phys.* **46** 464013
[17] Hofmann S, Gils K, Linden S, Iseni S and Bruggeman P 2014 *Eur. Phys. J.* D **68** 56
[18] Shao T, Zhang C, Fang Z, Yu Y, Zhang D, Yan P, Zhou Y and Schamiloglu E 2013 *IEEE Trans. Plasma Sci.* **41** 3069–3078
[19] Robert E, Sarron V, Darny T, Ri`es D, Dozias S, Fontane J, Joly L and Pouvesle J-M 2014 *Plasma Sources Sci. Technol.* **23** 012003
[20] Lommatzsch U, Pasedag D, Baalmann A, Ellinghorst G and Wagner H E 2007 *Plasma Process. Polym.* **4** S1041–5
[21] Cheng C, Liye Z and Zhan R J 2006 *Surf. Coat. Tech.* **200** 6659–65
[22] Szili E J, Al-Bataineh S A, Bryant P M, Short R D, Bradley J W and Steele D A 2011 *Plasma Process. Polym.* **8** 38–50
[23] Deng X, Leys, Vujosevic D, Vuksanovic V, Cvelbar U, De Geyter N, Morent R and Nikiforov A 2014 *Plasma Process. Polym.* **11** 921–30
[24] Fakhouri H, Ben Salem D, Carton O, Pulpytel J and Arefi-Khonsari F 2014 *J. Phys. D: Appl. Phys.* **47** 265301
[25] Mariotti D and Sankaran M 2011 *J. Phys. D: Appl. Phys.* **44** 174023

[26] Mariotti D, Patel J, Svrcek V and Maguire P 2012 *Plasma Process. Polym.* **9** 1074–85
[27] Mitra S, Svrcek V, Mariotti D, Velusamy T, Matsubara K and Kondo M 2014 *Plasma Process. Polym.* **11** 158–63
[28] Lee S W, Liang D, Gao X P A and Sankaran R M 2011 *Adv. Funct. Mater.* **21** 2155–61
[29] Lee S W, Mattevi C, Chhowalla M and Sankaran R M 2012 *J. Phys. Chem. Lett.* **3** 772 − 7
[30] Colomo V, Fabiani D, Focarete M L, Gherardi M, Gualandi C, Laurita R and Zaccaria M 2014 *Plasma Process. Polym.* **11** 247–55
[31] Weltmann K D, Brandenburg R, von Woedtke T, Ehlbeck J, Foest R, Stieber M and Kindel E 2008 *J. Phys. D: Appl. Phys.* **41** 194008–14
[32] Shen J, Cheng C, Fang S, Xie H, Lan Y, Ni G, Meng Y, Luo J and Wang X 2012 *Appl. Phys. Express* **5** 036201
[33] Fridman G, Peddinghaus M, Ayan H, Fridman A, Balasubramanian M, Gutsol A, Brooks A and Friedman G 2006 *Plasma Chem. Plasma Process.* **26** 425–42
[34] Kim G C and Lee H J and Shon C H 2009 *J. Korean Phys. Soc.* **54** 628–32
[35] Kim C H, Bahn J H, Lee S H, Kim G Y, Jun S I, Lee K and Baek S J 2010 *J. Biotech.* **150** 530–8
[36] Keidar M, Walk R, Shashurin A, Srinivasan P, Sandler A, Dasgupta S, Ravi R, Guerrero-Preston R and Trink B 2011 *Br. J. Cancer* **105** 1295–301
[37] Kurita H, Nakajima T, Yasuda H, Takashima K, Mizuno A, Wilson J I B and Cunningham S 2011 *Appl. Phys. Lett.* **99** 191504
[38] Yan X, Xiong Y, Zou F, Zhao S, Lu X, Yang G, He G and Ostrikov K 2012 *Plasma Process. Polym.* **9** 59–66
[39] Huang J, Li H, Chen W, Lv G H, Wang X Q, Zhang G P, Ostrikov K, Wang P Y and Yang S Z 2011 *Appl. Phys. Lett.* **99** 253701
[40] Joh H M, Kim S J, Chung T H and Leem S H 2012 *Appl. Phys. Lett.* **101** 053703
[41] Volotskova O, Hawley T S, Stepp M A and Keidar M 2012 *Sci. Rep.* **2** 636–45
[42] Kolb J F, Mattson A M, Edelblute C M, Hao X, Malik M A and Heller L C 2012 *IEEE Trans. Plasma Sci.* **40** 3007–26
[43] Jijie R, Luca C, Pohoata V and Topala I 2012 *IEEE Trans. Plasma Sci.* **40** 2980–5
[44] Zhao S, Xiong Z, Mao X, Lu X, He G, Han F and Yang G 2012 *IEEE Trans. Plasma Sci.* **40** 2179–84
[45] Brulle L, Vandamme M, Ries D, Martel E, Robert E, Lerondel S, Trichet V, Richard S, Pouvesle J-M and Le Pape A 2012 *PLOS One* **7** e52653
[46] Lu X, Laroussi M and Puech V 2012 *Plasma Sources Sci. Technol.* **21** 034005
[47] Stoffels E, Flikweert A J, Stoffels W W and Kroesen G 2002 *Plasma Sources Sci. Technol.* **11** 383–8
[48] Robert E, Barbosa E, Dozias S, Vandamme M, Cachoncinlle C, Viladrosa R and Pouvesle J-M 2009 *Plasma Process. Polym.* **6** 795–802
[49] Schmidt-Bleker A, Norberg S A, Winter J, Johnsen E, Reuter S, Weltmann K D and Kushner M J 2015 *Plasma Sources Sci. Technol.* **24** 035022
[50] Weltmann K D, Kindel E, Brandendburg R, Meyer C, Bussiahn R, Wilke C and von Woedtke T 2009 *Contrib. Plasma Phys.* **49** 631–40
[51] Kim J Y, Ballato J and Kim S O 2012 *Plasma Process. Polym.* **9** 253–60
[52] Kim K, Kim G, Hong Y C and Yang S S 2010 *Microelectron. Eng.* **87** 1177–80
[53] O'Neill F T, Twomey B, Law V J, Milosavljevic V, Kong M, Anghel S D and Dowling D 2012 *IEEE Trans. Plasma Sci.* **40** 2994–3002
[54] Deng X L, Nikiforov A Y, Vanraes P and Leys C 2013 *J. Appl. Phys.* **113** 023305
[55] Xiong Q, Nikiforov A Y, Li L, Vanraes P, Britun N, Snyders R, Lu X P and Leys C 2012 *Eur. Phys. J.* D **66** 281
[56] Hong Y, Lu N, Pan J, Li J, Wu Y and Shang K F 2013 *J. Electrost.* **71** 93–101
[57] van Gessel A F H, Hrycak B, Jasinski M, Mizeraczyk J, van der Mullen J J A M and Bruggeman P J 2013 *J. Phys. D: Appl. Phys.* **46** 095201
[58] Xiong Q, Nikiforov A Y, Gonzalez M A, Leys C and Lu X P 2013 *Plasma Sources Sci. Technol.* **22** 015011
[59] Olszewski P, Wagenaars E, McKay K, Bradley J W and Walsh J L 2014 *Plasma Sources Sci. Technol.* **23** 015010
[60] Nastuta A V, Topala I and Popa G 2011 *IEEE Trans. Plasma Sci.* **39** 2310–1
[61] Babaeva N Y and Kushner M J 2014 *Plasma Sources Sci. Technol.* **23** 015007
[62] Robert E, Sarron V, Riès D, Dozias S, Vandamme M and Pouvesle J-M 2012 *Plasma Sources Sci. Technol.* **21** 34017
[63] Puač N, Maletić D, Lazović S, Malović G, Đorđević A and Petrović Z Lj 2012 *Appl. Phys. Lett.* **101** 024103
[64] Xiong Z and Kushner M J 2012 *Plasma Sources Sci. Technol.* **21** 034001
[65] Naidis G V 2013 *Plasma Sources Sci. Technol.* **22** 035015
[66] Robert E *et al* 2013 *Clin. Plasma Med.* **1** 8–16
[67] Urabe K, Sands B L, Ganguly B N and Sakai O 2012 *Plasma Sources Sci. Technol.* **21** 34004
[68] Wu L, Lane J, Cernansky N P, Miller D L, Fridman A and Starikovkiy A Y 2011 *Proc. Comb. Inst.* **33** 3219–24
[69] Hu J T, Liu X Y, Liu J H, Xiong Z L, Liu W D, Lu X P, Iza F and Kong M G 2012 *Phys. Plasmas* **19** 063505
[70] Sands L B, Ganguly N B and Tachibana K 2008 *IEEE Trans. Plasma Sci.* **36** 4
[71] Urabe K, Sands L B, Sakai O and Ganguly B N 2011 *IEEE Trans. Plasma Sci.* **39** 2294–5
[72] Cha M S, Lee S M, Kim K T and Chung S H 2005 *Comb. Flame* **141** 438–47
[73] Horst R M, Verreycken T, Veldhuizen E M and Bruggeman P J 2012 *J. Phys. D: Appl. Phys.* **45** 345201
[74] Park D, Fridman G, Fridman A and Dobrynin D 2013 *IEEE Trans. Plasma Sci.* **41** 1725–30
[75] Gucker S N, Garcia M C and Foster J E 2013 *Proc. XXXI ICPIG* (Granada, Spain)
[76] Nie Q Y, Cao Z, Ren C S, Wang D Z and Kong M G 2009 *New J. Phys.* **11** 115015
[77] Xiong Q, Nikiforov A Y, Lu X P and Leys C 2010 *J. Phys. D: App. Phys.* **43** 415201
[78] Wagenaars E, Gans T, O'Connell D and Niemi K 2012 *Plasma Sources Sci. Technol.* **21** 042002
[79] Urabe K, Ito Y, Tachibana K and Ganguly B N 2008 *Appl. Phys. Express* **1** 66004
[80] Schulz-von der Gathen V, Schaper L, Knake N, Reuter S, Niemi K, Gans T and Winter J 2008 *J. Phys. D: Appl. Phys.* **41** 194004
[81] Voráč J, Dvořák P, Procházka V, Ehlbeck J and Reuter S 2013 *Plasma Sources Sci. Technol.* **22** 025016
[82] Geiswiller J, Robert E, Huré L, Cachoncinlle C, Viladrosa R and Pouvesle J M 1999 *Meas. Sci. Technol.* **9** 1537–42
[83] Robert E, Hure L, Cachoncinlle C, Viladrosa R and Pouvesle J M 1999 *Meas. Sci. Technol.* **10** 789–95
[84] Sobota A, Guaitella O and Garcia-Caurel E 2013 *J. Phys. D: Appl. Phys.* **46** 372001
[85] Wu S and Lu X 2014 *Phys. Plasma* **21** 023501
[86] Petrović Z Lj, Škoro N, Marić D, Mahony C M O, Maguire P D, Radmilović-Rađenović M and Malović G 2008 *J. Phys. D: Appl. Phys.* **41** 194002
[87] Kuschel T, Stefanović I, Malović G, Marić D and Petrović Z Lj 2013 *Plasma Sources Sci. Technol.* **22** 045001

[88] Stefanović I, Berndt J, Marić D, Šamara V, Radmilović-Radjenović M, Petrović Z Lj, Kovačević E and Winter J 2006 *Phys. Rev.* E **74** 026406
[89] Belvin A, Fletcher J and Hunter S R 1976 *J. Phys. D: Appl. Phys.* **9** 1671–9
[90] Malović G, Strinić A, Živanov S, Marić D and Petrović Z Lj 2003 *Plasma Sources Sci. Technol.* **12** S1–7
[91] Petrović Z Lj and Phelps A V 2009 *Phys. Rev.* E **80** 016408
[92] Boselli M, Colombo V, Ghedini E, Gherardi M, Laurita R, Liguori A, Sanibondi P and Stancampiano A 2014 *Plasma Chem. Plasma Process.* **34** 853–69
[93] Starikovskiy A, Yang Y, Cho Y I and Fridman A 2011 *Plasma Sources Sci. Technol.* **20** 024003
[94] Puač N, Petrović Z Lj, Malović G, Đorđević A, Živković S, Giba Z and Grubišić D 2006 *J. Phys. D: Appl. Phys.* **39** 3514
[95] Lazović S *et al* 2010 *New J. Phys.* **12** 083037
[96] Miletić M, Mojsilović S, Okić Đorđević I, Maletić D, Puač N, Lazović S, Malović G, Milenković P, Petrović Z Lj and Bugarski D 2013 *J. Phys. D. Appl. Phys.* **46** 345401
[97] Lazović S, Maletić D, Leskovac A, Filipović J, Puač N, Malović G, Joksić G and Petrović Z Lj 2014 *Appl. Phys. Lett.* **105** 124101
[98] Puač N, Živković S, Selaković N, Milutinović M, Boljević J, Malović G and Petrović Z Lj 2014 *Appl. Phys. Lett.* **104** 214106
[99] Puač N, Petrović Z Lj, Živković S, Giba Z, Grubišić D and Đorđević A R 2005 *Plasma Processes and Polymers* (New York: Wiley) Chap 15 p 193
[100] Sakiyama Y, Graves D B and Stoffels E 2008 *J. Phys. D: Appl. Phys.* **41** 095204
[101] Sakiyama Y and Graves D B 2006 *J. Phys. D: Appl. Phys.* **39** 3451–6
[102] Kieft I E, van der Laan E P and Stoffels E 2004 *New. J. Phys.* **6** 149
[103] Wagenaars E, Bowden M D and Kroesen G M W 2005 *Plasma Sources Sci. Technol.* **14** 342
[104] Marić D, Škoro N, Malović G, Petrović Z Lj, Mihailov V and Djulgerova R 2009 *J. Phys. Conf. Ser.* **162** 012007
[105] Li S, Ouyang J-T and He F 2010 *Chin. Phys. Lett.* **27** 065201
[106] Petrović Z Lj and Phelps A V 1996 *IEEE Trans. Plasma Sci.* **24** 107–8
[107] Živanov S, Živković J, Stefanović I, Vrhovac S and Petrović Z Lj 2000 *Eur. Phys. J. AP* **11** 59–69
[108] Škoro N, Marić D and Petrović Z Lj 2008 *IEEE Trans. Plasma Sci.* **36** 994
[109] Marić D, Hartmann P, Malović G, Donkó Z and Petrović Z Lj 2003 *J. Phys. D: Appl. Phys.* **36** 2639–48
[110] Marić D, Savić M, Sivoš J, Škoro N, Radmilović-Radjenović M, Malović G and Petrović Z Lj 2014 *Eur. Phys. J.* D **68** 155
[111] Urošević V V, Božin J V and Petrović Z Lj 1983 *Z. Phys.* A **309** 293
[112] Tachibana K and Phelps A V 1987 Excitation of the 1s5 and 1s4 levels of neon by low-energy electrons *Phys. Rev.* A **36** 999
Erratum 1988 *Phys. Rev.* A **37** 1786
[113] Marić D, Kutasi G M, Donkó Z and Petrović Z Lj 2002 *Eur. Phys. J.* D **21** 73–81
[114] Jelenak Z M, Velikić Z B, Božin J V, Petrović Z Lj and Jelenković B M 1993 *Phys. Rev.* E **47** 3566
[115] Božin J V, Jelenak Z M, Velikić Z V, Belča I D, Petrović Z Lj and Jelenković B M 1996 *Phys. Rev.* E **53** 52
[116] Phelps A V http://jila.colorado.edu/~avp/collision_data/electronneutral/Electron.txt
[117] Phelps A V 1992 *J. Phys. Chem. Ref. Data* **21** 883–97
[118] Phelps A V 1991 *J. Phys. Chem. Ref. Data* **20** 557–73
[119] Škoro N, Marić D, Malović G, Graham W G and Petrović Z Lj 2011 *Phys. Rev.* E **84** 055401(R)
[120] Stojanović V *et al* 2015 unpublished

6.4 Paper IV

iCCD Imaging of the Transition From Uncoupled to Coupled Mode in a Plasma Source for Biomedical and Materials Treatment Applications

DOI: 10.1109/TPS.2014.2321012

iCCD Imaging of the Transition From Uncoupled to Coupled Mode in a Plasma Source for Biomedical and Materials Treatment Applications

Simone Bianconi, Francesca Cavrini, Vittorio Colombo, Matteo Gherardi, Romolo Laurita, Anna Liguori, Paolo Sanibondi, and Augusto Stancampiano

***Abstract*— Intense and energetic atmospheric plasma was achieved by jet-to-jet coupling using an array of plasma jets arranged in an axisymmetric structure. To highlight the effects of pulse repetition frequency, peak voltage and mass flow rate on the transition from a coupled mode to an uncoupled one, qualitative results coming from iCCD imaging of a nanopulsed *Gatling machine gun*-like plasma source will be shown. Moreover, results on surface modifications and bacterial inactivation will be presented.**

***Index Terms*— Atmospheric-pressure plasmas, bacterial inactivation, plasma diagnostics, plasma sources, surface modification.**

A PARTICULAR type of plasma source, reminding the shape of a Gatling machine gun (Fig. 1), has been recently developed to generate high intensity, high ionization rate plasmas at 1 atm, overcoming some of the limitations of classical atmospheric pressure plasma jets [1]. Gatling sources are an array of plasma jets, adjacent to one another, that rely on jet-to-jet coupling phenomenon to merge plasma plumes in a single combined intense jet [2], able to achieve surface modification including etching [3].

The Gatling plasma source adopted in this paper is an array of seven PTFE tubes, one in the center and six surrounding it, having inner–outer diameters of 1–1.6 mm. The tubes are arranged in an axisymmetric structure. As powered electrodes, 6-mm wide aluminum tapes are placed 10 mm from the end of each tube. The source is driven by a generator producing pulses with a rise time of 9 ns and peak voltages (PV) in the range 7–20 kV into a 100–200 Ω load impedance. As working gas 99.999% pure helium is used.

The occurrence of jet-to-jet coupling for the Gatling source impinging on borosilicate glass at different operating conditions was investigated with an iCCD camera (Princeton Instruments PIMAX3) having exposure time down to 3 ns. A synchronous pulses generator (BNC 575 digital pulse/delay generator) is used to time the generator and the oscilloscope (Tektronix DPO 4034), that in turn triggers the iCCD camera.

Surface modification of silicone films treated with the Gatling source was evaluated through static water contact angle (WCA) measurements (Kruss drop shape analysis system DSA 30). Antibacterial effect of the plasma source was assessed by treating a *Bacillus atrophaeus* (ATCC 9372) suspension in NaCl 0.9% swabbed uniformly across a trypticase soy agar plate with 5% sheep blood. The number density of the swabbed solution was found to be 4×10^6 colony forming units ml^{-1}, using a dilution technique. After treatment, the agar plates were incubated at 37 °C for 24 h. During plasma treatment, substrate materials were placed on a grounded aluminum plate, 8 mm from the tip of the plasma source.

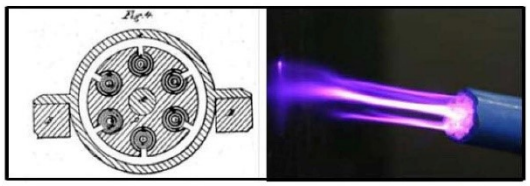

Fig. 1. Detail of a drawing in the "Machine Gun" US 36,836 patent by R.J. Gatling (1862) and a picture of the Gatling-gun like plasma source.

Gatling sources are known to exhibit either an uncoupled mode or a coupled one; the transition from the former to the latter has been reported in the literature only as an effect of decreasing gas flow rate (GFR) [2]. In fact, as shown by iCCD images in Fig. 2(b), a transition from uncoupled [Fig. 2(a)] to coupled [Fig. 2(c)] mode occurs changing GFR from 8 to 2 slpm, at a constant PV of 28 kV and for a 476 Hz pulse repetition frequency (PRF). Moreover, we observed such a transition also increasing PRF from 476 to 1000 Hz (PV fixed at 28 kV and GFR at 5.5 slpm), as shown in Fig. 2(d). An increase in PV was found to intensify the coupling effect, resulting in modification of the shape and emission intensity of the discharge [Fig. 2(e)]. Fig. 2(f) shows a reduction of WCA with respect to pristine (107°) when treating (PV: 28 kV, PRF: 476 Hz) for 1 s silicone films in uncoupled (GFR: 5.5 slpm; WCA: 77°) or coupled (GFR: 2 slpm; WCA: 50°) mode. Fig. 2(g) shows that a 60-s treatment (PV: 27.2 kV, PRF: 476 Hz) of *B. atrophaeus* can induce a growth inhibition area with diameter 4 and 8 mm for uncoupled (GFR: 5.5 slpm) and coupled mode (GFR: 2 slpm), respectively.

Manuscript received November 1, 2013; revised February 26, 2014; accepted April 26, 2014. Date of publication May 16, 2014; date of current version October 21, 2014. This work was supported in part by the COST Action MP1101 Biomedical Applications of Atmospheric Pressure Plasma Technology and by the COST Action TD1208 Electrical Discharges with Liquids for Future Applications.

The authors are with the Department of Industrial Engineering and Industrial Research Centre for Advanced Mechanics and Materials, Alma Mater Studiorum-Università di Bologna, via Saragozza 8, Bologna 40123, Italy (e-mail: vittorio.colombo@unibo.it).

Digital Object Identifier 10.1109/TPS.2014.2321012

REFERENCES

[1] S. Kim, J. Y. Kim, D. Y. Kim, and J. Ballato, "Intense plasma emission induced by jet-to-jet coupling in atmospheric pressure plasma arrays," *Appl. Phys. Lett.*, vol. 101, no. 17, p. 173503, 2012.

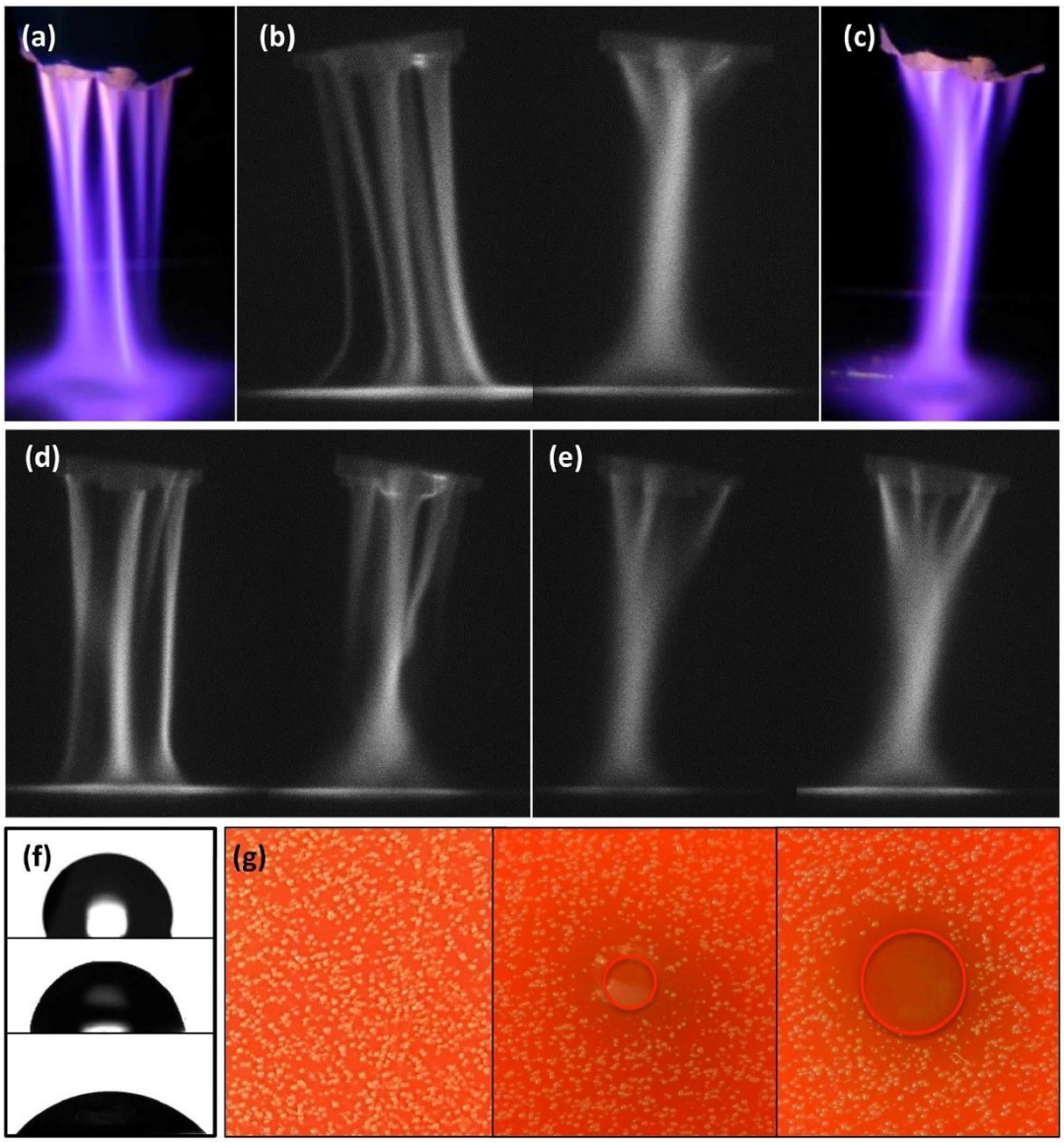

Fig. 2. Low-speed images of the Gatling source in uncoupled (a) and coupled (c) modes. iCCD images (3-ns exposure time) of transition from uncoupled to coupled mode by GFR reduction (b) and PRF increase (d). Intensification of coupling effect by PV increase (e). WCA changes on silicon film (f) from pristine to treated in uncoupled and coupled mode, respectively (from top to bottom). Control and growth inhibition area of *B. atrophaeus* (g) for plasma treatment in uncoupled and coupled mode, respectively (from left to right).

[2] J. Y. Kim, J. Ballato, and S. Kim, "Intense and energetic atmospheric pressure plasma jet arrays," *Plasma Process. Polym.*, vol. 9, no. 3, pp. 253–260, 2012.

[3] J. Furmanski, J. Y. Kim, and S. Kim, "Triple-coupled intense atmospheric pressure plasma jet from honeycomb structural plasma device," *IEEE Trans. Plasma Sci.*, vol. 39, no. 11, pp. 2338–2339, Nov. 2011.

6.5 Paper V

High-speed multi-imaging of repetitive unipolar nanosecond-pulsed DBDs.

DOI: 10.1109/TPS.2014.2330954

High-Speed Multi-Imaging of Repetitive Unipolar Nanosecond-Pulsed DBDs

Marco Boselli, Vittorio Colombo, Emanuele Ghedini, Matteo Gherardi, Romolo Laurita, Anna Liguori, Paolo Sanibondi, and Augusto Stancampiano

***Abstract*— Dielectric barrier discharges (DBDs) are being studied for a wide range of biomedical and industrial applications. In this paper, qualitative results coming from synchronized high-speed and Schlieren multi-imaging of a unipolar nanosecond-pulsed DBD are presented, with the final aim of showing plasma structure, filament movement, and refractive index gradients in different interelectrode gaps and counter electrode materials.**

***Index Terms*— Atmospheric-pressure plasmas, plasma diagnostics, plasma sources, pulsed power supplies.**

THE study of plasma sources dealing with biomedical applications or thermosensitive materials treatment can take advantage from diagnostics of the discharge to gather more knowledge on the complex interaction between plasma and the substrates and to tailor the source to specific applications. In this paper, we focus on the high-speed multi-imaging of a DBD, where plasma is ignited between two electrodes, at least one of which is commonly covered with a dielectric [1]. The material to be treated can be positioned within the interelectrode gap or can act as the counter electrode in the common configuration for the treatment of living tissue [2]. The DBD source consists of a cylindrical copper electrode (diameter 26.2 mm) surrounded by a 6 mm thick dielectric plastic layer (polyetherimide), a 0.5 mm thick quartz disk covering the electrode plane surface facing the plasma region and, as a transparent grounded counter electrode, either ITO-coated plastic (450–650 nm indium tin oxide coating on 1.3 mm PET layer) or salted water [1]. The DBD is driven by a pulser with a rise time of 9 ns and peak voltages in the range 7–20 kV into a 100–200 Ω load impedance, with a maximum pulse repetition rate of 1 kHz. Among the main advantages of plasmas generated by nanopulsed power supplies is the effectiveness in treating nonuniform surfaces [3]. The concurrent use of high-speed and Schlieren imaging, enabling the visualization of plasma microdischarges related to a single voltage pulse together with the synchronized imaging of the refractive index gradients induced by them, was implemented according to the setup shown in Fig. 1. High-speed cameras were synchronized and triggered using a DPO4034 Tektronix oscilloscope. The NAC Memrecam K3R (1000 frames/s, 10 μs shutter) was connected to a Z-type Schlieren setup, while a NAC-GX3 (1000 frames/s, 1 ms shutter) captured, using a double mirror, a side view (at 45° with respect to the K3R Schlieren observation perspective) of the plasma region and a bottom one through the transparent substrate. In Fig. 2, results for both salted water and ITO-coated substrates are shown for three interelectrode gap widths at 1, 5 and 8 mm. With ITO substrate at 1 mm, the plasma discharge appears as a uniform glow where no microdischarges can be discerned. Increasing the gap width, transition from a diffuse to a filamentary discharge occurs. In Schlieren images, refractive index gradients are observed in correspondence with filaments for the cases at 5 and 8 mm. The addition of salt greatly increases the electrical conductivity of water inducing the formation of a filamentary discharge typical of metallic counter electrode materials, even with 1 mm gap. A transient for the case with ITO-coated substrate with gap width at 8 mm is shown in Fig. 3. Spatial distribution of refractive index gradients changes accordingly to filament movements. Analyzing the bottom view frames and assuming linear trajectories between the contact points of subsequent microdischarges in a moving filament, its velocity on the substrate was estimated between 0.2 and 0.3 mm/ms.

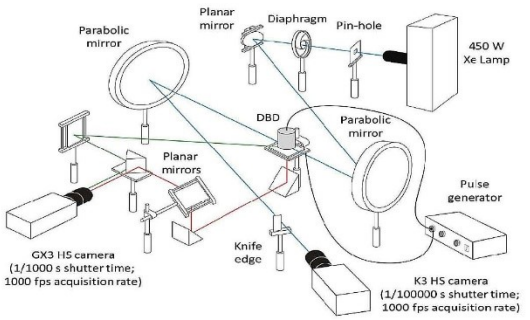

Fig. 1. Three-view high-speed multi-imaging and Schlieren setup.

Manuscript received November 1, 2013; revised April 11, 2014; accepted June 8, 2014. Date of publication June 27, 2014; date of current version October 21, 2014. This work was supported in part by the COST Action MP1101 Biomedical Applications of Atmospheric Pressure Plasma Technology and by the COST Action TD1208 Electrical Discharges with Liquids for Future Applications.

The authors are with the Department of Industrial Engineering and Industrial Research Centre for Advanced Mechanics and Materials, Alma Mater Studiorum-Università di Bologna, via Saragozza 8, Bologna 40123, Italy (e-mail: vittorio.colombo@unibo.it).

Digital Object Identifier 10.1109/TPS.2014.2330954

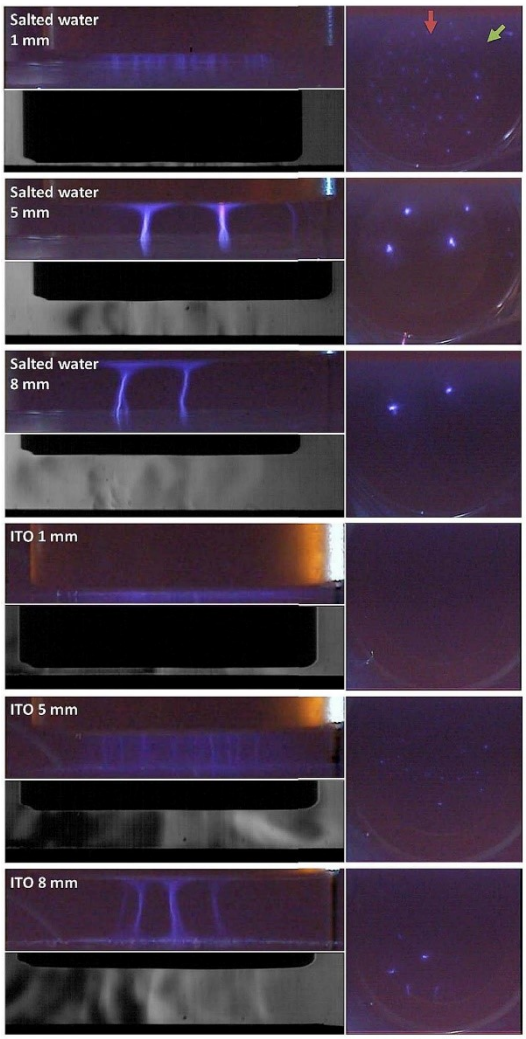

Fig. 2. Horizontally flipped Schlieren, lateral and bottom HS imaging of the DBD source on top of salted water and ITO substrate for different electrode gap widths. Green and red arrows: lateral HS and Schlieren observation points, respectively, which are the same for all cases. Peak voltage and operating frequency at 23 kV and 1000 Hz, respectively.

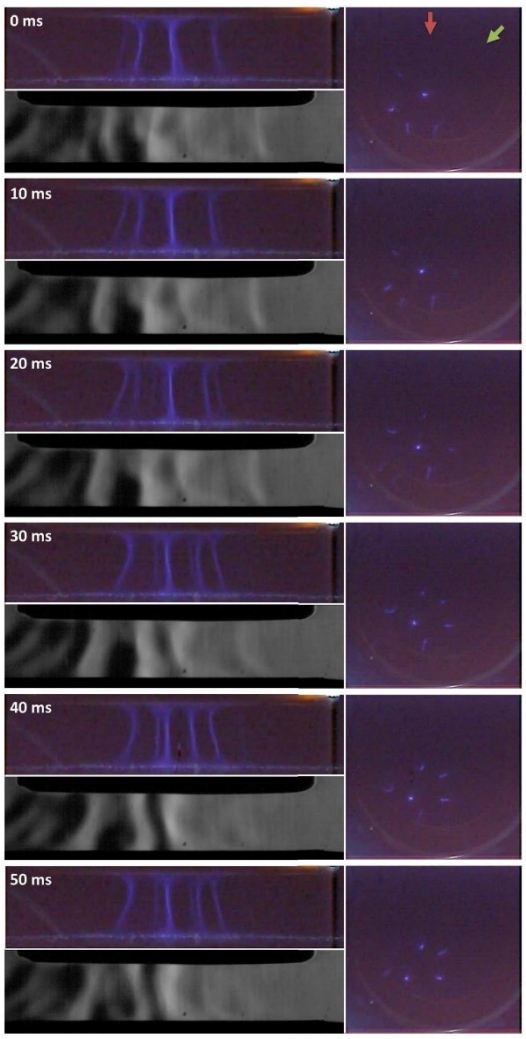

Fig. 3. Horizontally flipped Schlieren, lateral and bottom HS imaging during a transient of the DBD source on top of ITO substrate, for 8 mm electrode gap width. Green and red arrows: lateral HS and Schlieren observation points, respectively, which are the same for all cases. Peak voltage and operating frequency at 23 kV and 1000 Hz, respectively.

REFERENCES

[1] U. Kogelschatz, "Dielectric-barrier discharges: Their history, discharge physics, and industrial applications," *Plasma Chem. Plasma Process.*, vol. 23, no. 1, pp. 1–46, Mar. 2003.

[2] A. Gutsol, A. Fridman, G. Friedman, G. Fridman, and M. Balsubramanian, "Methods for non-thermal application of gas plasma to living tissue," WO 2006/116252 A2, Nov. 2, 2006.

[3] A. Fridman, H. Ayan, D. Staack, G. Fridman, A. Gutsol, Y. Mukhin, A. Starikovskii, G. Friedman, "Application of nanosecond-pulsed dielectric barrier discharge for biomedical treatment of topographically non-uniform surfaces," *J. Phys. D, Appl. Phys.*, vol. 42, no. 12, p. 125202, 2009.

6.6 Paper VI

Atmospheric Non-Equilibrium Plasma Promotes Cell Death and Cell-Cycle Arrest in a Lymphoma Cell Line

DOI: 10.1002/ppap.201500033

Atmospheric Non-Equilibrium Plasma Promotes Cell Death and Cell-Cycle Arrest in a Lymphoma Cell Line

Matteo Gherardi,* Eleonora Turrini, Romolo Laurita, Elena De Gianni, Lorenzo Ferruzzi, Anna Liguori, Augusto Stancampiano, Vittorio Colombo,* Carmela Fimognari

Atmospheric non-equilibrium plasma is drawing interest as a promising tool for cancer treatment due to its blend of physical and chemical components that can exert anti-tumor effects. In this work, we investigate the effects of plasma treatment, performed by means of a wand electrode DBD driven by nanosecond high voltage pulses, on the viability, proliferation, and cell-cycle distribution of cells of mouse lymphoma. Results for direct treatment, with cell exposed to plasma while suspended in culture medium, and indirect treatment, where cells were added to culture medium previously activated by plasma treatment, are compared. A qualitative characterization by means of high-speed and iCCD imaging of the plasma discharges produced for the different operating conditions adopted in biological experiments, as well as a semi-quantitative study of the reactive species produced by plasma treatment in the culture medium, are also presented.

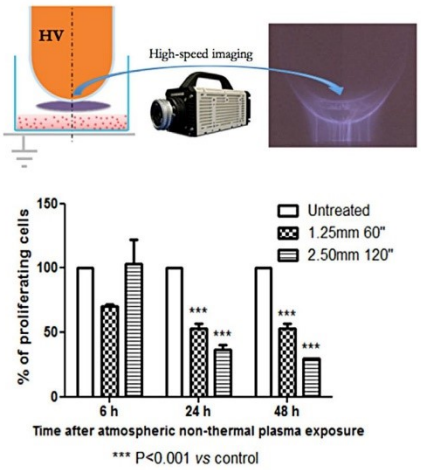

M. Gherardi, R. Laurita, A. Liguori, A. Stancampiano, V. Colombo
Department of Industrial Engineering (DIN), Alma Mater Studiorum-University of Bologna, Via Saragozza 8, 40123 Bologna, Italy
E-mail: matteo.gherardi4@unibo.it
E. Turrini, L. Ferruzzi, C. Fimognari
Department for Life Quality Studies, Alma Mater Studiorum-University of Bologna, Corso d'Augusto 237, 47921 Rimini, Italy
E. De Gianni
Advanced Mechanics and Materials, Interdepartmental Center for Industrial Research (AMM-ICIR), Alma Mater Studiorum-University of Bologna, Piazza Malatesta, 29/30, 47923 Rimini, Italy
V. Colombo
Advanced Mechanics and Materials, Interdepartmental Center for Industrial Research (AMM-ICIR), Alma Mater Studiorum-University of Bologna, Via Saragozza 8, 40123 Bologna, Italy
E-mail: vittorio.colombo@unibo.it

1. Introduction

Despite improvements in survival rates, cancer is still the second leading cause of death in Western countries.[1] While the rapidly expanding knowledge of cancer pathogenesis at the molecular level is providing new targets for drug discovery and development, the multiple genetic and molecular alterations involving transformation, dysregulation of apoptosis, proliferation, invasion, angiogenesis, and metastasis[2] make cancer an extremely complex disease.

Currently, the treatment of cancer largely revolves around chemotherapy, with new therapeutic approaches under investigation, alone or in combination with conventional chemotherapy. Despite the development of multiple new agents, antitumor therapies are strongly limited by the

Plasma Process. Polym. **2015,** DOI: 10.1002/ppap.201500033

low therapeutic index of most of the adopted drugs and by the development of chemoresistence. In particular, the onset of chemoresistance frequently hampers the successful treatment of cancer either at the initial presentation or following primary or subsequent relapses,[3] and relapse continues to be the most common cause of death.[4] Thus, cancer remains a formidable therapeutic challenge that requires the identification and the development of novel agents for the treatment of this disease.

Atmospheric non-equilibrium plasmas are encountering increasing interest as a novel anti-tumor agent, since they provide a blend of physical and chemical components (reactive species, charged particles, and UV radiation) which was demonstrated to exert anti-tumor effects by some pioneering work both on in vivo and in vitro models.[5,6] However, the mechanism of plasma-cell interaction is still not completely understood, as well as the selectivity associated to the various plasma generated species. Different species were demonstrated to mediate either "plasma-killing" (for the case of singlet oxygen, O) or "plasma-healing" (for the case of nitrogen oxide, NO) effects.[7] Gweon et al.[8] considered reactive oxygen species (ROS) responsible for the dissociation of integrin and the consequent detachment of human liver cancer cells (SK-HEP-1). Ishaq et al.[9] demonstrated that plasma treatment induced apoptosis in melanoma cells and, differently from the previous works, focused their attention on intracellular ROS levels. On the other hand, Volotskova et al.[10] demonstrated that plasma treatment enhances the oxidative stress of cells in the S phase of the cell cycle. Interestingly, recent studies [11] have reported that plasma not only affects cancer cells when they are directly exposed to it or suspended in the culture medium being treated, but also when they are subject to indirect treatment, being suspended in a medium that was previously treated and activated by plasma. Tanaka et al. [12] demonstrated that, when treated by plasma activated medium, glioblastoma human brain tumor cells were induced to undergo apoptosis, through AKT down-regulation; moreover, they also demonstrated in vitro and in vivo that plasma-activated medium has an anti-tumor effect on chemo-resistant epithelial ovarian carcinoma cells.[13]

These observations together with the rapidly expanding knowledge of cancer biology have fueled a growing interest in exploiting cold plasma as an interesting strategy in the oncological field endowed with the potential of shifting the current paradigm of cancer treatment and enabling the transformation of cancer treatment technologies.

In this work, we focused on the fundamental mechanisms of plasma interaction with cancer cells, investigating cell viability, proliferation, and cell-cycle distribution of L5178Y lymphoma cells treated by a wand electrode dielectric barrier discharge (DBD)[14] driven by unipolar nanosecond high voltage pulses.[15] Plasma direct treatment was performed keeping constant the electrical parameters (peak voltage and pulse repetition frequency), while adopting two different combinations of treatment time and gap width between the tip of the plasma source and the liquid; the differences between the plasma discharges generated in the considered operating conditions were highlighted and analyzed through iCCD and high speed (HS) imaging, which are often used for qualitative characterization of non-equilibrium plasmas.[16–25] Flow cytometry was employed to evaluate cell viability at 6, 24, and 48 h after plasma treatment, as well as to analyze cell-cycle distribution after cell culture for 24 and 48 h. Finally, a comparison of the effects of direct and indirect treatments, where cancer cells were exposed to a previously plasma treated culture medium instead of being directly exposed to plasma treatment, and the semi-quantitative measurement of nitrites, nitrates and peroxides in the plasma treated medium were carried out to support the evaluation of the observed cell response to plasma exposure.

2. Experimental Section

2.1. Plasma Device

The wand electrode DBD plasma source used in this work, represented in Figure 1, consists of a cylindrical brass electrode, with a 10 mm diameter, having a semispherical tip, with curvature radius of approximately 5 mm. The electrode is covered with borosilicate glass (relative permittivity $\varepsilon_r = 4.7$) as dielectric layer with a thickness of 1 mm. The plasma source is driven by a commercial pulse generator producing high voltage pulses with a slew rate of few kV/ns, a peak voltage (PV) of 7–20 kV into a 100–200 Ω load impedance and a maximum pulse repetition frequency (PRF) of 1000 Hz.

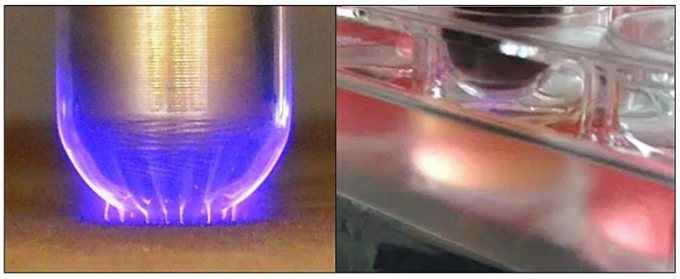

Figure 1. Wand electrode DBD discharge on a grounded plate (left) and on liquid culture medium during cell treatment (right).

2.2. Plasma Device Characterization

A high-speed camera (Memrecam GX-3-NAC Image Technology) was used to visualize the behavior of the plasma discharge in contact with 1 mL of Dulbecco's modified Eagle's medium (DMEM) contained in a 24 wells plate, representative of the operating conditions adopted for the treatment of cancer cells as later described in section 2.4; for these tests, the 24 wells plate was slightly modified, removing part of the plastic walls to allow an optimal visualization of the plasma region. Results will be presented for the camera being operated either at 500 fps (frames per second) and 1/500 s shutter time or at 100 fps and 1/100 s shutter time; as the shutter time was equal or superior to the pulse period, no means of synchronization was necessary. The setup adopted for high-speed imaging characterization is reported in Figure 2.

Temporal evolution of the plasma discharge in contact with DMEM has been investigated by means of an iCCD camera (Princeton Instruments PIMAX3). A synchronous pulse generator (BNC 575 digital pulse/delay generator) was used to synchronize the high voltage generator and the oscilloscope (Tektronix DPO 40034) adopted to trigger the iCCD camera, as schematically represented in Figure 3; to allow an optimal visualization of the plasma region, the same modified 24 wells plate adopted for high speed imaging test was used for iCCD experiments. The plasma discharge temporal evolution during an entire pulse was reconstructed from sequential frames acquired at time steps of 1 ns and with an exposure time of 3 ns.

2.3. Cell Cultures

For the experiments, L5178Y TK ± clone (3.7.2C) cells of mouse lymphoma (LGC Standard, Teddington Middlesex, UK) were grown in suspension and propagated in DMEM (from LGC Standard) supplemented with 4 mM L-glutamine, 10% inactivated fetal bovine serum, 1% penicillin/streptomycin solution, 0.1% pluronic (all obtained from Sigma, St Louis, MO, USA). To maintain the exponential growth, the culture was divided every third day by dilution to a final concentration of 1–2 $\times 10^5$ viable cells/mL. Cells were cultured at 37°C/5% CO_2.

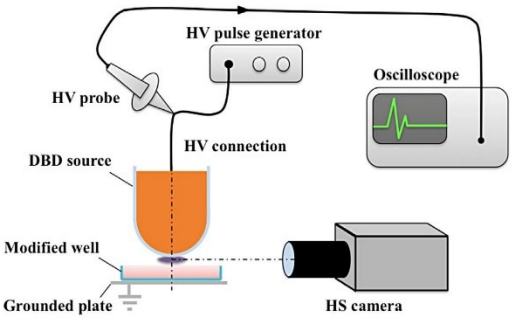

Figure 2. Representation of the setup for high speed imaging characterization of the wand electrode DBD discharge during the treatment of DMEM.

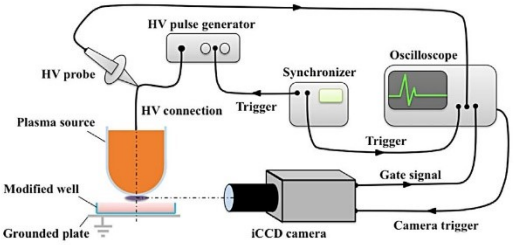

Figure 3. Representation of the setup for iCCD imaging characterization of the wand electrode DBD discharge during the treatment of DMEM.

2.4. Plasma Treatment

Plasma treatment of lymphoma cells was performed either in direct both indirect configuration. In direct configuration, 5 $\times 10^5$ cells in 1 mL complete medium were seeded in a monolayer through centrifugation and directly exposed to plasma treatment in a 24 wells plate; two different sets of operating conditions were considered: in the first case (T1), a 60 s treatment was performed keeping a 1.25 mm distance between the tip of the plasma source and the surface of the liquid medium (gap); in the second case (T2), a 120 s treatment was performed setting the gap at 2.50 mm. During the experiments, PV and PRF were kept constant at 20 kV and 500 Hz, respectively. These two operating conditions were selected after a series of preliminary tests; in particular, for each of the two mentioned gaps, preliminary treatments were performed for several different treatment times, after which cell viability was assayed: we selected the operating conditions that resulted in a significant reduction of cell viability, but still higher than 50% (normalized to the cell viability of untreated cells), necessary to perform the cell proliferation experiments.

In indirect configuration, 1 mL of complete medium not containing lymphoma cells was exposed to plasma treatment in a 24 wells plate; 5 00 000 lymphoma cells were added to the medium immediately after plasma treatment. A comparison of the effects of direct and indirect treatments was carried out for the following operating conditions: PV 20 kV, PRF 500 Hz, gap 1.25 mm, and various treatment times (30, 45, 60, 90, and 120 s).

Setups for direct and indirect treatments are schematically reported in Figure 4A and B, respectively.

2.5. Biological Assays

For direct treatment, cell viability and proliferation were determined after 6, 24 and 48 h from atmospheric non-equilibrium plasma exposure of cells at the two different experimental conditions; for the comparison between direct and indirect treatments, cell viability was determined after 6, 24, and 48 h from atmospheric non-equilibrium plasma exposure of cells (direct treatment) or 6, 24, and 48 h after cells were added to the plasma treated culture medium (indirect treatment). Briefly, 25 μL of cell suspension were mixed with 225 μL of Guava ViaCount Reagent (Merck Millipore, Hayward, CA, USA) containing 7-aminoactinomycin D (7-AAD), a fluorescent intercalator of DNA, and incubated

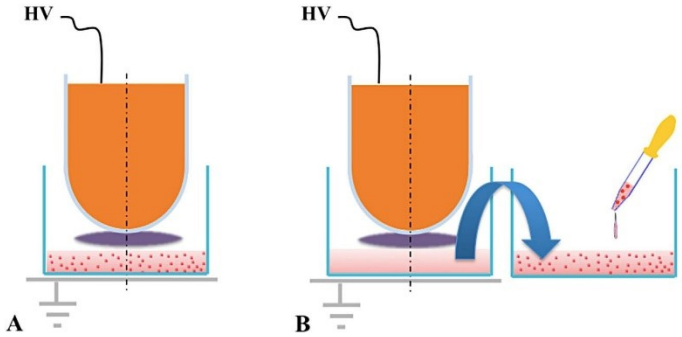

Figure 4. DBD plasma treatment of lymphoma cells: A) direct treatment setup; B) indirect treatment setup.

in the dark at room temperature for 5 min before the flow cytometric analysis, performed using the guava easyCyte 5HT (Merck Millipore).

To evaluate cell-cycle distribution, cells were treated at the two established experimental conditions and cultured for 24 and 48 h, then permeabilized with ice-cold ethanol for 30 min and stained with 200 μL of Guava Cell Cycle reagent (Merck Millipore), containing propidium iodide (PI), for 30 min in the dark. At the end of the incubation, cells were analyzed via flow cytometry.

All results are expressed as mean ± SEM (Standard Error of the Mean). Differences among exposure conditions at different time points (6, 24, 48 h) were evaluated by One-way ANOVA repeated, followed by Bonferroni as post hoc test. For all statistical analysis, GraphPad InStat version 5.0 (GraphPad Prism, San Diego, CA, USA) was used and $P < 0.05$ was considered significant.

2.6. Measurement of Nitrites, Nitrates, and Peroxides in Cell Culture Medium

Semi-quantitative analysis of nitrites (NO_2^-), nitrates (NO_3^-), and peroxides (H_2O_2) produced after exposure to plasma in 1 mL complete medium were performed by means of Quantofix analytic strips. All the measurements were effectuated immediately after the end of the treatments.

3. Results and Discussion

3.1. High Speed Imaging and iCCD Imaging of the Plasma Discharge

A qualitative investigation of the plasma discharge produced during the treatment of 1 mL of cell culture medium not containing Lymphoma cells was performed by means of HS and iCCD imaging; for the following operating conditions: PV 20 kV, PRF 500 Hz, gap 1.25 mm (T1 case) and PV 20 kV, PRF 500 Hz, gap 2.50 mm (T2 case). The described experimental setup and the considered operating conditions were identical to those adopted for biological tests.

Concerning HS imaging, two different frame rates were used, 100 and 500 fps; the HS camera shutter was kept open and, subsequently, exposure time was imposed by the frame rate (Figure 5). Considering the PRF adopted in the experiments, images recoded at 500 frames/s show the discharge produced during a single pulse of the driving electrical signal, while images recoded at 100 frames/s are accumulated over five subsequent pulses.

The reported HS images immediately highlight the effect of a variation of gap width, and thus of electrical field in the gap, on the plasma discharge aspect; for the smallest gap width (T1 case), the discharge appears characterized by several microdischarges located close to the tip of the plasma source. In this case, for the longest exposure time (100 fps image), a faint glow appears in the gap region and a larger number of filaments are observed with respect to the image taken at 500 fps, as a consequence of the accumulation of five subsequent discharges; the comparison between images taken at 100 and 500 fps highlights also that during subsequent pulses, for the selected operating conditions, the microdischarges form in different locations,

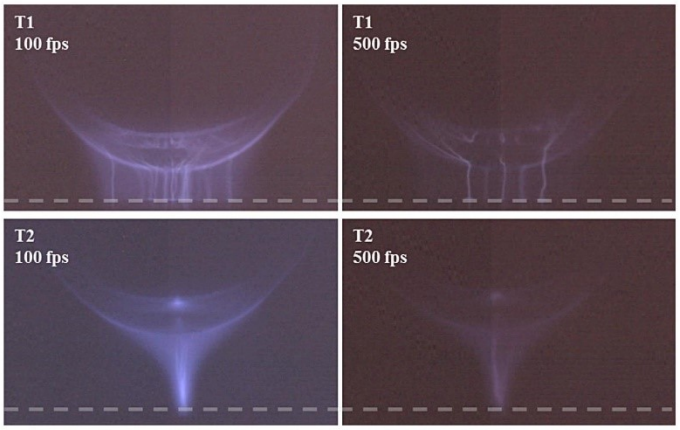

Figure 5. HS images of the plasma discharge during the treatment of culture medium (the dashed line indicates the culture medium surface) for both selected operating configurations (top: T1, bottom: T2). Acquisitions were realized at two different frame rates (left: 100 fps, right 500 fps).

Plasma Process. Polym. **2015,** DOI: 10.1002/ppap.201500033

DOI: 10.1002/ppap.201500033

with no significant memory effect observed,[26] possibly as a consequence of the adopted value of PRF and the unevenness of the liquid surface acting as a second electrode. When the gap between the plasma source and the culture medium surface is larger (T2 case), the plasma discharge appears completely different from the previous case, being characterized by a single filament located at the tip of plasma source, where the gap is the smallest and the electric field is the highest. The single filament has a funnel-like shape, which appears broader at the upper electrode, due to charge distribution and electric field distortion at the dielectric surface, and more collimated close to the culture medium surface; moreover, in case T2 images taken at different exposure times seem to show that filament produced during successive pulses are formed always in the same position, along the axis of the plasma source.

iCCD imaging, being characterized by exposure times of few nanoseconds, allows for the investigation of the plasma behavior with greater time resolution than HS images,[16–22] and was here used to investigate the temporal evolution of a single discharge event. Due to iCCD technology limitations, only one acquisition per voltage pulse can be gathered and thus the analysis of the discharge evolution along the voltage pulse is based on the assumption of repeatability of the plasma discharge characteristics in every high voltage pulse; this assumption was verified comparing three different acquisitions and observing that plasma evolution during the pulses was similar in all the cases. In our experiments, the exposure time was set at 3 ns (gate time) and the voltage pulse was scanned with time steps of 1 ns, obtained progressively increasing the trigger delay time.

In Figure 6, eight subsequent frames representing the plasma evolution are shown for each operating condition (T1 and T2); for clarity purposes, the gate opening of the first (one, colored in green) and last acquisitions (eight, colored in

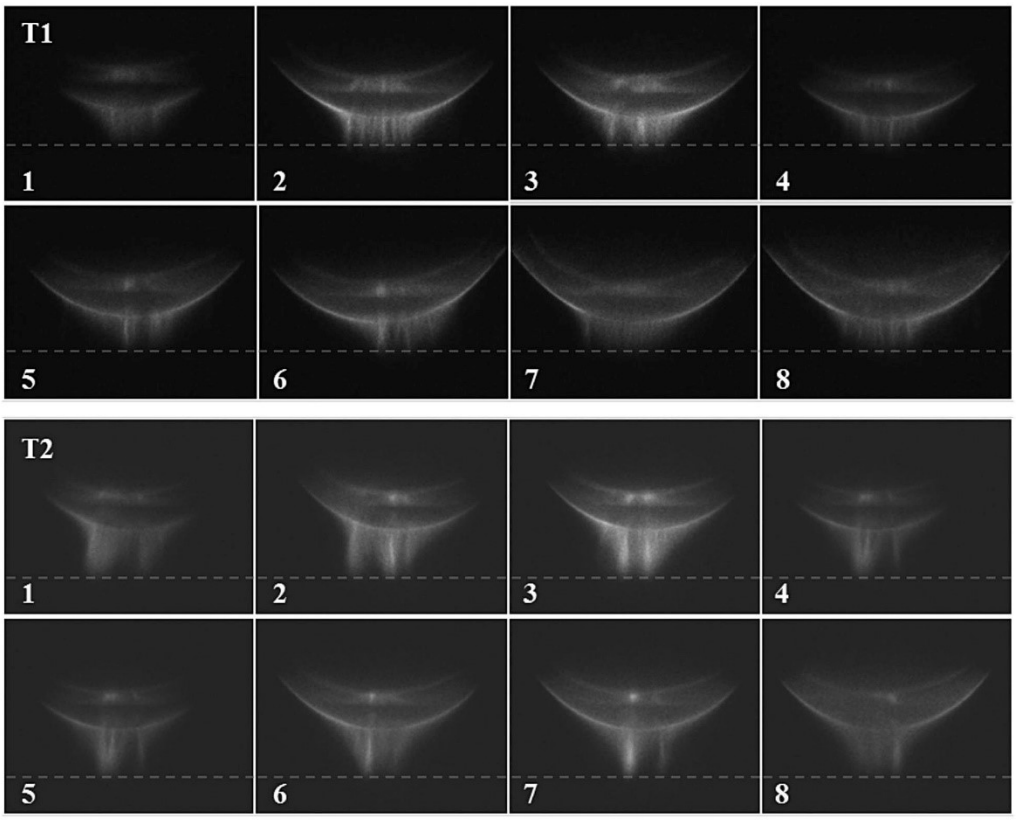

Figure 6. iCCD images depicting the temporal evolution along the voltage pulse of the plasma discharge formed in contact with 1 mL of culture medium (the dashed line indicates the culture medium surface), for both operating configurations adopted for cancer cell treatment (T_1, T_2). The start of each acquisition (3 ns exposure) is delayed of 1 ns with respect to the previous one.

red) are plotted against the recorded voltage waveform in Figure 7.

From iCCD acquisitions, the discharge structures for T1 and T2 cases turn out to be more similar to each other than previously observed by means of HS imaging. Indeed, the first plasma luminous emission appears almost at the same time, corresponding to the initial part of the voltage ramp, in both cases; moreover, the third frame, collected in correspondence of the maximum peak voltage, is the most luminous for both T1 and T2 cases. Most interestingly, a multi-filamentary structure is observed in both operating conditions; while this behavior was already observed by means of HS imaging in T1 conditions, only a single filament along the axis of the plasma source could be seen for the T2 case in HS pictures. This is probably because in HS imaging acquisition no light signal intensification is applied, therefore the signal of short living or low emitting microdischarges could be shadowed by the presence of a longer living or higher emitting microdischarge; indeed, almost all iCCD images for T2 case show the presence of a microdischarge near the axis of the source, while other shorter living microdischarges appear and disappear in subsequent frames.

3.2. Studies of Cell Viability, Proliferation, and Cell-Cycle Progression for Direct Plasma Treatment

Plasma induced a decrease in cell viability after 48 h from treatment, as revealed by the number of cells permeable to 7-AAD, a fluorescent compound with strong affinity for DNA that remains excluded from viable cells with intact membrane. After 60 s of L5178Y plasma exposure at the distance of 1.25 mm the percentage of viable cells was 57.3% compared to 71.2% of untreated cells (Figure 8). The highest cytotoxic effect was induced by cells exposure to plasma for 120 s at the distance of 2.50 mm (43% living cells compared to 71.2% of untreated cells) (Figure 8).

Furthermore, non-equilibrium plasma affected cells proliferation both after 24 and 48 h from the exposure

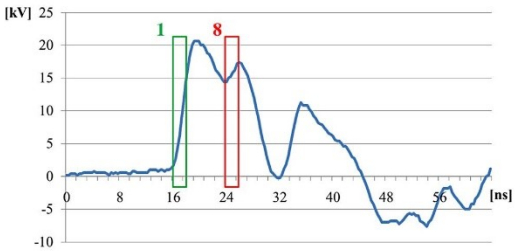

Figure 7. Measured voltage waveform with superimposed exposure gates for the first (one, green) and last (eight, red) iCCD frames.

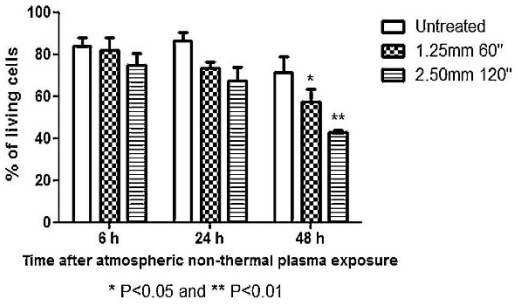

Figure 8. Percentage of living cells after 6, 24, and 48 h from direct atmospheric non-equilibrium plasma exposure.

(Figure 9). The highest effect was observed at the exposure condition 2.50 mm for 120 s, where it was possible to observe 36.7% proliferating cells after 24 h from the treatment and 30.0% after 48 h (Figure 9).

In order to investigate non-equilibrium plasma effects on cell-cycle progression, cells were treated with a reagent containing PI, a red fluorescent intercalating agent that allows to evaluate DNA content. During cell-cycle S phase, cells duplicate their content of DNA that will be double in G2/M phase compared to G0/G1 phase, as well as PI fluorescence. After 24 h from the treatment, it was possible to observe an accumulation of cells in G2/M phase, as showed in Figure 10A, for both exposure conditions (1.25 mm, 60 s 65.3% cells and 2.50 mm, 120 s 55.9% cells vs. 39.6% of untreated cells) (Figure 10B). After 48 h from plasma exposure, the accumulation of cells in G2/M phase was statistically significant for the exposure condition 2.50 mm, 120 s (52.2% cells vs. 42.8% of untreated cells) (Figure 10C).

On the basis of our results, the cell-cycle arrest is reversible for the 60 s and 1.25 mm condition; indeed, in that condition, we observed an accumulation of G2-cells at 24 h post-treatment but not at 48-h post-treatment. This

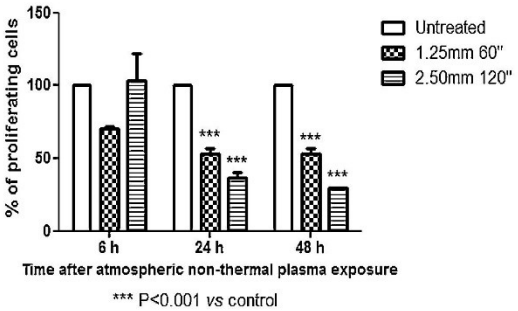

Figure 9. Percentage of proliferating cells after 6, 24, and 48 h from direct atmospheric non-equilibrium plasma exposure.

Plasma Process. Polym. **2015,** DOI: 10.1002/ppap.201500033

DOI: 10.1002/ppap.201500033

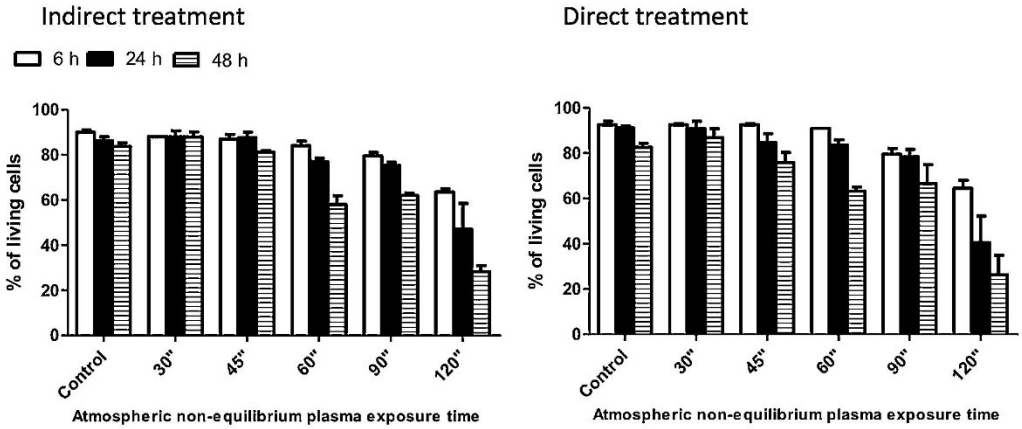

Figure 11. Percentage of living cells after direct and indirect plasma treatment for different treatment times. Data were collected 6, 24, and 48 h after cells were added to atmospheric non-equilibrium plasma treated medium (indirect treatment) or 6, 24, 48 h after atmospheric non-equilibrium plasma exposure of cells (direct treatment). Operating conditions: PV 20 kV, PRF 500 Hz, and gap 1.25 mm.

presented; moreover, also results for plasma treatment performed with gap width 1.25 mm and treatment time 120 s, which is shown in Figure 11 to induce the lowest cell viability among the tested treatments, are presented as a means of comparison and discussion.

For all the tested conditions, a significant increase of NO_2^-, NO_3^-, and H_2O_2 can be observed with respect to the untreated cell culture medium. For the cases T1 and T2, the measured concentration of all reactive species fell in the same range; since viability, proliferation, and cell-cycle progression tests showed different results for conditions T1 and T2, we would have to conclude that the limited sensitivity of the analytic strips prevents us from drawing further conclusions on the relative importance of the various reactive species on the modulation of cell response to plasma exposure. Despite this limited sensitivity, a significantly higher nitrite concentration with respect to the T1 and T2 treatments was measured for the case with a 1.25 mm gap and for 120 s, while nitrate and peroxide concentrations were measured in the same range. Nitrites were previously suggested to possibly have a significant role in plasma oncology [29] and to be linked to the reduction of cell viability after plasma treatment;[30,31] accordingly, we measured the highest concentration of nitrites for the case inducing the highest reduction of cell viability: considering only the 48 h culture times, the treatment performed with a 1.25 mm gap and for 120 s resulted in a percentage of viable cell of 26%, while treatment T1 and T2 resulted in percentages of 57.3% and 43%, respectively.

4. Conclusion

Atmospheric non-equilibrium pressure plasma has encountered a great interest as a novel anti-tumor agent since it was demonstrated by early works, both on in vitro and in vivo models, that the wide blend of chemical and physical reactive components could exert anti-tumor effects.[32–37] Beside few pioneering studies,[5,6] plasma-cell interaction mechanisms are still mostly unsolved and thus are an extremely relevant subject of current cutting edge researches.[38,39] With the aim to contribute to garner knowledge on the fundamental aspects of plasma interactions with cancers cells, the effects of the plasma

Table 1. Nitrite, nitrate, and peroxide concentrations in the untretated and in the plasma treated cell culture medium. All treatments were performed at PV 20 kV and PRF 500.

Operating conditions	NO_2^- (mg/L)	NO_3^- (mg/L)	H_2O_2 (mg/L)
Untreated	0	0	0
Gap 1.25 mm, treatment time 60 s (T1)	5–10	100–250	3–10
Gap 2.5 mm, treatment time 120 s (T2)	5–10	100–250	3–10
Gap 1.25 mm, treatment time 120 s	10–20	100–250	3–10

Plasma Process. Polym. **2015,** DOI: 10.1002/ppap.201500033

DOI: 10.1002/ppap.201500033

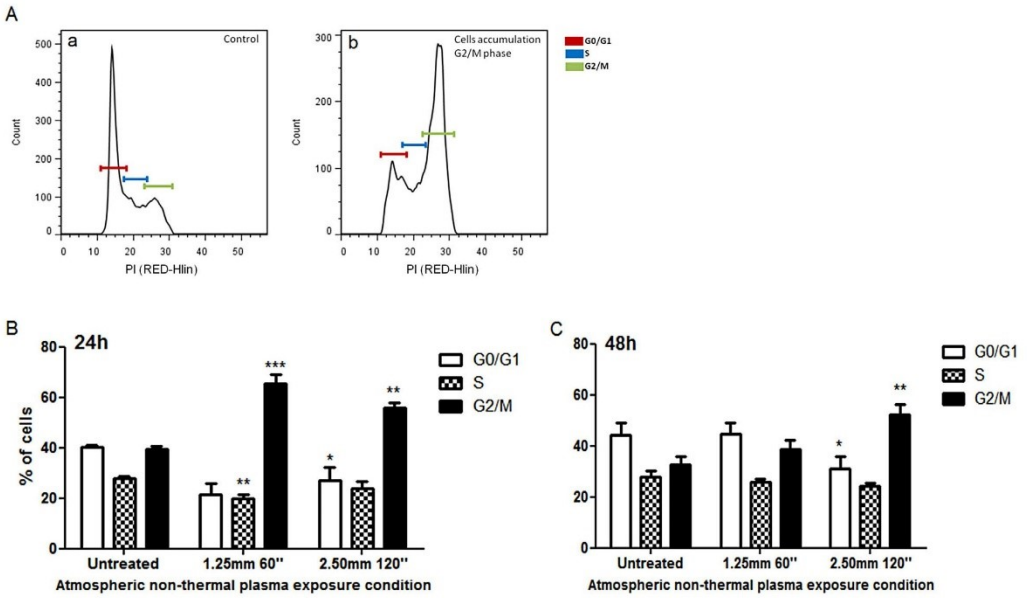

* P<0.05, ** P<0.01 and *** P<0.001

Figure 10. Fluorescence histograms representing cell-cycle distribution of untreated cells (Aa) and of cultures directly treated with plasma, where a plasma-induced G2/M phase accumulation is evident (Ab). Cell-cycle distribution after 24 (B) and 48 h (C) from atmospheric non-equilibrium plasma exposure.

means that cells can overcome the plasma-induced cell-cycle arrest and start proliferating. The 120 s and 2.50 mm condition is able to induce a stronger antiproliferative effect, from which cells cannot rescue; in this case, we can conclude that the cell-cycle arrest induced by plasma is irreversible.

Taken together, these results demonstrate that the growth inhibition of lymphoma cells induced by plasma treatment is imputable to cell death and cell-cycle arrest in which G2 accumulation is a key event. The simultaneous appearance of G2 block and cell death suggests that cell death is a primary direct effect due to plasma treatment, and not a secondary effect due to the cells' inability to overcome growth arrest and proceed through the cell cycle.

3.3. Comparison of Direct and Indirect Plasma Treatment

Results for cell viability after direct and indirect plasma treatment at different treatment times, PV 20 kV, PRF 500 Hz, and gap 1.25 mm are reported in Figure 11. As revealed by the number of cells permeable to 7-AAD, the longer the treatment time (from 30 to 120 s) and the culture time after plasma treatment (6, 24, and 48 h), the higher the reduction in cell viability; no relevant difference can be observed between direct and indirect treatment results. Similar results were obtained with a gap of 2.50 mm and identical treatment times (data not shown). This suggests that the chemistry induced by plasma treatment in the culture medium plays the leading role in plasma reduction of cancer cells viability; similar considerations were previously reported by Vandamme et al.[27] and Mohades et al.,[28] who compared the effects of direct and indirect treatment on glioblastoma U87MG and SCaBER bladder cancer cells, respectively.

3.4. Measurement of Nitrites, Nitrates, and Peroxides in Cell Culture Medium

Results for the concentration of NO_2^-, NO_3^-, and H_2O_2 produced in 1 mL of complete cell culture medium after plasma treatment, semi-quantitatively measured by means of analytic strips, are reported in Table 1. In particular, results for treatments carried out in the same operating conditions (T1 and T2) adopted for studies of cell viability, proliferation, and cell-cycle progression are

treatment on the viability, proliferation, and cell-cycle distribution of L5178Y TK± clone (3.7.2C) cells of mouse lymphoma have been presented in this paper.

Plasma treatments were performed by means of a wand electrode DBD driven by unipolar nanosecond high voltage pulses, either in direct configuration, with cells exposed to plasma while suspended in DMEM, or indirect configuration, where cells were added to DMEM previously activated by plasma treatment. In direct configuration, two different sets of operating conditions were considered, varying the distance between the tip of the plasma source and the surface of the liquid medium and the treatment time; qualitative differences between the plasma discharges produced in the two operating conditions were highlighted by means of HS and iCCD imaging. Plasma treatment was observed to reduce the percentage of viable cells in both the evaluated operating conditions, with the highest cytotoxic effect for the case with longest exposure time and largest gap width. Moreover, plasma treatment was shown to significantly reduce cell proliferation and to induce a statistically significant accumulation of cells in G2/M phase.

Furthermore, results for direct treatment were compared with results for indirect treatment of cancer cells: no differences were observed for cell viability in the two cases, suggesting that the leading role in plasma treatment of cancer cells is played by the reactive species produced in the culture medium. Semi-quantitative measurements of nitrites, nitrates, and peroxides highlighted the production of significant concentrations of reactive species in the culture medium after plasma treatment; despite their sensitivity limitations, the adopted analytic strips hinted at a connection between nitrite concentration and the reduction of cell viability, supporting data and speculations presented in other works.[29–31] Therefore, future activities will be focused on a more detailed identification and quantification of the reactive species produced by plasma treatment in the culture medium and in the investigation of their role in the mechanisms of plasma interaction with cancer cells.

Acknowledgements: This work was partially supported by COST Action MP1101 "Biomedical Applications of Atmospheric Pressure Plasma Technology," by COST Action TD1208 "Electrical discharges with liquids for future applications," and by the 2007–2013 Emilia Romagna Regional Operational Programme (POR) of the European Regional Development Fund (FESR).

Received: February 24, 2015; Revised: April 20, 2015; Accepted: May 8, 2015;DOI: 10.1002/ppap.201500033

Keywords: cell-cycle analysis; cell viability; dielectric barrier discharge; lymphoma; plasma treatment of cancer

[1] A. Jemal, R. Siegel, J. Xu, E. Ward, *CA. Cancer J. Clin.* **2010**, *60*, 277.
[2] D. Hanahan, R. A. Weinberg, *Cell* **2000**, *100*, 57.
[3] A. Arcangeli, S. Pillozzi, A. Becchetti, *Curr. Med. Chem.* **2012**, *19*, 683.
[4] J. E. Karp, D. D. Ross, W. Yang, M. L. Tidwell, Y. Wei, J. Greer, D. L. Mann, T. Nakanishi, J. J. Wright, A. D. Colevas, *Clin. Cancer Res.* **2003**, *9*, 307.
[5] M. Keidar, R. Walk, A. Shashurin, P. Srinivasan, A. Sandler, S. Dasgupta, R. Ravi, R. Guerrero-Preston, B. Trink, *Br. J. Cancer* **2011**, *105*, 1295.
[6] M. Vandamme, E. Robert, S. Pesnel, E. Barbosa, S. Dozias, J. Sobilo, S. Lerondel, A. Le Pape, J. M. Pouvesle, *Plasma Process. Polym.* **2010**, *7*, 264.
[7] H. J. Lee, C. H. Shon, Y. S. Kim, S. Kim, G. C. Kim, M. G. Kong, *New J. Phys.* **2009**, *11*, 115026.
[8] B. Gweon, M. Kim, D. B. Kim, D. Kim, H. Kim, H. Jung, J. H. Shin, W. Choe, *Appl. Phys. Lett.* **2011**, *99*, 063701.
[9] M. Ishaq, S. Kumar, H. Varinli, Z. Han, A. E. Rider, M. D. M. Evans, A. B. Murphy, K. Ostrikov, *Mol. Biol. Cell* **2014**, *25*, 1523.
[10] O. Volotskova, T. S. Hawley, M. A. Stepp, M. Keidar, *Sci. Rep.* **2012**, *2*, 636.
[11] T. Adachi, H Tanaka, S. Nonomura, H. Hara, S. Kondo, M. Hori, *Free Radical Bio. Med.* **2015**, *79*, 28.
[12] H. Tanaka, M. Mizuno, K. Ishikawa, K. Nakamura, H. Kajiyama, H. Kano, *Plasma Med.* **2011**, *1*, 265.
[13] F. Utsumi, H. Kajiyama, K. Nakamura, H. Tanaka, M. Mizuno, K. Ishikawa, H. Kondo, H. Kano, M. Hori, F. Kikkawa, *PLoS ONE* **2013**, *8*, e81576.
[14] G. Fridman, M. Peddinghaus, H. Ayan, A. Fridman, M. Balasubramanian, A. Gutsol, A. Brooks, G. Friedman, *Plasma Chem. Plasma Process* **2006**, *26*, 425.
[15] M. Boselli, V. Colombo, E. Ghedini, M. Gherardi, R. Laurita, A. Liguori, P. Sanibondi, A. Stancampiano, *IEEE ICSD*. Bologna, Italy **2013**.
[16] T. Shao, Z. Niu, C. Zhang, Y. Yu, H. Jiang, W. Li, P. Yan, Y. Zhou, *IEEE Trans. Plasma Sci.* **2011**, *39*, 2062.
[17] H. Luo, Z. Liang, B. Lv, X. Wang, Z. Guan, L. Wang, *Appl. Phys. Lett.* **2007**, *91*, 221504.
[18] M. Teschke, J. Kedzierski, E. G. Finantu-Dinu, D. Korzec, J. Engemann, *IEEE Trans. Plasma Sci.* **2005**, *33*, 310.
[19] F. Massines, A. Rabehi, P. Decomps, R. B. Gadri, P. Ségur, C. Mayoux, *J. Appl. Phys.* **1998**, *83*, 2950.
[20] S. Bianconi, F. Cavrini, V. Colombo, M. Gherardi, R. Laurita, A. Liguori, P. Sanibondi, A. Stancampiano, *IEEE Trans. Plasma Sci.* **2014**, *42*, 2746.
[21] M. Boselli, V. Colombo, M. Gherardi, R. Laurita, A. Liguori, P. Sanibondi, E. Simoncelli, A. Stancampiano, *IEEE Trans. Plasma Sci.* **2015**, *43*, 713.
[22] T. Shao, C. Zhang, Y. Yu, Z. Fang, P. Yan, *EPL* **2012**, *97*, 55005.
[23] S. F. Mirala, E. Monette, R. Bartnikas, G. Czeremuszkin, M. Latreche, M. R. Wertheimer, *Plasmas Polym.* **2000**, *5*, 63.
[24] M. Boselli, V. Colombo, E. Ghedini, M. Gherardi, R. Laurita, A. Liguori, P. Sanibondi, A. Stancampiano, *IEEE Trans. Plasma Sci.* **2014**, *42*, 2744.
[25] M. Boselli, V. Colombo, E. Ghedini, M. Gherardi, R. Laurita, A. Liguori, P. Sanibondi, A. Stancampiano, *Plasma Chem. Plasma Proc.* **2014**, *34*, 853.
[26] U. Kogelschatz, *Plasma Chem. Plasma Proc.* **2003**, *23*, 1.
[27] M. Vandamme, E. Robert, S. Lerondel, V. Sarron, D. Ries, S. Dozias, J. Sobilo, D. Gosset, C. Kieda, B. Legrain, J.-M. Pouvesle, A. Le Pape, *Int. J. Cancer* **2012**, *130*, 2185.
[28] S. Mohades, N. Barekzi, M. Laroussi, *Plasma Process. Polym.* **2014**, *11*, 1150.

[29] D. B. Graves, *Plasma Process. Polym.* **2014**, *11*, 1120.
[30] A. R. Gibson, H. O. McCarthy, A. A. Ali, D. O'Connell, W. G. Graham, *Plasma Process. Polym.* **2014**, *11*, 1142.
[31] J. Liebmann, J. Scherer, N. Bibinov, P. Rajasekaran, R. Kovacs, R. Gesche, P. Awakowicz, V. Kolb-Bachofen, *Nitric Oxide* **2011**, *24*, 8.
[32] I. E. Kieft, *PhD Thesis*, Technische Universiteit Eindhoven, Eindhoven, **2005**.
[33] G. Fridman, A. Shereshevsky, M. M. Jost, A. D. Brooks, A. Fridman, A. Gutsol, V. Vasilets, G. Friedman, *Plasma Chem. Plasma Process.* **2007**, *27*, 163.
[34] Z. Xianhui, L. Maojin, Z. Rouli, F. Kecheng, Y. Size, *Appl. Phys. Lett.* **2008**, *93*, 021502.
[35] G.-C. Kim, H. J. Lee, C.-H. Shon, *J. Korean Phys. Soc.* **2009**, *27*, 628.
[36] Y. Xu, X. Zilan, Z. Fei, Z. Shasha, L. Xinpei, Y. Guangxiao, H. Guangyuan, K. Ostrikov, *Plasma Process. Polym.* **2011**, *9*, 59.
[37] S. Kalghatgi, C. Kelly, E. Cerchar, J. Azizkhan-Clifford, *Plasma Med.* **2011**, *1*, 249.
[38] Y. Ma, C. S. Ha, S. W. Hwang, H. J. Lee, G. C. Kim, K.-W. Lee, K. Song, *PLoS ONE* **2014**, *9*, e91947.
[39] N. Kaushik, N. Kumar, C. H. Kim, N. K. Kaushik, E. H. Choi, *Plasma Process Polym.* **2014**, *11*, 1175.

6.7 Paper VII

Cold atmospheric plasma treatment affects early bacterial adhesion and decontamination of soft reline palatal obturators

Submitted to Journal of Biomedical Materials Research: Part B - Applied Biomaterials 2016

Title: Cold atmospheric plasma treatment affects early bacteria adhesion and decontamination of soft reline palatal obturators

Authors: Anna Liguori [*,a], Andrea Cochis [*,b,c,d], Augusto Stancampiano [*,a], Romolo Laurita [a], Barbara Azzimonti [c,e], Rita Sorrentino [e], Elena Varoni [d], Marta Petri [b], Vittorio Colombo [a,f], Matteo Gherardi [a,f,**], and Lia Rimondini [b,c,**]

* These authors contributed equally to this work

Authors Affiliations:

[a] Department of Industrial Engineering (D.I.N.), Alma Mater Studiorum-Università di Bologna (BO), Italy

[b] Laboratory of Biomedical Materials, Department of Health Sciences, Università del Piemonte Orientale, Novara (NO), Italy

[c] Consorzio Interuniversitario Nazionale per la Scienza e Tecnologia dei Materiali (INSTM), Firenze (FI), Italy, Local Unit Università del Piemonte Orientale

[d] Department of Biomedical Sciences, Surgery and Dentistry, Università degli Studi di Milano, Milano (MI), Italy

[e] Laboratory of Applied Microbiology, Department of Health Sciences, Università del Piemonte Orientale, Novara (NO), Italy

[f] Industrial Research Centre for Advanced Mechanics and Materials (C.I.R.I.-M.A.M.), Alma Mater Studiorum-Università di Bologna (BO), Italy

** *Corresponding Authors:*

Prof. Lia Rimondini

Laboratory of Biomedical Materials

Università del Piemonte Orientale

Department of Health Sciences, Via Solaroli 17, 28100 Novara (NO), Italy.

Tel.: +39 0321660673

Fax.: +39 0321620421

E-mail address: lia.rimondini@med.uniupo.it

Dr. Matteo Gherardi

Department of Industrial Engineering (D.I.N.),
Alma Mater Studiorum-Università di Bologna
Via Saragozza 8, 40123 Bologna (BO), Italy
Tel: +39 0512093978
E-mail address: matteo.gherardi4@unibo.it

Highlights.

1. Cold atmospheric plasma treatment affects bacteria adhesion
2. Cold atmospheric plasma treatment is effective for palatal obturators decontamination
3. Cold atmospheric plasma is effective towards both early and mature biofilm
4. Cold atmospheric plasma treatment does not affect polymer mechanical performances
5. Palatal obturators treated by cold atmospheric plasma are not toxic for human primary cells

Abstract.

Objectives: evaluation of anti-adhesion and decontamination activity of cold atmospheric plasma towards biofilm formation onto soft reline oral palatal obturators.

Methods: the ability of cold atmospheric plasma to prevent biofilm formation and reduce bacteria viability was evaluated by two dielectric barrier discharge plasma sources against the oral biofilm formers *Streptococcus mutans* and *Aggregatibacter actinomycetemcomitans*. Reline specimens were either plasma treated before being infected with 24 hours old biofilm or else infected with 90 minutes (early biofilm) or 24 hours (mature biofilm) old biofilm prior to be plasma treated; specimens were exposed to plasma for 30, 60 and 120 seconds. Afterwards, bacteria number and viability were evaluated by CFU and XTT assays. Finally, viability and morphology of human primary fibroblasts and keratinocytes cultivated onto plasma treated specimens were assayed by MTT.

Results: both plasma sources resulted effective towards the selected strains. Plasma treatment of sterile reline specimens affected subsequent bacteria adhesion, leading to a CFU number and ~~bacteria~~ viability 2 logs and 50%, respectively, lower than untreated controls ($p<0.05$). The anti-adhesion efficacy was noticeable towards early biofilm: after 120 s of plasma treatment, CFUs were reduced of 3 logs and viability decreased of around 60% ($p<0.05$). Significant results were also observed for mature biofilm: CFUs and viability were reduced of around 2 logs and 40% ($p<0.05$), respectively, after 120 s exposure. Finally, MTT did not reveal toxic effects towards human cells.

Significance: plasma represents a very promising ~~solution~~ tool for decontaminating soft reline oral palatal obturators and for inducing a reduction of early bacteria adhesion.

Keywords: cold atmospheric plasma, oral biofilm, soft reline oral palatal obturator, *in vitro* cytocompatibility.

1. Introduction.

Cancer involving upper gums, palate and oral sinus accounts for 1-5% of malignant neoplasms of head and neck ~~neoplasms~~ [1]. Most of them are deeply invasive because late diagnosed. In these cases, the treatment of choice are surgical deep resection including palate- and maxillectomy followed by reconstructive approaches. These latter include, at the best, plastic surgical reconstructions such as free microvascularized flaps (osteo-musculocutaneous of the internal iliac crest, osteo-cutaneous flap of the fibula or scapula, fascia, or osteo-cutaneous radial flap or pedicled flaps such as temporalis muscle flap) [2-4].

However, when the breach is wide, patients are required to temporary of definitively wear custom-made removable palatal obturators, to replace the lacking tissues and to restore masticatory, deglutition, speech functions, and cosmetic appearance [1]. Among the large number of materials suitable for this purpose, soft reline holds a relevant position since it is easily moldable and possesses, thanks to its sponge-like return, the mechanical characteristics required to sustain the typical values of the compressive oral forces. Unfortunately, because of the sophistication of the raw material and the custom-made production process, soft reline oral palatal obturators are quite expensive; therefore, an eventual implant failure might be severely resource- (because of the implants cost) and time-(because of the long production process) consuming. Severe bacteria biofilm contamination of the device is one of the major causes of failure of prosthetic rehabilitations in many body districts [5]. Sometime medical-devices infections are threats for general health and life. Therefore, preventive and therapeutic approaches to counteract or remove biofilm contamination from medical-devices, even palatal obturators, are mandatory for clinical success [6-9].

Conventional methods based on the use of antimicrobial agents have been already demonstrated to be often ineffective against bacteria within a biofilm; therefore, the ability to destroy these living organisms is critical and the development of an alternative technique is demanded. Cold atmospheric plasma (CAP) potentially offers a good alternative to conventional antimicrobial approaches, thanks to its characteristic blend of several and synergic biologically active agents; namely, ultra-violet radiation, neutral or excited atoms and molecules, negative and positive ions, free radicals and free electrons [10-13], which are effective in disrupting individual micro-organisms [14-18] and are not influenced by mechanisms of microbial resistance to antibiotics (innate or acquired) [10]. Since among the biologically active components of plasma, charged particles and electric field are also included, it is proposed that they can affect the cell membrane causing electrostatic disruption or at least permeabilization for a very short time [19-21]. As a consequence, plasma-derived ROS/RNS molecules can penetrate the cell membrane [22-23] inducing further chemical reactions inside the

cytoplasm and leading to the oxidization of cellular proteins and microbial DNA [11, 24-26]. In this regards, Park et al. reported about the possibility to induce *B. subtilis*, *E. coli*, *P. aeruginosa* and *S. typhimirium* disruption within 20 s of exposure to a microwave Ar plasma at atmospheric pressure [27].

Interestingly, some literature results report the effective use of CAP for biofilm disinfection or inactivation [28,29]. The remarkable study carried out by Joaquin et al. [30], about the investigations of the effects induced by CAP on living biofilm-forming bacterial cells, suggests that they go through sequential physiological and morphological changes before becoming inactivated by plasma and that longer treatment time than for the case of planktonic bacteria are necessary to ensure a complete inactivation.

This inactivation potential of CAP, together with the possibility to maintain relatively low temperature (below 40°C), enable to extend plasma treatment to living tissues and thermo-sensitive materials. Nowadays several studies are focusing on the biomedical applications of plasma, a field usually referred to as *Plasma Medicine* [13,31,32], which includes also dental applications [33]. While a rather significant number of works highlight the effectiveness of CAP for bacteria and biofilm inactivation, to the best of our knowledge, the investigation of the potentialities of CAP treatment in preventing bacteria adhesion and biofilm formation has not been widely performed yet.

Here we report the results concerning the treatment of soft reline oral shutters by means of two CAP sources, with the aim of evaluating their effectiveness in preventing biofilm adhesion and enabling biofilm decontamination. The ability of CAP in preventing biofilm adhesion was evaluated by contaminating with 24 hours old biofilm sterile specimens previously exposed to plasma treatment, while the efficacy in reducing bacteria viability was tested treating with plasma specimens previously contaminated with 90 min (early) and 24 hours (mature) old biofilm. In both cases, *Streptococcus mutans* and *Aggregatibacter actinomycetemcomitans* were chosen since they are strongly related to biofilm formation in the oral cavity. Finally, since the soft reline palatal obturators are properly designed to replace resected tissues, the viability of human primary cells cultivated directly onto the surface of plasma treated specimens has been evaluated.

2. Materials and Methods.

2.1. Specimens preparation

Soft reline was prepared following the manufacturer's instructions (Reline Soft, GC Europe N.V., Leuven, Belgium); afterwards, polymers were cut in order to realize square specimens (5 mm per side) with a thickness of 2 mm. Prior to plasma treatment experiments, specimens were sterilized by ethanol (70% v/v in PBS) immersion overnight followed by three washes in phosphate buffered saline solution (PBS, pH 7.4, 10 min each).

2.2 Plasma sources

In order to evaluate the effectiveness of CAP in preventing bacteria adhesion and in biofilm decontamination, two dielectric barrier discharge (DBD) plasma sources were tested. Schematics and pictures of both adopted plasma sources are presented in Figure 1.

The first plasma source, named DBD-Rod, consists of a cylindrical brass electrode, with a 10 mm diameter, having a semispherical tip, with curvature radius of approximately 5 mm. The electrode is covered with borosilicate glass (relative permittivity ε_r=4.7) as dielectric layer with a thickness of 1 mm. When operated, the plasma source is positioned near, or even in contact with, a grounded electrode realised with an aluminium plate [32]. The DBD-Rod plasma source was driven by a micropulsed generator producing high-voltage nearly sinusoidal pulses having a peak voltage (PV) of 15.4 kV, frequency (f) of 40 kHz, pulse duration of 250 μs and fixed pulsed repetition frequency (PRF) of 1000 Hz.

The second plasma source used in this work, named DBD-Plate, is composed by a POM-C plate (1mm thickness, relative permittivity ε_r=3.4), used as dielectric layer, and an aluminium foil (6x6 cm) adherent to the top surface of the dielectric plate as the high voltage electrode. An aluminium plate, placed in front of the the bottom surface of the dielectric barrier, was employed as grounded electrode. The DBD-Plate plasma source was driven by a micropulsed generator different from the previous one and producing high-voltage sinusoidal pulses having a peak voltage (PV) of 12 kV, frequency (f) of 20 kHz, pulse duration of 4 ms and fixed pulsed repetition frequency (PRF) of 100 Hz.

In this work, the distance between the dielectric surface and the grounded plate was kept constant and equal to 3 mm for both plasma sources and specimens were placed on the grounded plateduring the treatments.

2.3. Mechanical characterization

With the aim of evaluating the potential effects of plasma treatment on the mechanical properties of the reline polymer, stress-strain tests were carried out both on untreated and treated specimens.

Stress–strain measurements were performed with an Instron 4465 (ITW Test and Measurements, Torino, Italy) tensile testing machine on rectangular samples (8 mm x 0.1 mm). The gauge length was 13 mm and the cross-head speed was 50 mm/min. At least five samples were tested for each condition and results were evaluated as the average value ± standard deviation.

2.4. *In vitro* plasma antibacterial activity

2.4.1. Bacteria Strains and Growth conditions

Two exponentially growing oral biofilm former strains were used for the evaluation of plasma induced antibacterial activity: *i*) *Streptococcus mutans* (DSMZ 20523, Leibniz Institute DSMZ-German Collection of Microorganisms and Cell Cultures, Braunschweig, Germany) and *ii*) *Aggregatibacter actinomycetemcomitans* (DSMZ 11123). Bacteria were cultivated in blood agar plates (Sintak S.r.l., Corsico, Milan, Italy) at 37°C in aerobic conditions for 48 hours until single round colonies were obtained. Single colonies were inoculated into fresh LB medium and grown at 37°C in a Gallenkamp orbital shaker incubator at 120 rpm until a $1x10^7$ cells/ml broth culture was obtained, according to McFarland 1.0 standard.

2.4.2. Evaluation of plasma activity in preventing bacteria adhesion

Sterile reline specimens were treated with both DBD sources for 30, 60 and 120 seconds. Then, samples were placed into a 24 multiwell plate (Nunclon Delta Surface, Thermo Scientific, Rodano, Milan, Italy) and submerged with 1 ml of LB medium containing $1x10^7$ bacterial cells (prepared as described in paragraph 2.4.1). Plate was incubated for 90 minutes at 37°C in agitation (120 rpm, adhesion phase) [34]. Finally, supernatants containing floating planktonic cells (separation phase) were removed and specimens were washed carefully with PBS. The number of biofilm viable colonies was evaluated by the Colonies Forming Unit (CFU) count, while bacteria viability was determined by the colorimetric metabolic 2,3-bis (2-methoxy-4-nitro-5-sulphophenyl)-5-[(phenyl amino) carbonyl]-2H-tetrazolium hydroxide assay (XTT, Sigma, Milan, Italy) assay, as previously described. Briefly, bacteria colonizing surface were detached by means of sonicator and vortex (30 seconds each, 3 times), collected in PBS and used to obtain 6 ten-fold dilutions; then, 20 ml of each dilutions were spotted onto LB agar plates and incubated for 24 hours at 37°C. The final CFU number was calculated as follows [35]:

$CFU = [(number\ of\ colonies \times dilution\ factor)^{(serial\ ten\text{-}fold\ dilution)}]$

Bacteria viability was evaluated by adding 50 ml of XTT solution (3mg/ml in acetone containing 1μM menadione) to each well; plate was incubated for 4 hours in the dark and the optical density was evaluated by a spectrophotometer (SpectraCount, Packard Bell, Chicago, USA) at 490 nm wavelength. Specimens not subjected to plasma treatment were used as control and bacteria viability

onto these samples was considered as 100% and assumed to express the viability onto plasma treated specimens. Experiments were performed in triplicate.

2.4.3. Evaluation of plasma activity in decontaminating early biofilm

Sterile untreated specimens were placed into a 24 multiwell plate (Nunclon Delta Surface, Thermo Scientific) and submerged with 1 ml of LB medium containing $1x10^7$ bacteria cells (prepared as described in paragraph 2.4.1). Plate was incubated for 90 minutes at 37°C in agitation at 120 rpm (adhesion phase). Then, supernatants were extracted in order to remove floating planktonic cells (separation phase) [34], and plasma treatment was directly performed onto 90 minutes bacteria cells (early biofilm) colonizing the surface of specimens for 30, 60 and 120 seconds by using both the DBD plasma sources. Twenty minutes after the plasma treatment, CFU count and XTT assay were performed, as described in paragraph 2.4.2. Infected and untreated specimens were used as control and bacteria viability onto these samples was considered as 100%. Experiments were performed in triplicate.

2.4.4. Evaluation of plasma activity in decontaminating mature biofilm

Sterile untreated specimens were infected as described in paragraph 2.4.1. After the separation phase, samples containing biofilm were rinsed with 1ml of fresh medium and cultivated for 24 hours at 37°C to promote biofilm maturation. Then, supernatants were removed and plasma treatment was directly performed onto 24 hours bacteria cells (mature biofilm) colonizing the surface of the specimens for 30, 60 and 120 seconds by using both plasma sources. After 20 minutes, CFU and XTT analysis were performed as described above. Infected and untreated specimens were used as control and bacteria viability onto these samples was considered as 100%. Experiments were performed in triplicate.

2.5. *In vitro* cytocompatibility

2.5.1. Human Primary Cells

Cytocompatibility of plasma treated soft reline specimens was evaluated against pooled primary human gingival fibroblasts (HGFs) and skin keratinocytes (HEKs). HGFs were isolated from discarded normal human gingiva, surgically resected from healthy patients who underwent ~~to~~ impacted third molars extraction, after obtaining informed consent. Briefly, thin mucosa specimens were collected by dermatome and the epithelial layer detached by enzymatic digestion using a 0.5% dispase solution (in PBS) at 4°C overnight. Afterwards, dermal layer was minced with surgical blades and digested for further 30 min at 37°C with a collagenase/dispase/trypsin solution (1 mg mL^{-1} collagenase, 0.3 mg mL^{-1} dispase, 0.25% trypsin in PBS, all from Sigma) [36]. Obtained cells were cultivated in α-MEM (Sigma) supplemented with 10% heat-inactivated foetal bovine serum FBS (Sigma-Aldrich, Italy)) and 1% antibiotics-antimycotics (Anti-Anti, Sigma) at 37°C in a humidified

5% CO_2 atmosphere. HEK were obtained from Clonetics (Euroclone, Milan, Italy) and maintained in EpiLife® Medium (Invitrogen, Milan, Italy). Before confluence, both eukaryotic cell types were trypsinized, re-suspended, plated for the experiments and used within fifteen population doublings.

2.5.2. Evaluation of cytocompatibility of plasma treated soft reline specimens

Sterile specimens were plasma treated with both DBD sources for 30 and 120 seconds. Then, a defined number ($5x10^4$ cells/specimen) of eukaryotic cells were seeded onto plasma treated reline surfaces; samples were incubated for 24 hours at 37°C, 5% CO_2. After 24 hours, eukaryotic cell viability was determined by the colorimetric metabolic assay 3-(4,5-dimethylthiazol-2-yl)-2,5-diphenyltetrazolium bromide (MTT, Sigma). Briefly, 20 µL of MTT solution (3 mg mL^{-1} in PBS) were spotted into each well; plates were incubated for 4 hours in the dark in incubator at 37°C. Afterwards, medium was removed and formazan crystals on the wells bottom were solved with 100 µL of DMSO. Finally, 50 µL aliquots were collected from each well and the optical density measured by the spectrophotometer at 570 nm. Eukaryotic cells were also cultivated onto untreated reline to confirm its cytocompatibility, while eukaryotic cells cultivated onto polystyrene wells were considered as 100% and assumed to express the viability onto plasma treated specimens. Furthermore, cells morphology, spread and density were visually checked by light microscope (Leica AF 6500, Leica Microsystems, Basel, CH). Experiments were performed in triplicate.

2.6. Statistical analysis of data

Statistical analysis of data was performed using the Statistical Package for the Social Sciences (SPSS v.20.0, IBM, Atlanta, GA, USA). Data were statistically compared by one-way ANOVA, followed by Sheffe's test for post-*hoc* analysis in case of independent samples and by Friedman's ANOVA, followed by Conover's test, in case of dependent samples, Two-samples comparisons were done using Mann-Whitney'U test. Significance level was set at $p<0.05$.

3. Results.

3.1. Mechanical characterization

The mechanical characterization was performed on untreated and 30, 60 and 120 seconds plasma treated soft reline polymers, with the aim to garner some knowledge about the possible variation induced in the material by plasma treatment in terms of elastic modulus, stress at break and deformation at break.

Tensile mechanical properties of the samples treated with both DBD plasma sources are reported in Table 1, where elastic modulus E, stress at break σb, and deformation at break εb are listed. Figure 2 a and Figure 2 b show a representative stress–strain curve of specimens treated by DBD-Rod and DBD-Plate, respectively. From the obtained results, no significant alteration of mechanical performances of the soft reline polymer was found even after 120 seconds of plasma treatment.

3.2. Evaluation of plasma activity in reducing bacteria adhesion

DBD-Rod and DBD-Plate sources, used to treat soft reline palatal obturators before bacterial contamination (as schematized in Figure 3 a), turned out to be effective in preventing bacteria adhesion for both the selected biofilm formers. In particular, the CFUs counts highlighted that on plasma treated samples the CFU number was approximately 2 logs lower than the one registered on untreated control (CNT) ($p<0.05$, indicated by #), as reported in Figure 3 b-e (left histograms). Moreover, as shown in Figure 3 b-e (right histograms), also the bacteria viability evaluated on the soft reline palatal obturators resulted to be affected by plasma treatment, since a loss of bacteria viability of 40-60% for plasma treated samples with respects to the untreated ones ($p<0.05$, indicated by *) was found.

3.3. Evaluation of plasma activity in decontaminating early and mature biofilm

Plasma treatment of previously infected specimens (schematized in Figure 4 a and Figure 5 a) led to a significant decrease of CFU number and bacteria viability for both early and mature biofilm, even after a short treatment time (30-120 seconds). As it can be observed comparing Figure 4 and Figure 5, plasma treatment is more effective on early biofilm.

In fact, both DBD-Rod (Figure 4 b and c) and DBD-Plate (Figure 4 d and e) induced at least a 3 Logs reduction of the CFUs number (b-e, left histograms) and a 40-60% loss in terms of bacteria viability (b-e, right histograms), for both the selected early biofilm formers. All the results obtained for plasma treated specimens were statistically significant in comparison to untreated controls ($p<0.05$, indicated by the # for CFUs counts and by the * for viability assay).

Significant results were also obtained when plasma treatment was performed onto specimens infected by mature biofilm (Figure 5), even though the inhibition values resulted to be lower than the one obtained in the case of early biofilm. In fact, for the two considered biofilm formers, plasma treatment was able to induce 2 Logs reduction of the CFUs number (Figure 5 b-e left histograms) and 20-40% loss in terms of bacteria viability (Figure 5 b-e right histograms). Also in this case results were statistically significant in comparison to untreated controls ($p<0.05$, indicated by the # for CFUs counts and by the * for viability assay). No differences were observed between DBD-Rod and DBD-plate sources.

3.3. Evaluation of cytocompatibility of plasma treated soft reline specimens

Cytocompatibility of untreated soft reline specimens (reported as polymer control in Figure 6) was evaluated, considering eukaryotic cells cultivated onto polystyrene surface (reported as polystyrene control in Figure 6) as positive control and 100% viability. Results showed that both HEKs and HGFs were able to grow onto the specimens surface and no difference ($p>0.05$) with respect to the polystyrene control was observed, as reported in Figure 6 a-b and d-e. Also, reline specimens were subjected to plasma treatment performed under the same operating conditions implemented for bacterial decontamination, in order to assess the possible cytotoxic effects of plasma treated specimens. Results confirmed that plasma treatment of soft reline specimens did not affect their cytocompatibility; in fact, an almost insignificant, when compared to the controls (polystyrene and polymer, $p>0.05$), decrease of the eukaryotic cells viability ratio was registered only after 120 seconds plasma treatment. Furthermore, also the visual observation confirmed that, after 24 hour of cultivation, morphology, spread and density of both HEKs (Figure 6 c) and HGFs (Figure 6 f) cultured onto treated specimens were comparable with those of eukaryotic cells cultured on both the controls.

4. Discussion.

The decontamination of soft reline palatal obturators, worn by patients who suffered from oro-nasal communication as a replacement of lacking soft tissues, represents a challenge for clinicians [37]. In fact, in most cases, due to the inefficacy of conventional methods in reducing the microbial load, the removal and substitution of contaminated implants are required; this procedure is expensive and time consuming because each obturator needs a custom-made molding procedure in order to fit with patients' tissue defect [38]. Since the bacterial and fungal biofilm contamination is the most recognized cause of prosthetic stomatitis [39] and, in case of immunocompromised patients also a potentially life-threatening condition [40], innovative methods able to affect biofilm adhesion onto

sterile soft reline palatal obturators and to induce a reduction of microbial load onto contaminated scaffolds are strongly demanded.

In the present work, the efficacy of plasma treatment for biofilm formation was investigated in a pilot study using two bacteria strains, one belonging to Streptococcus family and one to the subgingival putative periodontal and peri-implant pathogens. The choice of the reported bacteria strains instead of the most common Candida spp, involved in stomatitis etiology, was due to the remarkable role of bacteria both in the early adhesion phase of biofilm formation [41], even when Candida spp are involved, and in enhancing Candida virulence and pathogenicity [42]

The obtained results highlighted the possibility to employ plasma to reduce bacteria adhesion onto sterile soft reline obturators as well as the bacteria load of the contaminated ones. When soft reline specimens were plasma treated prior to their infection (Figure 3), bacteria number and viability after 90 minutes of incubation were found to be lower than the ones evaluated onto the untreated samples: these preliminary results demonstrate that plasma treatment can affect the chemical characteristic of the soft reline polymer surface, at least for the considered elapsing time between the plasma exposure and the contamination. As documented, bacterial adhesion onto surfaces is linked to the chemico-physical properties and functional groups exhibited by the material at its interface with the cells [43]. When polymeric surfaces are subjected to cold plasma treatment performed using oxygen containing gas, as in our case (ambient air), the introduction of oxygenated functional groups occurs [44, 45], contributing to prevent the initial bacterial adhesion [46]. While effective in temporally modifying the surface chemical characteristics of the soft reline specimens plasma treatment did not induce any significant alteration of their bulk mechanical properties. This is of extreme importance since the choice of soft reline as constituting material is mainly based on its unique mechanical characteristics that are able to withstand compressive oral forces while granting comfort to the patients.

Regarding the investigation of the capability of plasma in decontaminating biofilm infected surfaces, very promising results were observed towards early biofilm (Figure 4); in fact, both plasma treatment were found to induce a strong decrease of bacteria load and viability, suggesting that plasma was able to penetrate the biofilm matrix. A noticeable reduction of CFUs number and viability loss was also observed by performing plasma treatment of mature biofilm (Figure 5). However, since the obtained reduction turned out to be less relevant than the one evaluated in the case of early biofilm inactivation, it can be supposed that the penetration of biologically active agents of plasma through the matrix of the mature biofilm is rather slow and unable to eradicate all the mature biofilm layers for the adopted treatment times. In light of this consideration, as a future investigation, the effect of longer plasma treatment time on the mature biofilm inactivation will be investigated, evaluating at the same time the cytocompatibility of the soft reline specimens, which for treatment time up to 120 s did not turn

out to be compromised. Since the appliance of plasma onto reline prosthesis surface did not affect human cells viability or morphology (Figure 6), the reactive species anchored to the surface are assumed to be effective againstbacteria but not toxic for eukaryotic cells.

Conclusions.

The possibility of effectively bacterial decontaminatingsoft reline palatal obturators, in order to prevent their failure and replacement, represents nowadays a challenge for clinicians. In the present work, we have shown that the direct application of cold atmospheric plasma represents a suitable procedure able to significantly reduce bacterial contamination, even in a single short time treatment, and to prevent bacteria adhesion on sterile soft reline specimens. In future works, different elapsing times between the plasma treatment and the contamination of the sterile specimens will be investigated to evaluate the recovery over time of the antibacterial properties induced by the plasma treatment.

Considering the preliminary *in vitro* data, the process turns out to be not toxic for human cells. Therefore, even if more *in vitro* and *in vivo* data are still necessary, it is possible to state that plasma can be considered as a very promising solution for the soft reline decontamination.

Acknowledgements.

Work partially supported by COST Action MP1101 “Biomedical Applications of Atmospheric Pressure Plasma Technology”. Prof. Maria Letiza Focarete is acknowledged for her support in performing stress-strain measurements.

Funding.

AC and BA were partially supported by PRIN 2010–2011 (PRIN 20102ZLNJ5_006), financed by the Ministry of Education, University and Research (M.I.U.R.).

References

1. Tirelli G, R Rizzo R, Biasotto M, Di Learda R, Argenti B, Gatto A, Bullo F. Obturator prostheses following palatal resection: clinical cases. Acta Otorhinolaryngol Ital 2010;30: 33–9.
2. Chiapasco M, Biglioli F, Autelitano L, Romeo E, Brusati R. Clinical outcome of dental implants placed in fibula-free flaps used for the reconstruction of maxillo-mandibular defects following ablation for tumors or osteoradionecrosis. Clin Oral Implants Res 2006;17:220-8.
3. Rogers SN, Lowe D, McNally D, Brown JS, Vaughan ED. Health-related quality of life after maxillectomy: a comparison between prosthetic obturation and free flap. J Oral Maxillofac Surg 2003;61:174-81.
4. Genden EM, Wallace D, Buchbinder D, Okay D, Urken ML. Iliac crest internal oblique osteomusculocutaneous free flap reconstruction of the postablative palatomaxillary defect. Arch Otolaryngol Head Neck Surg 2001;127:854-61.
5. Al Mohajer M, Darouiche RO. The expanding horizon of prosthetic joint infections. J Appl Biomater Funct Mater 2014;12:1-12.
6. Song F, Koo H, Ren D. Effects of Material Properties on Bacterial Adhesion and Biofilm Formation. J Dent Res 2015;94:1027-34.
7. Percival SL, Suleman L, Vuotto C, Donelli G. Healthcare-associated infections, medical devices and biofilms: risk, tolerance and control. J Med Microbiol 2015;64:323-34.
8. Crnich CJ, Drinka P. Medical device-associated infections in the long-term care setting. Infect Dis Clin North Am 2012;26:143-64.
9. Heuer W, Elter C, Demling A, Neumann A, Suerbaum S, Hannig M, Heidenblut T. Analysis of early biofilm formation on oral implants in man. J Oral Rehabil 2007;34:377-82.
10. Laroussi M, Kong MG, Morfill G, Stolz W, editors. Plasma medicine. Cambridge: Cambridge University Press; 2012.
11. Dobrynin D, Friedman G, Fridman A, Starikovskiy A. Inactivation of bacteria using dc corona discharge: role of ions and humidity. New J Phys 2011;13:103033.
12. Stoffels E, Sakiyama Y, Graves DB. Cold atmospheric plasma: Charged species and their interactions with cells and tissues. IEEE T Plasma Sci 2008;36:1441-57.
13. Kong MG, Kroesen G, Morfill G, Nosenko T, Shimizu T, van Dijk J, Zimmermann JL. Plasma medicine: an introductory review. New J Phys 2009;11:115012.
14. Laroussi M. *IEEE* T *Plasma* Sci 2002;30:1409-15.

15. Brandenburg R, Ehlbeck J, Stielber M, Woedtke T, Zeymer J, Scluter O, Weltmann KD. Antimicrobial treatment of heat sensitive materials by means of atmospheric pressure RF-driven plasma jet. Contribution to Plasma Physics 2007;47:72-9.
16. Cooper M, Fridman G, Staack D, Gutsol A, Vasilets VN, Anandan S, Cho YI, Fridman A, Tsapin A. Decontamination of Surfaces From Extremophile Organisms Using Nonthermal Atmospheric-Pressure Plasmas. *IEEE* T *Plasma* Sci 2009;37:866-71.
17. Machala Z, Chladekova L, Pelach M. Plasma agents in bio-decontamination by dc dischargers in atmospheric air. J Phys D 2010;43: 222001.
18. Deng X, Shi J, Kong MG. Physical mechanism of inactivation of Bacillus subtilis spores using cold atmospheric plasmas. *IEEE* T *Plasma* Sci 2006;34:1310-6.
19. Laroussi M, Mendis DA, Rosenberg M. Plasma interactions with microbes. New J Phys 2003;5:41.1.-41.10.
20. Klampfl TG, Isbary G, Shimizu T, Li YF, Zimmermann JL, Stolz W, Schlegel J, Morfill GE, Schmidt HU. Appl Environ Microbiol 2012:78:5077-82.
21. Leduc M, Guay D, Leask RL, Coulombe S. Cell permeabilization using a non-thermal plasma. New J Phys 2009;11:115021.
22. Pompl R, Jamitzky F, Shimizu T, Steffes B, Bunk W, Schmidt HU, Georgi M, Ramrath K, Stolz W, Stark RW, Urayama T, Fujii S, Morfill GE. The effect of low-temperature plasma on bacteria as observed by repeated AFM imaging. New J Phys 2009;11:115023.
23. Montie TC, Kelly-Winterberg K, Reece Roth J. An overview of research using the one atmosphere uniform glow discharge plasma (OAUGDP) for sterilization of surfaces and materials. IEEE T Plasma Sci 2000;28:41-50.
24. Oehmigen K, Hähnel M, Brandenburg R, Wilke C, Weltmann KD, von Woedtke T. The role of acidification for antimicrobial activity of atmospheric pressure plasma in liquids. Plasma Process Polym 2010;7:250-7.
25. Joshi SG, Cooper M, Yost A, Paff M, Ercan UK, Fridman G, Friedman G, Fridman A, Brooks AD. Nonthermal dielectric-barrier discharge plasma-induced inactivation involvesoxidative DNA damage and membrane lipid peroxidation in Escherichia coli. Antimicrob Agents Chemother 2011;55:1053-62.
26. Cooper M, Fridman G, Fridman A, Joshi SG. Biological responses of Bacillus stratosphericus to floating electrode-dielectric barrier discharge plasma treatment. J Appl Microbiol 2010;6:2039-48.

27. Park BJ, Lee DH, Park JC, Lee IS, Lee KY, Hyun SO, Chun MS, Chung KH. Sterilisation using a microwave-induced argon plasma system at atmospheric pressure. Phys Plasm 2003;10:4539–44.
28. Abramzon N, Joaquin JC, Bray J, Brelles- Mariño G. Biofilm destruction by RF high-pressure cold plasma jet. IEEE T Plasma Sci 2006;34:1304-9.
29. Alkawareek MY, Algwari QT, Laverty G, Gorman SP, Graham WG, O'Connell D, Gilmore BF. Eradication of Pseudomonas aeruginosa biofilms by atmospheric pressure non-thermal plasma. PLoS One 2012;7:e44289.
30. Joaquin JC, Kwan C, Abramzon N, Vandervoort K, Brelles-Mariño G. Is gas-discharge plasma a new solution to the old problem of biofilm inactivation? Microbiology 2009;155:724-32.
31. Fridman G, Friedman G, Gutsol A, Shekhter AB, Vasilets VN, Fridman A. Applied plasma medicine. Plasma Process Polym 2008;5:503–533.
32. Gherardi M, Turrini E, Laurita R, De Gianni E, Ferruzzi L, Liguori A, Stancampiano A, Colombo V, Fimognari C. Atmospheric Non-Equilibrium Plasma Promotes Cell Death and Cell-Cycle Arrest in a Lymphoma Cell Line Plasma Process Polym 2015; DOI: 10.1002/ppap.201500033.
33. Arora V, Nikhil V, Suri NK, Arora P. Cold Atmospheric Plasma (CAP) in Dentistry. Dentistry 2014;4:189.
34. Cochis A, Azzimonti B, Della Valle C, Chiesa R, Arciola CR, Rimondini L. Biofilm formation on titanium implants counteracted by grafting gallium and silver ions. J Biomed Mater Res A 2015; 103: 1176–1187.
35. Harrison JJ, Stremick CA, Turner RJ, Allan ND, Olson ME, Ceri H. Microtiter susceptibility testing of microbes growing on peg lids: a miniaturized biofilm model for high-throughput screening. Nat Protoc 2010;5:1236-54.
36. Azzimonti B, Cochis A, Beyrouthy ME, Iriti M, Uberti F, Sorrentino R, Landini MM, Rimondini L, Varoni EM. Essential Oil from Berries of Lebanese Juniperus excelsa M. Bieb Displays Similar Antibacterial Activity to Chlorhexidine but Higher Cytocompatibility with Human Oral Primary Cells. Molecules 2015;20:9344-57.
37. Goiato MC, dos Santos DM, Moreno A, Santiago JF Jr, Haddad MF, Pesqueira AA,Miyahara GI. Prosthetic treatments for patients with oronasal communication. J Craniofac Surg. 2011;22:1445-7
38. Beumer J, Curtis TA, Marunick MT. Maxillofacial rehabilitation: prosthetic and surgical consideration. St. Louis: Medico Dental Medial Intl Inc; 1996. pp. 387–399.

39. Webb BC, Thomas CJ, Willcox MD, Harty DW, Knox KW. Candida-associated denture stomatitis. Aetiology and management: a review. Part 2. Oral diseases caused byCandida species. Aust Dent J. 1998;43:160-6. Review
40. Miller DJ. Diagnosis and Management of Candida and Other Fungal Infections of the Head and Neck. Curr Infect Dis Rep. 2002 Jun;4(3):194-200
41. Valentini F, Luz MS, Boscato N, Pereira-Cenci T. Biofilm formation on denture liners in a randomised controlled in situ trial. J Dent. 2013 May;41(5):420-7.
42. Cavalcanti YW, Morse DJ, da Silva WJ, Del-Bel-Cury AA, Wei X, Wilson M,Milward P, Lewis M, Bradshaw D, Williams DW. Virulence and pathogenicity of Candida albicans is enhanced in biofilms containing oral bacteria. Biofouling.2015;31:27-38.
43. Campoccia D, Montanaro L, Arciola CR. A review of the biomaterials technologies for infection-resistant surfaces. Biomaterials 2013; 34: 8533-8554.
44. Desmet T, Morent R, De Geyter N, Leys C, Schacht E, Dubruel P. Nonthermal Plasma Technology as a Versatile Strategy for Polymeric Biomaterials Surface Modification: A Review. Biomacromolecules 2009; 10: 2351-2378.
45. Jacobs T, Morent R, De Geyter N, Dubruel P, Leys C. Plasma surface modification of biomedical polymers: influence on Cell-Material Interaction. Plasma Chem. Plasma Process. 2012,;32: 1039-1073.
46. Triandafillu K, Balazs D J, Aronsson B O, Descouts P, Tu Quoc P, van Delden C, Mathieu H J, Harms H. Adhesion of Pseudomonas aeruginosa strains to untreated and oxygen-plasma treated poly(vinyl chloride) (PVC) from endotracheal intubation devices. Biomaterials 2003; 24 1507–1518.

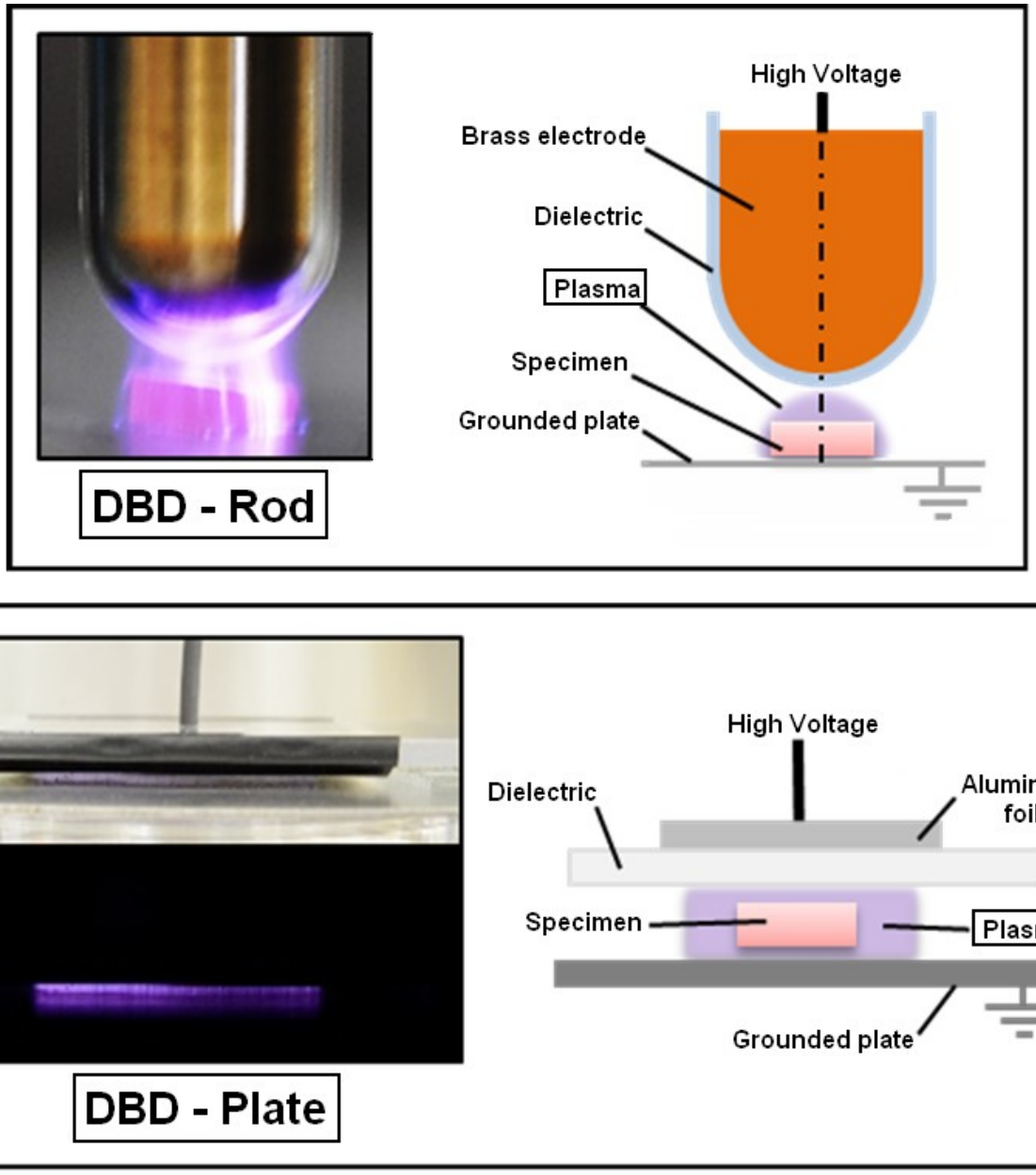

Figure 1. DBD-Rod (upper panel) and DBD-Plate (lower panel), pictures of the discharge during operation (left figures) and schematics representations of the sources (right figures).

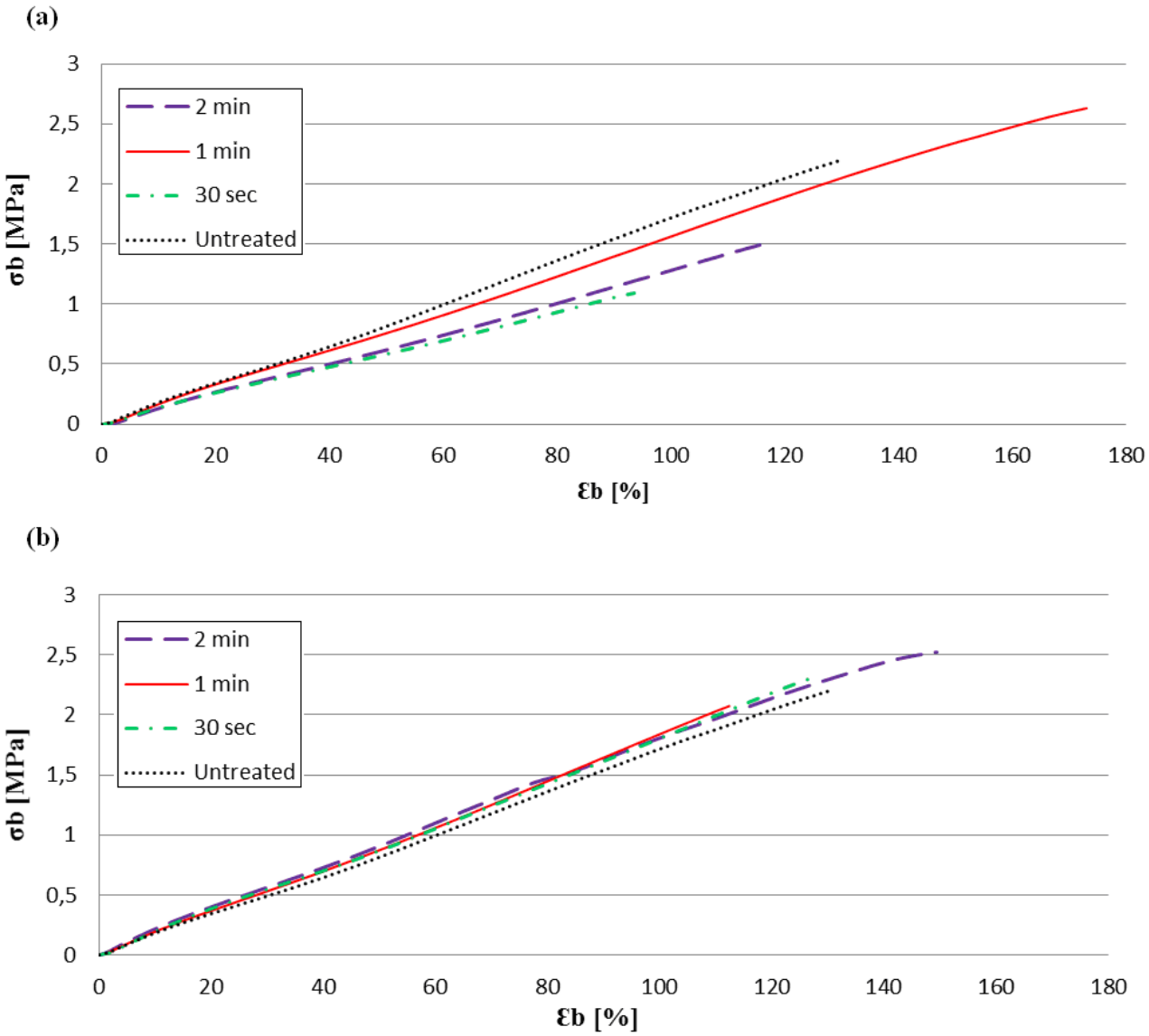

Figure 2 a-b. Stress-strain curves of DBD-Rod (a) and DBD-Plate (b) plasma treated samples for 30 s, 1 min and 2 min and untreated samples.

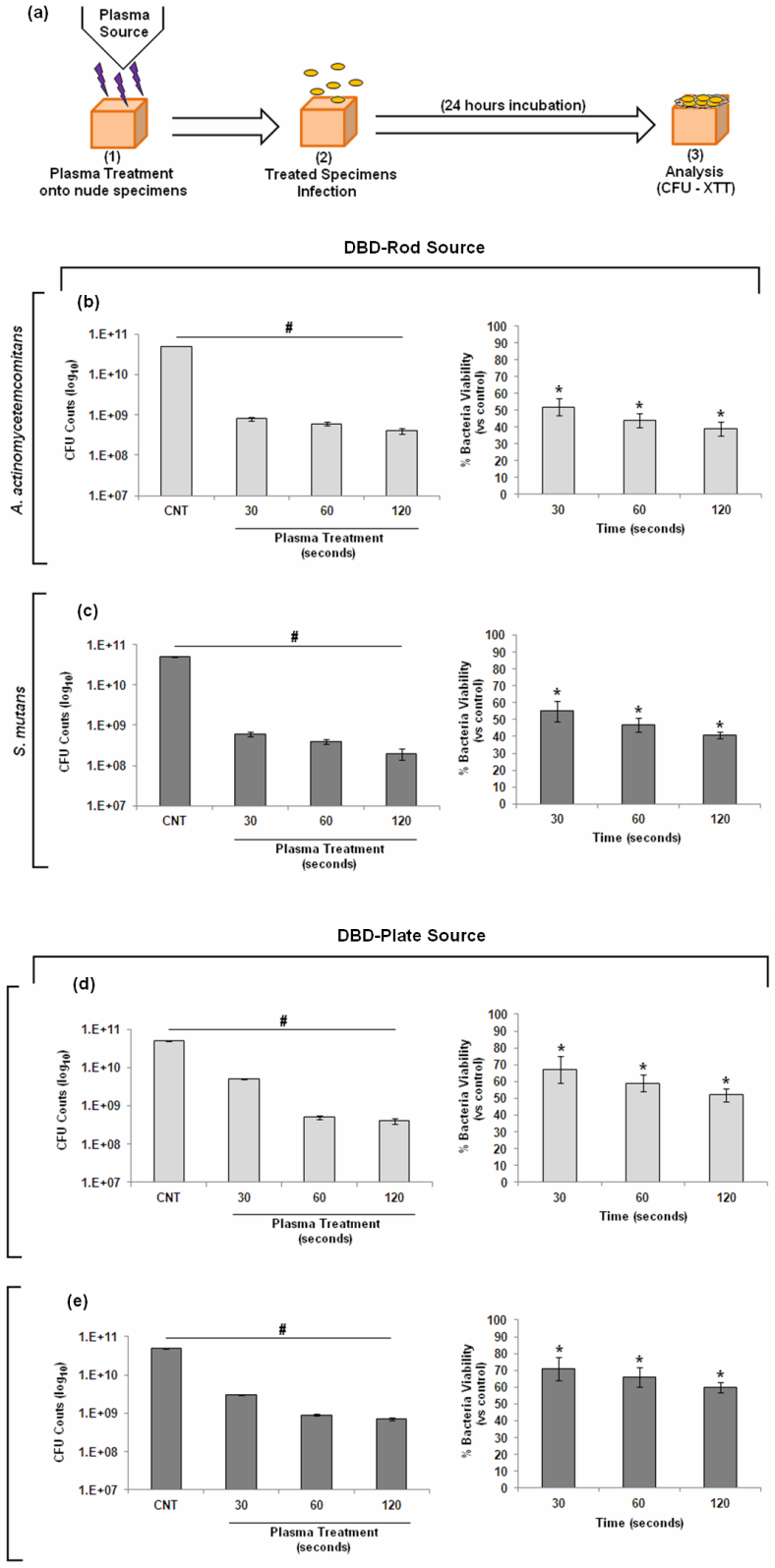

Figure 3 a-e. Schematic representation of the experimental protocol (a); assessment of the capability of DBD-Rod and DBD-Plate plasma source in affecting *A.actinomycetemcomitans* (b and d) and *S.mutans* (c and e) *adhesion*, by means of CFUs counts (b-e left histograms) and evaluation of bacteria viability (b-e right histograms). Results were statistically significant in comparison with untreated controls (CNT) for both CFUs ($p<0.05$, indicated by the #) and viability assessed by XTT ($p<0.05$, indicated by the *). Bars represent mean values and standard deviations

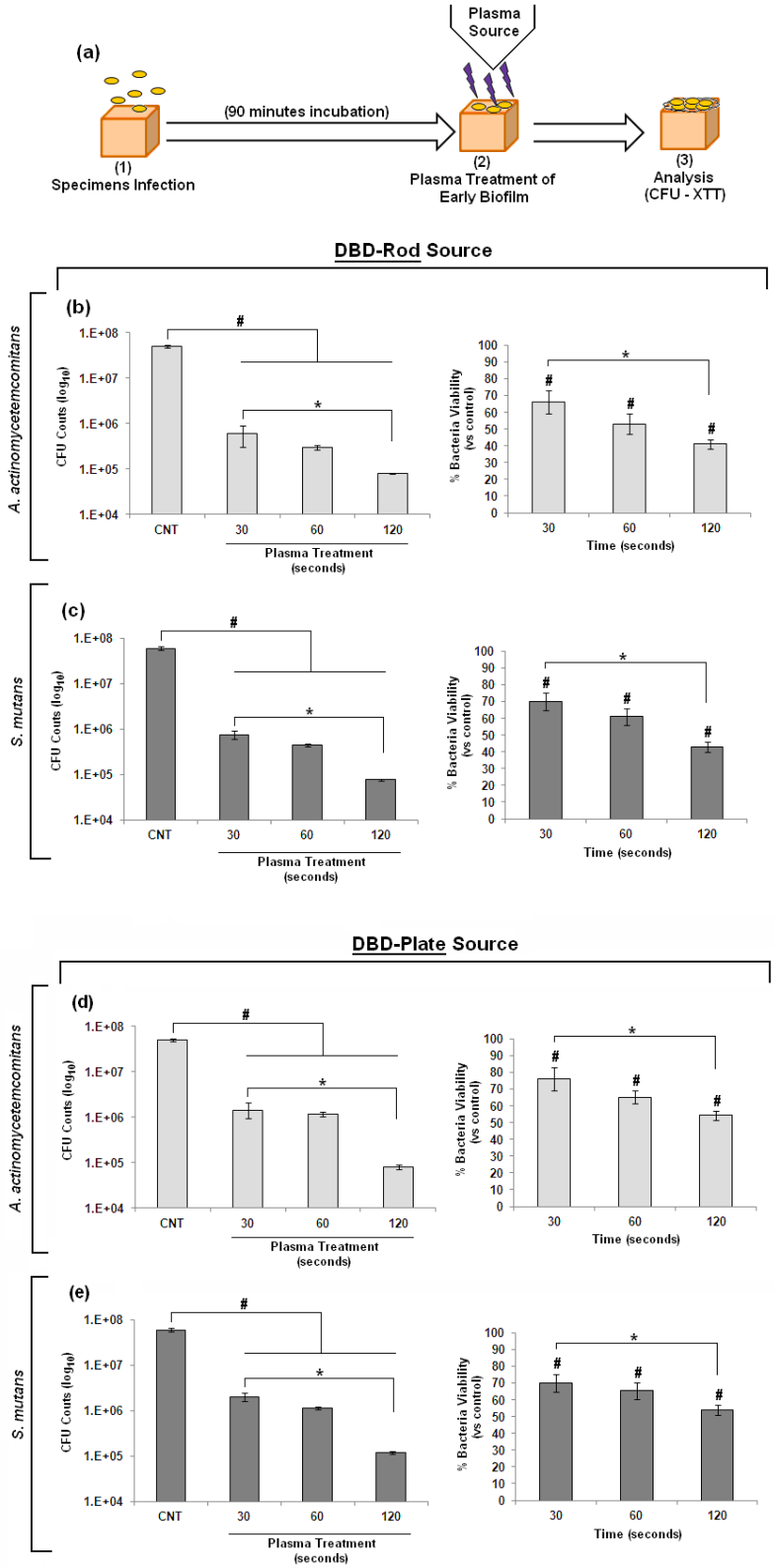

Figure 4 a-e. Schematic representation of the experimental protocol (a); assessment of the effectiveness of DBD-Rod and DBD-Plate plasma source in decontaminating *A.actinomycetemcomitans* (b and d) and *S.mutans* (c and e) *early* biofilm, by means of CFUs counts (b-e left histograms) and evaluation of bacteria viability (b-e right histograms). Results were statistically significant in comparison with untreated controls (CNT) for both CFUs ($p<0.05$, indicated by the #) and viability ($p<0.05$, indicated by the *). Bars represent means and standard deviations.

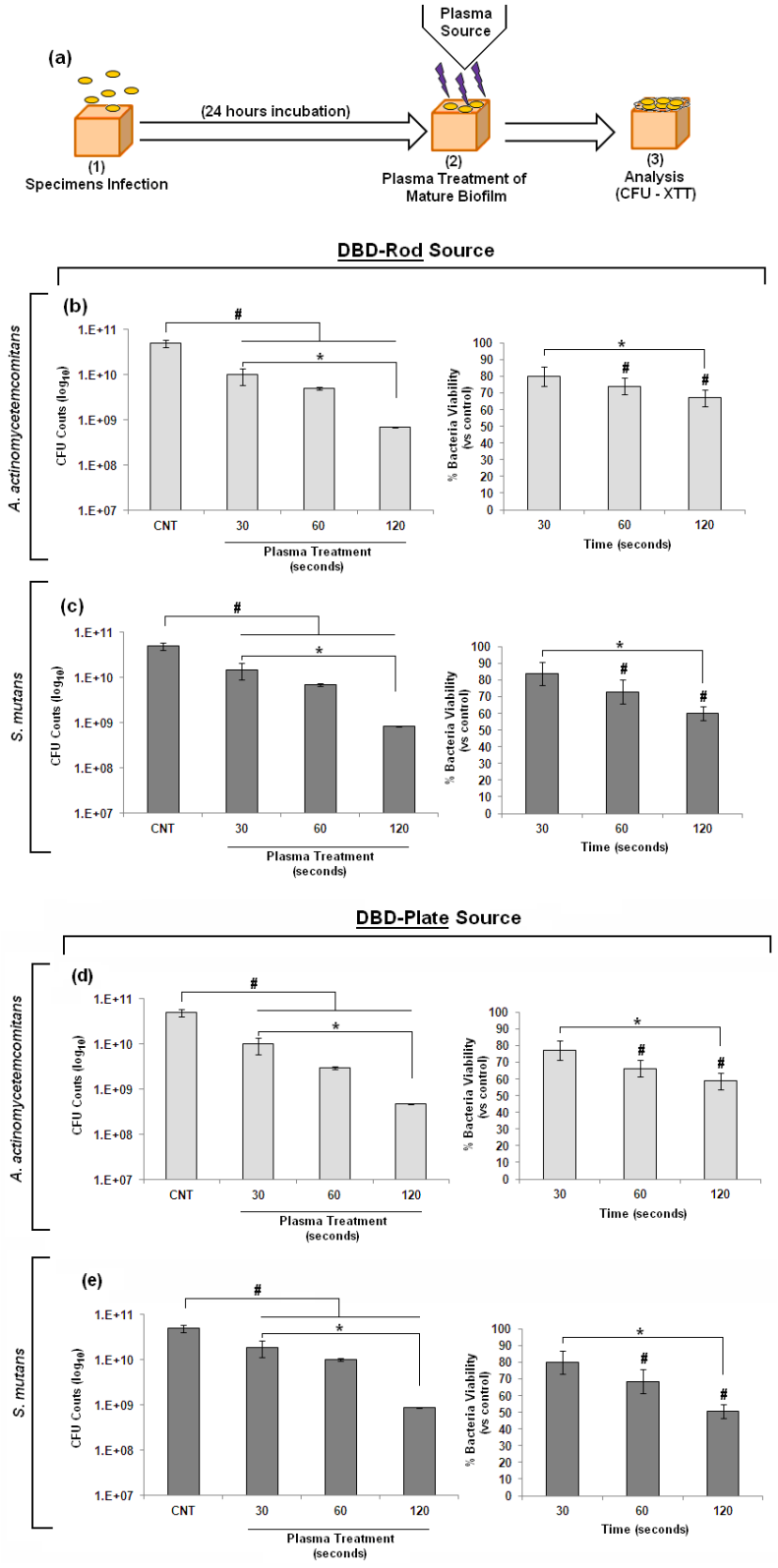

Figure 5 a-e. Schematic representation of the experimental protocol (A); assessment of the effectiveness of DBD-Rod and DBD-Plate plasma source in decontaminating *A.actinomycetemcomitans* (B and D) and *S.mutans* (C and E) *mature* biofilm, by means of CFUs counts (B-E left histograms) and evaluation of bacteria viability (B-E right histograms). Results were statistically significant in comparison with untreated controls (CNT) for both CFUs ($p<0.05$, indicated by the #) and viability ($p<0.05$, indicated by the *). Bars represent means and standard deviations.

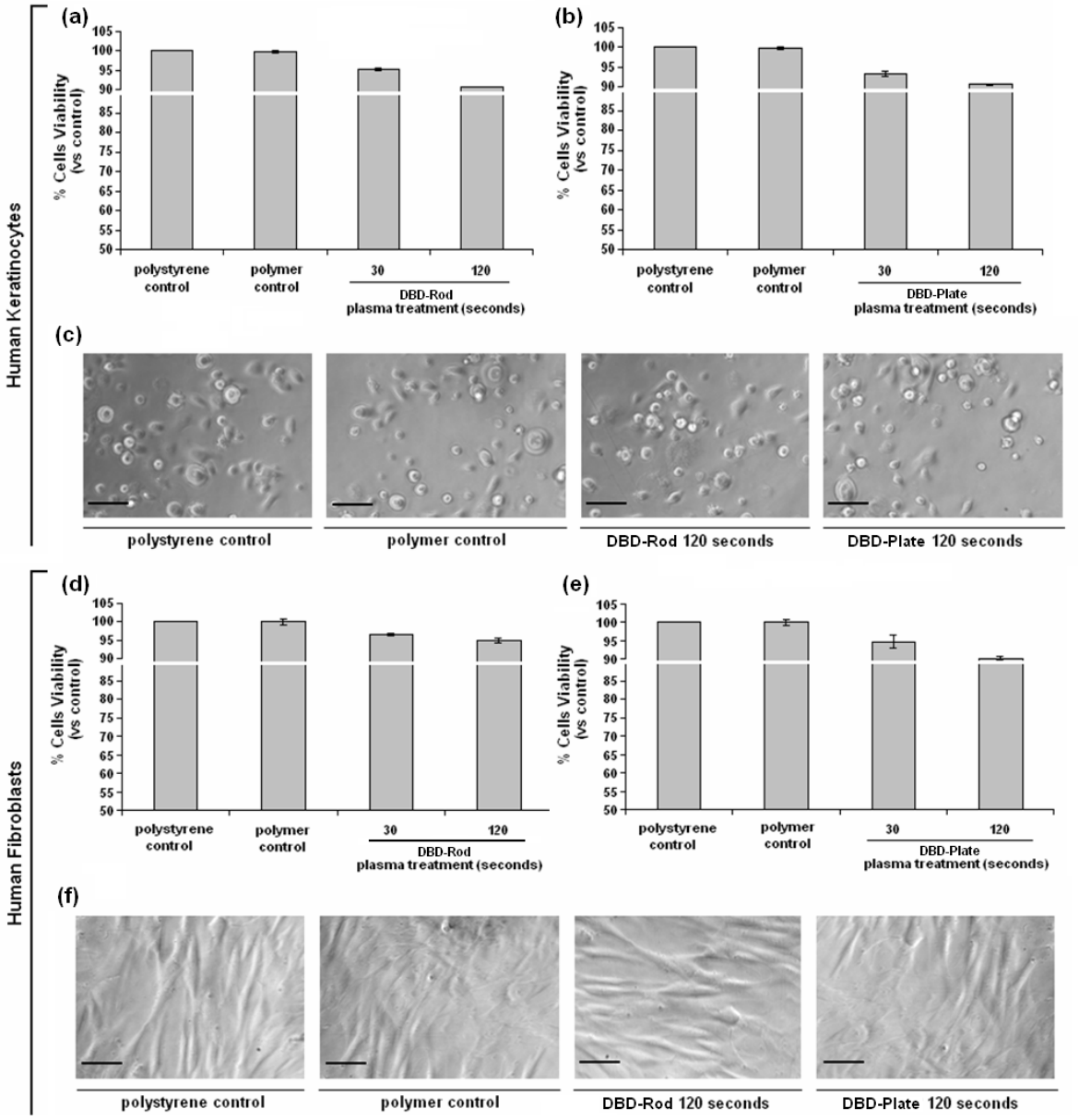

Figure 6 a-f. Assessment of cyotocompatibility of plasma treated soft reline specimens, by means of the evaluation of eukaryotic cell viability and visual observation. The viability and morphology of HEKs (a-c, upper panel) and HGFs (d-f, lower panel) grown onto plasma treated specimens were comparable towards controls cultivated onto untreated reline (polymer control) and polystyrene wells (polystyrene control). No statistically significant differences ($p>0.05$) were detected between treated and control groups.

Acknowledgments

Though only my name appears on the cover of this dissertation, many people have contributed to its production. To them I owe my gratitude. They have made this dissertation possible and my Ph.D period an experience that I will cherish forever.

I would like to express my sincere gratitude to my advisor Prof. Vittorio Colombo for the opportunity to achieve this Ph.D, for the continuous support, for his patience, motivation, and immense knowledge. His guidance helped me through all these three years. I could not have imagined having a better advisor and mentor for my Ph.D study. It was a privilege and honour to be one of his students.

A special thanks goes to Matteo Gherardi, for his friendship, his continuous support, his suggestions, his teachings and all the time he dedicated to me, including the one spent to read this thesis. Thank you for all this and for helping me growing as a research scientist.

I can not but thank Romolo Laurita, for suffering me every morning through all these years. Most of all I thank him for being the very first one to convince me to enter in the field of plasma technology when I was still a master student.

Many thanks goes to my fellow labmates Marco Boselli, Anna Liguori, Enrico Traldi, Emanuele Simoncelli and Anna Miserocchi for all the experiments, all the discussions on plasma physics and random stuff, all the jokes and all the fun. More than everything, thank you for all your help.

Last but not the least, I would like to thank Tito Stancampiano and Elisabetta Golinelli, for being my parents. As a young researcher I have learn that the number of failures is generally a hundred times the number of successes. For this reason, I can not but be impressed by the way the manage to give me the best childhood I could ever imagine, and on their first try. I thank them, and my sister too, for supporting me spiritually throughout writing this thesis and my life in general.